GEOLOGICAL SURVEY EXPLANATORY REPORT SHEET 36

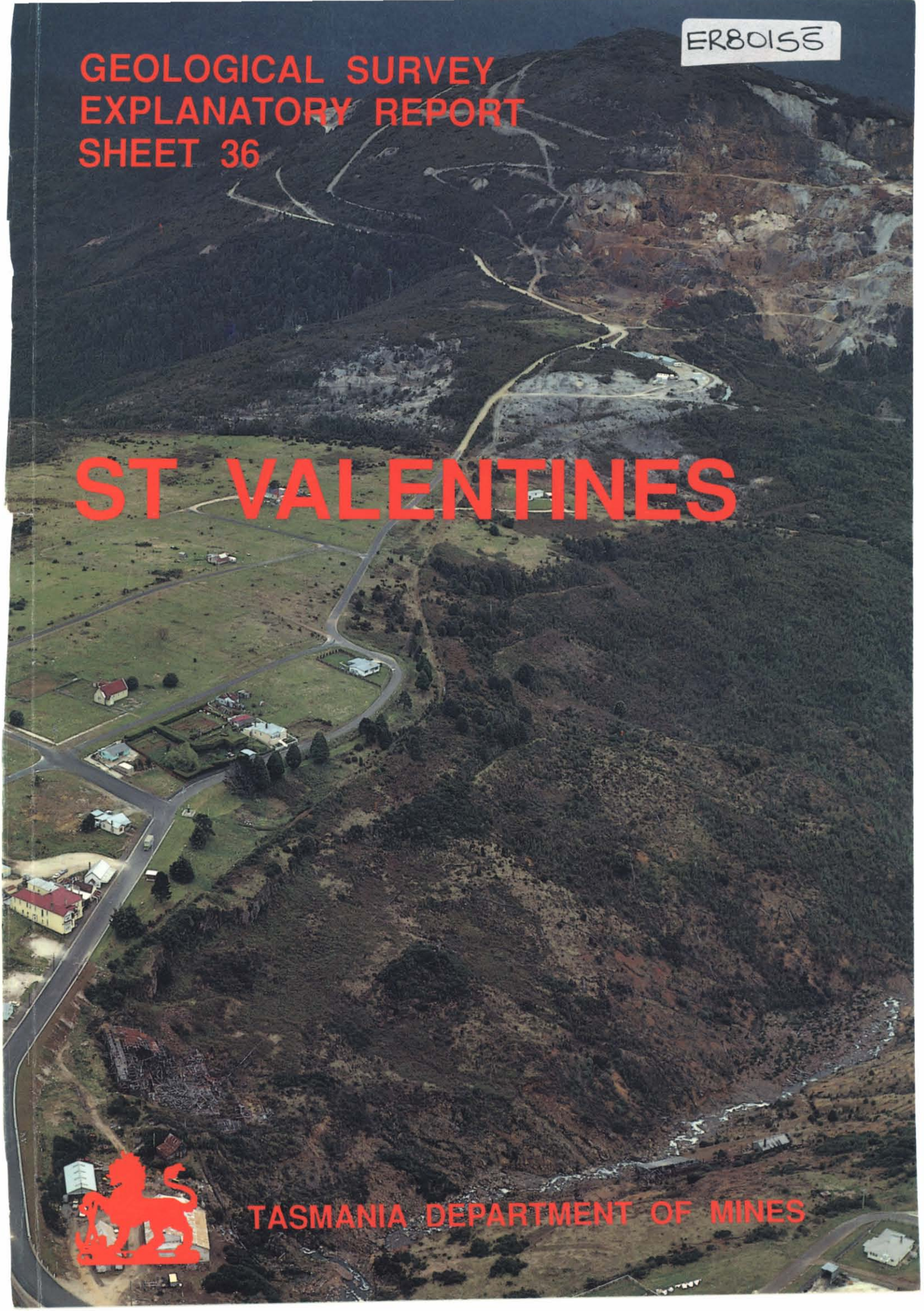

ST VALENTINES

TASMANIA DEPARTMENT OF MINES

1989

TASMANIA DEPARTMENT OF MINES

GEOLOGICAL SURVEY EXPLANATORY REPORT

GEOLOGICAL ATLAS 1:50 000 SERIES SHEET 36 (8015N)

ST VALENTINES

compiled by D. B. SEYMOUR, B.Sc. (Hons), Ph.D.

with contributions by P. W. BAILLIE, B.Sc., M.Sc. (Hons), P. R. WILLIAMS, B.Sc. (Hons), Ph.D., D. B. SEYMOUR, B.Sc. (Hons), Ph.D., P. G. LENNOX, B. Sc. (Hons), Ph.D., A. V. BROWN, B.Sc. (Hons), Ph.D., J. L. EVERARD, B.Sc. (Hons), G. R. GREEN, B.Sc. (Hons), Ph.D.

and appendices by N. J. TURNER, B. Sc. (Hons); P. W. BAILLIE, B.Sc., M.Sc. (Hons) and J. B. JAGO, B.Sc. (Hons), Ph.D.; J. L. EVERARD, B.Sc. (Hons); A. V. BROWN, B.Sc. (Hons) , Ph.D. and P. R. WILLIAMS, B.Sc. (Hons), Ph.D.

DEPARTMENT OF MINES, GPO BOX 56, ROSNY PARK, TASMANIA 7018

ISBN 0 7246 2003 6

SEYMOUR, D. B. (comp.) 1989. Geological atlas 1:50 000 series. Sheet 36 (8015N). St Valentines. *Explan. Rep. geol. Surv. Tasm.*

ISBN 0 7246 2003 6

TECHNICAL EDITOR: E. L. Martin

TEXT INPUT: Claire Humphries

LINE ART / CAD: A. Hollick, J. S. Ladaniwskyj, R. M. Turvey

PHOTOGRAPHS: R. S. Bottrill, J. L. Everard, E. L. Martin, D. B. Seymour

CONTENTS

LIST OF PLATES

LIST OF FIGURES

LIST OF TABLES

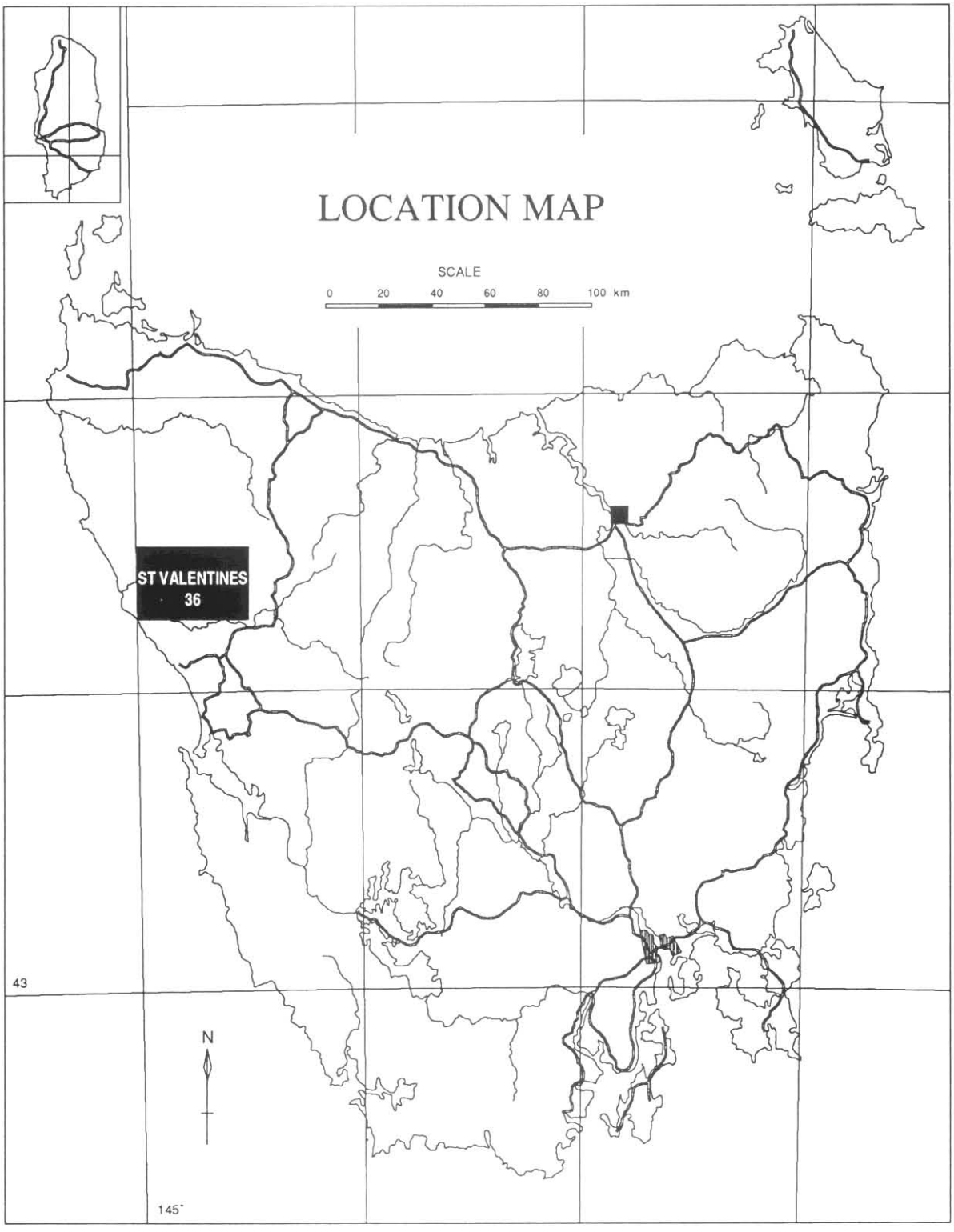

Figure 1. Location map

5 cm

INTRODUCTION

The St Valentines Quadrangle lies to the south of the Burnie Quadrangle and to the north of the Mackintosh Quadrangle in the north-west of Tasmania. It lies between latitudes 41°15′S and 41°30′S and between longitudes 145°30′E and 146°00′E (fig. 1), and has a land area of approximately 1160 km^2.

Over much of the region covered by the Quadrangle, generally subdued topography has developed on an extensive undisturbed cover of Tertiary basalt, into which the Hellyer River is deeply incised. The remainder of the region, underlain by Precambrian and Palaeozoic rocks, is more rugged. In the west, deeply dissected and heavily vegetated country in the Arthur River catchment is developed on Proterozoic, ?Eocambrian-?Early Cambrian and Carboniferous-Permian rocks. The highest country occurs in the south-east, where generally open alpine or sub-alpine vegetation has developed on ridges of ?Late Cambrian-Early Ordovician siliceous sedimentary rocks. The highest point (Black Bluff, 1339 m, DQ125104) occurs here, where the drainage generally forms part of the Leven River catchment. The Quadrangle takes its name from the second highest point, St Valentines Peak (1106 m, CQ958208), composed of ?Late Cambrian-Early Ordovician conglomerate, near the centre of the Quadrangle.

Forestry is the most significant land use in the region although mining and agriculture are also important.

The mining town of Waratah, which once served the Mt Bischoff tin-mining field (Groves *et al.*, 1972), is the largest permanent settlement in th region. Smaller settlements are the railway service centres of Guildford and Hampshire, and rural settlements in the Leven River valley at Heka and south of the Loongana Range near the eastern boundary of the Quadrangle.

In part due to forestry operations, access is good over most of the Quadrangle. Mapping was carried out using contoured base maps at a scale of 1:20 000. Most of the fieldwork was carried out by five geologists in summer field seasons between 1976-1977 and 1978-1979, from Waratah and local base camps, some of which in the less accessible south-eastern part of the region were walked in. The work of D. B. Seymour in the south-eastern part of the quadrangle formed part of a Ph.D. study at the University of Tasmania. This report was compiled by D. B. Seymour using the data of, and unpublished reports written by, P. W. Baillie, P. R. Williams, P. G. Lennox, A. V. Brown, J. L. Everard, G. R. Green, and the Ph.D. thesis of Seymour (1980). The individual geologists responsible for the information given are acknowledged where appropriate. The work was supervised by Dr Emyr Williams.

The Denison Subgroup and Gordon Subgroup were recently raised to Group status (Burrett *et al.*, 1984). However, to maintain consistency with the legend on the St Valentines map, the Subgroup terminology is retained in the stratigraphic nomenclature in these explanatory notes. Stereographic projections (stereoplots) of structural data are all lower-hemisphere equal-area projections, and Grid North is always used as reference for directional data. Grid references are given to the nearest 100 m in the form CQ958208. The convention for conversion to Universal Grid References is indicated on the map sheet. Registered rock sample numbers are given either in the forms 80-2, 79-15, 78-410 etc. (the first two digits indicating year of registration) or 001616, which refer to the Department of Mines collection, or in the form UTGD48378 which refer to the collection of Geology Department, University of Tasmania.

STRATIGRAPHY

Proterozoic

P. R. Williams

Precambrian rocks crop out in three areas on the western side of the St Valentines Quadrangle - around Mt Bischoff, and in the Arthur River basin, north of the Wandle River and in the north-western corner of the Quadrangle. The sequences consist of interbedded quartzite and phyllitic siltstone, the quartzite occurring in beds usually less than one metre in thickness. At Mt Bischoff and also in the Arthur River [CQ751227] beds of carbonate rich rock (dolomite) occur in the sequence.

The quartzite beds are usually fine- to medium-grained and are composed of quartz and shale fragments, densely packed, in a matrix of fine-grained quartz and opaque material in approximately equal proportions. The rock is composed of about 30% shale rock fragments which have a good disoriented cleavage. Quartz grains typically contain a ring of opaque inclusions, interpreted as the original grain boundary. This suggests that substantial quartz overgrowth has occurred, probably during diagenesis. The shape of the original grains suggests that they were moderately well rounded. The quartz commonly has undulose extinction and some shows deformation lamellae. Some samples also contain biotite and detrital muscovite. A well-defined cleavage is usually present, defined by the alignment of deformed lithic fragments (e.g. 78-376, 78-411, and samples from CQ752292). The lithology is lithic arenite, conspicuously with no feldspar component.

Siltstone beds in the Precambrian sequence are composed of angular clasts in a matrix of sericite and quartz. These rocks also contain small biotite flakes and accessory tourmaline. The siltstone invariably shows one well well-developed cleavage and one other cross-cutting cleavage direction. the micaceous and opaque material is often concentrated in discrete discontinuous seams. In the very fine-grained rocks bedding is defined by differing concentrations of micaceous material. The cleavage is very strongly developed and is the dominant feature of the rock. In some samples (e.g. from CQ751293, CQ752295 and CQ742240), the dominant cleavage is a crenulation cleavage, deforming a penetrative fabric which was initially at a low angle to bedding. The crenulation limbs are strongly enriched in opaque material. A sample from CQ752295 has abundant detrital white mica, and shows the variable development of cleavage seams parallel to the crenulation limbs, dependent on the composition of the host bed. The cleavage forms across graded layers, grading from coarse quartz silt to micaceous material. The thickness of the graded units is up to 3 mm. A sample from CQ750293 shows the effect of pressure solution on thin silty layers, which become discontinuous with removal of silica and concentration of opaque minerals and mica in cleavage seams.

In the Arthur River [CQ751227] the dolomite unit is composed of laminated units of dolosiltite with a siliceous cement and micaceous matrix. The cement is optically continuous silica and comprises about 50% of the rock. Some discrete carbonate horizons occur which are composed of 100% dolomite, but these are now discontinuous. The optical continuity of the silica cement suggests that it is diagenetic. A pyroclastic rock is interbedded with the Precambrian quartzite in the Arthur River [CQ751227]. It is composed of very angular fragments of quartz and plagioclase in a chloritic matrix, and has a well-defined cleavage. There are also abundant fragments of a homogeneous, high-relief mineral with a rusty colour and masked interference colours, and some chert fragments and opaque grains. It is an intermediate lithic crystal tuff. In the Mt Bischoff area the dolomite which hosts the ore-body has been described by Groves and

Solomon (1964), who also report chemical analyses of the unit. These authors suggested that the rock is sedimentary in origin and is concordant with the surrounding quartzite and slate.

The Proterozoic rocks are thus dominantly lithic arenite interbedded with siltstone and mudstone. Bedding thickness of the lithic arenite ranges up to one metre, but is often less than 0.5 m. Sedimentary structures preserved in the quartzite include parallel lamination, small scale cross-bedding, some sole-marks, graded bedding, and rare ripple marks. The monotonous interbedding of arenite and siltstone in association with graded bedding, parallel lamination and small scale cross-bedding, suggests that these rocks may represent the deposits of low-energy turbidity currents. The polymict nature of the rocks suggests a low-rank quartzose metamorphic provenance, deficient in feldspar. Lithologically the rocks are similar to the Oonah Formation to the south, and are probably of similar age, based on their structural history (see Structural Geology section). They are also a probable correlate of the Burnie Formation, to the north. They are the same sequence of rocks mapped as Burnie Formation in the Burnie Quadrangle (Gee, 1977), although Gee reports that the rocks on the Burnie foreshore are quartzwacke rather than lithic arenite, and usually occur in thicker beds. It is possible that the Proterozoic rocks on the St Valentines Quadrangle were deposited further from the source of generation of the turbidity currents which deposited the Burnie Formation rocks on the north coast.

?Eocambrian - ?Early Cambrian

AREAS NORTH AND SOUTH OF MT BISCHOFF

P. R. Williams

The Precambrian rocks of the Mt Bischoff area are overlain unconformably by a sequence of red pelite, feldspathic sandstone, sandstone, spilite and chert. The nature of the contact between the two sequences was established in the Don Hill area south of Mt Bischoff by Groves (1971), who argued that deposition was against an active fault. The relationship on the northern side of Mt Bischoff is apparently similar. South of Mt Bischoff the overlying rocks are well exposed in creek sections, at Don Hill, in the Waratah River and along the Magnet Tram, where they are dominantly greywacke and siltstone with occasional interbedded basic igneous rocks. Greywacke beds are up to 2 m thick. In the Waratah River [CQ771114], the greywacke sequence contains units consisting of large disoriented blocks which have been incorporated into a bedded greywacke matrix. The blocks consist of both quartzite and finely contorted siltstone and are up to 7 m in length. Quartzite blocks retain their internal bedding structure, which is parallel to the external bedding. These features suggest that the sediment pile was mobilised as a coherent slump sheet, the slump incorporating blocks of partly consolidated material as it moved downslope. The blocks of quartzite are compositionally identical to quartzite of the Mt Bischoff Precambrian sequence. In addition to this, evidence of instability of the sediment pile is suggested by bedding distortion and intraformational faulting. At CQ771114 a rotational fault plane is preserved which is interpreted as a relict slip plane of a submarine slide. The fault only affects a 10 m stratigraphic thickness and is thus inferred to be an open-cast structure. This evidence of instability of the earliest sediments overlying the Proterozoic rocks was also reported by Groves (1971), who described similar slump blocks from the Don Hill area [CQ767115]. It supports the hypothesis that the Don Hill Proterozoic rocks were being actively uplifted during deposition of the early Cambrian rocks.

North of Mt Bischoff the ?Eocambrian-?Early Cambrian rocks extend continuously from the North Valley mine workings [CQ760140] northwards to the Wandle River area [CQ760226]. Further isolated outcrops of these rocks occur as far north as CQ760286. The sequence is fairly homogeneous, consisting of interbedded basaltic pillow lavas, very fine-grained reddish brown pelitic sedimentary rocks, and greywacke beds up to 2 m thick. In addition units of chert are present, often as distinct mappable units. The proportion of the three major components is variable, and units composed dominantly of basaltic pillow lavas have been distinguished separately. This division is somewhat arbitrary, but in areas shown as dominantly pillow lava, greywacke is almost absent. Pelitic sedimentary rocks and minor chert are interbedded with the lava flows.

North of the intersection of Wandle Road and Belmont Road, graded greywacke beds, pelitic sedimentary rocks and basalt are equally abundant. Basaltic pillow lavas occur in flows up to 3 m thick, and occasional sills of basalt have chilled margins on both sides of the intrusion. Chert horizons are present at Belmont Road [CQ770182], Munday Road [CQ772215], and as isolated basement highs protruding through the basalt plateau at CQ800236 and CQ805220. The chert is a primary chemical deposit, as there is a very finely preserved bedding lamination. The chert is commonly white to pale green in colour and occurs in well-laminated beds up to 0.2 m thick. Individual beds are separated by thin mudstone horizons. Occasional chert breccia horizons consist of small angular chert fragments (~15 mm) in a chert matrix. The chert is usually surrounded by pelitic sedimentary rocks, although a few greywacke beds are present close to the Belmont Road chert horizon.

The association of basaltic pillow lava, greywacke, reddish brown argillite and chert is also present in the Luina Beds to the north-west of the St Valentines Quadrangle and the rocks described here are probably a direct continuation of that sequence. No fossils have been found in either sequence, and it is inferred that they are Eocambrian or Early Cambrian in age.

In thin section the greywacke is composed dominantly of quartz, plagioclase and minor rock fragments. The grains range in size from silt to medium sand, indicating the extremely poor sorting of the deposits. The grains are very angular. Occasional flakes of detrital muscovite occur. Rock fragments include quartzite with a well-defined mosaic texture which closely resembles metaquartzite from the Tyennan region. Shale fragments and carbonate grains are also present, as are some composite quartz-plagioclase grains. Biotite flakes, opaque mineral grains, chlorite, garnet and accessory corundum are also present. The presence of garnet and metaquartzite suggests that there was a sediment contribution from the metamorphic rocks of the Tyennan region. Sample 78-397 from CQ756110 shows similar features but contains much more abundant chlorite and a higher percentage of opaque minerals in the matrix. The feldspar component consists of both K-feldspar (perthite) and plagioclase. The plagioclase composition is consistent between samples, with a maximum extinction angle on combined Carlsbad-albite twins of 20° (andesine). Some samples show a very strong grain alignment parallel to bedding. Usually two sets of cleavage surfaces are present in addition to this, defined by spaced seams enriched in fine-grained mica and opaque minerals.

Detrital muscovite flakes are deformed by rotation into parallelism with the seam direction (e.g. 78-381, CQ755106). Typical samples of greywacke were collected from the Arthur River [CQ742240], from the Magnet Tram area (78-381, CQ757106) and from the Waratah River (78-397, CQ771110).

The fine-grained rocks in the sequence are typified by silty mudstone from the Magnet Tram (78-362, CQ759085) and fine-grained reddish pelite from Wandle Road. The silty

mudstone is composed of angular quartz grains elongate parallel to a pervasive cleavage at an angle of about 5° to bedding. In the matrix, fine-grained mica and larger detrital muscovite flakes are also aligned in this direction. Detrital tourmaline is present. The rock is finely laminated, but no secondary cleavage surfaces are apparent. At CQ759085 on the Magnet Tram, quartz veining or silicification of sediments occurs over 20 m of outcrop (e.g. 78-361).

The reddish pelitic sediments are evenly fine grained, consisting of mica flakes about 14 μm long in a rust-coloured homogeneous matrix. Abundant dispersed quartz grains occur which are less than 7 μm in diameter. They are equidimensional. In the field the rock has a hackly to conchoidal fracture, but the thin sections show a strong dimensional orientation of mica flakes, representing a well-developed cleavage. This surface is gently crenulated, but no marked mineral segregation occurs in the axial surface direction of the crenulations.

In thin section, the chert consists of laminated very fine-grained silica with well-developed spaced sigmoidal cleavage seams at an angle to the layering. The rock contains a small percentage of opaque minerals. The banding is discontinuous, and produces undulating surfaces with clear silica forming lozenges enclosed by dusty layers. Two opposed seam directions are present, suggesting that these may represent conjugate fracture surfaces. The silica in the rock tends to form optically continuous patches and no alignment of fabric elements associated with the seams is visible. This suggests that the rock deformed in a brittle manner. A typical sample is 78-366 [CQ767182].

Spherulitic quartzite crops out at some localities (e.g. CQ750151). It may form a continuous horizon. It is composed of spherulites of fine-grained quartz in a matrix of undeformed interlocking quartz crystals. The spherulites tend to be circular to hexagonal in cross section, and some have concentric rings. The outer rim is always fine grained, but the core area may be either coarse-grained quartz or fine-grained cherty material. The spherulites form a continuous framework. They are variable in size from 2 - 4 mm. The material cementing the spherulites is clear, undeformed vein quartz which forms crystals growing at right angles to the spherulite boundaries. The grain size of the crystals decreases close to the spherulite boundaries. Iron oxide forms part of the cement, and also partly replaces the interior of the spherulites. Rare cuspate remnants of fine-grained vein quartz occur in the centre of hematitic fillings, suggesting that the quartz filled small vugs incompletely filled by iron oxide. It is inferred that the rock was deposited as spherulites, and the voids were later filled by iron oxide and quartz. Silicification has altered the spherulites in some samples, but well-preserved spherulites with both quartz and iron oxide cement were present in one sample. It is probable that the rock was originally an aggregate of calcareous pisoliths which have been completely replaced by silica and iron oxide.

Basaltic extrusive rocks are the other dominant component of the sequence, north of Mt Bischoff. The rocks in areas mapped as dominantly pillow lavas are identical to the basaltic rocks occurring in more pelitic or greywacke-rich parts of the succession. The basalts form pillow lavas, as shown on the Wandle Road, where cuspate chert bodies have formed in the interstices between pillows, and discontinuous bedded lenses of mudstone occur within areas of basalt. The lenses are sometimes gently deformed. In addition basaltic lapilli tuff is present (e.g. 78-391, CQ757155). At the junction of the Wandle and Arthur Rivers, probable pyroclastic deposits are composed of very angular albite fragments, abundant chlorite and opaque mineral grains and rare basaltic fragments. In addition angular quartz fragments are present. The albite is usually untwinned, but some grains show albite twinning. The presence of quartz and the absence of igneous textures suggests that the rock is a crystal tuff. A typical sample is 78-410 [CQ752225] which has a grain size of about 0.2 mm and is a mafic rock. It has a well-defined grain alignment which represents either a compaction or flow foliation.

?CAMBRIAN SEQUENCE IN THE HELLYER RIVER AREA

P. G. Lennox
P. R. Williams

In the Hellyer River, from CQ855285 south to CQ846244 a sequence of folded and cleaved graded greywacke beds interbedded with thin mudstone and siltstone units forms an uplifted block faulted against Permian tillite to the north and west, and overlain elsewhere by Tertiary basalt or sediments. In thin section the greywacke is very similar to greywacke from the Arthur River area. The unfossiliferous nature of the sequence and lithological similarity with the ?Eocambrian-?Early Cambrian sequences to the west suggest correlation with those rocks.

In hand specimen (80-35, 80-40, 80-41) the greywacke is a poorly cleaved, greenish grey, poorly sorted clastic rock containing angular quartz grains and abundant white mica platelets. In thin section (80-21) it consists of poorly sorted 40-600 μm diameter quartz grains (80%) with straight to scalloped margins and undulose extinction, microcline feldspar up to 400 μm across (10%), ?muscovite needles (30 × 400 μm) and rare chert grains, in a sericite and quartz matrix. There are rare large, cleaved, sometimes sigmoidal muscovite grains.

The contact between the Cambrian greywacke and Tertiary basalt is exposed in two localities - the Basils Road extension into Lockwood Creek [CQ866275] and in a tributary of the Hellyer River at CQ855251. Whereas the contact at the former locality is sharp, at the latter locality an approximately 2 m thick, closed-framework quartz-pebble conglomerate

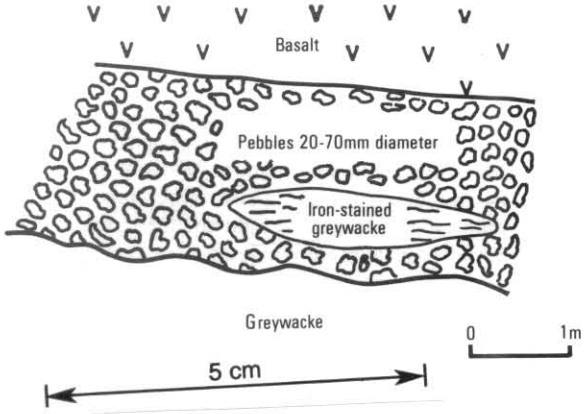

Figure 2. Contact between Tertiary basalt and ?Eocambrian-?Early Cambrian greywacke, in tributary of Hellyer River at CQ855251. (P.G.L.).

containing occasional blocks of greywacke occurs between the basalt and the greywacke (fig. 2).

Middle Cambrian

WINTER BROOK AREA

D. B. Seymour

The pre-Denison Subgroup rocks in the Winter Brook area appear to have relatively simple structure, with bedding generally dipping steeply south-eastward to southward, and consistently southward stratigraphic younging (the latter based on evidence at only a small number of localities however). This lead Seymour (1980) to suggest the following

partial composite stratigraphic section, based on a section line which straddles the boundary between St Valentines and Sheffield Quadrangles:

TOP of partial composite section (near DQ181090 on Devonport Mine track)

Unit		*(m)*
6	Altered intermediate lava (?andesite)	800+
5	Mostly thin-bedded siltstone with some thin units of ashflow tuff	250
	(Interval covered by Tertiary basalt and other superficial deposits)	1100
4	Acid agglomerate and/or volcaniclastic conglomerate, crystal-lithic lapilli tuff and volcanic wacke	650
3	Thinly interbedded siltstone and?intermediate lithic-crystal airfall tuff	350
2	Acid crystal-vitric ashflow tuff (some welded)	700
1	Thinly interbedded siltstone, sandstone and crystal-vitric tuff, large rhyolite masses (?domes or intrusions) at DQ181132 and DQ187136	250
	Total	4100

BASE of partial composite section (at DQ163128 in Winter Brook)

The stratigraphy is discussed in greater detail in Weste (1978). Most of the rocks are strongly altered to mineralogies of quartz + albite + sericite ± chlorite ± carbonate ± iron oxides, the term sericite meaning very fine-grained pale-coloured phyllosilicate minerals. The alteration is most noticeably developed in the ashflow tuffs, the lithic-crystal tuffs of Unit 3, the coarse fragmental rocks of unit 4, and the ?andesites of unit 6. In many cases the alteration products appear to have been deformed or recrystallised during Devonian cleavage development and therefore pre-dated it.

The nature of original lithologies is in some cases obscured by the alteration, as exemplified by a quartz porphyry from DQ132115, 1.3 km north-east of the summit of Black Bluff (plate 1). As is commonly the case in the volcanic rocks in this area, the quartz phenocrysts, although embayed, are little affected by the alteration and many still have the equant shape due to the bipyramidal habit inherited from the high-temperature β form. The light-coloured irregular blebs in the rock (see plate 1) are composed almost entirely of very fine-grained pale-coloured phyllosilicates (sericite), while the matrix appears to consist of very fine-grained quartz, ?feldspar and sericite. The blebs could represent either completely altered feldspar phenocrysts (in which case the original rock was a quartz-feldspar porphyry) or sericitised devitrified glass shards, which would make the original rock a crystal-vitric tuff. The ?subhedral outline shape of some of the blebs favours the first interpretation, but many are also irregular and cuspate. Crystal shapes may have become distorted due to volume change associated with the alteration.

Plate 2 shows a lithic-crystal tuff from Unit 3, thinly interbedded with laminated siltstones in a quarry at DQ187129 east of St Valentines Quadrangle boundary. This lithology probably represents a ?reworked airfall tuff. Crystal clasts are dominantly feldspar, with subordinate quartz. The lithic fragments include both volcanic lithologies and foliated metamorphic rocks. Furthermore, if it is assumed that all of the fragments in this deposit were volcanic ejecta, the metamorphic clasts imply the presence of Precambrian basement below this area at the time of volcanism. Most of the obvious alteration of this rock is confined to the matrix and is dominantly chloritic. Iron oxide grains are common and seem to be associated with the chloritic alteration. The feldspars have a less altered appearance but are turbid and are all of albite composition. Unless considerable Fe and Mg have been introduced it seems likely that the original bulk composition of this rock was intermediate.

Despite the alteration, textures in some cases indicate probable ashflow origin of some of the tuffs. Plate 3 shows a sample of one of the tuff units constituting a minor part of Unit 5, from DQ193103 on the Devonport Mine track. The discontinuous elongate light-coloured areas now mainly consist of fine-grained anhedral quartz and feldspar, and alternate with the darker matrix (which has a dominantly sericitic alteration) to produce a crude fine layering in the rock. Heavily embayed quartz phenocrysts and occasional heavily altered (sericitised) feldspar phenocrysts are present and the layering tends to wrap around them. As well as the 'primary' embayment of the quartz phenocrysts, some initial dissolution of them and later optically continuous overgrowth of quartz on them appears to have occurred during the (probably hydrothermal) alteration. The crude layering is probably partly a result of diagenetic compactional flattening of original fragments of pumice or vesicular lava, but its appearance has probably also been enhanced by tectonic flattening associated with the development of cleavage, the trace of which is sub-parallel to the trace of the layering in the section shown. The main microtextural effect of the tectonic deformation is a preferred orientation of very fine-grained phyllosilicates in the matrix. Examination of the fine structure of the matrix favours the conclusion that the mechanism responsible for the development of the tectonic fabric was dominantly recrystallisation rather than re-orientation of existing grains.

The original porphyritic texture of the altered andesites of Unit 6 is still discernible in most samples (e.g. sample UTGD48375) and relict flow-banding is visible at outcrop scale at some localities (e.g. DQ180094, sample UTGD48378). The fine-grained groundmass has a patchy chloritic alteration, and all of the phenocrysts except for large embayed quartz euhedra have been almost completely altered. The feldspars are now composed of assemblages of fine-grained pale phyllosilicates and ?carbonate minerals, while rarer, darker phenocrysts with crystal outlines similar to hornblende have a fine-grained chloritic alteration. Iron oxide grains are scattered throughout the rock, and appear to be at least partly a by-product of the alteration of the ferromagnesian phenocrysts.

No biostratigraphic information has so far been obtained from the sedimentary rocks within the Winter Brook sequence.

MOUNT TOR - TWO HUMMOCKS AREA

D. B. Seymour
P. W. Baillie

The pre-Denison Subgroup rocks in this part of the Quadrangle outcrop in four disconnected areas separated by Tertiary basalt cover. Several distinct types of felsic volcanic rocks are present, with interbedded sedimentary rocks, but none have been mapped out on a regional scale. To date no fossils have been found in any of the sequences. P.W. Baillie gives the following petrographic descriptions of some of the main lithologies present.

Several varieties of vitric tuff have been recognised. Coarse-grained types (e.g. from DQ058108, DQ016055, DQ007144) contain collapsed pumice fragments several millimetres in length, together with crystals of feldspar and (minor) quartz, in a matrix originally composed largely of glass shards. Less coarse-grained varieties (e.g. from DQ044133, DQ051133, DQ009140) consist almost entirely of a mass of relict glass shards up to 2 mm in length. Very fine-grained varieties (e.g. from DQ032087, DQ027088,

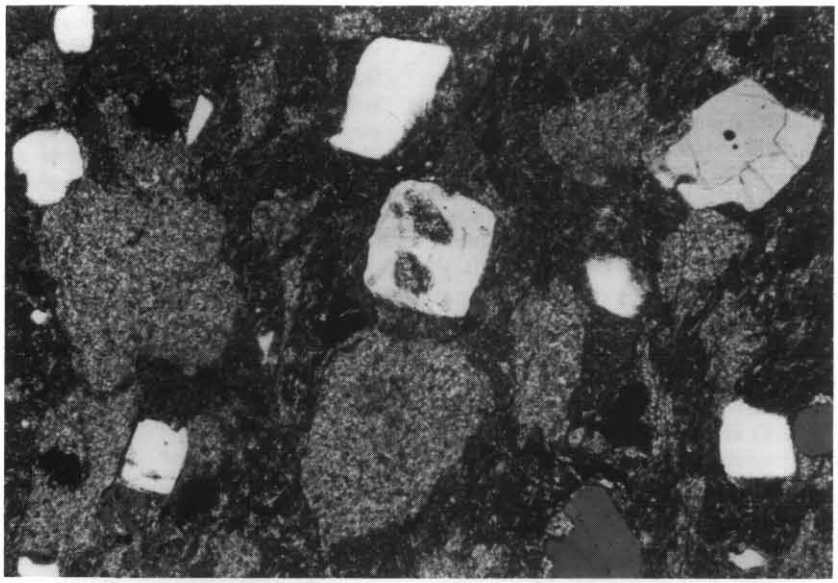

Plate 1. Altered quartz-feldspar porphyry or ?crystal-vitric tuff from pre-Denison Subgroup sequence, DQ132115, Winter Brook area. Sample UTGD48398. Crossed polars.

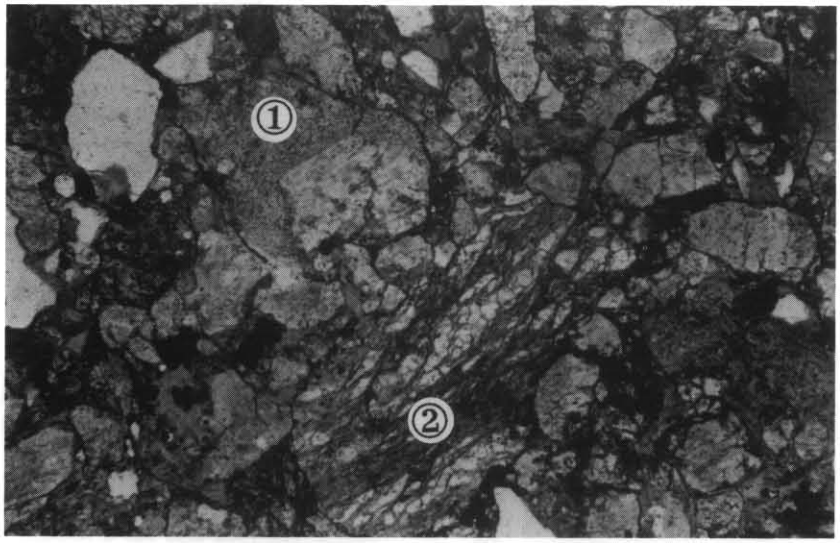

Plate 2. ?Reworked, airfall lithic-crystal tuff from pre-Denison Subgroup sequence, DQ187219, Winter Brook area. Lithic fragments include: ① feldspar porphyry and ② quartz-mica schist. Sample UTGD48372. Plane polarised light.

Plate 3. Altered, crudely-layered ?ashflow tuff from pre-Denison Subgroup sequence, DQ193103, Winter Brook area. Sample UTGD48383. Plane polarised light.

DQ027107, DQ023110, DQ008140) consist of shards and volcanic ash.

Another major pyroclastic lithology is vitric-crystal tuff, containing crystals of feldspar and (minor) quartz in a matrix consisting largely of glass shards (e.g. from DQ045102, DQ014053, DQ014051).

Lavas are apparently uncommon, but two types have been recognised. The first, sampled from the southern-most outcrop area (e.g. from DQ017060, DQ017056) is a feldspar-phyric rock with a groundmass displaying a prominent spherulitic texture. Altered phenocrysts were probably originally ferromagnesian minerals, perhaps hornblende. Blebs of mosaic quartz present are probably secondary. The other lava type is represented by a single sample (from DQ050098) and consists of phenocrysts of feldspar in an igneous groundmass.

Epiclastic sedimentary rocks range from tuffs which have undergone only a little reworking (e.g. samples from DQ061108, DQ040118, DQ016087) to lithic wackes showing features consistent with deposition by turbidity currents (e.g. from DQ038113). Laminated mudstones in the sequence may contain significant proportions of reworked volcanic ash.

The following partial composite section (Seymour, 1980) covers most of the exposed stratigraphy in the largest of the four outcrop areas, and is based on a section line perpendicular to the local strike of bedding, from DQ044122 near the Leven River bridge to DQ064108 some 2.5 km to the south-east. Lithological descriptions are modified after those given by Seymour (1980) and the section line is almost coincident with part of Section C-D on the St Valentines map:

TOP of partial composite section

Unit		*(m)*
5	Thinly interbedded laminated blue-grey siltstone, massive lithic wacke, and coarse lithic conglomerate or agglomerate. Minor lithic-crystal tuff	250+
4	Altered thin-bedded green vitric-crystal tuff (quartz-feldspar bearing). Some probable ashflows. Chloritic alteration	700
3	Interbedded massive very fine-grained blue-grey siliceous sedimentary rock (?fine airfall tuff) and thinly bedded laminated blue-grey siltstone	400
2	Intermediate ?intrusive (chloritic alteration)	400
1	Thinly interbedded light green laminated siltstone and altered crystal-vitric tuff (feldspar bearing) with chloritic alteration. Minor massive very fine-grained grey siliceous sedimentary rock (?fine airfall tuff)	200+
	Total	1 950

BASE of partial composite section

The identification of Unit 2 as an intermediate intrusive is taken from the report of Rogers (1976), which includes a description identifying the rock as a fine-medium grained pyroxene microdiorite. The unit was shown as a basic ?volcanic rock in Seymour (1980), but this was based only on field identification of the lithology. Rogers (1976) also appears to consider most of Unit 5 to belong to the Denison Subgroup correlate rather than to the underlying sequence (see also Structural Geology section herein).

There appears to be some indication of cyclicity in the volcanism, both on a large scale with units dominated by fine-grained sedimentary rocks interspersed with the volcanic-dominated units, and also on a finer scale, for example within Units 1 and 4 which in part display thin alternations of laminated siltstone and crystal-vitric tuff. Many of the fine-grained rocks may contain a considerable contribution of very fine ashfall material, particularly the massive siliceous lithologies in Units 1 and 3.

Another short partial section was observed by Seymour (1980) in limited exposures in quarries near DQ009142 on Black Marsh Road south-east of Two Hummocks. The sequence here has moderate to steep dips to the ENE and is right-way up:

TOP of partial section

Unit		*(m)*
	Coarse siliceous conglomerate (basal unit of Denison Subgroup correlate)	
	(?Unconformity)	
4	Thinly interbedded siltstone and well-laminated dark grey shale	20+
3	Thinly interbedded light green claystone and shale	52
2	Light green crystal-vitric tuff (ash-flow) with bedding foliation, eutaxitic texture and well-preserved devitrified glass shards. Chloritic alteration	48
1	Thinly interbedded light green siltstone and shale	54
	Total	174

BASE of partial section

Pike (1964, pp. 27-28) reported an altered ?rhyolitic lava cropping out on Black Marsh Road south of the quarries, and apparently underlying unit 1 above. The tuff of Unit 2 contains very delicately preserved devitrified glass shards (plate 4), now composed of mosaics of fine-grained anhedral quartz. The rock also has a foliation which is parallel to bedding in the sedimentary rocks above and below Unit 2. The foliation is defined by discontinuous elongate chloritic layers, one of which can be seen in Plate 4, and which probably represent a eutaxitic texture produced by compaction of an ashflow tuff deposit. Parts of Unit 1 contain what appear to be accretionary lapilli composed of fine-grained material and up to 40-50 mm diameter, and both this unit and Unit 3 may include a significant contribution from very fine ashfall material.

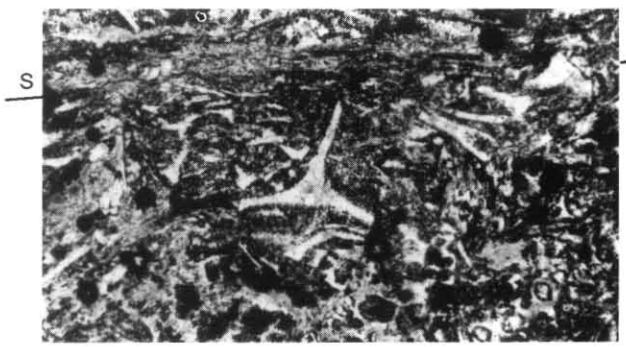

Plate 4. Altered?ashflow tuff from pre-Denison Subgroup sequence, DQ008143 near Two Hummocks. Note the delicately preserved glass shards. S is layering, which is parallel to bedding in enclosing rocks. Sample UTGD48414. Plane polarised light.

ST VALENTINES PEAK AREA

P. G. Lennox

The two best exposures of the pre-Denison Subgroup sequence in this area outcrop on roads un-named on the Hellyer 1:100 000 topographic map. The road off Guildford Road which ascends Companion Hill is herein called PMG Road, while the roughly east-trending road on the northern flanks of St Valentines Peak is herein called Black Pit Road, in line with previous practice.

A folded dominantly non-volcanic clastic sequence is exposed in the valley between Companion Hill and St Valentines Peak. Jago *et al.* (1975) have outlined the Cambrian stratigraphy, and although there is broad agreement herein as to the sequence of lithologies, there is disagreement as to their thickness (see table 1). The Cambrian sequence is folded into an anticline trending almost N-S with the oldest unit exposed in the core.

Table 1
COMPARATIVE THICKNESSES, PRE-DENISON SUBGROUP SEQUENCE, ST VALENTINES PEAK AREA.
(Calculated values are based on generalised dip and strike of strata and assume no repetition by folding.
(P. G. Lennox)

	Thickness (m)					
	Jago *et al.* (1975)		P. G. Lennox			
	PMG Road Companion Hill	Black Pit Road St Valentines Peak	PMG Road		Black Pit Road	
			Calculated	Measured	Calculated	Measured
TOP						
Conglomerate, meta-sandstone and metasiltstone	~18	–	30	31	47	18
Laminated and non-laminated hornfels	~375	230	430	127	<127	61
Contact metasomatic rock ("augen hornfels")	n.a.	100	n.a.	–	65	25
Meta-sandstone and meta-siltstone	n.a.	75-100	n.a.	–	–	–
Welded tuff	n.a.	100	n.a.	–	–	50
Cherty pyritic meta-siltstone and meta-sandstone	n.a.	>100	n.a.	–	70	90

The oldest unit is exposed in two quarries; one on Black Pit Road [CQ952228] and the other off Guildford Road near its junction with 29 Mile Road [CQ944209]. In both areas it consists of massive, cherty, pyritic meta-siltstone and meta-sandstone with persistent faint laminations defining the bedding. In thin section (80-24) it exhibits a cherty groundmass containing abundant scattered darkly translucent, reddish brown iron oxides and hydroxides, and opaque minerals 0.05 mm in diameter.

Sample 80-12 is a pyritic black chert with 20-30 mm thick layering. In thin section the square 3 mm diameter ?pyrite crystals display skeletal growth of acicular ?hornblende crystals and are rimmed with smaller intergrown pyroxene crystals. Intergrown scapolite and pyroxene (?diopside) crystals which occur in this sample indicate the regional metamorphism which has resulted from proximity to a granite body. This unit of pyritic meta-siltstone and meta-sandstone is 90 m thick and is overlain by welded tuff. The contact is not exposed.

The welded tuff outcrops in a quarry adjacent to Guildford Road 0.5 km south of the Black Pit Road intersection [CQ947220], and also in a small quarry 300 m east of the Guildford Road - 29 Mile Road junction [CQ948213]. In hand specimen (80-25) it consists of a pale grey silty matrix enclosing angular to well-rounded, cream to dark grey bodies commonly 1-2 mm across (rarely up to 5 mm across) forming 20-30% of the rock. In thin section the bodies consist of coarse- to fine-grained chert and sericite. Jago *et al.* (1975) considered this unit to be about 100 m thick, although only a 50 m section outcrops in the quarry.

According to Jago *et al.* (1975) the welded tuff is overlain by about 75 to 100 m of poorly exposed meta-sandstone and meta-siltstone. Unfortunately quarrying and regrowth have obscured the nature of the unit overlying the welded tuff. There is a single outcrop of spotted hornfels on Black Pit Road (80-10, CQ953224).

The green and white striped hornfels overlying the welded tuff was considered by Jago *et al.* to be 100 m thick. Assuming an average dip, no folding and consistent strike of bedding the 'augen-hornfels' was calculated to be about 65 m thick. Only 25 m of section was measured at its outcrop on Black Pit Road [CQ954222]. In thin section the rounded green ovoids consist of skeletal black hematite, altered intergrown amphiboles (?tremolite), epidote minerals, diopside and scapolite. The creamy-white ground-mass in thin section consists of translucent, brown, fine-grained granular ?dolomite (80-11).

The overlying unit of laminated and non-laminated, slightly pyritic, pale grey hornfels crops out on both Black Pit Road [CQ956223] and PMG Road [CQ941230]. Jago *et al.* (1975) estimate it is about 375 m thick on the western limb, while it was measured at about 130 m and calculated as 430 m. On the eastern limb Jago *et al.* (1975) estimate the thickness as about 230 m, and it was calculated to be about 217 m. Only 61 m was measured in the field. In thin section the hornfels (80-34) is a translucent grey, extremely fine-grained chert with rarely visible quartz grains. Characteristically the hornfels weathers to a buff-coloured mudstone, occasionally with a spheroidal weathering pattern (PMG Road, 60 m downhill of the conglomerate/mudstone contact).

The nature of the contact between the Cambrian sequence and the overlying basal conglomerate of the Denison Subgroup correlate was examined in some detail. The contacts in the 'Brambles' quarry on Black Pit Road [CQ958224] and in a cutting on PMG Road, Companion Hill [CQ939228] are easily accessible. The contact on Black Pit Road is exposed over 40 m of quarry cliff, and the bedding attitudes in the conglomerate and in the underlying meta-siltstone and meta-sandstone are almost parallel. Where the contact is not part of a fault it appears to be erosional with 0.4-0.69 m deep troughs cut into the underlying sequence (fig. 3). The contact

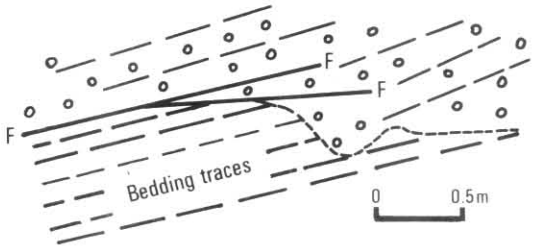

Figure 3. Contact between basal conglomerate of the Denison Subgroup and underlying Cambrian metasiltstone, Black Pit Road. Bedding either side of the contact appears parallel. (P.G.L.)

on PMG Road, Companion Hill is only exposed over 2-3 m, and although sharp is not completely planar. As in the Black Pit Road outcrop, bedding attitudes either side of the contact on PMG Road are not markedly different. Thus the base of the Denison Subgroup correlate in this area appears to be an erosional unconformity and not a paraconformity (*cf.* Jago, 1973).

The sequence underlying the contact consists of interbedded meta-siltstone and meta-sandstone with up to 0.5 m thick horizons or lenses of breccia, grit and pebble conglomerate (fig. 4*a, b*). In the quarry on Black Pit Road these horizons are from 5 mm to 0.8 m thick, range from grit to pebble conglomerate, and occur between 4-10 m below the contact. In contrast the 7 mm to 0.45 m thick lenses on PMG Road are breccias or microbreccias and occur 3-5 m below the contact. Jago *et al.* (1975) consider this upper Cambrian unit of meta-sandstone and meta-siltstone to be about 18 m thick on PMG Road. It was measured as being 30 m thick. On Black Pit Road it was calculated to be about 47 m thick, whilst only 18 m was measured.

NATIVE TRACK TIER AND ADJACENT AREAS

P. W. Baillie

Cambrian rocks considered to be in part correlates of the Mount Read Volcanics crop out extensively in the north-eastern part of the Quadrangle, from the Native Track Tier area [*c.* DQ100200] to Milligan Creek in the north-east corner [DQ160327].

In the *Milligan Creek area* the sequence consists of interbedded siltstone, lithic wacke and conglomerate containing angular granules of quartz and sedimentary rock fragments in a ferruginous sandy matrix. In thin section (78-10) the quartz clasts are seen to comprise metamorphic and vein quartz, suggesting origin from a Precambrian terrain. The lithic wacke beds are often graded and occur in beds less than 50 mm in thickness. Detailed petrography is rendered difficult by thermal metamorphism caused by nearby Devonian granite.

Cambrian fossils were found in float composed of siltstone and very fine sandstone at DQ160311. Conglomerate similar to that which occurs near Milligan Creek is also present in this area, and is also seen in thin section (78-22) to consist of quartzose clasts derived from a metamorphic terrain and sedimentary rock fragments. The fossils are essentially the same as those described by Jago (1976) from the Radfords Creek Group in the Sugarloaf Gorge and are of late Middle Cambrian age of *Lejopyge laevigata* II Zone or *L. laevigata* III Zone. It is noteworthy that this locality is only about 60 m from outcropping siliceous conglomerate, a correlate of the Denison Subgroup.

In a quarry on the South Riana Road, some 5 km south of South Riana [DQ143295] the contact between the Denison Subgroup correlate and the underlying volcanic rocks is exposed. The volcanic rocks are felsic vitric tuffs, with a prominent flattening of glass shards sub-parallel to bedding in the overlying conglomerate. In thin section (78-30 to 78-32) the volcanic rocks are seen to be strongly altered to quartz-mica-carbonate mineralogies, and to have originally been composed largely of glassy material, ?lithic fragments and biotite. The rocks probably originated from ash flows.

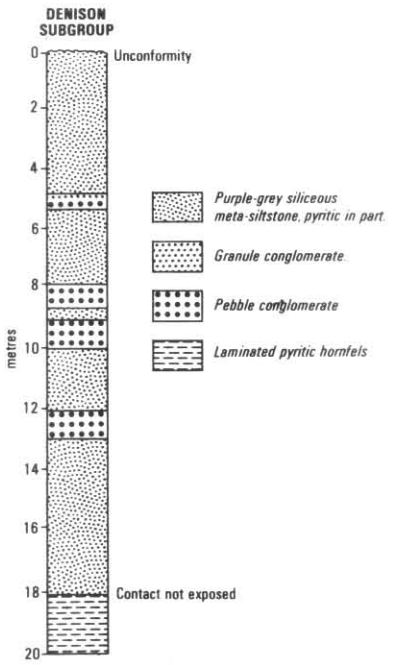

Figure 4a. Stratigraphic section of exposed units below Denison Subgroup correlate, Brambles quarry, Black Pit Road, St Valentines Peak area. (P.G.L.)

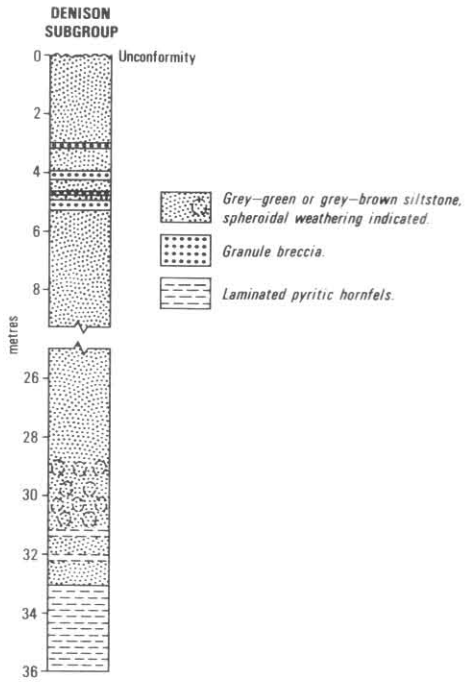

Figure 4b. Stratigraphic section of exposed units below Denison Subgroup correlate, PMG Road, Companion Hill, St Valentines Peak area. (P.G.L.)

The sequence in the *Loyetea Peak area* [DQ124254] consists only of sedimentary rocks. In thin section (e.g. 78-90) the sandstones are seen to be quartzose lithic wackes comprising sub-angular clasts of metamorphic and plutonic quartz, vein quartz, metaquartzite and mica, together with sedimentary rock fragments including siltstone and chert, and rare felsic volcanic clasts, in a clayey matrix.

A significant area of Cambrian rocks is exposed in the *Native TrackTier area,* in the core of a major anticline trending E-W. The rocks crop out from the Leven river [DQ161220] on the eastern edge of the Quadrangle, through Native Track Tier [DQ110210], to the Mt Everett area [DQ065210]. Contiguous rocks on the Sheffield Quadrangle were mapped as Gog Range Greywacke (Jennings *et al.*, 1959), which is a mixed sequence of 'greywacke' and felsic volcanic rocks of probable Late Cambrian age (Jennings, 1979).

Two broad associations can be recognised in the Native Track Tier area and are separated by a postulated major fault in the vicinity of Laurel Creek [DQ093235]. Volcanic rocks are a major component of the rocks east of Laurel Creek, but are very rare to the west of the postulated fault.

The section exposed in the Leven River [DQ158230 to DQ164207] consists dominantly of tuffs with lesser epiclastic sedimentary rocks, agglomerate, lavas and ?intrusive rocks. Several types of tuff are present. The most common type (e.g. 78-754, 78-757) is a fragmental rock containing clasts ranging from fine ash to about 10 mm, and comprising lithic volcanic fragments, felted sericite masses that were probably originally vitric clasts, and altered crystals of feldspar. The matrix appears to be largely composed of altered vitric material.

Vitric ash deposits are also present (e.g. 78-751, 78-758). 78-758 consists of devitrified glass shards 0.5-1.0 mm in length in a matrix of glass shards within which Y-shaped fiamme and shards with remnant vesicles can be distinguished. This rock also preserves traces of original bedding.

Sample 78-759 shows strong flow-banding on a scale of 1-8 mm and is feldspar-phyric, containing phenocrysts less than 3 mm in length. Apatite is common in the rock, which was probably a lava. Sample 78-756 is also feldspar-phyric but does not exhibit flow-banding. Incipient snowflake texture is present in the rock, which may be an intrusive.

A very mixed sequence is present in the central part of the Native Track Tier area, comprising both volcanic and sedimentary rocks. The contact between the volcano-sedimentary sequence and the overlying siliciclastic rocks (Denison Subgroup correlate) is exposed at several localities in the area, including a quarry on the Native Track Tier Road [DQ086220] and also at several localities on the prominent line of hills which define the northern limb of the major anticline in the area (e.g. DQ107223, DQ128235). The contacts are either erosional or apparently conformable. A new fossil locality was found which indicates that the volcano-sedimentary sequence is in part of late Middle Cambrian age in either the *Lejopyge laevigata* III Zone or the *Damesella torosa - Ascionepea janitrix* Zone (Baillie and Jago, 1985). This, together with the nature of the contact with overlying Denison Subgroup correlates suggests that the volcano-sedimentary sequence is a correlate of the Tyndall Group of western Tasmania (Corbett, 1981). This has important economic ramifications in that in western Tasmania, with the possible exception of the Lake Dora area, the Tyndall Group is unmineralised (Corbett, 1981).

In this tract of country volcanic rocks consist of pyroclastic, extrusive, and epiclastic varieties. The most common type of tuff found is a crystal lithic tuff (e.g. 78-734, 78-805, 78-807, 78-745) containing crystal clasts up to 5 mm in diameter of feldspar and minor quartz, together with volcanic rock fragments (mainly felsic), and occasional metamorphic rock fragments (including rodded quartz). Sample 78-731 is chloritised and contains clasts including altered feldspar crystals, minor quartz crystals, lithic fragments (mainly felsic volcanic rocks) and devitrified glass fiamme, in a volcanic matrix containing abundant devitrified shards. The rock is an altered crystal lithic vitric tuff.

Andesitic ?extrusive rocks have been recognised in the area (e.g. 78-735, 78-769, 78-742, 78-744, 78-746), but cannot be mapped out on a regional scale. In thin section the rocks may be vesicular (e.g. 78-742) and contain altered phenocrysts of feldspar in an altered, often spherulitic matrix containing oriented feldspar laths and some quartz.

Fine-grained ash tuffs are also present (e.g. 78-737) and are usually so altered as to make recognition of original character extremely difficult.

Sedimentary rocks include laminated mudstone, greywacke and conglomerate.

As noted earlier the sequence is somewhat different to the west of Laurel Creek [DQ070220], where volcanic rocks form only a minor part of the sequence. In this area there appears to be a change from dominantly lithic wacke in lower parts of the section to quartz sandstone in the upper parts of the section.

The lithic wackes (e.g. 78-782, 78-797) are very poorly sorted and occur in beds less than 200 mm in thickness. The beds are usually graded and sometimes have laminae developed in the upper portion of the bed. In thin section they are seen to have originated from a dual provenance, containing both volcanic and metamorphic rock fragments. The volcanic fragments consist of chloritised fine-grained volcanic rocks, felsic volcanics and some volcanic quartz; the metamorphic rock fragments include metaquartzite, metamorphic quartz, metachert and vein quartz which may also show evidence of strain. These rocks are interbedded with commonly laminated siltstone (e.g. 78-783) and occasional beds of more siliceous sandstone.

In the upper parts of the sequence well-sorted quartz sandstone becomes dominant (e.g. at DQ053205). Beds are generally massive and 100-250 mm in thickness. The sandstone is interbedded with laminated siltstone. Indeterminate brachiopods and polymerid trilobites were the only fossils found in this sequence.

Denison Subgroup Correlates

BLACK BLUFF RANGE AREA

D. B. Seymour

The basal contact of the Denison Subgroup correlate in the Black Bluff Range area is an inferred angular unconformity in some places, and an inferred or observed erosional surface with approximate conformity in bedding attitudes above and below the contact in other places. This contrasts with the situation in the Native Track Tier and St Valentines Peak areas, where no significant angular unconformities have been observed or inferred (P.W.B. and P.G.L.).

The available structural evidence suggests that the Denison Subgroup correlate rests with high-angle angular unconformity on the underlying volcano-sedimentary sequence in all parts of the Winter Brook area and the small inlier around DQ150080 south-west of Tiger Plain (see Section E-F on the St Valentines map, and Structural Geology section herein). At a more detailed level, such a relationship can be strongly inferred over short distances on the ground at several localities. Thus, on the banks of a creek at DQ166087 east of Tiger Plain the exact contact between a thin sequence of fine-grained volcaniclastic sedimentary rocks and underlying altered crystal-vitric tuff is not exposed but its

position can be approached very closely (within 1-2 m) from above and below. Compositional layering in the tuff dips steeply to the south-west at 70°, while thin bedded red-brown hematitic pebbly laminated quartz siltstone immediately overlying the inferred unconformity dips to the SSE at 20°. Angular pebbles in the siltstone are composed of volcanic quartz and volcanic lithic fragments. The siltstone persists for a stratigraphic interval of some 20 m and is then abruptly but conformably overlain by thin bedded slightly hematitic quartz arenite typical of the Denison Subgroup correlate throughout the Black Bluff Range area. Further east, at DQ180091 on the track to the old Devonport mine (on Sheffield Quadrangle), flow banding in an altered intermediate lava dips to the ENE at 40°, while some 100 m further SSE and about 50 m vertically above this point, bedding in quartz arenite close to the base of the Denison Subgroup correlate dips to the south-east at about 30° The contact is not exposed but possible angular unconformity is suggested. At DQ155082 at the northern edge of the small inlier of pre-Denison Subgroup volcanic rocks south-east of Tiger Plain, thin compositional layering in altered crystal-vitric tuff dips to the SSE at 85°. Immediately overlying the tuff (i.e. within 1-2 m), thick bedded pebbly coarse quartz arenite of the Denison Subgroup correlate dips to the north-east at 22°, which again strongly suggests the presence of angular unconformity although the actual contact is not exposed.

In the western part of the Black Bluff Range area, the overall structure suggests that high-angle angular unconformities are not present, although consideration of the structural pattern within the area of pre-Denison Subgroup rocks immediately west of Mt Tor suggests a large-scale low-angle unconformity (see Structural Geology section). On a finer scale, near-parallelism of bedding attitudes in conglomerate above the contact and tuff below the contact at Two Hummocks (DQ003145, P.W.B.) suggests local structural conformity (although probably still with an erosional break). A similar relationship probably exists in the Leven River at DQ047139.

In Tor Creek, near DQ094133, interbedded quartz sandstone and siliceous conglomerate of the Denison Subgroup overlie an erosional surface developed on a strongly cleaved probable volcanic rock with very strong ferruginous alteration and relict ?vesicular texture (samples 001616, 001618). The basal part of the conglomeratic sequence contains angular boulders up to one metre in diameter of the ferruginous rock. Because of the structural position at this locality it seems unlikely that the ?volcanic rock belongs to the pre-Denison Subgroup sequence, and it is tentatively correlated with an apparently similar hematitic ?lava described by Weste (1978), from some 30 m above the base of the Denison Subgroup correlate in the Mt Jacob area [*c.* DQ210090] east of the Quadrangle boundary.

In the Black Bluff Range area, the dominantly quartzose clastic sedimentary rocks of the Denison Subgroup correlate generally do not fall naturally into a lower terrestrial conglomerate sequence and an upper marine sandstone sequence. This apparently is the case in some other parts of northern Tasmania, for example in the Fossey Mountains area (Mt Claude-Mt Roland-Gog Range) where Jennings (1958, 1963) defined the Roland Conglomerate and the Moina Sandstone, which together would now be considered to be stratigraphically equivalent to the Denison Subgroup. No attempt has therefore been made to subdivide the Denison Subgroup correlate in the Black Bluff Range area into comparable formations, although lithofacies similar to those recorded in the Roland Conglomerate and the Moina Sandstone are present. The main difference compared with the Fossey Mountains and Dial Range areas is the relative unimportance of coarse siliceous conglomerates, and the fact that where they do occur it is not always at the base of the sequence.

The geological cross-sections suggest that the Denison Subgroup correlate is considerably thicker (perhaps more than 1000 m) in much of the Black Bluff Range area than in the areas bordering Native Track Tier to the north, where for example on the Loongana Range it appears to be only about 350 m thick (compare Sections C-D and E-F on the St Valentines map). The thickness also decreases to the south, on the southern extension of the Black Bluff Range and the neighbouring Bonds Range on the Mackintosh Quadrangle, where it decreases to as little as 100 m in places (Seymour, 1980).

A number of lithofacies were recognized by Seymour (1980) within the Denison Subgroup correlate in the Black Bluff Range area:

I Polymict lithic (commonly volcaniclastic) conglomerate and wacke

II Medium- to coarse-grained hematitic siliceous conglomerate

III Lithic (commonly chert) breccia with quartz arenite matrix

IV Pebbly quartz arenite with trough and (minor) planar cross-lamination

V Pebbly quartz arenite and quartzwacke, with abundant bedding-perpendicular worm burrows

VI Thinly interbedded fine-grained quartz arenite and laminated hematitic siltstone, with bioturbation and marine trace fossils in the siltstone beds

Lithofacies I

This lithofacies tends to occur in the basal parts of the sequence. Fine-grained volcaniclastic conglomerate occurs in a few thin beds close to the base of the Denison Subgroup correlate on the south-western shore of Paddys Lake, 0.5 km east of the summit of Black Bluff [DQ131103]. This rock is hematitic and red-brown in colour. The most common clast compositions are altered quartz-feldspar porphyry and volcanic quartz, the former sub-rounded and the latter sub-angular. There is a continuous variation in grain size from the largest grains (about 10 mm in diameter) down to the matrix, which is in places visibly a result of degradation of the lithic fragments. Minor thin beds of siliceous conglomerate (Lithofacies II) occur in close association with this lithology at this locality, and the sequence passes rapidly upwards into thin bedded pebbly quartz arenite (Lithofacies IV).

Lithofacies I also includes rocks containing clasts which are not recognisably of volcanic derivation, but some of which may still have been derived from the sedimentary parts of the pre-Denison Subgroup sequence. An example is a red-brown hematitic lithic fine conglomerate (sample UTGD48403) from within 100 m of the base of the sequence at DQ169080, about one kilometre south-east of Tiger Plain. Clast compositions in decreasing order of importance in this rock are hematitic siltstone, metamorphic quartz, metaquartzite and quartz-mica schist, and volcanic quartz. Nearly all of the clasts are subangular, maximum grain size is about 10 mm and sorting is very poor. Considerable tectonic strain has been absorbed mainly by the matrix and the siltstone clasts, and so grain shapes of the latter are not original.

The short sequence of volcaniclastic pebbly siltstone occurring in the basal part of the sequence at DQ166087 east of Tiger Plain may also be considered to belong to Lithofacies I.

Lithofacies II

This lithofacies includes medium- to coarse-grained siliceous conglomerates similar to lithologies described from the

Roland Conglomerate in the Fossey Mountains area (Jennings, 1958, 1963), the basal unit of the Owen Conglomerate in the Queenstown area (Banks, 1962), and the Reeds Conglomerate in the type area of the Denison Subgroup on the Denison Range (Corbett and Banks, 1974, 1975). However, in the Black Bluff Range area such conglomerates are never thickly developed, and often do not occur right at the base of the sequence, as is commonly the case in other areas.

The presence of a thin unit of coarse siliceous conglomerate at the base of the sequence has been inferred along the southern boundary of the Winter Brook belt of pre-Denison Subgroup rocks, particularly to the east of the St Valentines Quadrangle boundary. The steep N-facing slopes here are mostly covered by talus deposits and bedrock outcrop is very poor; the presence of conglomerate is mainly inferred from its occurrence as boulders in the talus. The conglomerate unit was shown on the Tasmanian Department of Mines 1 mile series Sheffield Sheet (Jennings *et al.*, 1959) as about 100-150 m thick.

Thin units of coarse siliceous conglomerate also commonly occur some distance above the base of the Denison Subgroup correlate in the Black Bluff Range area. Where this is the case the conglomerate commonly overlies one of the finer grained lithofacies, in some places with low-angle angular unconformity. Some examples are:-

(1) At DQ112110, 1.5 km WNW of the summit of Black Bluff, a 10 m thick unit of very coarse siliceous conglomerate conformably overlies thinly interbedded hematitic fine quartz arenite and laminated siltstone with flame structures and ball and pillow structure (?Lithofacies VI). The latter are underlain by fine siliceous conglomerate, while the coarse conglomerate is overlain by thin bedded ferruginous pebbly quartz arenite with ripple marks (Lithofacies IV). The conglomerate consists of fairly well sorted sub-rounded to rounded clasts of massive metaquartzite, foliated metaquartzite and vein quartz up to 0.3 m or so in long dimension, and has a clast-supported fabric. The matrix consists of quartz arenite. Many of the clasts, particularly those composed of foliated metaquartzite, are disc-shaped. The clasts have a well developed preferred orientation parallel to bedding, with some tendency towards imbrication. The conglomerate unit includes a few thin quartz arenite layers.

(2) At DQ142091, 2 km south-east of the summit of Black Bluff, thin bedded coarse quartz arenite with ripple marks is overlain by about 10 m of medium-grained siliceous conglomerate. The contact is a low-angle (up to about 20°) angular unconformity, the arenite having the steeper dip. The base of the conglomerate at this locality is about 300 m above the base of the sequence. The conglomerate appears to grade upwards into fine conglomerate and coarse pebbly quartz arenite of Lithofacies IV.

(3) A similar situation to (2) also occurs at DQ142082, one kilometre to the south, where thin bedded pebbly quartz arenite (Lithofacies IV) is overlain by fine- to medium-grained siliceous conglomerate, again with low-angle angular unconformity.

The siliceous conglomerates occupying the lower parts of the Denison Subgroup correlate in other areas have been interpreted as the deposits of terrestrial alluvial fans by various authors. The conglomerates described above are similarly interpreted, on the basis of:

(1) their oxidised nature
(2) apparent lack of lateral continuity of individual units
(3) their bimodal fabrics (pebbles and cobbles in sand matrix)
(4) absence of silt- and clay-size material
(5) their unfossiliferous nature

It should be re-emphasised that the coarse siliceous conglomerates make up only a minor part of the Denison Subgroup correlate in most of the Black Bluff Range area. However, two of the other lithofacies, namely Lithofacies III and IV, have also been interpreted as terrestrial deposits (see later discussion), and may have also been deposited in an alluvial fan environment. Together, Lithofacies I to IV inclusive make up a major part of the sequence throughout the Black Bluff Range area.

Bull (1972) recognised the following types of deposits in alluvial fan environments:

(1) water-lain sediments
  (a) channel deposits
  (b) sheetflood deposits
  (c) sieve deposits
(2) debris-flow deposits

The coarse siliceous conglomerates in the Black Bluff Range area probably represent more than one of these types. For example, a basal conglomerate resting on volcanic rocks at DQ067038 on the southern Black Bluff Range (south of St Valentines Quadrangle) is devoid of bedding, stratification and grading, and has a bimodal fabric consisting of randomly oriented (except right at the base) large subangular to subrounded clasts of metaquartzite in an abundant poorly sorted matrix containing a significant contribution from the immediately underlying bedrock (Seymour, 1980). Under the criteria listed by Bull (1972, p.69) the final mode of emplacement of this deposit was almost certainly as a debris flow, although the metaquartzite clasts may have undergone other modes of transport in the journey from their source area. In contrast, the coarse conglomerate described from DQ112110 in example (1) above has a better sorted population of rounded large clasts with either bedding-parallel preferred orientation or slight imbrication, and forming a clast-supported fabric whose pore space is filled by quartz arenite. This deposit most probably represents channel lag material. Channel fill is probably also represented by some of the more fine grained conglomerates transitional between Lithofacies II and IV, some of which display trough cross-stratification.

Lithofacies III

This lithofacies comprises fine- to medium-grained lithic breccias with a usually hematitic sandy matrix varying from quartz arenite to quartz-lithic wacke. Most of the quartz in the matrix is of metamorphic origin. The dominant composition of the larger clasts is white, pink and brown chert, which is commonly slightly argillaceous. Less common are clasts of foliated and unfoliated metaquartzite. All of the large clasts are angular or subangular, but the chert clasts tend to be somewhat more angular than the metaquartzite clasts. The overall fabric is distinctly bimodal.

Rocks transitional between this lithofacies and fine- to medium-grained siliceous conglomerate occupy the basal 50 m or so of the sequence at Mt Tor [DQ074128]. However, the lithofacies does not only occur in the basal part of the sequence. Fine- to medium-grained siliceous conglomerate overlying the minor angular unconformity within the sequence at DQ142082 (see Lithofacies I) grades upwards into rocks characteristic of Lithofacies III. Occurrences of Lithofacies III at DQ104062 in the central part of the Black Bluff Range are high in the sequence, probably within 100-150 m of the base of the Gordon Subgroup correlate.

Rocks of Lithofacies III are commonly red-brown in colour, mainly due to the hematitic nature of the matrix. Together with the lack of fossils and common presence of trough cross-stratification, this indicates terrestrial deposition. In the alluvial fan model the lithofacies may represent deposits of braided distributary streams (sheetflood sediments of Bull, 1972, p.66). The provenance of the chert clasts, however, remains a problem.

Lithofacies IV

Pebbly medium to coarse quartz arenite is typical of this lithofacies. The pebbles are subrounded to subangular, generally up to about 7 mm in diameter, and are often concentrated at certain horizons. They constitute up to about 10% of the rock, and are composed of metaquartzite and chert, the former predominating. The remainder of the rock is a poorly to moderately sorted slightly hematitic quartz arenite consisting of mostly subangular grains of metamorphic quartz having low sphericity, in an argillaceous matrix. Blue-green tourmaline is a common accessory mineral.

In outcrop, the rock is often thick bedded, and trough cross-lamination is common. Marine fossils are apparently absent. The colour is usually light grey to mottled light grey-brown, indicating a lower degree of oxidation than is present in Lithofacies III. Texturally this lithofacies could represent a more mature, less pebbly variant of Lithofacies III, while the less oxidised nature suggests that it is more a marginal marine facies.

Lithofacies IV occurs at or very close to the base of the Denison Subgroup correlate south of St Valentines Quadrangle at DQ111032 on Bonds Range. The mineralogy indicates that the sediment was predominantly derived from the Precambrian basement rocks of the Tyennan region.

Lithofacies V

This lithofacies consists of bioturbated quartz arenite and quartz wacke, characteristically containing abundant bedding-perpendicular worm burrows, the density of which is often so great that it is difficult to identify original undisturbed sediment. This is a characteristic common to certain lithofacies within the Moina Sandstone in the Fossey Mountains area to the east (Jennings, 1958, 1963), which lead early workers to refer to that formation as the 'Tubicolar Series'. The higher percentage of argillaceous matrix compared with the arenites of Lithofacies IV may be at least partly a result of the bioturbation, as evidenced by higher matrix:grain ratios within burrow fill in those examples in which unburrowed material is still present (e.g. sample UTGD48402). The dominant clast composition is metamorphic quartz, and as is the case in Lithofacies IV, blue-green tourmaline is a common accessory mineral. The sorting of the quartz clasts is somewhat better than in Lithofacies IV, but they are still dominantly subangular. Rocks of Lithofacies V are nearly always mottled light grey to grey-green in colour, indicating lack of oxidation.

The characteristics of Lithofacies V suggest a marine-dominated (probably intertidal) environment of deposition. Lithofacies V tends to be more dominant in the upper parts of the Denison Subgroup correlate in the Black Bluff Range area, but this is by no means a universal rule. Hence, rocks characteristic of the lithofacies occur close to the base of the sequence south of St Valentines Quadrangle near DQ111032 on Bonds Range.

Lithofacies VI

This lithofacies makes up only a minor part of the Denison Subgroup correlate in the Black Bluff Range area. It consists of thinly interbedded dark red-brown hematitic laminated siltstone and pale-coloured fine quartz arenite. In some places the siltstone beds are very minor or absent. Where they are present they are sometimes bioturbated. South of St Valentines Quadrangle at DQ077056 on the Black Bluff Range, trace fossils which have been identified as trilobite feeding burrows were found in the top surface of one of these siltstone beds (sample UTGD48419). The arenite beds are much less hematitic and commonly contain ripple marks, ripple-drift cross-lamination, and occasionally small scale trough cross-lamination.

In some places Lithofacies VI forms the upper part of a sequence consisting of Lithofacies II-III-IV-VI. It is interpreted as a lower intertidal to subtidal marine facies, the siltstone forming in shallow lagoon or bay conditions and the arenite representing laterally migrating shallow bars. An alternative is that the whole assemblage formed in intertidal conditions, the siltstone representing intertidal mudflats and the arenite representing intertidal channels. The presence of trilobite feeding burrows, however, argues against intertidal conditions.

Palaeocurrents and provenance

A limited amount of palaeocurrent evidence from the Denison Subgroup correlate in the Black Bluff Range area was given by Seymour (1980), and is illustrated in Figure 5. With one exception the indicated currents are from directions ranging from east to south, although most are from the south-east, particularly in the southern part of the area shown. Most of the palaeocurrent determinations are from Lithofacies IV, and of these most were taken from planar-tabular cross-laminated units. Palaeocurrents determined from current ripples usually give greater scatter, although only one of the determinations shown (the one 2 km south-east of Black Bluff) disagrees markedly with the others. It seems possible that ripple asymmetry may have been misread at this locality.

The mineralogy of the quartz arenites of Lithofacies IV, V and VI is consistent with sediment derivation from the Precambrian basement rocks of the Tyennan region which lies generally to the south-east of the Black Bluff Range area, and the palaeocurrents are mostly also consistent with this. Although no palaeocurrents have been recorded from Lithofacies I, II and III, similar provenance is indicated by the composition of much of the gravel- to boulder-grade material in Lithofacies II, and of the arenite matrix and some of the pebbles in Lithofacies III. The white, pink and brown chert (jasper) angular pebble-grade material in Lithofacies III, which commonly forms a major component of the deposit, does not appear to have an obvious provenance in either the Precambrian basement of the Tyennan region or in the pre-Denison Subgroup volcano-sedimentary sequences in the immediate vicinity. Lithofacies I generally displays evidence of very local provenance.

ST VALENTINES PEAK AREA

P. G. Lennox

Siliceous conglomerate

The contact between the fossiliferous Cambrian sequence and basal quartz-(chert) conglomerate of the Denison Sub-group correlate crops out on PMG Road, Companion Hill [CQ939228] and on Black Pit Road [CQ958224].

A chain and compass traverse through the Black Pit Road conglomerate section reveals folds trending approximately N-S with vertical axial surfaces (see fig. *5a, b*). There are a number of prominent joint orientations which make determination of bedding difficult.

The W-dipping, N-trending conglomerate ridge east of St Valentines Peak (hereafter called 'Little Valentines Ridge') appears to be a fault block which is terminated at its southern end by another normal fault in the valley of a tributary of Old Park Creek [CQ970204].

The conglomerate at both localities consists of beds of coarse pebble conglomerate interbedded with small-pebble to granule conglomerate. The sorting is commonly poor with the pebbles usually white, grey or crimson chert or quartz in a coarse to medium sandstone matrix. Where the conglomerate

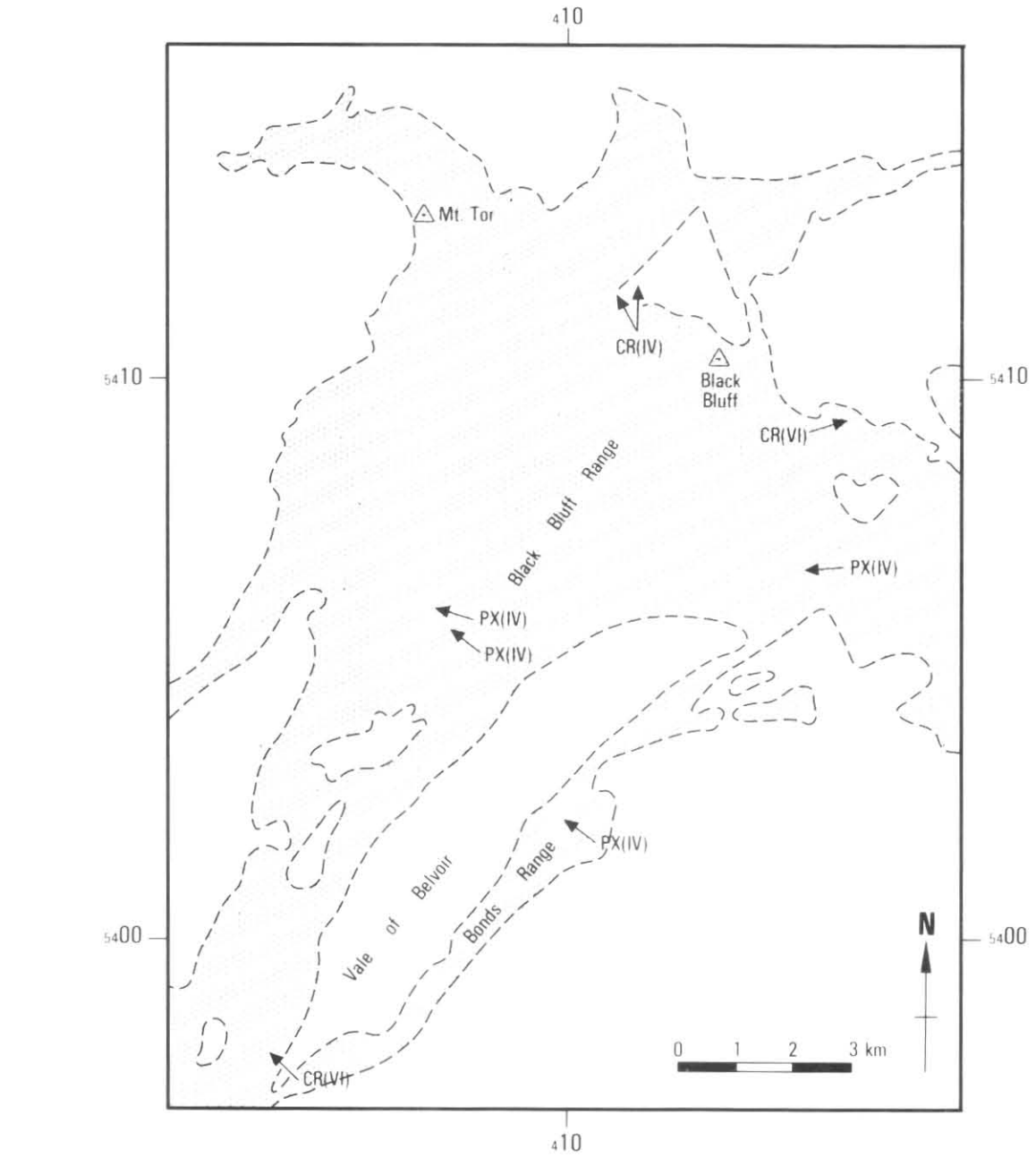

Figure 5. Extent of outcrop of Denison Subgroup correlates in the Black Bluff Range area on St Valentines and Mackintosh Quadrangles, showing palaeocurrent directions from Seymour (1980). Symbols: PX - planar cross-lamination; CR - current ripples; lithofacies indicated in parentheses. (D.B.S.)

has undergone thermal metamorphism and metasomatism as a result of close proximity to the granite (e.g. Kara Mine Road, CQ967273), it loses its highly siliceous, tough and non-friable character and becomes friable and discoloured to a pale greenish grey colour. Although there are abundant horizons of aligned pebbles defining bedding, grading is not a common feature. As Jago *et al.* (1975) noted, the sequence lacks distinct bedding planes. Occasional horizons of micaceous siltstone (PMG Road, CQ937227) or black mudstone (Black Pit Road, CQ965230) occur within the conglomerate.

The contact between the conglomerate and the rocks overlying it on the western side of Companion Hill is obscured by basalt. Near the basalt outcrop blocks of conglomerate up to 5 m in diameter form a scree zone at the base of the very steep western face of Companion Hill. On Black Pit Road the upper contact is exposed in a number of localities which are, north to south: Kara Mine (HEC power line) Road [CQ972273 and CQ972267]; Old Park Creek tributary [CQ969235]; and Black Pit Road [CQ968234 and CQ967225].

On the Kara Mine (HEC powerline) Road the altered conglomerate sequence displays a progressive decrease in pebble size from west to east. Altered conglomerate interbedded with coarse sand-grade quartzite gives way to poorly bedded, well jointed saccharoidal quartzite, with the actual change being obscured by overlying Tertiary basalt. Further south altered, small-pebble conglomerate gives way to a 40 m section of altered silty mudstone containing aplite dykes, which in turn gives way to aplitic, equigranular granite. This area is considered to be near the closure of the St Valentines Anticline and the sequence here would be expected to dip and face to the east. In fact although the Cambrian outcrops show dips to the east, all of the Denison Subgroup conglomerate and mudstone outcrops show dips to the west. There is no reliable grading in the conglomerate, nor graded silt horizons in the mudstone, so the overall west to east decline in the size of the pebbles in the conglomerate must be taken as the only indication of easterly facing in the sequence.

The contact between the Denison Subgroup conglomerate and the overlying sequence exposed in a tributary of Old Park

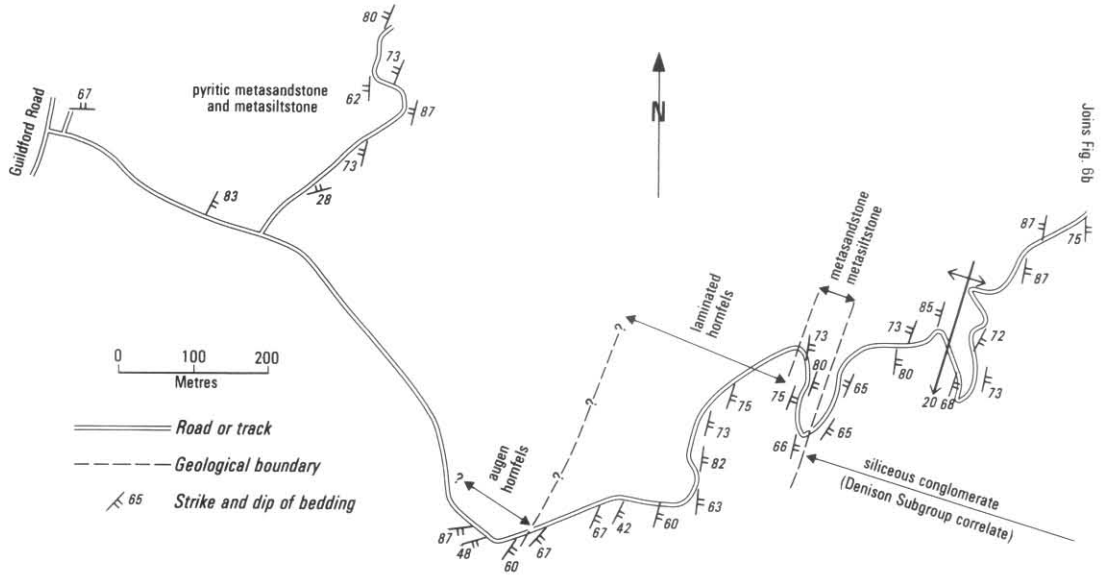

Figure 6a. Black Pit Road (western section), St Valentines Peak area. (P.G.L.)

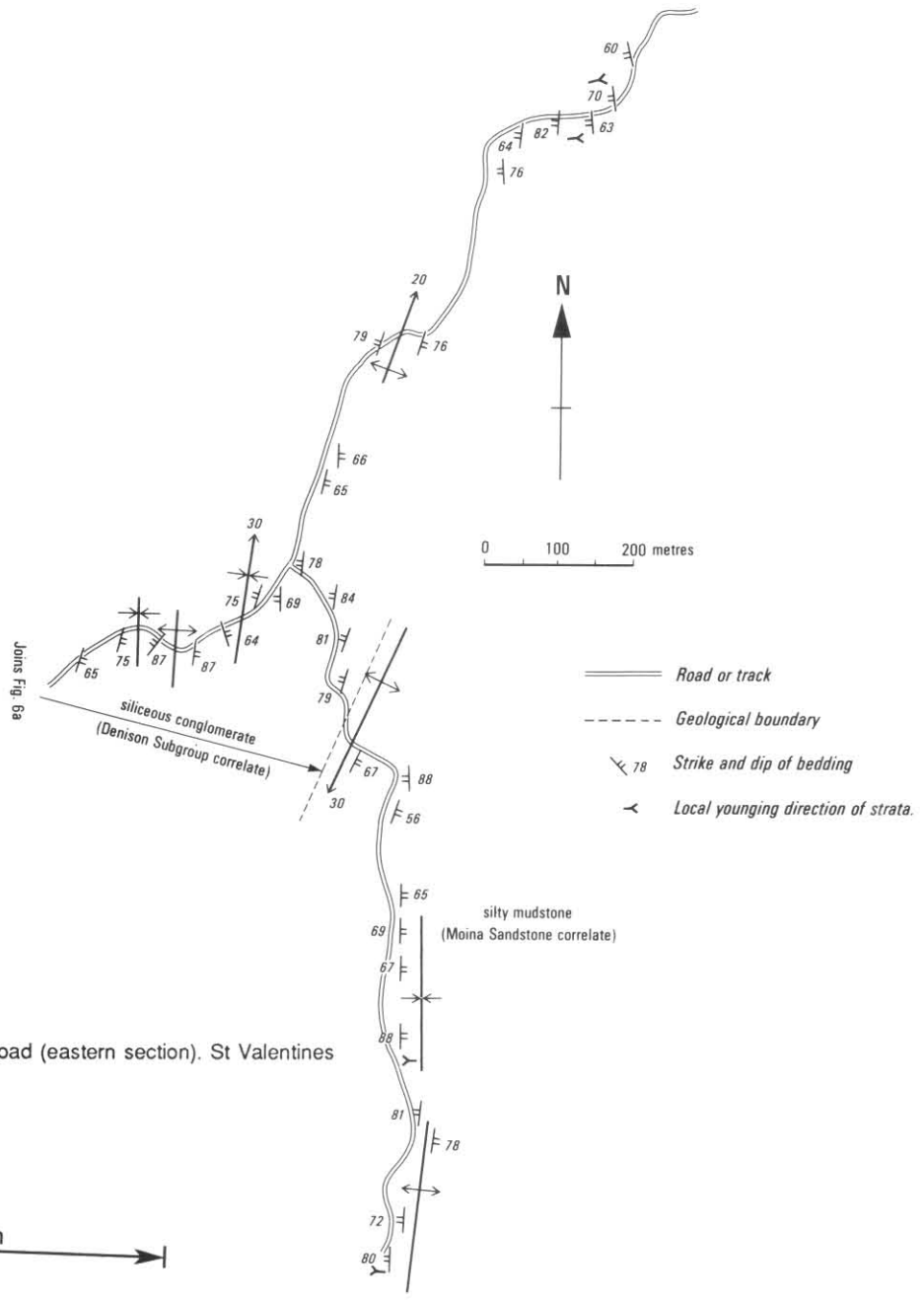

Figure 6b. Black Pit Road (eastern section). St Valentines Peak area. (P.G.L.)

Creek appears to be transitional over a 30 m section. Conglomerate gives way to pyritic laminated hornfels, quartzite (50-100 mm thick beds), quartz-pebble conglomerate, augen-hornfels and finally a continuous outcrop of interbedded dark and light grey, very fine-grained, siliceous skarn. The contact exposed on a track off Black Pit Road [CQ968234] closely resembles that on the Kara Mine (HEC powerline) Road. The lithological change is abrupt and the sequence above the conglomerate consists of extremely altered silty mudstone with calcareous horizons. It dips to the west and appears to dominantly young to the west on the basis of cross-lamination and grading.

The contact exposed on Black Pit Road on the eastern flank of St Valentines Peak [CQ967225] may be faulted, as the quartzite unit exhibits near-vertical planar joint faces (sub-)parallel to the contact. The unit above the quartzite is a dark greenish black, very fine grained, highly siliceous ?calcsilicate or laminated mudstone. The black, conchoidally fractured, very fine grained rock in thin section (80-43) exhibits a translucent brown groundmass with scattered poorly defined quartz grains (apparently aligned) and a lepidoblastic sericite fabric.

The upper and lower contacts of the conglomerate forming Little Valentines Ridge are not exposed.

Moina Sandstone correlate

The Moina Sandstone correlate crops out in a 250 m wide linear zone trending N-S parallel with and adjacent to the Emu River [CQ983278]. The isolated outcrops within the thinning basalt cap south of this zone (e.g. CQ982262), to the east of the Kara mine workings, are predominantly recrystallised quartzites (80-28, 80-30). They consist of equigranular monocrystalline quartz which is optically continuous in plane polarised light. In crossed-nicols the quartz mass consists of generally polygonal quartz grains with undulose extinction, between 30 and 90 μm across. At the margin of the grains feathery sericite aggregates or small interlocking phenocrysts of epidote predominate. New quartz crystals with straight margins are visible in some parts of the thin sections, forming within large quartz grains or overlapping their margins (80-28). This outcrop of thermally metamorphosed Moina Sandstone lies on the western side of a broad syncline trending N-S (half-wavelength 4-5 km) and would be expected to dip and face east. However, in only one instance does the outcrop dip to the east. The discrepancy may be in part due to the smaller scale folding within the sequence as evidenced by the one kilometre half-wavelength antiform within the siliceous skarn outcrop on Kara Road near Highwood Hill [CQ987250].

The 9 km long, 0.5-1 km wide linear outcrop on the eastern side of the synform forms an arcuate W-dipping belt which is faulted at its southern end against well cleaved, fossiliferous Bell Shale correlate. The two main outcrops, in gravel pits on Blythe Road [DQ019247] and in the Blythe River upstream of Blythe Road [DQ022205], consist of white, well bedded, well sorted, saccharoidal medium sand-grade quartzite. The displacement of this belt by faults, as proposed by Pike (1964), is discussed in the Structural Geology section.

Although the outcrop between St Valentines Peak and Little Valentines Ridge would be identified as thermally metamorphosed, ?Moina Sandstone on stratigraphic grounds, it is in part lithologically unlike any other outcrops on the Quadrangle. An aeromagnetic anomaly trending N-S in this valley was drilled by Comalco Pty Ltd and determined to be a small lens of magnetic skarn. Magnetite skarn is the host rock for the wolframite mineralisation at the Kara mine. The outcrops range from black, conchoidally fractured, highly siliceous mudstone (80-43) to recrystallised, extremely fine-grained hornfels (80-37, 80-38, 80-39), very like the Kara mine outcrops (80-28, 80-30).

AREAS ADJACENT TO NATIVE TRACK TIER

P. W. Baillie

Rocks correlated with the Denison Subgroup (Corbett, 1975) crop out in a number of areas in the north-eastern part of the map sheet. The contact with the underlying volcano-sedimentary sequence was observed at several localities during mapping and in every case the relationship was either an erosional break or apparent conformity. No angular unconformities were observed.

Quartz sandstone sequence, Mt Everett (Ods)

As noted earlier the Cambrian rocks are different on either side of the postulated major fault in the Laurel Creek area [DQ093235]. To a lesser extent the same is true of the Denison Subgroup correlates, and the Mt Everett sequence has thus been differentiated from the other sequences as Ods.

In its upper parts the Cambrian sequence in this area (€ms) consists predominantly of quartz sandstone, cross-bedded in part, in which indeterminate marine fossils have been found. These beds appear to be gradational into a sequence of quartz sandstone which is pebbly in part and which is correlated with the Denison Subgroup. The boundary between the two sequences is not distinct and is shown as an inferred boundary on the map sheet, approximately corresponding to the change from marine to non-marine sedimentation.

Higher in the sequence, near the summit of Mt Everett [DQ050207], rocks correlated with the Denison Subgroup consist of well-bedded, well-sorted, very coarse quartz sandstone and minor granule conglomerate.

The sequence appears to be similar to that described on the Denison Range by Corbett (1975), in particular the Great Dome Sandstone.

It is strange that both the Cambrian sequence and the Denison Subgroup correlate are apparently unique in the Mt Everett area. One possibility is that this sequence (Ods) was present in other areas between the volcanic rocks and Denison Subgroup conglomerate, but was removed by erosion (erosional breaks have been observed at this level) prior to deposition of the conglomerate. Another possibility is that a facies change, perhaps somehow related to movement on the Laurel Creek Fault, persisted in the area over most, if not all, of the Late Cambrian, and some of the Early Ordovician. Exposure and access are not good in this area and resolution of the problem requires much further work.

Siliceous conglomerate (Odc)

Conglomerate sequences, contiguous with the Roland Conglomerate of the adjoining Sheffield Quadrangle (Jennings *et al.*, 1959) are exposed over much of the north-eastern portion of the St Valentines Quadrangle.

The unit is similar to 'Owen-type' conglomerate seen at many other localities in the West Coast Range and consists of thick bedded, generally structureless, white or pink, granule to cobble conglomerate containing usually well-rounded clasts of vein quartz, or siliceous clasts derived from a metamorphic terrain - such as orthoquartzite, laminated quartzite, quartz-mica schist, together with some chert. The conglomerates are sometimes imbricate and less commonly cross-bedded. Interbedded lenses of coarse to very coarse quartz sandstone are commonly cross-bedded.

Access is difficult on the Loongana Range and the only rock-type observed was ferruginous pebble conglomerate [DQ140177].

The unnamed range of hills on the northern side of the major anticlinal structure in the Native Track Tier area [DQ108224] consist largely of siliceous conglomerate. Steep cliffs are present above the underlying volcano-sedimentary rocks. The conglomerate sequence consists dominantly of pebble to cobble conglomerate, with individual beds up to one metre in thickness and occasional interbeds of very coarse quartz sandstone. Clasts are almost entirely composed of quartzite, with lesser laminated quartzite and very minor chert. The clasts are usually well-rounded and in some places have an imbricate fabric. The sandstone interbeds are lenticular and show medium- to large-scale trough cross-bedding.

In a quarry on the Native Track Tier road at DQ087220 conglomerate has been deposited in an erosional channel developed in purple turbiditic siltstones of the underlying volcano-sedimentary sequence. The conglomerate is well sorted and contains pebbles and cobbles of quartzite, vein quartz and chert in a silty matrix.

On Loyetea Peak [DQ126253] the sequence consists of interbedded pink to purple, granule and cobble conglomerate and very coarse sandstone. Clasts are composed of vein quartz and quartzite. Bedding thickness varies from approximately one metre in the conglomerate to less than 200 mm in the sandstones.

In the Leven River in the gorge immediately upstream of Gunns Plains [DQ160230] the conglomerate sequence consists of pebble and granule conglomerate in which chert clasts comprise up to 20% of some beds.

Towards the north-east corner of the map sheet [DQ142296] the sequence is also chert-rich and consists of pink-coloured granule and pebble conglomerate with unusually well-rounded clasts of vein quartz, quartzite and chert in a coarse sandy matrix.

The sedimentary features of the conglomerate sequences such as channelling, trough cross-bedding, thick bedding and imbricate fabric, suggest that deposition took place under terrestrial conditions perhaps in the upper part of a braided stream system or the lower part of an alluvial fan system.

Moina Sandstone correlates (Odm)

In the neighbouring Sheffield Quadrangle the Roland Conglomerate is overlain by the Moina Sandstone, a 'sequence of quartz sandstone and shale with minor grit and some conglomerate beds' (Jennings, 1979). The formation is characteristically bioturbated at several horizons and displays abundant tubicolar casts.

Rocks contiguous with the Moina Sandstone crop out extensively in eastern parts of the St Valentines Quadrangle, and also in other areas, including Mt Pearse [CQ843049] in the south-west of the sheet. Extensive mobilisation of material on hillslopes by periglacial processes during the Pleistocene has resulted in much of the Moina Sandstone being covered by scree, making mapping of the formation very difficult. It is largely for this reason that the undifferentiated Denison Subgroup symbol (Odu) is used in certain areas of the map, i.e. areas where it was not possible to differentiate between the conglomerate and overlying sandstone sequences.

Rocks considered to be correlates of the Moina Sandstone crop out from east of Laurel Creek [DQ088223] to the Puffers Creek area [DQ112234] and also in the downfaulted fault block to the north of this area [DQ097243]. The rocks overlie conglomerate sequences and consist of medium to very coarse grained quartz sandstone occurring in beds less than one metre in thickness, but usually of the order of 200 mm, together with minor interbedded siltstone or micaceous mudstone. Bioturbation is not common, nor were any diagnostic fossils collected.

It is probable that parts of the sequences mapped as Moina Sandstone and correlates are lateral equivalents of sequences mapped as Roland Conglomerate and correlates.

MT CATTLEY, GRASSTREE RIDGE AND MT PEARSE

P. W. Baillie
P. R. Williams

At Mt Cattley [DQ045060] the lower part of the Denison Subgroup sequence consists dominantly of cobble conglomerate with bedding thicknesses usually greater than one metre (P.W.B.). Clast shape varies from sub-angular to well rounded and clasts consist of quartzite, schistose quartzite, vein quartz and minor chert in a very coarse quartz sandstone matrix. Very coarse sandy layers or lenses are generally less than 100 mm in thickness, and some have internal laminae and/or contain pebbles. Some show trough cross-lamination.

Correlates of the Moina Sandstone occur on Grasstree Ridge [CQ980130], where the rocks consist of white, often bioturbated fine- to coarse-grained quartz sandstone and minor granule conglomerate (P.W.B.). A few indeterminate bryozoa are present in some beds.

A sequence of siliceous sandstone and conglomerate at Mt Pearse [CQ842050] is heavily bioturbated, contains abundant worm tubes and is lithologically similar to late Cambrian and Early Ordovician sandstone (Moina Sandstone) in other parts of Tasmania (P.R.W.). It is continuous with rocks mapped as such on the Mackintosh Quadrangle. On the western edge of Mt Pearse, a ridge of granule to pebble conglomerate occurs against the surrounding basalt plateau. The clasts are usually well-rounded and form a continuous framework, although some beds contain dispersed pebbles in a coarse-grained sandstone matrix. The clasts range up to 0.1 m in diameter and are usually metaquartzite. Oblate clasts are invariably imbricate. At CQ840051 the clast size in conglomerate increases to 0.4 m. The conglomerate beds are interbedded with ferruginous coarse to medium-grained sandstone composed of well-rounded grains of quartz and quartzite. Vertical worm burrows and complete bioturbation are common in the sandstone beds, and cross-bedding is ubiquitous. Current directions are from and to the NNE. The grain size of the sequence exposed at Mt Pearse decreases upwards. The siliceous sandstone and conglomerate sequence is surrounded by Tertiary basalt.

Gordon Subgroup correlates

LOONGANA AREA

D. B. Seymour

Carbonate lithofacies stratigraphically equivalent to the Gordon Subgroup occur in a large syncline in the Loongana area [*c.* DQ145145] near the eastern margin of the Quadrangle. The axis of the syncline is horizontal and trends ESE-WNW, and it is an asymmetric structure with a long northern limb and short southern limb. The southern boundary of the limestone may be a fault against the Denison Subgroup correlate. An early report on the limestone at Loongana was given by Hughes (1957), although he gave no details of the lithofacies.

The maximum exposed section of limestone at Loongana is estimated herein to total about 1150 m. The top of the limestone is not exposed. The base is exposed to the east of the Quadrangle boundary in the Leven River near DQ179164, where lithofacies transitional between the limestone and bioturbated quartz arenites of the Denison Subgroup correlate are only developed to a minor extent. The basal 10-15 m of the limestone sequence consists of micrite containing sparse oncolites and small specimens of the gastropod *Maclurites*

sp., and may have been deposited in a lower intertidal to shallow subtidal environment. Most of the remainder of the sequence consists of dolomicrites which are often bioturbated, with common dolomitised bedding - perpendicular worm burrows. These are interpreted as intertidal sediments. They include a few minor shell beds and calcarenite beds which may represent intertidal channels. Towards the upper part of the sequence dolomitisation becomes better developed and algal-laminated dolomicrites appear. Some of these may have been deposited in supratidal environments. Stromatolitic algal-laminated dolomicrites occur near the top of the exposed section at Taylors Flat [DQ143143].

Burrett (1978, pp. 88-90) obtained the following biostratigraphic information from the limestone at Loongana, based on conodont microfaunas:

(1) Location: the oncolitic micrite close to the base of the sequence

Contents: *Phragmodus flexuosus* Moskalenko
Panderodus serpaglii sp. nov.

Indicated age: Chazyan (early-Middle Ordovician)

(2) Location: about 22 m above base of sequence

Contents: *Phragmodus flexuosus* Moskalenko
Belodina compressa (Branson and Mehl)

Indicated age: Blackriveran (middle-Middle Ordovician)

(3) The youngest indicated age obtained by Burrett from the Loongana sequence was Rocklandian (late-Middle Ordovician)

ST VALENTINES PEAK AREA

P. G. Lennox

G. R. Green has subdivided the Gordon Subgroup correlate in this area into two lithologies: siliceous hornfels and magnetite skarn. The latter is the host rock for the Hampshire Silver mine and Kara No. 1 (scheelite) mine. The siliceous hornfels forms the core of a N-trending syncline, and is poorly exposed over most of this area, while the magnetite skarn crops out at three isolated localities.

The western contact of the siliceous hornfels in Old Park Creek appears faulted against sedimentary rocks considered to overlie the conglomerate of the Denison Subgroup correlate [CQ970235]. The southern contact is a normal fault against fossiliferous calcareous mudstone of the Bell Shale correlate.

Pike (1964) postulated a number of approximately east-west faults and a curved hinge line to the N-trending regional synform (see Structural Geology section).

In hand specimen (80-29, CQ988263) the hornfels consists of mottled, light and dark grey layers and has a sub-conchoidal fracture. In thin section the 0.5 mm thick layers consist of a ?dolomitic groundmass with minor recrystallised quartz grains and altered sericite blades. Hand specimens from outcrops at Blythe River (80-16, 80-17) are (sub-)conchoidally fractured, grey, massive, well cleaved, calcsilicate rocks which are in part pyritic and fossiliferous. In thin section 80-17 is a stylolitic well-cleaved crystalline dolomitic mudstone with fossils possibly after ?bivalves or *?Tentaculites* (S. M. Forsyth, pers. comm.).

GUNNS PLAINS AREA

P. W. Baillie In the north-eastern corner of the Quadrangle, limestones which are correlated with the Gordon Subgroup (Corbett and Banks, 1974) crop out in the Gunns Plains area [DQ150290], and near Laurel Creek in the vicinity of Peak Hill Farm [DQ105260].

Because of overall poor exposure and lack of any good sections no attempt was made to subdivide the limestone sequences as has been done successfully in the Florentine Valley of southern Tasmania (Corbett and Banks, 1974; Brown *et al.*, 1982).

At most localities the limestone consists of fine-grained grey micrite and interbedded brown dolosiltite. Stylolites are common. Coarser grained bioclastic limestones also occur.

The limestone of the Gunns Plains area has been described by Hughes (1957).

Biostratigraphic aspects are discussed by Banks and Burrett (1980) and Webby *et al.* (1981).

Eldon Group Correlates

FLORENCE QUARTZITE CORRELATE (Df)

P. G. Lennox

Near the centre of the Quadrangle there are two isolated outcrops of cleaved siltstone [CQ956145] and saccharoidal quartz-conglomerate and quartzite [CQ956139] which Pike (1964) assigned to the Florence Quartzite correlate on the basis of their locality and lithology. He also considered the nearby NE-trending ridge bounded by Blythe Road, Rabbit Plain Road and Guildford Road to be underlain by Florence Quartzite correlate. Regrowth has obscured outcrop on this ridge, preventing confirmation of Pike's conclusion. On the map the ridge has been shown as consisting of Tertiary basalt.

BELL SHALE CORRELATE (Db)

P. G. Lennox

In the headwaters of Old Park Creek and the Blythe River, cleaved fossiliferous calcareous mudstones with some interbeds of fine-grained sandstone outcrop are faulted against Gordon Subgroup and Denison Subgroup correlates to the north and probably also to the north-west, and are covered by Tertiary basalt elsewhere.

The outcrop of weathered, pale brown, well-bedded mudstone on Peak Plain Road [CQ977192] contains abundant fossils typical of the Bell Shale at Zeehan. M. J. Clarke has identified *Isorthis* sp., a strophomenid *cf. Cymostrophia, Favosites, ?Hysterolites* sp., *Notanoplia pherista* Gill and nautiloids. The Bell Shale at Zeehan does not contain the advanced *Hysterolites* sp. present in this outcrop. M. J. Clarke considers that this Bell Shale correlate may possibly be younger than that at Zeehan, although this has not been proved.

Pike (1964) considered that the area in the upper reaches of the Blythe River centred around DQ005175 is underlain by Eldon Group correlates other than the Bell Shale. Fossils from three localities [DQ003168, CQ998168, CQ995169] include *Lissatrypa* sp. (V124), *Pleurodictyum* sp., crinoid ossicles (V126), *?Strophochonetes* or *Plectambonites* sp., and *?Isorthis* sp. (V128), all of which indicate Bell Shale correlate.

Parmeener Supergroup correlates

WYNYARD TILLITE CORRELATE

P. R. Williams
P. G. Lennox

A sequence of tillite and rhythmites covering a large area of the north-west corner of the St Valentines Quadrangle is continuous with the Carboniferous Wynyard Tillite in the Burnie Quadrangle (Gee, Gulline and Bravo, 1968). The

outcrop extends from the Hellyer Gorge area [CQ850290] west to the Arthur River [CQ750290]. The stratigraphic section in the western area differs from that in the Hellyer Gorge area. At Hellyer Gorge the section from 250 m above sea level to 520 m above sea level is entirely composed of thickly bedded tillite, containing polymict fragments in a dark grey calcareous matrix. However, in the western area tillite is restricted to thin horizons in the lower part of the section, which is composed dominantly of interbedded mudstone and sandstone (rhythmites) from 225 m above sea level to 370 m above sea level. Clearly this represents a major facies change, the area of deposition of thick rhythmites probably occurring in a part of the basin below the general level of ice grounding. The section contains abundant sedimentary structures indicating ice advance over the rhythmites for short periods of time. A stratigraphic section of the rhythmite rich area is shown in Figure 7, which is similar to the section by Gulline in Gee (1977).

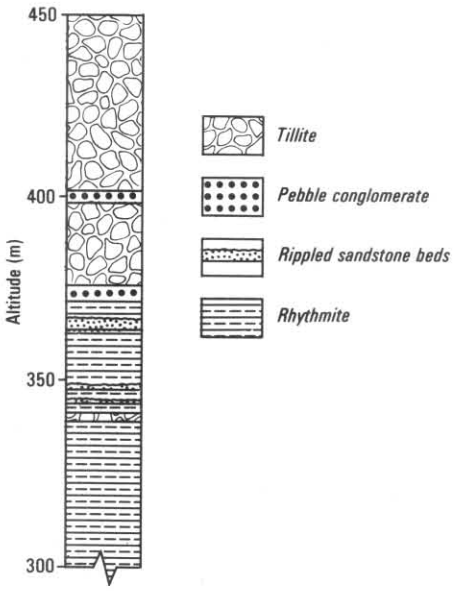

Figure 7. Partial stratigraphic section of Wynyard Tillite, western part of the St Valentines Quadrangle. (P.R.W.)

Palaeocurrent directions within the rhythmite sections are determined from cross-laminated ripple-marks present in interbedded turbidite sandstone. They are invariably from a south-westerly quadrant. This direction is consistent with the direction of scouring at the base of tillite beds which overlie rhythmites. Sedimentary structures present include mounds of tillite which contain rhythmites on one side of the mound and tillite on the other. These are both overlain by tillite. These tillite mounds may represent terminal moraines, in front of which fine-grained sediments accumulated. Channels cut into interbedded tillite and rhythmite are present, and may represent deep ice scour. The scours are filled with tillite. In addition, three examples of large scale deformation associated with ice-loading have been noted. On Parrawee Creek Road [CQ772301] soft-sediment folds with a wavelength of about 3 m occur, forming a conjugate fold pair. One fold has a shallowly dipping axial surface and an overturned limb, whereas the other is an open S-fold. Sandstone beds are severely distorted by pull-apart fractures, and behaved as competent units during the deformation. On Saxons Road [CQ768310] tillite has been forcibly emplaced into the rhythmite sequence causing deformation and overturning. At Wandle Road [CQ775256] an overfold with a half wavelength of 3 m and a horizontal axial surface is probably due to slumping caused by ice loading of partly consolidated till. The forms of some of these structures are shown in Figure 8.

In other respects the tillite section is similar to that described by Gulline in Gee (1977).

P. G. Lennox describes the faulted contact in the Hellyer River [CQ853290] between the tillite and ?Eocambrian-?Early Cambrian greywacke as a 6 m × 5 m zone of mixing.

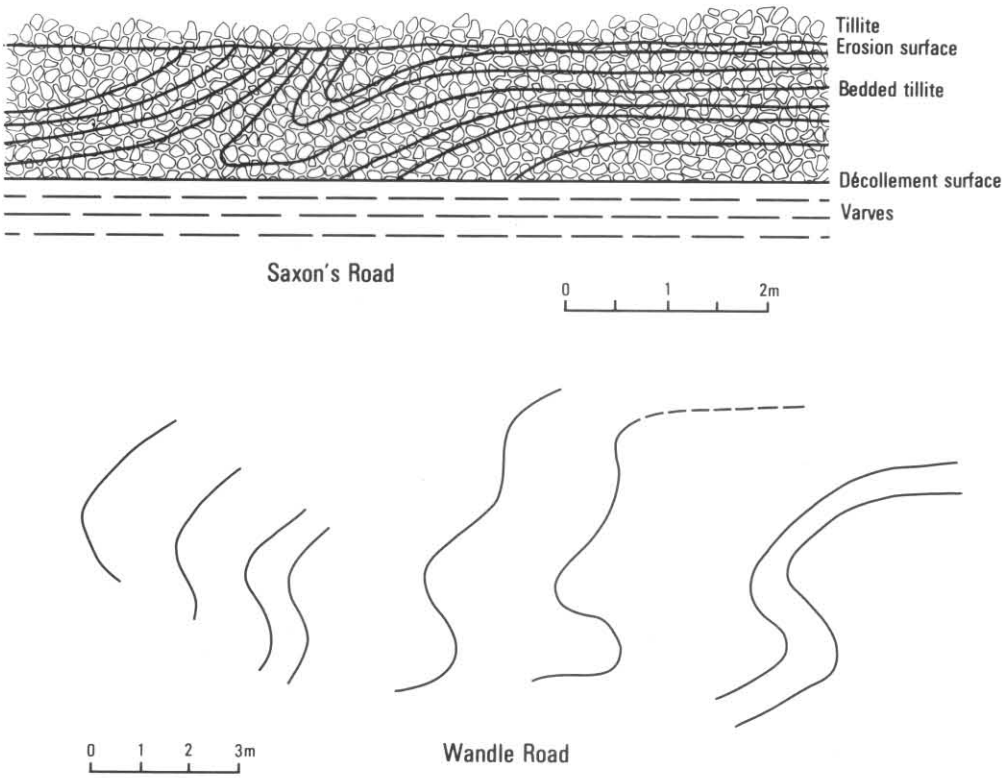

Figure 8. Deformation associated with ice loading, Wynyard Tillite correlate, as seen in road cuttings in western part of St Valentines Quadrangle. (P.R.W.)

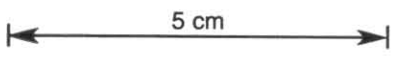

This zone contains angular boulders of pink equigranular granite with tourmaline-filled vugs, micrite with ?oncolites and dolosiltite layers, and occasional boulders of quartzite and cleaved schist, in a pale grey claystone matrix with an almost horizontal planar fabric.

INGLIS SILTSTONE CORRELATE

P. R. Williams

A sequence of interbedded sandstone and mudstone overlying the tillite at CQ771320 is correlated with the Inglis Siltstone. Graded sandstone beds up to 0.7 m thick occur at the base of the section. The sequence passes upwards into medium- to fine-grained, polymict feldspathic lithic sandstone.

At CQ838306 in Hellyer Gorge, a lens of oil shale occurs in mudstone overlying the tillite, close to the contact with the tillite. The sequence is correlated with the Inglis Siltstone, although outcrop in this area is very poor. No fossiliferous horizons have been discovered.

Tertiary

EXTENT AND PHYSIOGRAPHY

J. L. Everard

Tertiary basalt covers about 640 km^2, or about 55%, of the St Valentines Quadrangle. As discussed below, drilling has shown that in places the basalt is over 300 m thick and may consist of fifty or more flows, often with intercalated or underlying layers of sediment.

In the central and southern parts of the quadrangle, the basalt has almost completely filled in the earlier topography to produce a plateau at an elevation of about 600 to 700 m above mean sea-level, except for Mt Pearse, Grasstree Ridge and the Two Hummocks which project through the basalt as basement highs. To the north and northeast, where it is dissected by the Emu, Blythe, Leven and other coastal rivers, the basalt is probably much thinner, but more or less extends to the coast near Burnie (Gee, *et al.*, 1967). In the north-east, the Hellyer River has cut through more than 250 m of basalt to reach Eocambrian basement at CQ846241. However, near Waratah the basalt appears to be less than 100 m thick in places, since basement is exposed at an elevation of 500 to 600 m, not far below the edge of the basalt plateau. The lack of basalt at lower elevations in the valley of the upper Arthur River suggests that the valley post-dates the volcanism.

Outlying areas of basalt, typically capping hills and ridges at an elevation of 500 to 600 m, occur further west on the Magnet Quadrangle. Brown (1986, p. 66-68, 164) has shown that, in the Savage River-Luina area, these basalt outliers are chemically similar to analyses from the lower part of the basalt pile in drill holes east of Waratah. Thus it is likely that the outliers are remnants of a continuous basalt plateau which was originally even more extensive than at present.

To the south, the main continuous area of basalt extends to northern parts of the Mackintosh Quadrangle (Barton, *et al.*, 1966) where the Coldstream, Hatfield and Que Rivers have dissected the plateau and cut down to the mainly Cambrian basement. Basalt outliers north-west of Mt Romulus [CP940860] and capping Lynch Hill [CP731826] (Brown, *ibid.*) suggest that the basalt was originally more extensive to the south as well.

Similarly, basalt outliers in the east near Loongana suggest that the main body of basalt originally extended into the Leven River valley which may therefore pre-date the volcanism.

A small area of basalt shown in the Leven River at DQ051131 is now known to be part of a larger, probably Cambrian, mafic intrusive (J. Pemberton, pers. comm.).

FEEDERS

During mapping a probable feeder was discovered on a hill near South Riana at DQ157310, in the extreme north-east of the quadrangle (P.W.B.). Numerous spinel lherzolite nodules up to 100 mm in diameter occur in a strongly alkaline basanite (sample EV1, table B2). This is the most under-saturated basalt so far analysed from the quadrangle.

In Catley Creek at DQ046086, the exposed contact of an unusual fine-grained augite-phyric alkali basalt dips steeply south-east, subconcordant with steeply-dipping Cambrian sediments, and may represent a sill-like feeder. Jointing in the basalt is roughly parallel to the contact. Further north in Cattley Creek at DQ040112, field relations are less clear, but also suggest a possible feeder (J. Pemberton, pers. comm.).

Edwards (1950) quotes an analysis of a strongly alkaline olivine-titanaugite-phyric basalt (analysis Oc37, table B2) from a 'prominent point of eruption east of [the] Emu Bay railway line, a short distance north of Hampshire Railway Station'. This appears to refer to Coastview Hill [CQ987323] which may therefore also be the site of a feeder.

Doubtless other, probably volumetrically more significant feeders or fissures were involved in the extrusion of the basalt, but remain undetected and possibly concealed beneath hundreds of metres of flows. Pyroclastic depositional features such as cinder or scoria cones which would indicate a feeder are very susceptible to erosion and apparently have not been preserved.

THICKNESS AND PRE-BASALT TOPOGRAPHY

Information on the thickness of the basalt in the St Valentines Quadrangle and adjacent areas is available from several sources. In a few dissected areas, such as in the Hellyer River valley, the thickness can be observed directly, whilst elsewhere drill holes provide some information. Estimates have also been made by geophysical methods.

Drilling has been carried out by both mineral exploration companies and the Department of Mines. The basalt-covered area has attracted mineral exploration because of the proximity of major ore deposits, notably Mt Bischoff (Sn) and Que River (Ag-Pb-Zn), and the likelihood that the highly prospective Mt Read Volcanics occur concealed beneath the basalt. In 1983 BHP drilled nine holes (WA1-7, WY1-2), eight of which penetrated through basalt cover to basement, over geophysical anomalies in the western part of the Quadrangle (Anon, 1983, 1984, *a-b*). In 1986 the Department of Mines commenced the Sub-Basalt Drilling Project (SBDP) in an effort to obtain data on basalt thickness, basement lithologies and geophysical properties in the basalt-covered area (Baillie, *et al.*, 1987). At the time of writing (June, 1988) data on seven holes is available (Baillie, 1987*a-c*; Baillie and Green, 1988*a, b*; unpublished data). Localities and summary logs of all holes are given in Figure 9. (*Note:* Data for hole WY2 are incorrectly shown on the printed colour map).

Several attempts to use geophysical methods have been made, both to determine the thickness of the basalt cover and to detect features and generate drilling targets in the underlying basement. Leaman (1986), who summarises the various problems encountered, has used aeromagnetic data, with some control from gravity and B.H.P. drill hole information, to estimate the total thickness of the basalt (fig. 10) and pre-basalt topography (fig. 11) in an area of about 150 km^2 north-east of Waratah. Subsequent drilling in this area (holes SBDP1, 4 and 5) has proved basalt thicknesses in good agreement with Leaman's estimates. Note that, as substantial thicknesses of Tertiary sediments underlie the basalt in some drill holes, the base of the basalt does not necessarily correspond to the unconformity with basement.

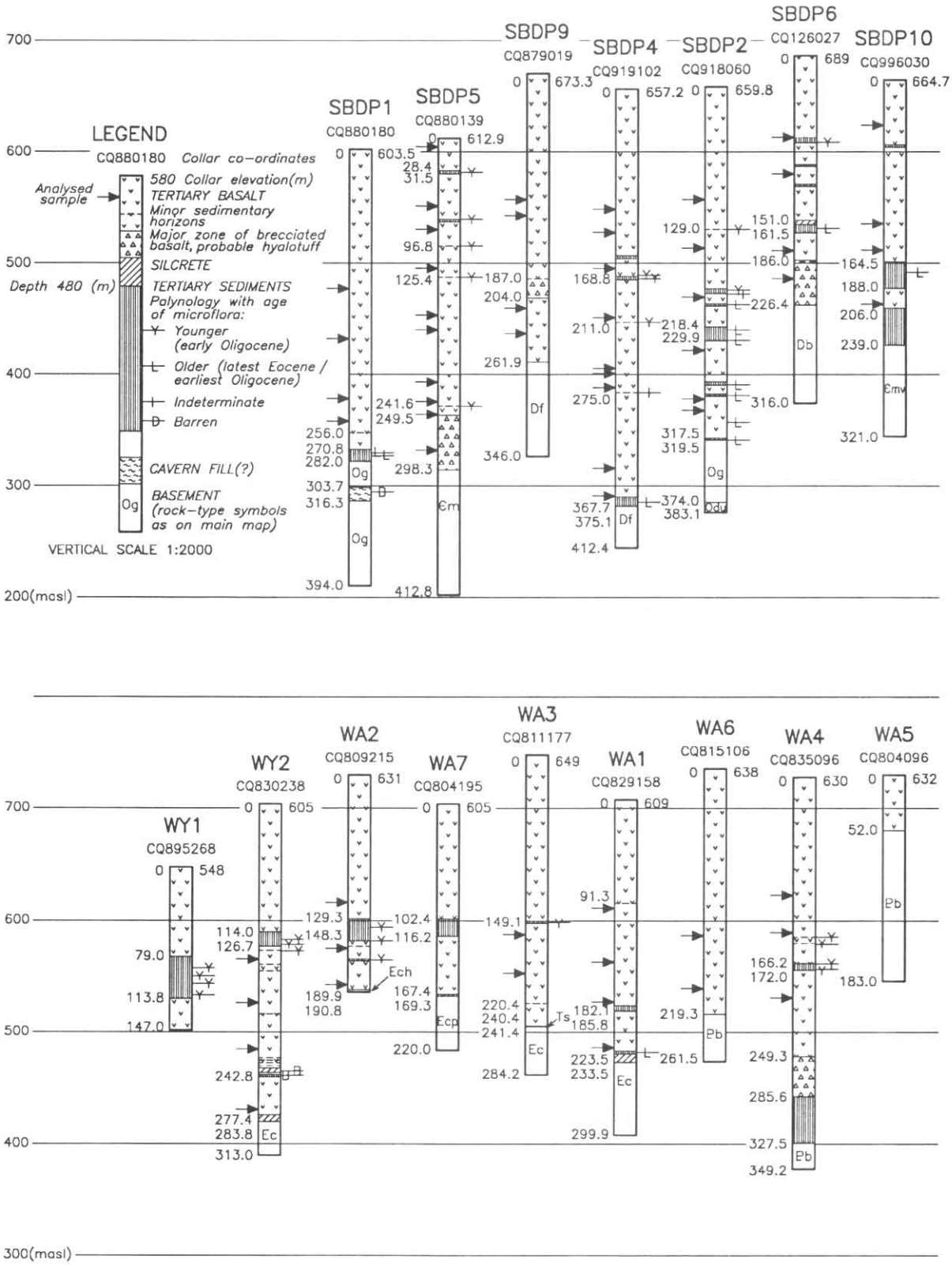

Figure 9. Graphic logs of sub-basalt drill holes, St Valentines Quadrangle and adjacent areas. Data from Baillie (1987*a-c*); Baillie and Green (1988*a-c*), Unpublished data); anon (1983,1984*a-b*).

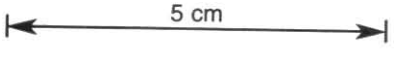

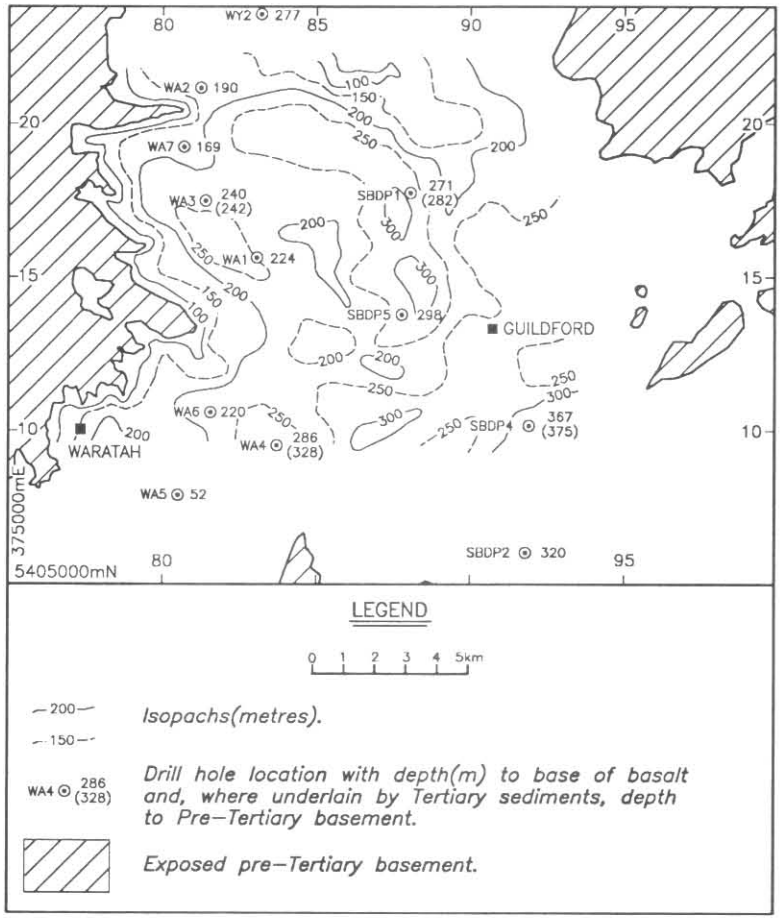

Figure 10. Known and estimated thickness of Tertiary basalt in the Waratah-Guildford area. Contoured estimates from the geophysical interpretation of Leaman (1986).

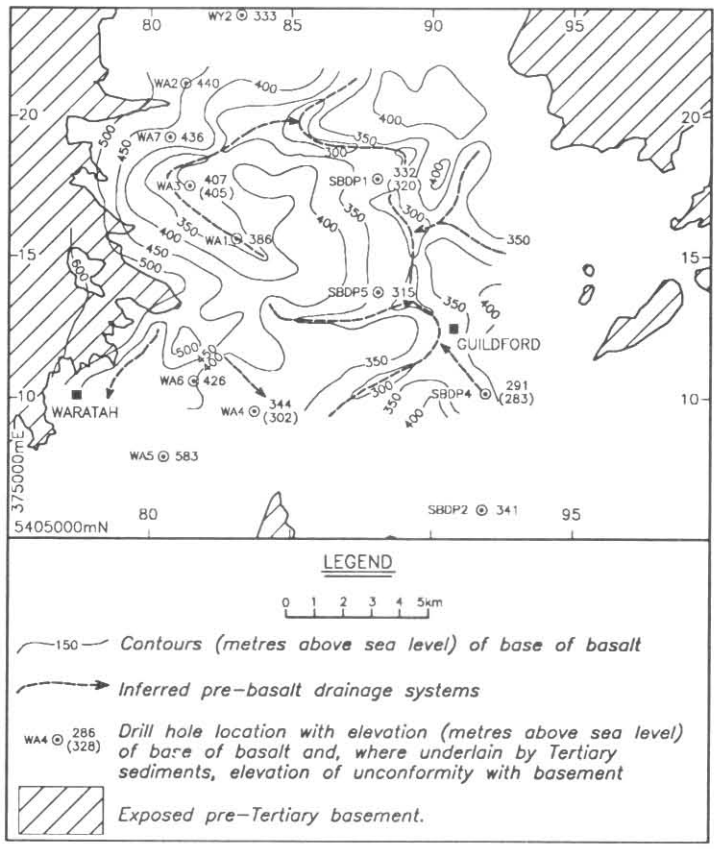

Figure 11. Inferred pre-basalt topography, Waratah-Guildford area. Re-drawn from the geophysical interpretation of Leaman (1986) with additional drill hole data.

5 cm

The above information indicates that, away from the margins and the deeply incised Hellyer valley, the basalt in the south-western corner of the Quadrangle, around Guildford, is usually over 200 m thick. The maximum proven thickness of basalt is 367 m (375 m to basement) in hole SBDP4.

The inferred pre-basalt topography in the Guildford area (fig. 11) had a relief of over 300 m, much greater than the present relief. A basement high of over 600 m above present sea level exists to the west of the area, where the basalt cover thins and disappears. Although the possibility that some deep sediment-filled valleys underlie the basalt precludes any certainty, a major north-south trending drainage system with several tributaries appears to lie just west of Guildford, in roughly the same position as the present-day Hellyer River. The geophysical interpretation gives no indication as to the dip of the main channel, but in the absence of post-basalt faulting or tilting, drainage is likely to have been to the north, as basement occurs at much higher elevations to the south of the basalt, on the Mackintosh Quadrangle. A complex history of valley fill by sedimentation and successive lava flows, with the formation of lakes and drainage diversion, is likely and probably the valley axes shifted several times.

Little information is available on the thickness of the basalt in other parts of the quadrangle. Preliminary results of a drill hole (SBDP15) near Wattle Park Road [CQ993111] indicate a thickness of 134.5 m of basalt overlying Cambrian volcanics (P. W. Baillie, pers. comm.).

In the northern and north-eastern parts of the quadrangle, generally alkaline basalts east of Hampshire and in the Loyetea area surround numerous inliers of basement and are probably relatively thin. They have chemical similarities to some basalts from the lower part of the pile in some drill holes (e.g. SBDP6), but on the other hand may represent a different phase of volcanism altogether.

SUB-BASALT GEOLOGY

Information available from sixteen drill holes which have passed through the basalt into basement (fig. 9) together with the exposed areas of basement shown on the Mackintosh (Barton, *et al.*, 1966) and St Valentines map sheets, enables some inferences to be made as to the underlying geology.

Hole SBDP6 and 9 (Baillie and Green, 1988*a, b*) encountered rocks correlated with the Siluro-Devonian Eldon Group which may be exposed nearby around CQ950010 in an area shown as undifferentiated Ordovician-Silurian siltstone and sandstone on the Mackintosh Quadrangle (Barton, *et al.*, 1966). This indicates that a down-thrown fault block exists between the Cambrian sequence in the Hatfield-Que River area to the south of the basalt and the Ordovician Denison Sub-group correlate of the Mt Pearse-Moory Mountain inlier. The latter appears to extend north-east (SBDP2, Baillie, 1987*b*) to similar rocks exposed on Grasstree Ridge. To the north there is another fault-bounded block of Eldon Group (SBDP4, Baillie, 1987*c*) which also appears to extend north-east to small inliers north-west of Talbots Lagoon and, with cross-faulting, to the Old Park Road area. The main Cambrian volcanic belt lies further east (SBDP10, SBDP15, data unpublished) and is exposed at Two Hummocks. Hole SBDP1 (Baillie, 1987*a*) encountered limestone correlated with the Ordovician Gordon Subgroup, whilst SBDP5 (G. R. Green, pers. comm.) encountered a lithicwacke-mudstone sequence which has been correlated with the Cambrian Dundas Group.

The basement lithologies reached in holes WA1, 2, 3, 7 and WY2 (volcanics, shale, chert and dolomite) and WA4, 5 and 6 (black shale, minor sandstone and dolomite) are correlated with the Eocambrian Crimson Creek Formation and the Precambrian Oonah Formation respectively. They represent extensions of the known rock distribution exposed west of the Murchison Highway, beyond the basalt plateau.

Leaman (1986) has made inferences as to the basement geology in the region north-east of Waratah, based on lineaments and properties interpreted from aeromagnetic and gravity data. A large isolated deep magnetic anomaly near CQ830130 may represent a large basalt feeder, but is considered by Leaman more likely to be a feature of the basement.

In summary, the available drilling results suggest that the basalt was extruded into a Tertiary valley system that had developed on a highly faulted basement, comprising more downthrown blocks of Ordovician-Devonian rocks than was previously suspected.

GENERAL CHARACTERISTICS OF BASALTS

Particularly in regions of subdued topography, the basalt is poorly exposed and much of the area has been mapped from float. Surface samples of fresh basalt are typically dark grey, massive to slightly vesicular or amygdaloidal, fine-grained and speckly to aphanitic rocks in which olivine phenocrysts a few millimetres across and, less commonly, plagioclase microphenocrysts may be visible. The latter are abundant in one outcrop in Lockwood Creek [CQ873280](PGL). Vesicles and amygdales are usually small (mm) and rounded to elliptical but sometimes larger vugs a centimetre or more across are present. Sub-horizontal columnar jointing in basalt was noted in Lockwood Creek [CQ868279, CQ876279] and in a tributary of the East Cam River [CQ907319](PGL).

In drill holes the basalt is more vesicular in general appearance and, probably due to the effect of groundwater, usually more altered (*cf.* chemical analyses, table B2, appendix B). It is typically grey to dark grey, more rarely with a greenish, pinkish or mauve tint. It is sometimes massive, but more often very vesicular or amygdaloidal, with vugs up to 50 mm across. Rarely, elongation and alignment of vesicles and/or amygdales defines a flow direction (e.g. WY2/144 m).

The most common secondary minerals infilling amygdales are montmorillonite (typically blue-black to greenish with a waxy lustre), calcite and members of the zeolite group (table 2). Clear, striated crystals and needles of aragonite were recorded in one sample. The most common zeolite is chabazite ($CaAl_2Si_4O_{12}.6H_2O$), but herschelite ($Na_2Al_2Si_4O_{12}.6H_2O$), phillipsite ($(Na,K,Ca)_2Al_2Si_4O_{12}.4^1/_2H_2O$), heulandite ($CaAl_2Si_7O_{18}.6H_2O$), analcite ($NaAlSi_2O_6.H_2O$), gonnardite ($Na_2CaAl_4Si_6O_{20}.7H_2O$) and thomsonite ($NaCa_2Al_5\ Si_5O_{20}.6H_2O$) also occur. There is no clear zonation of zeolites mineralogy with depth on the data available. Other minerals reported in drill logs but not otherwise positively identified include agate (WY1/114), kaolinite, chlorite, 'iddingsite', 'bowlingite' and serpentine.

Veins of calcite are locally abundant and there are also rare veins of serpentine and chalcedony. Pyrite occurs in the basalt in hole WY2, both disseminated and in fractures. Olivine phenocrysts, where visible, are often altered to 'iddingsite' or 'bowlingite' (names given to poorly defined brown goethitic and green chloritic mixtures, respectively) and plagioclase laths may be altered to kaolinite.

Individual flows of basalt have been identified and logged in hole SBDP5 (Lucas, 1988) and in the fully cored parts of holes WY1, WY2, WA1-4 and WA6-7 (Anon, 1983, 1984*a, b*). A summary of this data is given in Table 3. The thickest flow (30.7 m) measured is the basal flow in hole WY2 (246.7-277.4 m) and consists of massive predominantly coarse-grained black basalt with transitional to mildly alkaline affinities (analysis 830766, table B2). However, many flows are less than one metre thick, with 100 mm being the minimum reported. Most holes have passed through tens of flows, with an average thickness in the range of 2.5 to 10

Table 2
AMYGDALE INFILLINGS IN BASALT

Hole	Depth (m)	Zeolite Group: Calcite	Aragonite	Montmorillonite	Chabazite	Herschelite	Phillipsite	Heulandite	Analcite	Gonnardite	Thomsonite
SBDP1	130.0	...	...	■	...	...	...	...	...	...	...
	141.7	■	...	■	...	■	■	...	...	...	...
	148.3	...	...	■	■	...	...	...	...	...	...
	188.5	...	...	■	■	...	■	...	...	...	...
	240.6	...	...	...	■	...	■	...	...	...	...
SBDP2	90.0	...	...	■	■	...	...	...	...	...	...
	114.4	...	...	...	■	...	...	■	...	...	...
	169.3	...	...	■	■	...	...	...	...	...	...
	275.4	■	...	...	...	...	...	...	...	...	...
SBDP4	138.8	■	...	■	■	...	...	■	...	...	...
	200.2	...	...	■	■	...	...	...	...	...	...
	208.0	...	...	...	■	...	...	...	...	...	...
	322.2	■	...	■	■	...	...	...	...	■	...
	332.0	■	...	...	■	...	...	...	■	...	■
SBDP5	8.8	...	...	■	■	...	...	...	...	...	...
	54.6	...	...	...	■	...	...	...	...	...	...
	64.0	...	...	...	...	...	■	...	...	...	...
	125.1	...	■	...	...	...	...	...	...	...	...
	175.9	...	...	...	■	...	...	...	...	...	...
	178.9	...	...	...	■	...	...	...	...	...	...
	182.9	■	...	...	...	...	...	...	...	...	...
	183.9	...	...	...	■	...	...	...	...	...	...
	192.9	...	...	...	■	...	■	...	...	...	...
SBDP6	90.5	■	...	■	...	...	...	...	...	...	...
	145.4	■	...	...	...	...	...	...	...	...	...
SBDP10	71.0	■	...	■	■	...	...	...	...	...	...
	113.2	■	...	■	...	...	...	...	...	...	...
	117.1	...	...	...	■	...	...	■	...	...	...

Determined by X-ray diffraction by R. N. Woolley.

m. Within any drill hole, there is no systematic variation in thickness, the flows neither consistently thickening or thinning upward. Likewise, it is impossible to correlate individual flows between drill holes, at least on the available data. It is likely that the basalt pile in the main area centred on Guildford is a highly complex, interdigitating and laterally variable sequence of overlapping flows, sediments and pyroclastics.

In the southern part of the basalt-covered area on the Mackintosh Quadrangle, the flows 'form several distinct topographic steps and the margins of multiple sheets form step-like features on the valley sides' (Collins *et al.*, 1981, p.64).

A pinkish or reddish-brown alteration at the top of some flows (e.g. SBDP2/133.8-135.0, 187.6-187.9; SBDP5/38.0-40.0, 69, 90, 128, 150, 163-167; SBDP9/103.5-104.5; SBDP10/116-118 m) is due to weathering and probably indicates subaerial extrusion of the basalt, followed by an appreciable time interval before burial beneath the succeeding flow. On the other hand, zones of brecciation, described below, are probably of hydrovolcanic origin, suggesting locally subaqueous deposition.

Table 3
THICKNESSES OF BASALT FLOWS

Hole	Interval (m)	Thickness (m) Total	Thickness (m) Flows*	No. of Flows	Flow thickness (m) Mean	Median	Max	Min
SBDP5	0-249.5	249.5	246.1	28	8.8	8.4	18.4	2.8
WY1	113.8-147.0	33.2	32.0	13	2.5	2.1	5.0	0.85
WY2	90.0-114.1	24.1	22.5	9	2.5	2.7	5.5	0.45
	126.7-277.4	150.7	123.7	45	2.75	1.3	30.7	0.10
WA1	90.5-182.1	91.6	91.4	16	5.7	5.9	10.8	0.7
	185.8-223.5	37.7	37.7	4	9.4	9.9	13.3	4.7
WA2	103.9-129.3	25.4	24.7	9	2.7	3.4	6.3	0.3
	148.3-190.0	41.6	38.3	13	2.9	1.7	10.8	0.15
WA3	141.6-149.1	7.5	7.5	1	–	–	–	–
	151.5-240.4	88.9	88.3	19	4.6	3.7	13.5	1.25
WA4	87.9-166.2	78.3	77.2	13	5.9	4.3	16.1	1.1
	172.0-249.3	77.3	77.3	18	4.3	3.4	16.0	0.50
WA6	140.0-219.3	79.3	79.3	15	5.3	3.8	20.2	0.8
WA7	72.5-102.4	29.9	29.9	4	7.5	7.0	14.9	1.0
	116.2-167.4	51.2	51.2	15	3.4	3.1	10.3	0.5

* Total thickness of identifiable flows; excludes minor zones of sediments, brecciation, etc.
Data for SBDP5 from Lucas 1988); other data from BHP Exploration Department Reports 83/2026, 84/2085, 84/2295.

BRECCIAS AND PILLOW LAVAS

everal major zones of brecciation are known, from mostly at or near the base of the basalt pile. The only recorded surface exposure is in the Hellyer Gorge section of the Murchison Highway [CQ821287], where a tuffaceous rock below the basalt is composed of scoriaceous basalt fragments and abundant volcanic glass fragments in a basaltic matrix. The rock probably formed as a result of extrusion into water with associated rapid chilling to produce the abundant glass fragments (P.R.W.).

Major intervals of basalt breccia occur in holes SBDP5, 6 and WA4, in each case overlain by more coherent lava flows (fig. 9).

In SBDP5, a remarkably uniform interval of matrix-supported breccia 48.8 m thick consists of sharply defined, irregularly shaped but more or less equant, angular clasts (2-15 mm) of pale yellow-brown glassy basalt, set in a darker green-grey glassy volcanic matrix containing white wisps of calcite (1-3 mm) (plate 5). There are occasional large clasts up to 100 mm long of massive or amygdaloidal, fine-grained basalt, with sharply defined, straight margins (J.L.E., P.W.B.). In thin section (SBDP5/280.8 m), the basalt fragments contain sparse olivine phenocrysts (<1 mm) set in a groundmass of sparse, very fine plagioclase laths (typically 50 × 10 μm) and yellow to yellow-brown, mostly devitrified glass. The matrix between the fragments is very fine and probably also results from the alteration of glass (J.L.E.). Chemically, the rock is an altered tholeiitic basalt (analysis 872682, table B2), and is very similar to the overlying lava flows, except for depleted Ba.

In SBDP6, the breccia is 40.4 m thick and consists of glassy debris and pillow lavas which are often broken with diffuse margins (Baillie and Green, 1988*a*). In thin section (SBDP6/202.8) the fragments are seen to consist of abundant euhedral fresh olivine phenocrysts (typically 500 μm-1.5 mm) set in a dark brown to black, somewhat altered glass which contains rather sparsely distributed narrow plagioclase laths (≤200 μm long) and very small augite and olivine granules (J.L.E.). A chemical analysis (874884, table B2) shows (in contrast to 872681) a strongly alkaline composition which is, however, again similar to that of the overlying flows.

Plate 5. Basalt breccia, probably hyalotuff, consisting of basalt clasts in a matrix of glass and calcite (white). Core from hole SBDP5, depth 269.9 m. Core diameter 46 mm.

In WA4, an interval of weathered, mottled grey-green basaltic breccia is 36.3 m thick. Some fragments are angular and vesicular, and calcite occurs between fragments (Anon., 1983).

Less extensive zones of basaltic breccia have also been recognised. In hole SBDP9, a strongly brecciated interval (187.0-204.0) is characterised by rapid change in lithology, inclusions of sediment and coal, and probable pillow lavas. Brecciation of probable primary origin is also present at SBDP1/214.5, 256 m; SBDP2/182.3-183.5 m, 208 m and SBDP10/99-101.5 m, 204.2-206.0 m (Baillie, 1987*a,b*, unpublished data).

The glassy nature of both the basaltic fragments and the matrix in the breccias indicates rapid quenching and is consistent with subaqueous chilling of the magma, either because it was erupted beneath water or because subaerially erupted flows entered water. Such an environment is consistent with the associated pillow lavas identified in SBDP6, and the non-marine, probably lacustrine sediments intercalated in the basaltic pile (see below).

The cause of the brecciation is less certain. A variety of processes are capable of producing fragmental deposits during subaqueous volcanism (e.g. Cas and Wright, 1984; Kokelaar, 1986; Wohletz, 1986). In this case, the glassy nature of the breccia suggests two possible mechanisms:

(1) phreatomagmatic (steam) explosivity, caused by the interaction of hot magma and an external body of water or water-saturated sediments,and the consequent explosive expansion of steam. This process is effective only at relatively shallow depths of probably less than a few hundred metres, and may also require a vigorous dynamic contact of water with magma, as high impact velocity or the action of surface water waves in the surf zone (Kokelaar, 1986). The debris produced by these processes is termed *hyalotuff* (Honnorez and Kirst, 1975).

(2) quench fragmentation, a non-explosive process in which rapid cooling produces thermal and tensile stresses, causing fragmentation. This process has also been called chill-shatter fragmentation (Cas and Wright, 1982) and cooling-contraction granulation (Kokelaar, 1986). It can occur in any depth of water, and is often associated with pillow lavas. The products are termed *hyaloclastite* (Rittmann, 1962).

The breccias intersected in drill holes have been called hyaloclastics (Baillie, 1987*a, b*, Baillie and Green, 1988*a, b*) but Baillie (pers comm.) considers them to be the result of phreatomagmatic explosions. Honnorez and Kirst (1975) suggest morphological criteria to distinguish true hyaloclastites of quench origin from material of explosive origin (hyalotuffs). Fragments in which more than 20% of the perimeter is planar rather than concave or convex are likely to be of quench origin. A cursory examination of the drill core strongly suggests that the breccias are of explosive origin and thus should be termed hyalotuffs. However, there is scope for a more detailed sedimentological study.

Pillow lavas are formed by non-explosive subaqueous volcanism, and require conditions of low magma viscosity (usually a basaltic composition) and high water/magma ratios. In this case, the magma becomes insulated from the cold water by either a quenched skin of chilled glass, or by a superheated layer of water vapour (Leidenfrost effect). They propagate by chilling to produce a glassy skin, rupture of the skin, and advance of fingers of lava (e.g. Moore, 1975; Williams and McBirney, 1979; Mills, 1984; Kokelaar, 1986).

PYROCLASTIC DEPOSITS

In the Hellyer River [CQ846243], basalt is underlain by about 10 m of basaltic tuff, consisting of fragments of vesicular to massive basalt up to 600 mm long, chert fragments and a tuffaceous matrix. Many fragments are extremely rich in plagioclase laths, their grain size varying between fragments. There are also rare fragments with dispersed feldspar laths and anhedral phenocrysts set in opaque glass. The matrix of the tuff is fine-grained and altered to a reddish-brown colour. Its composition cannot be determined optically, although some fine granular aggregates of a mineral with second-order interference colours may be amphibole (P.R.W.).

In hole WA7, 1.9 m of fine-grained dark green tuff was encountered beneath the basalt (167.4-169.3), just above a 200 mm coal seam resting on the unconformity with Cambrian basement. Accretionary lapilli are present in the tuff, suggesting an air-fall origin (Anon., 1984*a, b*).

Coarse-grained basaltic tuff is present within the basalt pile between 91.0-91.9 m in hole SBDP5 (P. W. Baillie, unpublished data).

SEDIMENTS AND SEDIMENTARY ROCKS (Ts)

Layers of Tertiary sediment, usually quite thin but sometimes tens of metres thick, often occur between basalt flows or beneath the basalt pile, resting on basement. Surface exposures are relatively rare, but have been depicted on the map where possible. The sediments vary greatly in grain size

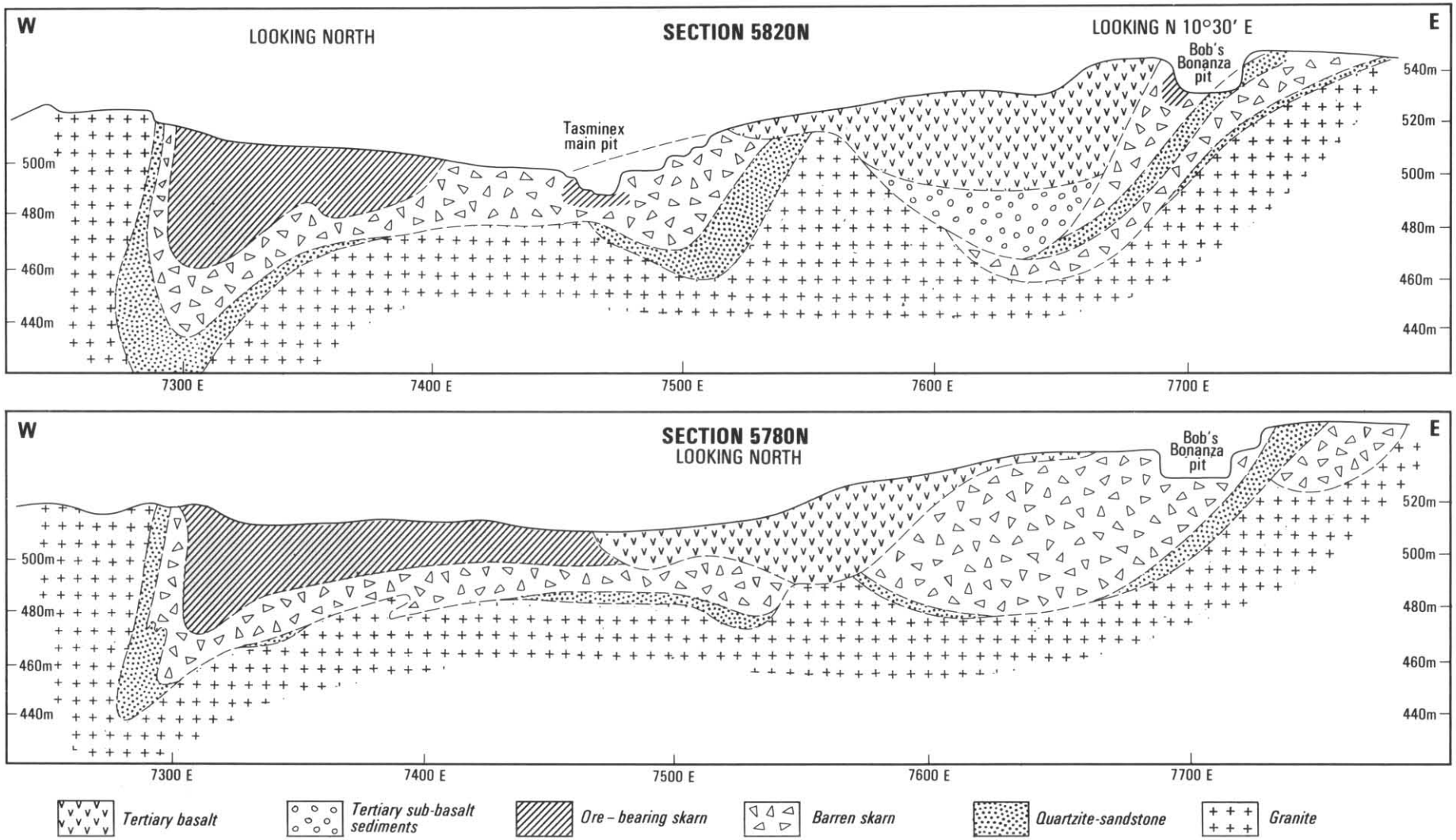

Figure 12. Interpretive geological cross sections, Kara No. 1 [CQ975258] to Bob's Bonanza [CQ977258]. (P.G.L., redrawn D.B.S., from draft by C. Whitehead, McIntyre Mines, October 1980).

5 cm

and degree of lithification, Carbonaceous siltstone, mudstone and claystone are most common, but conglomerate, basaltic sandstone, shale, gravel, sand, silt and clay have also been noted. Plant material is common and rare coal, lignite and peat occur. Silcrete (Tss) is discussed in the following section.

Near Mt Bischoff [CQ765116] steeply dipping sand and gravel up to 30 m thick underlies the basalt (P.R.W.). These deposits have been described by Groves and Solomon (1964) as locally derived conglomerates and gravels overlain by siltstone and sands. In the Waratah River, carbonaceous siltstone and occasional lignite occurs at the base of Waratah Falls (P.R.W.). Leaf impressions are present and microfossils indicate a late Oligocene to early Miocene age, according to Harris (1968, 1973). However, recent refinements to the palynological time scale suggest an early to late Oligocene age (S. M. Forsyth, pers. comm.).

Carbonaceous siltstone underlies the basalt at Wandle River [CQ806209]. A lens of similar carbonaceous siltstone with abundant leaf fossils also underlies the basalt on the western side of the Hellyer River valley near Parrawe [CQ840270] and extends for 3 km to the south [CQ838240] where it lies within the basalt. This suggests that an earlier phase of valley-filling basalt flows was followed by a much more extensive phase covering much of the area (P.R.W.). Siltstone samples from CQ838262 and CQ836242 contain spores indicating an Oligocene, probably early Oligocene age (Brown and Forsyth, 1984).

A mudstone bed 4 m thick, containing fossils of a fern-like plant, occurs beneath a basalt cap 5 m thick in a tributary of the Hellyer River at CQ857250. Intrabasalt mudstone is also exposed nearby in the Basil Road extension [CQ876277] (P.G.L.). Samples from both these localities also yielded an Oligocene microflora (Brown and Forsyth, 1984). Sediments were intersected at about the same elevation (450-500 m) to the west in drill holes WY2 (brown sericitic mudstone, sand, silt), WA2 (mudstone, clay, silt, gravel), WA7 (dark green to light grey laminated mudstone) and WA3 (mudstone) (Anon., 1983, 1984*a, b*). These also contain a similar microflora to that from the Hellyer River and Basils Road outcrops, and may represent parts of the same lake deposit (Brown and Forsyth, 1984).

A small creek draining Snowdon Plains south into the Hellyer River contains a boulder of laminated chocolate-brown claystone, 2-3 m thick and 5 m long. Float of micaceous mudstone occurs in the upper reaches of the East Cam River above its intersection with the Lockwood Creek Road [CQ893299]. Near Douglas Brook [CQ882313] a flat-lying white to pale grey mudstone with distinctive conchoidal sub-horizontal jointing occurs in isolated outcrop over a distance of about 750 m at the same elevation (P.G.L.).

Near the junction between the Lockwood Creek tributaries [CQ870281] two beds of micaceous mudstone 0.5 m thick are separated by a basalt rich in white feldspar phenocrysts and with joint fillings of epidote. Columnar-jointed basalt both underlies and overlies the mudstone beds. In the same area [CQ872283] numerous, in places plant-bearing, micaceous mudstone units up to 6 m thick have been observed (P.G.L.).

Drill hole WY1 intersected 34.8 m of light brown finely sericitic mudstone with abundant plant material, both overlain and underlain by basalt (Anon., 1984*a*).

The contact between Eocambrian or Early Cambrian greywacke and Tertiary basalt is exposed in the Hellyer River tributary at CQ857251, and marked by a well rounded quartz pebble conglomerate 2 m thick. Sub-basalt river gravels, sand and ferricrete (Tsf) have been identified by G. R. Green in the central northern part of the Quadrangle. Sub-basalt deposits, principally gravel, sand and minor clay, are notable in drill holes SBDP1, 4, 10 and WA4. In hole WA4, approximately 32 m of grey mudstone and light brown siltstone with chert pebbles is underlain by 10 m of gravel containing rounded quartzite and black shale clasts of Precambrian origin, resting on Precambrian basement (Anon., 1983).

Near the Kara No. 1 mine [CQ975258] extensive drilling has revealed probable Tertiary sediments underlying Tertiary basalt. The drilling has also shown the marked relief of the granite contact (up to 100 m) (P.G.L., see fig. 12).

In the southeastern part of the quadrangle, fossil logs are preserved in well-bedded sands and gravels exposed in the Leven River at DQ024098 (P.W.B.).

An interval of 3.1 m of an unconsolidated organic rich peaty horizon, sandy in its upper parts, occurs within the basalt in the upper part of hole SBDP5 (P.W.B.).

Brown clay and silty clay, encountered within Gordon Subgroup limestone in hole SBDP1 between 303.7 m and 316.3 m, is possibly a cave deposit. However, no palymorphs were found and thus its age remains indeterminate (Baillie, 1987*a*).

SILICIFIED QUARTZOSE SEDIMENTS (GREYBILLY - ?Tss)

Areas of this rock type are shown on the map at two localities, north of Loyetea Peak [DQ127270] and west of Mt Everett [DQ038201]. The rocks consist of pink or white coloured, fairly well sorted, commonly open-framework pebble conglomerate in which bedding is almost impossible to detect. They are highly siliceous and may have an almost conchoidal fracture. Because of their proximity to basalt they are probably silicified sub- or intra-basalt deposits (P.W.B.).

A similar interpretation has been applied to cemented breccia and siliceous conglomerate directly underlying the basalt at CQ770320 and CQ771182 in the western part of the quadrangle (P.R.W.).

In drill hole SBDP6 similar pinkish-coloured, very hard silicified conglomerate was encountered between 151.0 and 154.1 m, overlying 7.4 m of soft, grey-brown silt and clay. The silicification is clearly diagenetic and is related to the high permeability of the original gravel, in contrast to the underlying unaltered silt and clay which are relatively impervious to groundwater movements (Baillie and Green, 1988*a*).

Rocks logged as 'silcrete' were also encountered in drill holes WY2 and WA1. In both cases, several metres of silcrete associated with clay and silt rest on the unconformity with pre-Tertiary basement, and probably also represent silicified Tertiary gravels. Several thinner layers of 'silcrete' also occur within the basalt in hole WY2, between 230 and 240 m (Anon., 1983, 1984*a*).

These rocks could be termed greybilly because of their spatial relationship to basalt; the term silcrete is usually applied to similar material produced by deep weathering or pedogenesis.

PALYNOLOGY

The palynology of Tertiary sediments from St Valentines Quadrangle has been studied principally by S.M. Forsyth (in Brown and Forsyth, 1984) and by R. Morgan (in Baillie, 1987*a, b, c*; Baillie and Green, 1988*a, b*; unpublished data). Sample localities in each drill hole are shown in Figure B1. Two distinct microfloras of slightly differing age are present.

The older microflora is usually dominated by *Nothofagidites* spp., although locally *Cyathidites* spp., *Ischyosporites gremius* and *Phyllocladidites mawsonii* are also abundant. The assemblages are of low diversity but sufficient to allow assignment to the upper *Nothofagidites asperus* zone of the Gippsland and Bass Basins, which is of latest Eocene to

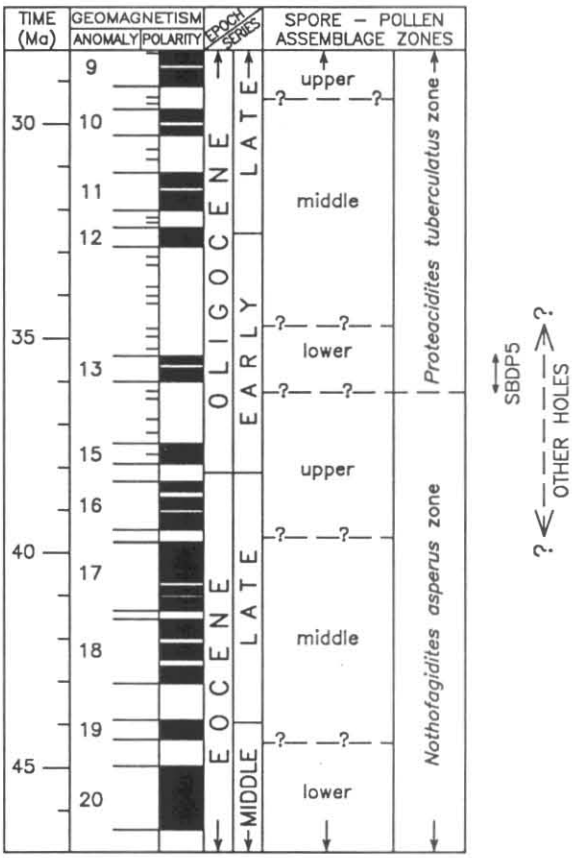

Figure 13. Constraints on the age of the Tertiary basalts. Absolute and geomagnetic time scale after La Becque *et. al.* (1977). Black blocks indicate normal polarity, white blocks indicate reversed polarity. Short lines refer to shorter events or intensity fluctuations. Spore-pollen assemblage zones after Partridge (1976).

earliest Oligocene age (fig. 13). Non-marine environments are indicated by the abundance of pollen and spores and the absence of marine indicators. Lacustrine environments are suggested at SBDP1/274.2-276.0 m and SBDP2/318.9, in sub-basalt sediments, by the presence of non-marine dinoflagellates (*Saeptodinium tasmaniense* and *?Trithyrodinium* sp.) and the freshwater alga *Botryococcus*. Spore colours are generally yellow, indicating immaturity for hydrocarbon generation. Locally darker brown to black assemblages are attributed to the local heating effects of the basalts.

The younger microflora is also dominated by *Nothofagidites* spp. and is of low to moderate diversity. It is characterised by the presence of *Cyatheacidites annulatus* which, together with other palymorphs, assign the assemblage to the lower *Proteacidites tuberculatus* zone (fig. 13) assuming that the zonal system developed by Stover and Partridge (1973) for the Gippsland Basin is applicable to Tasmania. An Oligocene, probably early Oligocene, age is indicated. Non-marine environments are indicated by the absence of marine indicators and the local presence of non-marine dinoflagellates and the freshwater alga *Botrycoccus*. Maturity for hydrocarbon generation, as indicated by spore colour, is very variable, probably also due to the effect of the basalts. Full details of sample localities and palymorphs identified are available in the reports quoted above.

In summary, the available palynological data indicate that the basaltic volcanism commenced in upper *N. asperus* zone time, but most of the basalt was extruded in lower *P. tuberculatus* zone time. According to the palynological time scale of Partridge (1976) this corresponds to an age of latest Eocene to Oligocene, probably early Oligocene (fig.13).

PALAEOMAGNETISM

Lucas (1988) has investigated in the laboratory the magnetic properties of 58 basalt samples taken from the core of hole SBDP5. Samples taken from the lower part of the hole, at depths ranging from 249.5 m to 152.0 m, corresponding to flows 1 to 11, are mostly reversely magnetised (i.e. exhibiting thermal remanent magnetism implying a geomagnetic field at the time of cooling that had an opposite polarity to that at present). The exceptions, which show normal polarity, are from 194.9 and 195.9 m, both from flow 7. Samples from the upper part of the hole, at depths above 152.0 m, corresponding to flows 12 to 28, all show normal polarity (Lucas, 1988).

When combined with the palynological data this information defines the age of the basalts in terms of the known geomagnetic time scale for the Cainozoic (La Brecque *et al.*, 1972). Palymorphs from intrabasalt sediments at 241.6 m (between flows 1 and 2) and at 30.7 m (between flows 26 and 27) both indicate an early Oligocene lower *P. tuberculatus* zone age (R. Morgan, unpublished data). According to the time scales of La Brecque *et al*, (1979) and Partridge (1976), only one reverse-to-normal polarity change, at 35.9 Ma, occurs in this interval (fig. 13). Thus the reversely magnetised basalt from 152.0 m to at least 241.6 m depth is correlated by Lucas with the reverse polarity event prior to magnetic anomaly 13, with the normal polarity observed in hole 7 probably corresponding to one of the two short events shown in Figure 13. The basalt from 152.0 m to at least 30.7 m depth is correlated with magnetic anomaly 13. There is evidence that flow 1, below the lowest dated sediment, and flows 27 and 28, above the highest dated sediment, are nearly contemporaneous with the rest of the basalt. On the other hand, the age of the underlying breccias below 249.5 m depth is uncertain; they may be significantly older than the overlying flows. The breccias have negligible remanent magnetisation (Lucas, 1988).

Assuming that Lucas's interpretation is correct, probably all flows in hole SBDP5 were extruded in a short interval between the base of the *P. tuberculatus* zone at about 36-36.5 Ma and the end of anomaly 13 at 35.3 Ma. However, the applicability to Tasmania of the palynological time scale of Stover and Partridge (1973), which is based on work in the Gippsland Basin, is questionable. It is uncertain whether the subdivisions of the *P. tuberculatus* zone defined there are recognisable in Tasmania, and by no means certain that they are of the same age. In particular, it is possible that the microflora assigned to the *P. tuberculatus* zone extends to younger ages. Thus the magnetic reversal observed at 152.0 m depth could represent the base of anomaly 13, 12, 11 or 10 and thus be as young as 30.0 Ma (Late Oligocene) (A. D. Partridge, S. M. Forsyth, pers. comm.). There are also doubts as to the precision of the geomagnetic time scale, since it is based on interpolation between 3.32 Ma and 64.9 Ma, assuming a constant rate of sea-floor spreading (La Brecque *et al.*, 1977). Unfortunately, basalt from the drill cores is invariably deuterically altered, and none suitable for radiometric dating, either in SBDP5 or the other holes, was seen (P. W. Baillie, pers. comm.).

Lucas (1988) also discusses the implications of the magnetic properties of the basalt for aeromagnetic surveys.

Quaternary

The Quaternary deposits of the St Valentines Quadrangle comprise deposits of glacial and glaciofluvial, periglacial, and fluviatile origin. Of note is the previously unrecorded recognition of till in the Leven River in the Gunns Plains area. Because of the lack of good sections a reliable stratigraphic framework cannot be erected.

TILLS

P. W. Baillie

Deeply weathered till (Qpw)

Deeply weathered deposits, interpreted as till, occur at several localities in the Leven Valley, from near Mt Tor [DQ067150] to the Gunns Plains area [DQ288162] on the eastern edge of the Quadrangle.

The deposits usually consist of very poorly-sorted, often angular clasts of very varied composition but including limestone, quartzite, siliceous conglomerate, felsic volcanic rocks and basalt, in a clay matrix. The clasts are often matrix-supported and the deposits are deeply weathered. The nature of the deposits strongly suggests that they are till and the degree of soil development suggests that the deposits are significantly older than the Last Glacial Stage.

Younger till (Qpg)

Paddys Lake [DQ132105] is dammed by a small moraine some 200 m in length. The moraine is composed of bouldery till derived from the nearby siliceous conglomerate sequences. The lake is formed in an amphitheatre-like depression that is considered to be a cirque.

This single occurrence is the only evidence of glaciation considered to belong to the late Last Glacial Stage known from the St Valentines Quadrangle.

OLDER ALLUVIUM (Qpa)

P. W. Baillie

The valley of the Leven River, from McHughs Flats [DQ096165] to the flats near Leven Cave [DQ160156] and also in the Gunns Plains area [DQ154265], contains large deposits of alluvial material that are currently being incised by the river. Near Mostyn Hardy Cave [DQ143146] these deposits are observed to overlie deeply weathered till.

The deposits range from coarse, often pebbly, sand to gravel composed of cobbles and occasionally boulders. Imbricate structure is very commonly developed in the gravels.

The deposits were clearly formed during periods of higher flow than those which occur at the present time but the time of formation remains conjectural.

SLOPE DEPOSITS (Qpt)

P. W. Baillie
P. R. Williams

Periglacial slope deposits are extensively developed in the mapped area and have been differentiated according to dominate clast type present.

On the eastern edge of the Quadrangle on the South Riana Road [DQ163295] basalt scree was observed to overlie deeply weathered till (P.W.B.).

Slope deposits are particularly well-developed on the dominantly E-facing slopes of the hills immediately to the west of the Leven River in the Gunns Plains area [DQ140280]. The total thickness is unknown but must be of the order of several tens of metres (P.W.B.).

Bedded screes are present in the Cattley Creek area [DQ032088], together with large amounts of apparently massive scree (P.W.B.).

The slope deposits described above are all relatively unweathered and are considered to have formed in the Last Glacial Stage.

In the Arthur River valley in the western part of the Quadrangle (P.R.W.), several small areas of slope deposits consisting of well sorted platy fragments of early Cambrian rocks with a local dip of up to 25°, are probably also periglacial slope deposits. Clay deposits are also present, interbedded with gravel which may represent outwash deposits. These have not been studied in detail. Vegetated scree deposits adjacent to Parrawee Creek may also represent deposits formed in a colder climate with less vegetation cover.

HOLOCENE DEPOSITS

Areas of alluvium associated with currently active streams are present in various parts of the Quadrangle. These deposits reflect local derivation and vary accordingly in their characteristics.

Marsh and swamp deposits are also directly related to present day drainage systems and are thus Recent. In the Waratah and Arthur Rivers, thick deposits of sand and gravel occur as a direct result of deposition of tailings generated from Magnet mine and the Mt Bischoff mine (P.R.W.).

METAMORPHISM

Contact metamorphism and metasomatism

P. W. Baillie
P. G. Lennox

Thermal metamorphism of the country rock and metasomatism of some limestone sequences accompanied emplacement of the Devonian Housetop Granite, and produced contact metamorphic aureoles and skarn respectively. In areas where limestone was metamorphosed, wollastonite-bearing calc-silicate hornfels was produced. These various effects on country rock have been differentiated on the map by overprints.

In non-limestone sequences the criterion used to delineate the metamorphic aureole was the presence of spotting in pelites, and to a lesser extent hornfelsing of sandstone sequences.

Magnetite-bearing skarn (after limestone) occurs in areas surrounding the Kara No. 1 mine [*c.* CQ975260] and the Kara No. 2 prospect [*c.* DQ025253], and also crops out poorly in the Peak Hill Farm area [DQ101258].

Mills (1971) has extensively dealt with the mineralogical changes resulting from the granite intrusion so these will be only briefly summarised.

The Cambrian sedimentary rocks on Black Pit Road and PMG Road have been metamorphosed and metasomatised by the granite. Many horizons in the pyritic metasiltstone and metasandstone unit on Black Pit Road [CQ952228] show spotting. Some horizons in the sequence elsewhere on Black Pit Road are also spotted. The 'augen-hornfels' outcrop on Black Pit Road [CQ954222] consists of ?tremolite-actinolite, epidote, diopside, scapolite and carbonate minerals, typical of a contact metasomatic rock. More calcareous units in the Cambrian sequence have been metasomatised and metamorphosed to skarn [CQ943237, CQ955222].

The conglomerate cropping out on Kara Mine Road has been altered to a less siliceous, friable rock by the adjacent granite.

The Cambrian sedimentary rocks appear to have been metamorphosed to at least hornblende-hornfels facies. Andradite garnet occurs in samples from the Kara Mine magnetite skarn, indicating even higher-grade facies.

The granite intrusion appears likely to have caused the scheelite mineralisation at Kara (Wolff, 1978).

The Gordon Subgroup correlate, Moina Sandstone correlate and Bell Shale correlate have all been altered at least in part due to the granite intrusion.

IGNEOUS ROCKS

?Eocambrian-?Early Cambrian

A. V. Brown
P. R. Williams

PILLOW BASALTS (Ecp)

Stratigraphic relationships within the ?Eocambrian-?Early Cambrian succession have been discussed in the Stratigraphy section herein. The basaltic rocks are dominated by pillow lavas, samples of which are equigranular to porphyritic with small phenocrysts of plagioclase and pyroxene. In thin section the phenocrysts are set in an intersertal groundmass of feldspar laths, pyroxene crystals and chlorite. Chlorite is light green with anomalous interference colours, and forms irregular patches partially enclosing both pyroxene and plagioclase grains. Pyroxene grains are normally subhedral and colourless with a biaxial positive figure, and an extinction angle of 37°, indicating augite. The pyroxene phenocrysts are usually twinned. Plagioclase phenocrysts are albite, based on extinction angles of combined Carlsbad-albite twins, and are similar to the groundmass plagioclase. Plagioclase phenocrysts range in size up to one millimetre in the groundmass but are usually around 0.2 mm. There are abundant opaque grains, partly altered to leucoxene, evenly scattered throughout the rock.

Basaltic lapilli tuff beds are poorly sorted, but totally composed of rounded fragments of basalt identical to that described above. The clasts have a fine-grained matrix which is dark grey under crossed nicols. The basalt fragments are variable in size, and range up to 20 mm across. Because the matrix of the tuff is composed entirely of crystals derived from basaltic magma and the groundmass of the crystals is very fine-grained, it is inferred that these rocks are probably auto-brecciated flows in which the fine-grained groundmass is probably devitrified basaltic glass.

Chemical analyses of four basalt samples from areas of Ecp are presented in Table 4, columns 1-4. When compared to other basalt samples taken from the 'Luina Beds and correlates in the Luina area', (Rubenach, 1973; Collins, 1983) they have a similar chemistry and strengthen the correlation proposed on lithological grounds and lateral continuation, of successions in the St Valentines Quadrangle with those to the west in the Luina area.

MAFIC INTRUSIVES (Em)

Intruding the greywacke-mudstone-chert-basalt (Ec, Ecp) succession in the Waratah River-Belmont Creek area [CQ770180], are several elongate bodies of mafic and ultramafic rocks (Em and Es). The intrusions are spatially related, but otherwise the relationship between the intrusive rocks is unclear.

The mafic intrusives (Em) occur as elongate, coarse-grained basaltic to doleritic bodies. One body, to the south of Deep Gully Creek [CQ755177] cross-cuts a chert bed of the Ec succession at a low angle. Other bodies in the area around Mine Creek and Belmont Creek, and a large outcrop in Anne Creek, have boundaries discordant with bedding in the surrounding rocks. North of Belmont Creek, fine-grained material occurs in continuity with material of doleritic grain-size, implying the presence of a chilled margin. The bodies are inferred to be dykes, although the possibility that some may be sills cannot be ruled out. The relationship between the basaltic-doleritic dykes and the ultramafic rocks could not be determined, although they are intruded in the same structural position.

The mafic intrusive rocks range in texture from basaltic with a grain size of about 0.02 mm, to doleritic with a grain size of about 2 mm. Rare gabbroic rocks are present with a 5 mm grain size. The fine-grained basaltic rocks are composed of patches of chlorite, large pyrite grains and abundant small anhedral grains of pyroxene which tend to aggregate in patches, in a matrix of altered laths of plagioclase. These are much more altered rocks than the basalts interbedded with the sedimentary rocks (Ecp), and the presence of fine-grained granular aggregates of small pyroxene grains has not been observed in the pillow lavas. Rare altered feldspar phenocrysts (plagioclase) are present and rare augite rosettes also occur.

The coarse-grained varieties contain subhedral augite crystals in a matrix of truncated feldspar laths (intergranular texture). Large chlorite phenocrysts with prismatic habit are clearly pseudomorphs of another ferro-magnesian mineral (sample 78-383). Other samples tend to be ophitic to sub-ophitic, and tremolite occurs as fibrous aggregates in anhedral patches. Rocks of intermediate grain size show less well-crystalline pyroxene. Very altered samples are common and are composed dominantly of chlorite and feldspar (albite) with abundant opaque minerals, crossed by veins of tremolite and of recrystallised fresh albite, and containing sericitic patches. The absence of this type of alteration in the basaltic lava flows in the sedimentary rock sequence suggests that it may be primary or deuteric alteration.

Chemical analyses of four samples of these mafic dykes are given in Table 4, columns 5-8. Petrographically and chemically similar rocks are found in the Cleveland and Dundas areas (Rubenach, 1973; Creenaune, 1980; Brown, 1986). In these areas they are described as low-titanium tholeiitic basalts and due to their interdigitation with basal Dundas Group conglomerate flows in the Ring River, are considered to be of middle-Middle Cambrian age (Brown 1986).

ULTRAMAFIC ROCKS (Es)

Field occurrence

Three main bodies and one smaller body of ultramafic rocks crop out in the Belmont Creek-Arthur River area. They occur as lensoidal bodies parallel to the regional bedding direction. Where the margins are exposed, they are sub-parallel to bedding. The northernmost body of ultramafic rock has a faulted margin on its northern side with mudstone of the country rock succession (Ec). The mudstone is highly fractured, the fractures being filled with quartz, or quartz and a mineral resembling stilpnomelane. There is no abundant permeation of quartz/stilpnomelane veins away from the contact zone with the ultramafic intrusion, which suggests that the emplacement event and vein formation may have been synchronous. The mudstone also contains abundant opaque minerals which are offset by the quartz veins. The opaque minerals are elongate in the cleavage direction, and the parts of the rock lying between fractures have been rotated, producing partial disorientation of the cleavage. This suggests that the fracturing and vein formation occurred after the main cleavage forming event. The veins are not folded and do not appear to be affected by the cleavage, suggesting that they are post-cleavage veins.

On the southern edge of the southernmost of the three main ultramafic bodies a sequence of greywacke beds with spotted pelitic tops crops out. Contact metamorphism of the sedimentary rocks indicates that the ultramafic body was intruded while still hot. The spots are deformed into diamond-shaped lozenges parallel to cleavage, hence metamorphism occurred prior to Devonian deformation. There are no other nearby igneous bodies, indicating that the contact metamorphism was due to the magma from which the ultramafic rocks formed. Poor exposure away from road sections does not allow a metamorphic aureole to be mapped out.

Table 4
WHOLE-ROCK MAJOR AND TRACE ELEMENT ANALYSES OF Ecp *AND* Em

	1	2	3	4	5	6	7	8
Reg. No	85-0019	85-0020	85-0021	84-0022	85-0037	85-0038	85-0039	85-0761
SiO_2	46.6	47.44	50.0	47.80	52.69	49.55	50.97	50.3
TiO_2	1.7	3.38	1.0	1.95	0.55	0.39	0.25	0.39
Al_2O_3	14.2	12.31	13.3	13.26	13.26	14.15	13.56	14.0
Fe_2O_3	3.3	9.15	2.5	3.09	5.54	3.78	3.55	3.1
FeO	9.2	4.67	8.0	9.68	7.41	7.10	7.41	6.9
MnO	0.22	0.27	0.19	0.18	0.19	0.18	0.18	0.20
MgO	7.5	5.54	8.2	6.34	5.00	7.55	6.79	7.7
CaO	9.7	7.89	9.1	8.83	6.34	8.65	10.27	8.6
Na_2O	2.8	3.39	2.2	3.33	5.18	2.82	3.83	3.7
K_2O	1.0	0.86	0.53	0.22	0.17	0.21	0.34	0.28
P_2O_5	0.07	0.36	0.16	0.21	0.07	0.06	0.05	0.03
L.O.I.	4.06	3.67	4.80	4.10	2.65	4.77	3.37	4.60
Total								
Mg*	52	43	59	48	42	56	53	59
Cr	171	146	289	153	81	295	81	258
Ni	103	79	106	92	63	104	73	119
Sc	41	33	41	35	54	56	33	51
V	390	420	320	360	370	290	420	280
Rb	20	8	12	4	4	5	10	4
Ba	710	950	145	350	140	130	950	410
Sr	484	288	147	222	210	171	107	226
Nb	4	15	4	7	4	4	4	4
Zr	111	216	80	111	22	17	9	5
Y	22	33	25	20	18	14	8	15

Columns 1-4: Pillow and massive basalts from the Ec succession.
Columns 5-8: Low-titanium basalts which intrude Ec.
Mg* = 100 Mg/(Mg+Fe+): Fe+ = Fe as FeO.
See Table 10 for location and sample details.
Analyses done by Department of Mines Analytical Laboratory Launceston.

Table 5
WHOLE ROCK MAJOR AND TRACE ELEMENT ANALYSES OF PICRITIC LAVAS AND Es

	1	2	3	4	5	6	7
Reg. No.	85-0766	85-0767	KI(8)	85-0762	85-0765	85-0763	85-0765
SiO_2	36.84	37.97	46.97	38.34	38.64	40.38	40.84
TiO_2	0.27	0.40	0.27	0.03	0.03	0.04	0.05
Al_2O_3	7.30	8.75	10.21	4.41	4.34	5.42	5.40
Fe_2O_3	1.93	2.01	2.95	5.23	3.47	3.12	3.02
FeO	5.60	6.49	7.01	5.28	5.51	5.81	6.49
MnO	0.13	0.16	0.19	0.15	0.16	0.17	0.16
MgO	22.58	23.51	17.64	31.89	32.94	31.04	32.42
CaO	7.43	5.43	9.72	4.26	4.05	4.11	4.15
Na_2O	0.42	0.23	1.19	0.03	0.10	0.07	0.21
K_2O	0.01	0.06	0.20	0.03	0.07	0.06	0.07
P_2O_5	0.05	0.05	0.03	0.01	0.02	0.02	0.03
CO_2	3.50	0.34	0	0.26	0.37	0.28	0.36
H_2O^-	5.18	4.28	3.4†	0.67	0.66	0.71	0.55
H_2O^+	8.52	8.27	0	8.93	8.65	7.88	5.71
Total							
Mg*	85	83	76	85	87	87	86
Cr	2800	2800	1975	3698	4249	4093	4360
Ni	1300	1150	693	1621	1703	1616	1657
Sc	20	28	37	17	17	19	19
V	105	145	180	68	69	83	81
Rb	6	6	9	4	4	4	4
Ba	25	27	204	13	9	42	29
Si	81	31	39	27	15	21	28
Nb	3	3	-	4	4	4	4
Zr	10	16	11	4	4	4	4
Y	8	13	12	4	4	4	4

Column 1-2: Picritic lavas.
Column 3: Average of eight analyses of picritic lava samples from King Island. Waldron et al. (1988), table 2, columns 1-8.
Columns 4-8: Ultramafic rocks.
See Table 10 for location and sample details.
Mg* = 100 Mg/(Mg+Fe+) Fe+ = total Fe as FeO.
† = Loss on ignition.
Analyses, with the exception of column 3, done by the Department of Mines Analytical Laboratory, Launceston.

Table 6
CHEMICAL ANALYSES (OXIDE MASS %) AND STRUCTURAL FORMULAE (O=4) OF OLIVINE FROM BODIES OF Es

	1	2	3	4	5	6	7	8	9	10	11	12	13
Reg. No.	85-0763	85-0768	85-0764	85-0769	85-0770	85-0771	85-0765	85-0777	85-0774	85-0075	85-0776	85-0772	85-0773
SiO_2	40.79	40.41	40.80	40.44	40.44	40.21	40.66	40.57	40.57	40.48	40.67	38.96	38.96
FeO	12.36	11.92	11.85	12.05	12.14	11.83	11.59	12.19	11.76	11.81	12.34	17.82	18.19
MnO	0.24	-	-	-	-	0.24	0.41	-	-	-	-	0.25	0.28
MgO	47.20	46.48	47.36	47.27	47.22	47.23	47.25	46.97	47.76	47.33	47.31	42.25	42.41
CaO	-	-	-	-	-	-	-	0.17	-	0.26	0.20_	0.34	0.27
NiO	-	0.30	-	-	0.35	-	-	0.36	0.39	0.38	-	-	-
Total	100.59	99.11	100.01	99.76	100.15	99.51	99.91	100.26	100.48	100.26	100.52	99.62	100.11
Si	1.0043	1.0084	1.0068	1.0022	1.0004	0.9996	1.0053	1.0029	0.9988	0.9998	1.0018	0.9966	0.9935
Fe	0.2545	0.2488	0.2446	0.2497	0.2512	0.2460	0.2397	0.2520	0.2421	0.2439	0.2542	0.3812	0.3879
Mn	0.0050	-	-	-	-	00.51	0.0086	-	-	-	-	0.0054	0.0060
Mg	1.7319	1.7285	1.7418	1.7459	1.7410	1.7498	1.7411	1.7305	1.7524	1.7421	1.7368	1.6107	1.6117
Ca	-	-	-	-	-	-	-	0.0045	-	0.0069	0.0053	0.0093	0.0074
Ni	-	0.0060	-	-	0.0070	-	-	0.0072	0.0077	0.0075	-	-	-
Total	2.9957	2.9916	2.9932	2.9978	2.9996	3.0004	2.9947	2.9971	3.0011	3.0002	2.9982	3.0034	3.0065
Mg*	87.2	87.4	87.7	87.5	87.4	87.7	87.9	87.3	87.9	87.7	87.2	80.9	80.6

Analyses 1-5 from Wandle Road body.
Analyses 6 from Deep Creek body.
Analyses 7 from Belmont Road body.
Analyses 8 from Luina - west body.
Analyses 9-11 from Luina - east body.
Analyses 12-13 from Whyte Hill - south body.
See Table 10 for details and location of samples.
Mg* = Mg Number = molecular proportions. 100 Mg/Mg+Fe).
Analyses by A.V. Brown using JEOL X5A Electron Microprobe, Central Science Laboratory University of Tasmania.

Table 7
CHEMICAL ANALYSES (OXIDE MASS %) AND STRUCTURAL FORMULAE (O= 6) FOR ORTHOPYROXENE FROM BODIES OF Es

	1	2	3	4	5	6	7	8	9	10	11
Reg. No.	85-0763	85-0768	85-0764	85-0769	85-0770	85-0771	85-0765	85-0777	85-0774	85-0775	85-0776
SiO_2	56.41	55.40	56.11	56.94	56.23	56.06	56.39	55.70	56.21	56.14	56. 24
TiO_2	-	-	-	-	-	-	-	0.38	-	-	-
Al_2O_3	1.64	1.60	1.44	1.24	1.23	1.57	1.46	1.15	1.58	1.65	1.49
Cr_2O_3	0.49	0.48	0.47	0.50	0.41	0.56	0.57	0.39	0.54	0.53	0.48
FeO	7.83	7.54	7.47	7.66	7.94	7.53	7.06	9.09	8.34	8.98	9.02
MnO	0.25	0.23	0.26	-	-	0.24	-	-	-	-	-
MgO	31.79	31.83	31.87	32.45	32.79	31.46	31.48	31.24	31.84	31.41	31.29
CaO	2.07	2.08	1.95	1.87	1.67	2.22	2.14	1.57	2.03	1.94	2.06
Total	100.48	99.16	99.57	100.66	100.27	99.64	99.10	99.52	100.54	100.65	100. 58
SI	1.9603	1.9511	1.9644	1.9698	1.9567	1.9633	1.9769	1.9623	1.9556	1.9558	1.9611
Ti	-	-	-	-	-	-	-	0.0101	-	-	-
Al	0.672	0.0664	0.0594	0.0506	0.0505	0.0648	0.0603	0.0478	0.0648	0.0678	0.613
Cr	0.0135	0.0134	0.0130	0.0137	0.0113	0.0155	0.0158	0.0109	0.0149	0.0146	0.0132
Fe	0.2276	0.2221	0.2187	0.2216	0.2311	0.2205	0.2070	0.2678	0.2427	0.2616	0.2630
Mn	0.0074	0.0069	0.0077	-	-	0.0071	-	-	-	-	-
Mg	1.6464	1.67-7	1.6629	1.6730	1.7--6	1.6420	1.6447	1.6402	1.6509	1.6308	1.6261
Ca	0.771	0.0785	0.0732	0.0693	0.0623	0.0833	0.0804	0.0593	0.0757	0.0724	0.0770
Total	3.9994	4.0090	3.9993	3.9981	4.0124	3.9966	3.9851	3.9983	4.0045	4.0030	4.0017
Mg*	87.9	88.3	88.4	88.3	88.0	88.2	88.8	86.0	87.2	86.2	86.1
Ca*	4.0	4.0	3.7	3.5	3.1	4.3	4.2	3.0	3.8	3.7	3.9
Mg*	84.4	84.8	85.1	85.2	85.3	84.4	85.1	83.4	83.8	83.0	82.7
Fe*	11.7	11.3	11.2	11.3	11.6	11.3	10.7	13.6	12.3	13.3	13.4

See Table 10 for details and location of samples.
Samples 85-0772 and 85-0773 did not contain orthopyroxene.
Mg* = Mg Number = molecular proportion 100 Mg/(Mg + Fe).
Ca* = molecular proportions 100 Ca/(Ca+Mg+Fe).
Mg* = molecular proportions 100 Mg/(Ca+Mg+Fe).
Fe* = molecular proportions 100 Fe/(Ca+Mg+Fe).
Analyses by A.V. Brown using JEOL X5A Electron Microprobe, Central Service Laboratory, University of Tasmania.

Table 8
CHEMICAL ANALYSES (OXIDE MASS %) AND STRUCTURAL FORMULAE (O = 6) FOR CLINOPYROXENE FROM BODIES OF Es

	1	2	3	4	5	6	7	8	9	10	11	12	13
Reg. No.	85-0763	85-0768	85-0764	85-0769	85-0770	85-0771	85-0765	85-0777	85-0774	85-0775	85-0776	85-0772	85-0773
SiO_2	52.89	52.81	53.86	53.45	53.21	53.44	53.34	52.67	52.33	53.46	51.70	50.66	50.24
TiO_2	-	-	-	0.33	-	-	-	0.40	-	-	0.26	1.19	1.31
Al_2O_3	2.80	2.85	2.48	2.28	2.37	2.21	2.21	2.41	4.27	3.00	3.26	4.36	3.52
Cr_2O_3	1.10	1.05	1.07	1.12	1.14	0.97	1.09	0.90	1.08	0.97	0.39	1.10	0.73
FeO	4.19	4.31	4.06	4.17	4.16	3.87	4.09	4.30	4.28	4.81	5.87	5.16	6.56
MnO	0.21	-	-	-	-	-	-	-	-	-	-	-	-
MgO	17.53	18.24	18.64	18.50	18.33	18.58	18.78	17.93	17.92	19.43	18.65	15.08	13.77
CaO	20.80	20.10	20.02	20.31	20.69	20.59	20.18	20.88	20.79	19.20	19.22	23.10	23.48
Na_2O	0.32	-	-	-	-	-	-	0.32	-	-	-	0.34	-
Total	99.84	99.36	99.83	100.16	99.90	99.66	99.69	99.81	100.67	100.87	99.35	100.99	99.61
Si	1.9298	1.9294	1.9429	1.9369	1.9357	1.9441	1.9407	1.9238	1.8908	1.9215	1.8994	1.8535	1.8757
Ti	-	-	-	0.0090	-	-	-	0.0110	-	-	0.0072	0.0327	0.0368
Al	0.1204	0.1228	0.1061	0.0974	0.106	0.0948	0.0948	0.1038	0.1879	0.1271	0.1412	0.1881	0.1549
Cr	0.0317	0.0303	0.0307	0.0321	0.0328	0.0279	0.0314	0.0260	0.0309	0.0276	0.0113	0.0318	0.0215
Fe	0.1279	0.1317	0.1232	0.1264	0.1266	0.1177	0.1245	0.1314	0.1293	0.1446	0.1804	0.1579	0.2048
Mn	0.0065	-	-	-	-	-	-	-	-	-	-	-	-
Mg	0.9532	0.9931	1.0077	0.9991	0.9938	1.0074	1.0183	0.9760	0.9650	1.0408	1.0211	0.8222	0.7662
Ca	0.8132	0.7868	0.7782	0.7886	0.8065	0.8026	0.7867	0.8172	0.8049	0.7395	0.7566	0.9056	0.9393
Na	0.0226	-	-	-	-	-	-	0.0227	-	-	-	0.0241	-
Total	4.0054	3.9941	3.9887	3.9894	3.9970	3.9945	3.9963	4.0117	4.0028	4.0011	4.0172	4.0159	3.9993
Mg*	88.2	88.3	89.1	88.8	88.7	89.5	89.1	88.1	88.2	87.8	85.0	83.9	78.9
Ca*	42.9	41.2	40.8	41.2	41.9	41.6	40.8	42.5	42.4	38.4	38.6	48.0	49.2
Mg*	50.3	52.0	52.8	52.2	51.6	52.3	52.8	50.7	50.8	54.1	52.1	43.6	40.1
Fe*	6.7	6.9	6.5	6.6	6.6	6.1	6.5	6.8	6.8	7.5	9.2	8.4	10.7

See Table 10 for details and location of samples
Mg* = Mg number = molecular proportion 100 Mg(Mg+Fe)
Ca* = molecular proportion 100 Ca/(Mg+Ca+Fe)
Mg* = molecular proportion 100 Mg/(Mg+Ca+Fe)
Fe* = molecular proportion 100 Fe/(Mg+Ca+Fe)
Analyses by A.V. Brown using JEOL X5A
Electron Microprobe, Central Science Laboratory, University of Tasmania

North of Belmont Creek [CQ766185], a body of ultramafic rock was emplaced into sedimentary sequences causing the formation of very indurated rocks with incipient metamorphic spotting and biotite development. The sedimentary rocks have been brecciated and the fractures filled with opaque minerals. The ultramafic rocks occur in concordant slivers from 30 to 150 m thick, within the surrounding sedimentary rocks, the finer grained ones of which are hornfelsic. In a costean at CQ767185, near Belmont Road, the ultramafic rocks have an irregular boundary against chert and mudstone of the country rock succession, which are also indurated.

Overall, the evidence strongly suggests that the ultramafic rocks were intruded as hot magma into the chert-greywacke-red pelite-pillow lava sequence (Ec). Later faulting has occurred along some primary boundaries and produced the lozenge-shaped outcrop pattern, but some boundaries are undisturbed. The age of emplacement of the ultramafic bodies is unknown. They post-date the Ec succession, which they intrude, and pre-date Devonian deformation, which produced structural modification of contact metamorphic effects.

Three small, ellipsoidal bodies of similar ultramafic rocks to those described above, were found to the west of the St Valentines Quadrangle in the Luina area (Brown, 1986, €bp, fig. 2,3). Field relationships of these bodies indicate that the ultramafic rocks intruded high-magnesian andesite lavas which are associated with the low-titanium tholeiite basalts and considered to be Middle Cambrian in age (Brown, 1986), implying that these ultramafic rocks are younger than Middle Cambrian.

A comparison of the ultramafic rocks in the western part of the St Valentines Quadrangle with ultramafic complexes elsewhere in Tasmania is discussed by Williams and Brown (1983), which is included as Appendix C.

Beneath the Tertiary basalt to the east of the ultramafic rocks a diamond drill hole (at CQ812177) intersected highly weathered olivine-phyric picritic basalts. These basalts have a composition which is consistent with having been the extrusive equivalents of the ultramafic rocks to the west, indicating that the ultramafic bodies are remnant feeder channels for a phase of picritic magma. Further west in the Luina area, to the south of Whyte Hill, is a 3 km long fault wedge of highly altered lavas (€bm?, fig. 2-3, Brown, 1986), which also probably belong to the picritic volcanism.

The picritic lavas occur as hyaloclastite, vesicular, pillow or sheet flows and contain inter-flow volcaniclastic lithicwacke units derived entirely from spalled glass and lava fragments. In thin section, samples of the picritic lava from the drill hole contain 2-3 mm long pseudomorphs after olivine and two size populations of spinel. The larger spinels are between 0.45-0.90 mm and euhedral, with the smaller ones being subhedral and 0.10-0.25 mm across. The groundmass of these lavas was originally glass.

The volcanic units in the Whyte Hill area are vesicular, pillow and sheet flows and now consist of chlorite/serpentine group mineral pseudomorphs of olivine, and calcite- and zeolite-filled amygdales, in a groundmass of fine-grained quenched pyroxene and devitrified glass. The pyroxene is now pseudomorphed by mainly amphibole minerals with minor grains of epidote. These lavas have a low spinel content.

Table 9

CHEMICAL ANALYSES (OXIDE MASS%) AND STRUCTURAL FORMULAE (O=32) FOR SPINEL FROM BODIES OF Es

	1	2	3	4-1	4-2	5	6	7	8	9	10-1	10-2	11	12-1	12-2	12-3	13-1	13-2	14
Registered No.	85-0763	85-0768	85-0764	85-0769		85-0770	85-0771	85-0765	85-0777	85-0774	85-0775		85-0776		85-0772		85-0773		85-0778
TiO_2	2.48	3.25	1.23	0.63	3.10	0.89	0.54	1.46	0.57	0.41	0.24	3.98	0.34	0.66	4.54	11.74	3.02	12.80	0.29
Al_2O_3	14.85	13.81	18.41	17.64	12.17	17.31	19.92	15.59	15.92	17.06	18.52	9.57	18.34	27.30	15.43	5.92	17.77	2.05	26.95
Cr_2O_3	38.71	37.83	40.53	45.17	43.09	44.98	41.04	44.21	45.87	45.61	45.40	39.31	44.89	26.02	26.19	15.02	27.19	10.03	40.83
FeO	32.13	33.21	28.20	25.06	32.80	24.78	24.91	27.08	26.97	24.84	22.74	39.54	24.14	36.19	45.48	60.93	42.64	70.15	14.47
MnO	0.48	0.31	0.45	-	-	-	0.55	-	-	-	-	-	-	-	-	0.97	-	2.53	-
MgO	10.63	10.03	12.03	12.15	9.26	12.14	13.30	11.39	10.65	11.81	12.75	7.30	12.05	10.43	8.41	5.39	9.27	1.93	17.25
Total	99.28	100.44	100.85	100.65	100.42	100.10	100.26	99.73	99.98	99.73	99.65	99.70	99.65	100.60	100.05	99.96	99.89	99.49	99.79
Ti	0.4800	0.6288	0.2299	0.1184	0.6084	0.1683	0.1000	0.2802	0.1096	0.0780	0.0452	0.8044	0.0452	0.1203	0.8823	0.4221	0.5787	2.7616	0.0513
Al	4.5134	4.1885	5.3943	5.1966	3.7438	5.1311	5.7834	4.6901	4.7999	5.0889	4.4627	3.0322	5.4627	7.7975	4.7005	1.9146	5.3379	0.6933	7.4701
Cr	7.8894	7.6939	7.9635	8.9231	8.8888	8.9408	7.9900	3.2574	5.4769	2.2747	7.5891	8.3521	8.9798	4.9836	5.3500	3.2574	5.4769	2.2747	7.5891
Fe^{3+}	3.1164	3.4888	2.4123	1.7618	2.7590	1.7599	2.1266	2.1110	1.8231	1.7098	1.5123	3.8113	1.5123	3.0987	5.0672	8.4059	4.6065	1.2704	0.8896
Fe^{2+}	3.8110	4.0869	3.4493	3.4753	4.3989	3.4509	3.0039	3.6683	3.9427	3.5466	3.2459	5.0761	3.2459	4.2341	4.7613	5.5709	4.4799	6.5601	1.9557
Mn	0.1048	0.0676	0.0947	-	-	-	0.1147	-	-	-	-	-	-	-	-	0.2254	-	0.6148	-
Mg	4.0842	3.8456	4.4560	4.5247	3.6011	4.5491	4.8814	4.3317	4.0573	4.4534	4.7541	2.9239	4.7541	3.7659	3.2387	2.2037	3.5201	0.8251	6.0443
Mg#	51.7	48.5	56.4	56.6	45.0	56.9	61.9	54.1	50.7	55.7	59.4	36.5	59.4	47.1	40.5	28.3	44.0	11.2	75.6
Cr*	63.6	64.8	59.6	63.2	70.4	63.5	58.0	65.5	65.9	64.2	62.2	73.4	62.2	39.0	53.2	63.0	50.6	76.6	50.4

See Table 10 for details and location of samples.

Cr* = molecular proportion 100 Cr/(Cr+Al).

Mg* = molecular proportion 100 Mg/(Mg+Fe).

Analyses by A. V. Brown using JEOL X5A Electron Microprobe, Central Science Laboratory, University of Tasmania.

Petrography

Samples from the ultramafic bodies grade from plagioclase- and clinopyroxene-bearing harzburgite at the base, to plagioclase-bearing poikilitic lherzolite at the top. Overall the bodies are massive with a small grain size variation. The tops are coarser than the bases and contain a larger percentage of euhedral crystals.

Olivine and accessory chrome spinel are the cumulus mineral phases, pyroxene and plagioclase being post-cumulus. No indication of layering or a mineral fabric (foliation) is evident and the distribution of plagioclase is irregular. In places, olivine crystals are mantled by a mesh of serpentine group minerals and outlined by fine-grained magnetite. Interstitial plagioclase occurs in cuspate patches and is usually highly altered, but occasional fresh subhedral grains are present.

In the northern part of the largest body, as exposed along the Wandle Road, the plagioclase-bearing harzburgite has a panidiomorphic granular texture, of rounded olivine and euhedral chrome spinel grains surrounded by anhedral post-cumulus granular orthopyroxene, with minor irregular patches of clinopyroxene and plagioclase. Olivine and pyroxene make up approximately 95% of the rocks in this area.

Traversing this body southwards, olivine grains become coarser and more crystalline; pyroxene remains dominantly granular, but some poikilitic orthopyroxene grains occur; and post-cumulus plagioclase increases in volume. The southern-most outcrop of this body consists of plagioclase-bearing poikilitic lherzolite. Olivine crystals are subhedral to euhedral, and both ortho- and clinopyroxene poikilitically enclose olivine and chrome spinel grains, as well as occurring as anhedral intergranular grains.

The second main body, exposed along Belmont Road, is very similar to the top part of the Wandle Road body but contains a greater percentage of post-cumulus plagioclase and is slightly coarser grained. Overall, euhedral to anhedral olivine crystals are poikilitically enclosed by anhedral pyroxene.

The three small bodies in the Luina-Whyte Hill area to the west are very similar in texture, contain the same mineralogy, but vary in grain size and degree of serpentinisation.

Chemistry

Major and trace element chemistry for two samples of the picritic lavas from the drill hole (table 4, columns 1 and 2) and a comparison with average analyses of the King Island picrite lavas (table 4, column 3) are presented. Analyses of two samples of the ultramafic rocks from each of the Belmont Road and Wandle Road bodies are also included in Table 5, columns 4 and 5, and 6 and 7 respectively.

Mineral chemistry for coexisting olivine, chrome spinel, orthopyroxene and clinopyroxene are given in Tables 6-9 for four samples from the Wandle Road body (between CQ762190 and CQ759186); one sample from each of the Deep Gully Creek [CQ758182] and the Belmont Road bodies [CQ768183]; two from the body to the south of Whyte Hill [CQ688072]; three from the body east of Luina [CQ657080] and two from the body to the west of Luina [CQ648079].

The coexisting mineral compositions of all samples from the Wandle Road body are very similar. The compositions within this body are also very similar to the samples analysed from the other two bodies in the Arthur River-Belmont Road areas and the two bodies at Luina. Samples from the body to the south of Whyte Hill do not contain orthopyroxene and have an overall lower magnesium content. When the magnetic map of this region is studied a linear trend exists between the rocks at Luina and those in the Wandle Road-Belmont Road area, indicating that this is a continuous zone of similar rocks.

Table 10
SAMPLE DETAILS

Table	Column	Regd No.	Field No.	Analysis No.	AMG Ref.	Sample description
1	1	85-0019	WA63	783165	CQ744278	Pillow-massive basalt (Ecp)
	2	85-0020	WA78	814513	CQ762225	Pillow-massive basalt (Ecp)
	3	85-0021	WA53	783164	CQ749271	Pillow-massive basalt (Ecp)
	4	85-0022	WA79	814514	CQ764283	Pillow-massive basalt (Ecp)
	5	85-0037	WA71	814511	CQ754176	Low-titanium tholeiite (Em)
	6	85-0038	WA77	814512	CQ772189	Low-titanium tholeiite (Em)
	7	85-0039	WA80	814515	CQ768187	Low-titanium tholeiite (Em)
	8	85-0761	WA25	783165	CQ767101	Low-titanium tholeiite (Em)
2	1	85-0766	C1729	830760	CQ811177	BHP. D.D.H. WA3:256 m
	2	85-0767	C1730	830761	CQ811177	BHP. D.D.H. WA3:264 m
	4	95-0762	BR1	813140	CQ768183	Belmont Road Quarry not Wandle Road body
	5	85-0765	WA75	814510	CQ768183	as listed in Table 1, Williams and Brown (1983)
	6	85-0763	WA66	814507	CQ762190	Wandle Road body not Belmont Road body
	7	85-0764	WA68	814508	CQ762189	as listed in Table 1, Williams and Brown (1983)
3	1	85-0763	WA66	814507	CQ762190	From northern margin of Wandle Road body
	2	85-0768	WA67	-	CQ762190	10 m S of northern margin of Wandle Road body
	3	85-0764	WA68	814508	CQ762189	40 m S of northern margin of Wandle Road body
	4	85-0769	WA69	-	CQ760187	200 m S of northern margin of Wandle Road body
	5	85-0770	WA70	-	CQ759186	Near southern margin of Wandle Road body
	6	85-0771	WA74	-	CQ758182	From Deep Gully Creek body
	7	85-0765	WA75	814510	CQ768183	From Belmont Road body
	8	85-0777	C1584	-	CQ648079	Luina West - fig. 2, Brown (1986)
	9	85-0774	C1927	-	CQ658080	Luina East - fig. 2, Brown (1986)
	10	85-0775	C1928	-	CQ658080	Luina East - fig. 2, Brown (1986)
	11	85-0776	C1929	-	CQ658080	Luina East - fig. 2, Brown (1986)
	12	85-0772	C1569	-	CQ688072	Whyte Hill South - fig. 2, Brown (1986)
	13	85-0773	C1887	-	CQ688072	Whyte Hill South - fig. 2, Brown (1986)
	14	85-0778	C1723	-	CQ811177	B.H.P. D.D.H. WA4:282 m

Table 11
ANALYSED SAMPLES, CAMBRIAN VOLCANIC AND VOLCANICLASTIC ROCKS, NATIVE TRACK TIER AND MT TOR - TWO HUMMOCKS AREA
(P.W.B.)

Field No.	Analysis No.	Grid. Ref	Rock type
VA1	791073	DQ104200	Andesite
VA2	791074	DQ103200	Andesite
VA3	791075	DQ093211	Crystal-lithic vitric tuff
PV23	791085	DQ008140	Ash tuff
PV49	791086	DQ027107	Vitric tuff
VA20	850087	DQ144222	Agglomerate
VA21	850088	DQ136218	Conglomerate
VA22	850089	DQ061135	Altered? basalt

Cambrian volcanic rocks

P. W. Baillie

As noted in the Stratigraphy section, correlates of the Mt Read Volcanics crop out in several areas in the eastern half of the St Valentines Quadrangle. Eight analyses and calculated Rittman norms of samples from the Native Track Tier and Mt Tor-Two Hummocks areas are shown in Tables 11, 12. Note that analysis 850088 is of an epiclastic conglomerate, and not an igneous rock.

The rocks vary in composition from ?basaltic (850089 is an altered rock) to rhyolitic. In general it appears that the samples from the Native Track Tier area are less silica-rich than those from the Mt Tor-Two Hummocks area. This difference was apparent during mapping. Unfortunately the stratigraphic relationship between the sequences in these two areas is unknown.

Also noteworthy is the closeness in composition between sample VA20 (analysis 850087) and the Comstock Tuff and correlates (Tyndall Group) of the Queenstown area, western Tasmania. This similarity is also remarkable in hand-specimens, which consist of blotchy pink and green, massive or banded agglomerate with clasts of both felsic and more mafic volcanic rocks, together with grains or crystals of quartz, feldspar and altered ferromagnesian minerals. In both the type area of the Comstock Tuff (the Comstock Valley) and where correlates crop out (near Lynchford, Corbett 1979) typical outcrops are large rounded tors. The rock under discussion in the Native Track Tier area outcrops similarly. No analyses are available of the Comstock Tuff, but Corbett (1979) published three of correlates from the Lynchford area. A comparison between these and the rock from Native Track Tier is shown as Table 13. It is not meant to imply that these are the same rocks, despite the chemical similarities and age equivalence (Baillie and Jago, 1985), but rather that very similar processes were going on at approximately the same time in different parts of the Mt Read volcanic belt.

Devonian

HOUSETOP GRANITE

P. W. Baillie
P. G. Lennox

The Housetop Granite is one of the major granitic bodies of north-west Tasmania and has its major area of outcrop on the St Valentines Quadrangle. Unlike the major granite bodies of north-east Tasmania the Housetop Granite is not composite and individual plutons cannot be mapped within the body. In general it can be described as equigranular to sparsely porphyritic, medium- to coarse-grained biotite granite with minor variants, the most important of which is a fine-grained porphyritic granite with phenocrysts of quartz and feldspar (quartz-feldspar porphyry). The granite has been radiometrically dated in the range 353-370 Ma (McDougall and Leggo, 1965; revised McDougall, 1983), i.e. Late Devonian to Early Carboniferous (Harland *et al.*, 1982).

In thin section most samples from the main body of the Housetop Granite show little variation (P.W.B.). The texture varies from porphyritic (VA4, VA6, see Table 14) to hypidiomorphic granular (VA7, VA9). Quartz and K-feldspar are present in approximately equal proportions, and together usually occupy greater than about 80% of the rock (visual estimate). The potash feldspar is often perthitic and may display simple twinning. Small inclusions of quartz, plagioclase and sometimes biotite may be present. Phenocrysts of K-feldspar may be up to 25 mm in length. Plagioclase occurs both as phenocrysts and in groundmass and is generally about one half as abundant as potash feldspar. Optical determination indicates that it is oligoclase. Biotite is pleochroic (α = yellow, $\beta = \gamma$ = dark brown) and occurs as subhedral laths, discrete grains, and as inclusions in K-feldspar and quartz. Opaque minerals include both ilmenite and magnetite, while accessory minerals include apatite and zircon.

The quartz-feldspar porphyries (VA4, VA12) consist of phenocrysts of quartz and feldspar in a fine- to medium-grained groundmass consisting of quartz, K-feldspar, oligoclase, biotite and opaque minerals (P.W.B.). Development of myrmekite is common. No obvious intrusive relationships were observed between this granite type and the coarser, equigranular varieties.

P. G. Lennox considered that the western marginal part of the main body of the Housetop Granite between Rogetta Road and Blythe Road is composed of adamellite, e.g. sample 80-27 from DQ033260 which is a pink-coloured fine- to medium-grained equigranular adamellite. Lennox also mapped and described the irregularly shaped body centred around CQ965260, as follows. Sample 80-9 [CQ963246] from the St Valentines Road contains abundant white feldspar phenocrysts (up to 20 mm across) and occasional black biotite aggregates (usually less than 5 mm across) in a grey medium-coarse grained quartz- two feldspar-biotite groundmass. In thin section the presence of angular biotite crystals within glomeroporphyritic feldspar grains, and recrystallised microphenocrysts of quartz and feldspar, indicate that the rock has undergone partial recrystallisation. The proportion of K-feldspar (40-50%) compared with relict Carlsbad-albite twinned feldspar (10-20%) indicate that the rock is an adamellite. A sample from CQ980260 in a small tributary of the Emu River east of the Kara Mine workings, contains 0.5 mm thick planar tourmaline-filled veins within medium- to coarse-grained equigranular granite. In thin section it consists of large mostly equant phenocrysts of albite, quartz and K-feldspar (up to 9 mm across). Some of the quartz phenocrysts are optically continuous in plane polarised light but are seen in X-nicols to consist of numerous polygonal quartz grains, indicating probable recrystallisation.

P. G. Lennox also reports a 40 m thick, very weathered and friable quartz-porphyry dyke intruding Cambrian rocks on Black Pit Road [CQ950226], and which consists of 0.5-1 mm diameter, mostly angular quartz grains (60-65%) in a cream-coloured claystone groundmass after ?feldspar.

Mapping of the main body of the Housetop Granite by P. W. Baillie has clearly demonstrated the presence of several right-angled bends in the granite/country rock boundary. This suggests that intrusion was controlled largely by pre-existing joints and that the mechanism of intrusion was probably by stoping. P. G. Lennox considers that the unusual shape of the offshoot body north of St Valentines Peak also reflects partial structural control of the path of intrusion.

Chemical analyses of representative types of Housetop Granite were obtained (P.W.B.) and are listed in Tables 14

Table 12

CHEMICAL ANALYSES AND RITTMANN NORMS, CAMBRIAN VOLCANIC AND VOLCANICLASTIC ROCKS, NATIVE TRACK TIER AND MT TOR - TWO HUMMOCKS AREA (P.W.B.)

Analysis No.	791073	791074	791075	791085	791086	850087	850088	850089
SiO_2	60.8	62.2	51.7	77.6	78.3	52.50	64.24	52.65
TiO_2	0.7	0.7	0.88	0.26	0.22	0.85	0.71	1.73
Al_2O_3	14.6	14.7	15.5	12.4	10.1	15.88	12.79	17.37
Fe_2O_3	1.3	1.9	3.8	0.04	0.15	3.08	2.54	2.86
FeO	5.6	4.6	4.8	1.3	2.7	4.88	4.90	8.41
MnO	0.19	0.14	0.12	<0.02	0.11	0.13	0.16	0.14
MgO	1.6	1.9	4.6	0.36	0.34	3.80	2.87	7.33
CaO	2.0	1.3	3.7	0.07	0.12	3.26	2.48	0.32
Na_2O	4.3	2.8	2.2	0.07	3.0	6.27	4.18	2.49
K_2O	3.7	5.4	3.7	3.9	2.5	1.02	1.91	0.61
P_2O_5	0.27	0.25	0.2	<0.04	0.05	0.21	0.22	0.16
CO_2	2.2	1.2	4.5	0.03	0.03	0.68	0.75	0.29
SO_3	-	-	-	-	-	0.14	0.08	0.01
F	0.11	0.13	0.12	0.16	0.13	-	-	-
H_2O^+	1.9	2.0	3.6	2.4	1.4	1.97	1.99	5.99
H_2O^-	0.23	0.34	0.73	0.85	0.32	-	-	-
Total	99.50	99.56	101.15	99.44	99.47	99.67	99.82	100.26
Trace Elements (ppm)								
Li	35	35	45	10	10	-	-	-
Sn	-	-	-	-	-	<4	<4	<4
Th	-	-	-	-	-	9	10	<4
Sr	221	90	54	<2	35	270	160	48
U	-	-	-	-	-	5	<5	<5
Rb	97	142	227	186	94	24	44	23
Y	40	36	20	35	33	32	27	23
Zr	207	205	99	211	224	122	153	120
Nb	10	11	8	13	12	9	8	7
Mo	-	-	-	-	-	<2	<2	<2
Ni	4	4	16	<4	6	13	30	185
Ba	1900	2130	759	304	1150	550	770	127
Cr	-	-	-	-	-	61	160	210
V	-	-	-	-	-	200	136	210
Sc	-	-	-	-	-	17	15	30
Pb	363	358	84	62	65	20	60	26
As	-	-	-	-	-	<10	10	<10
Bi	-	-	-	-	-	6	5	5
Ga	-	-	-	-	-	16	14	20
Zn	945	586	490	26	133	61	89	115
Cu	<5	50	<5	<5	60	27	31	130
Co	-	-	-	-	-	29	22	50
Ag	-	-	-	-	-	<5	<5	<5
Ce	-	-	-	-	-	88	115	43
La	-	-	-	-	-	36	33	15
Nd	-	-	-	-	-	34	28	12
RITTMANN NORMS								
Quartz	13.9	16.8	8.0	60.8	49.2	3.0	22.4	10.3
Sanidine	-	60.5	45.6	7.9	-	-	2.9	-
Anorthoclase	63.6	-	-	-	40.8	-	-	27.0
Plagioclase	-	-	-	-	-	75.4	53.6	-
Orthopyroxene	5.8	5.3	10.5	-	-	14.4	-	15.4
Magnetite	1.2	1.0	1.2	0.1	0.4	1.4	1.1	1.2
Calcite	3.8	2.4	7.2	0.1	0.1	1.7	1.8	0.5
Cordierite	11.7	14.0	27.5	6.2	7.2	3.6	6.3	45.7
Muscovite	-	-	-	24.5	-	-	-	-
Biotite	-	-	-	-	2.1	-	-	-
Ilmenite	-	-	-	0.3	0.1	-	-	-
Apatite	-	-	-	-	0.1	0.4	0.5	-

Analyses by Department of Mines Laboratory, Launceston

Table 13
COMPARISON OF ANALYSES OF LYNCHFORD TUFF SAMPLES WITH A LITHOLOGICALLY SIMILAR ROCK FROM THE NATIVE TRACK TIER AREA (P.W.B.)

	C12	C13	C14	850087
SiO_2	59.5	56.9	58.4	57.5
TiO_2	0.8	0.99	0.80	0.85
Al_2O_3	13.9	15.2	14.7	15.9
Fe_2O_3	3.2	3.1	2.4	3.1
FeO	4.6	6.1	5.6	4.9
MnO	0.15	0.22	0.19	0.13
MgO	3.7	4.4	4.5	3.8
CaO	4.3	3.6	3.5	3.7
Na_2O	6.0	4.8	5.3	6.3
K_2O	1.4	1.8	1.1	1.0
P_2O_5	0.16	0.15	0.19	0.21
CO_2	0.80	0.08	0.03	0.68
SO_3	0.30	0.21	0.21	0.14
H_2O^+	1.80	2.7	2.9	1.97
Total	99.93	100.50	100.09	99.67
Trace elements				
Ba	270	549	660	550
Co	22	18	23	29
Cr	142	25	50	61
Cu	14	10	18	27
Nb	-	6	9	9
Ni	19	11	16	13
Pb	13	<6	6	20
Rb	36	48	29	24
Sc	-	28	25	17
Sr	427	267	265	270
V	222	229	201	200
Y	23	20	21	32
Zn	79	66	58	61
Zr	76	151	164	122

Table 14
ANALYSED SAMPLES, DEVONIAN GRANITIC ROCKS FROM THE HOUSETOP GRANITE, ST VALENTINES QUADRANGLE (P.W.B.)

Field No.	Analysis No.	Grid Ref.	Rock type
VA4	791076	DQ096285	Medium-grained granite
VA5	791077	DQ096284	Quartz-feldspar porphyry
VA6	791078	DQ092265	Coarse-grained granite
VA7	791079	DQ075253	Coarse-grained granite
VA9	791081	DQ070255	Medfium-grained granite
VA10	791082	DQ078269	Coarse-grained granite
VA11	791083	DQ077268	Medium-grained granite
VA12	791084	DQ070260	Quartz-feldspar porphyry1
VA24	850091	DQ066337	Coarse-grained granite
VA25	850092	DQ102345	Coarse-grained granite

and 15 together with calculated CIPW Norms. The analyses indicate that textural variants within the pluton are chemically very similar and can be regarded as granites (*sensu stricto*). Chemical features including relatively low Al_2O_3, low MgO, high Na_2O and K_2O and high Nb suggest that the Housetop Granite may be similar to the A-type granites of Collins *et al.* (1982). In a study of north east Tasmanian granitoids McClenaghan (*in press*) used the K/Rb ratio to differentiate between true A-types and granites which resembled A-types, i.e. highly fractionated from non-fractionated granites. A comparison showing Housetop Granite K/Rb ratios with values for the Gabo and Mumbulla A-type granites of Collins *et al.* (1982) and the highly fractionated non A-type Lottah Granite of McClenaghan (1985) is shown as Table 16. This shows that the Housetop Granite is intermediate, i.e. moderately fractionated, and so the question as to whether the granites are A-types remains unresolved.

MT BISCHOFF PORPHYRIES

In the western part of the Quadrangle, anastomosing dykes and sills of quartz-orthoclase porphyry intrude the Mt Bischoff sequence of Precambrian rocks near the crest of the main antiformal flexure (Collins, 1982). They have been dated at 394±4 Ma and are similar in age to granitic rock of the Meredith Granite (353±7 Ma; Brooks, 1966) which crops out 6.5 km south-west of Waratah. The porphyries are genetically related to the tin mineralisation at Mt Bischoff (see Economic Geology section herein).

They consist of abundant bipyramidal quartz phenocrysts up to 5 mm in diameter, and lath-shaped phenocrysts of K-feldspar up to 5 mm in length, in a fine-grained groundmass of intergrown quartz and sericitised feldspar with minor muscovite as flakes up to 0.5 mm in length. Macroscopic features include flow banding and small swirls within the dykes and probable fault breccias along dyke margins (Collins, 1982).

STRUCTURAL GEOLOGY

Introduction

D. B. Seymour

In the structural notation on the map, the Precambrian rocks are treated separately from the ?Eocambrian-?Early Cambrian to Early Devonian rocks. Thus, D_1-D_4 structures in the former do not directly correspond to D_1-D_4 structures in the latter, although there is probable correlation of D_3 and D_4 in the Precambrian rocks with D_1 and $?D_3$ in the younger rocks, as discussed by P. R. Williams herein (see below).

The regional sequence of D_1-D_4 upright structures in the post-Precambrian, pre-Carboniferous rocks is considered to be due to deformation which occurred between the middle Early Devonian and late Middle Devonian (E. Williams, 1979). The work of Seymour (1980) in the Black Bluff Range and adjacent areas in the south-eastern part of the Quadrangle was the first indication of a 4-phase Devonian structural history, compared with a 2-phase history proposed earlier by E. Williams (1979). The correspondence between these interpretations and the structural notation on St Valentines Quadrangle is shown in Table 17. Of particular note is that Seymour (1980) recognised two distinct sets of structures, an earlier one of dominantly NE-SW trend and a later one of N-S trend, within the West Coast Range/Valentines Peak trend of Williams (1979). The name West Coast Range/Valentines Peak trend was retained by Seymour (1980), but to include only structures of more or less N-S trend in this region (table 17).

The recognition of four trend groups of Devonian structures in the region seems now well established. However, both the proposal that these represent a D_1-D_4 structural sequence, and the corresponding classification o minor structures at many localities on the map, are still largely interpretive due to the very small number of localities where overprinting relationships are apparent. In particular, the extension of the D_1-D_4 minor structure notation to the ?Eocambrian-?Early Cambrian rocks in the western part of the Quadrangle is based entirely on the conclusions of P. R. Williams regarding correlation with the structural sequence proposed by Seymour (1980) for the Black Bluff Range and adjacent areas in the eastern part of the Quadrangle.

In the ?Eocambrian-?Early Cambrian rocks P. R. Williams has also recognised an early deformation which produced isoclinal folds and widespread cleavage parallel to bedding,

Table 15
CHEMICAL ANALYSES AND CIPW NORMS OF HOUSETOP GRANITE (P.W.B.)

Analysis No.	791076	791077	791078	791079	791081	791082	791083	791084	850091	850092
SiO_2	76.5	76.4	73.3	75.7	75.5	77.1	76.1	76.3	73.21	76.17
TiO_2	0.16	0.11	0.23	0.22	0.15	0.15	0.14	0.15	0.33	0.18
Al_2O_3	11.7	11.9	12.9	11.7	11.7	11.5	11.6	11.7	12.91	12.15
Fe_2O_3	0.3	0.01	0.34	0.07	0.01	0.26	0.32	0.15	0.55	0.40
FeO	1.7	1.7	1.7	2.3	1.7	1.8	1.8	1.7	1.54	1.06
MnO	0.03	0.03	<0.02	0.03	<0.02	0.03	0.03	0.03	0.03	0.01
MgO	0.14	0.07	0.09	0.19	0.2	0.11	0.09	0.09	0.41	0.11
Ca	0.51	0.46	0.67	0.77	0.66	0.68	0.61	0.58	1.52	0.67
Na_2O	3.0	3.2	3.2	2.8	3.0	3.0	2.9	3.0	3.34	3.57
K_2O	4.5	4.5	5.9	5.0	5.2	5.1	5.1	5.2	4.95	5.03
P_2O_5	<0.04	<0.04	<0.04	<0.04	0.05	0.09	0.05	<0.04	0.06	0.02
CO_2	0.0	0.2	0.02	0.05	0.0	0.0	0.02	0.03	0.10	0.05
SO_3	-	-	-	-	-	-	-	-	<0.01	<0.01
F	0.18	0.22	0.16	0.16	0.20	0.21	0.16	0.17	-	-
H_2O^+	1.0	0.58	0.72	0.71	0.58	0.60	0.55	0.50	0.60	0.33
H_2O^-	0.03	0.13	0.15	0.22	0.24	0.35	0.39	0.20	-	-
Total	99.75	99.51	99.25	99.92	99.19	100.98	99.86	99.80	99.55	99.75
Trace Elements (ppm)										
Li	35	25	15	35	35	35	40	35	-	-
Sn	-	-	-	-	-	-	-	-	6	4
Th	-	-	-	-	-	-	-	-	32	49
Sr	10	6	32	28	11	14	8	10	79	32
U	-	-	-	-	-	-	-	-	13	12
Rb	339	385	383	359	414	354	449	460	250	300
Y	63	70	46	48	49	43	60	55	36	54
Zr	141	126	102	164	128	146	138	128	170	150
Nb	19	26	20	20	33	25	27	25	15	22
Mo	-	-	-	-	-	-	-	-	3	3
Ni	8	4	4	4	4	4	9	5	3	4
Ba	86	75	315	229	73	121	43	47	490	230
Cr	-	-	-	-	-	-	-	-	87	110
V	-	-	-	-	-	-	-	-	21	5
Sc	-	-	-	-	-	-	-	-	<7	<7
Pb	118	178	115	58	43	46	42	27	22	23
As	-	-	-	-	-	-	-	-	10	10
Bi	-	-	-	-	-	-	-	-	6	<5
Ga	-	-	17	13	15	17	17	15	14	17
Zn	19	12	14	13	22	20	30	19	24	19
Cu	<5	<5	<5	<U5	5	<5	<5	<5	7	8
Co	-	-	-	-	-	-	-	-	9	7
Ag	-	-	-	-	-	-	-	-	<5	<5
Ce	-	-	-	-	-	-	-	-	150	160
La	-	-	-	-	-	-	-	-	71	92
Nd	-	-	-	-	-	-	-	-	35	49
CIPW NORMS										
Q	39.9	38.9	29.9	37.1	35.9	38.1	37.6	36.7	30.6	34.2
Or	26.6	26.6	34.9	29.6	30.7	30.1	30.1	30.7	29.3	29.7
Ab	25.4	27.1	27.1	23.7	25.4	25.4	24.5	25.4	28.3	30.2
An	1.1	0.6	2.0	2.5	1.5	1.3	1.6	1.5	5.6	2.3
Co	1.5	1.6	0.5	0.8	0.6	0.6	0.7	0.6	-	-
Di	-	-	-	-	-	-	-	-	1.3	0.8
Hy	3.0	3.2	2.87	4.3	3.4	3.2	3.1	3.0	2.3	1.2
Mb	0.4	-	0.5	0.1	-	0.4	0.5	0.2	0.8	0.6
Il	0.3	0.2	0.3	0.4	0.3	0.3	0.3	0.3	0.6	0.3
Ap	0.1	0.1	0.1	0.1	0.1	0.2	0.1	0.1	-	-
Fl	0.4	0.5	0.3	0.3	0.4	0.4	0.3	0.4	-	-
Hap	-	-	-	-	-	-	-	-	0.1	0.1

Analyses by Department of Mines Laboratory, Launceston

Table 16
COMPARISON OF K/Rb RATIOS OF HOUSETOP GRANITE WITH A-TYPE GRANITES OF COLLINS et. al. (1982), McCLENAGHAN (1985) (P.W.B.)

	K_2O	Rb	K/Rb
791076	4.5	339	110
791077	4.5	385	97
791078	5.9	383	128
791079	5.0	359	116
791081	5.2	414	104
791082	5.1	354	120
791083	5.1	449	94
791084	5.2	460	94
850091	4.95	250	164
850092	5.03	300	139
Mumbulla (average)	-	-	172
Gabo (average)	-	-	204
Lottah (average)	-	-	49

in addition to structures associated with the polyphase Devonian deformation. The Middle Cambrian and younger rocks in the eastern part of the Quadrangle were apparently not affected by this early deformation, and it has not been indicated as part of the regional structural sequence on the map.

Points of structural interpretation are discussed in further detail in appropriate parts of the text.

Proterozoic rocks

P. R. Williams

Structural interpretation of the Mt Bischoff Precambrian rocks has been confused. Several interpretations of both mesoscopic and macroscopic structures have been put forward (Knight, 1953; Groves and Solomon, 1964; Groves, 1968; Groves *et al.*, 1972; Anderson and Hopwood, 1963; Lambert, 1969; Fitch, 1970), involving the interpretation of the major structure controlling the area as an anticlinorium with superimposed folds producing the varied (but unexplained) fold hinge orientations. No detailed analysis of orientation data was attempted by these authors, although Chappell (1971) divided the region into several structural domains. The connection between these domains was not established.

The method of analysis used here in determining the structural history is based on evidence of superposition of events, including cleavage over-printing, spatial analysis of the orientation of separate fold elements, and the development of accurate geological cross-sections.

STRUCTURAL HISTORY

First tectonic deformation event

The earliest tectonic folds in the area are isoclinal refolded folds, described in detail by Groves (1971) and reproduced in Groves, *et al.* (1972). Diagrams in these papers clearly show the effects of superposition of later folds on the early isoclinal structures, which produces complex interference patterns. Groves and Solomon (1964) also report isoclinal folds and suggest that they are tectonically insignificant. This opinion is reiterated by Groves in Groves *et al.* (1972), despite the use of these early structures to make structural comparison between the Mt Bischoff series and the overlying rocks (Groves, 1971). Lambert (1969) and Fitch (1970) report inverted drag folds and use these to infer that a large part of the sequence is overturned. This conclusion is not supported by Groves in Groves *et al.* (1972).

Early tight to isoclinal folds are abundant throughout the area, and are similar in form to those described from Don Hill (Groves, 1971). In addition isolated fold cores in phyllite are present, and there is a very well developed cleavage sub-parallel to bedding related to these folds over much of the Mt Bischoff region (fig. 14). In addition, the dominant vertical cleavage of E-W trend is a spaced crenulation cleavage produced by deformation of the earlier, shallowly dipping cleavage surface related to the isoclinal folds. In the profile section of the western side of Mt Bischoff (fig. 15) a macroscopic S-fold preserved between steeply northerly dipping surfaces is inferred to be an F_1 fold because it is unrelated in style to the major Mt Bischoff monocline and associated minor folds have the earliest cleavage as their axial surface cleavage. Mesoscopic isoclinal folds exposed in a quarry on the road to the PMG towers on Mt Bischoff summit are also related to major inversion of sedimentary facing and it is proposed that a macroscopic F_1 fold is present in that area.

Evidence of sedimentary facing in the Mt Bischoff series is sparse, but ripple-marks, cross-bedding and graded-bedding are present at various localities, and water-escape structures such as dish structure and convolute folds have all been used to determine facing. Sedimentary facing at various localities on the road to the North Valley workings unequivocally indicates that the beds are overturned. The presence of the major S-fold would therefore indicate that this section of Mt Bischoff is on the lower limb of a south-facing recumbent to reclined anticline. The opposite direction of fold facing inferred by Lambert (1969) and Fitch (1970) may be the result of inferring fold facing from F_1 folds rotated during D2. Unfortunately there is insufficient sedimentary facing evidence and incomplete preservation of unrotated D_1 folds to allow profiles of F_1 folds to be established on either vergence or cleavage/bedding criteria. Significantly, the

Table 17
COMPARATIVE TERMINOLOGY OF DEVONIAN DEFORMATION EVENTS IN TASMANIA (D.B.S.)

	E. Williams (1979)	Black Bluff Range Seymour (1980)		St Valentines Quadrangle	Structural trends St Valentines Quadrangle
LATE FOLD PHASE	Deloraine/Railton trend Zeehan/Gormanston trend	Deloraine/Railton trend	(latest)	D4 (latest)	NW-SE to NNW-SSE
EARLY FOLD PHASE	West Coast Range/ Valentines Peak trend	West Coast Range/ Valentines Peak trend		D3	N-S±10°
		Belvoir trend		D2	NE-SW to NNE-SSW
	Loongana-Wilmot trend	Early, broad E-W trending folds	(earliest)	D1 (earliest)	E-W±20°
		Loongana trend (relative timing unknown)			

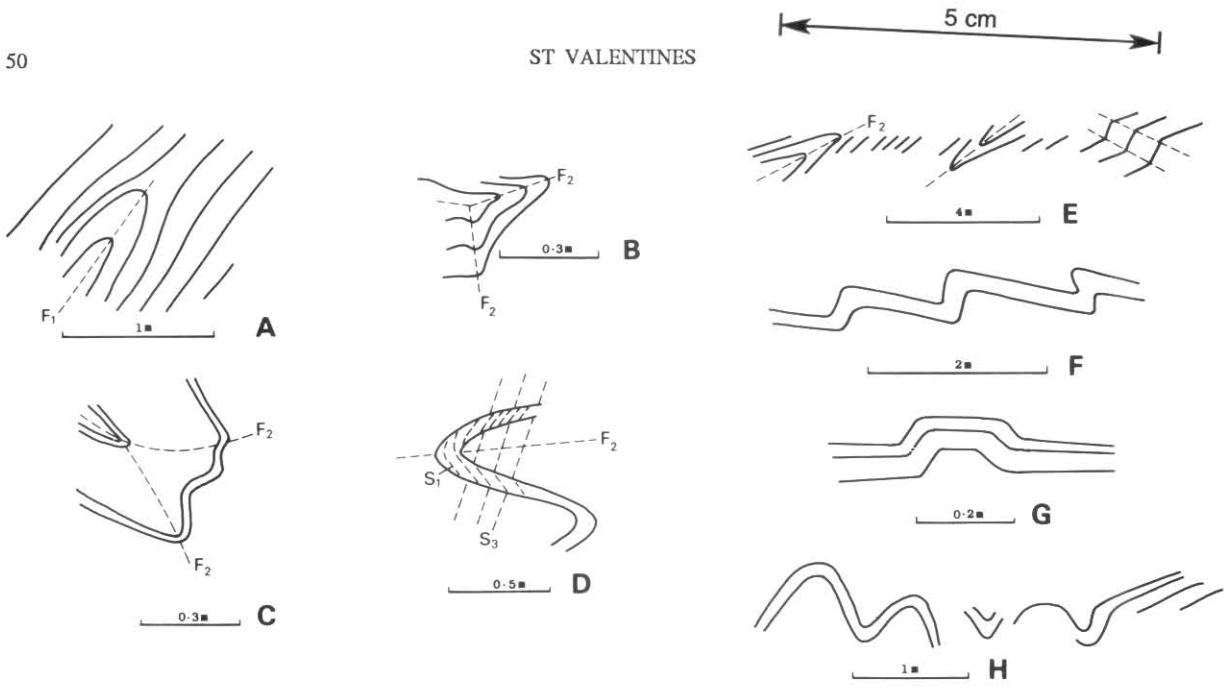

Figure 14. Mesoscopic fold styles at Mt Bischoff. A: Isolated isoclinal fold cores in phyllite; B: F_2 conjugate fold (from Groves, 1971); C: F_2 conjugate fold; D: Cleavage relationship within F_2 fold; E: Typical F_2 fold profile - fold hinge lines are typically non-parallel; F – H: F_3 fold styles. (P.R.W.)

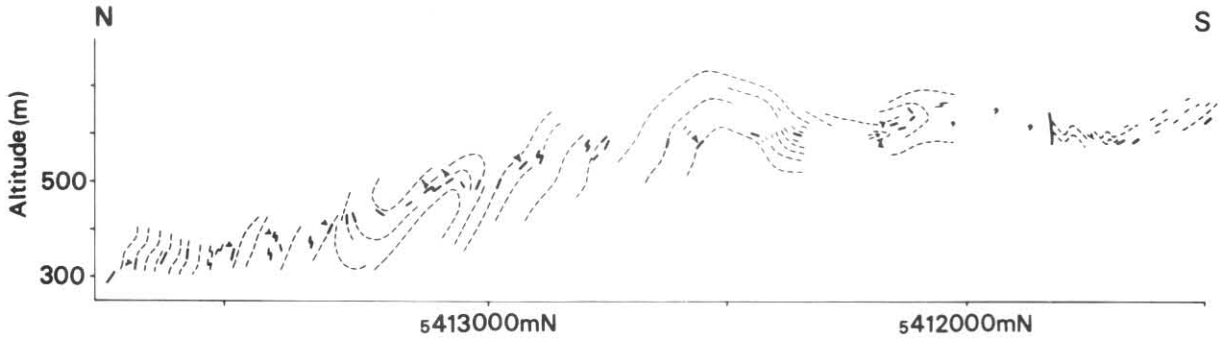

Figure 15. Accurately constructed profile section. Apparent dip of actual readings projected onto the section line indicated by heavy lines. Section is vertical, looking due east along AMG line 376000mE. V/H = 1. (P.R.W.)

sedimentary facing in the Waratah River section suggests that the beds are dominantly upright, which may indicate that the sequence there is on the opposite limb of an F_1 structure. This has not been confirmed by the orientation of F_1 mesoscopic folds and S_1 cleavages.

Second folding event

The second folding event is characterised by the development of conjugate styles are shown in Groves (1971) and Figure 14*b-e*. The varied form of the conjugate folds associated with the D_2 event are explained by the application of a stress field at an angle to the dominant anisotropy caused by the bedding and the cleavage formed during D_1. That the two fold sets, the very open folds and the tight folds which fold a cleavage (fig. 14*d*) belong to the same conjugate system is shown by the convergence of axial planes into a single surface (fig. 14*c*) and the highly variable hinge-line orientation of these folds. F_2 folds are the most abundant mesoscopic structures at Mt Bischoff, but are essentially coaxial with later F_3 folds. The plot of fold hinge-line orientation data on the North Valley road (fig. 16*a*) shows the wide scatter of points, with a concentration in an east-west direction. This plot includes F_3 folds which are more strongly directionally oriented.

Although the hinge lines of the F_2 folds are variably oriented, axial surface directions are more tightly grouped and lie on a great circle, the pole of which coincides with the overall statistical hinge direction (fig. 16*b*). The axial surface directions of D_2 conjugate fold sets vary according to the dip of external bedding, which defines the overall fold pattern of the Mt Bischoff area. A diagram showing the position of axial surfaces in relation to bedding shows that the axial surface direction of conjugates coincide when related bedding values are rotated to coincidence (fig. 17*a*). This is consistent with the rotation of early D_2 structures by D_3, explaining the variation of D_2 axial surface directions. Similarly the line of intersection of the axial surface of actual D_2 conjugate folds (representing the intermediate principal stress direction during D_2 are coincident for all sets irrespective of external bedding orientation (fig. 17*b*). This shows that D_2 and D_3 intermediate principal stress directions were coincident. This coincidence of D_2 and D_3 structures cannot be explained by superposition of the D_2 conjugate sets on an earlier fold (the major fold geometry), because it is not possible to generate the conjugate sets on both the steeply dipping section of structure (the northern side of Mt Bischoff) and the shallowly dipping section with a suitably oriented stress field. In addition, cleavage overprinting of the D_2 folds has been observed (fig. 14*d*), and that cleavage is axial planar to D_3 folds.

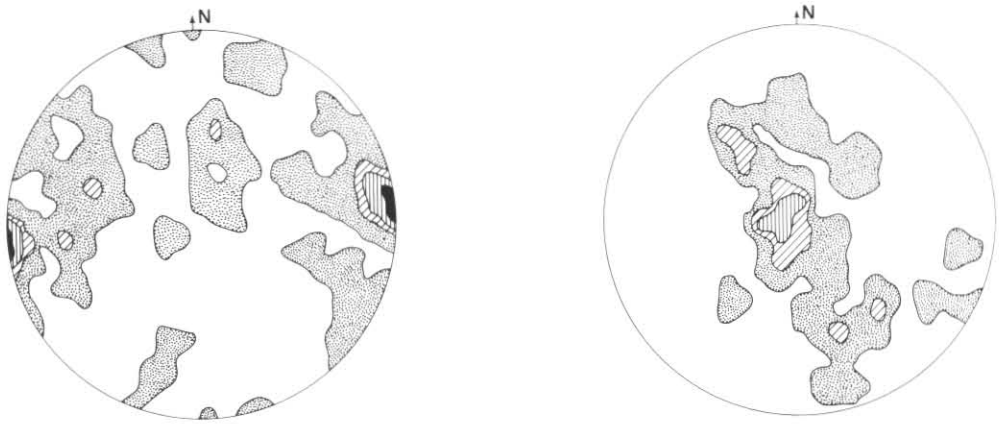

Figure 16. A: Orientation of all fold hinge lines from west of Mt Bischoff summit. Lower hemisphere equal area projection of 56 values contoured at 1, 5, 7, 11% per 1% area. B: Orientation of F_2 axial surfaces from west of Mt Bischoff summit. Lower hemisphere equal area projection of poles to surfaces contoured at 1, 6, 10% per 1% area. (P.R.W.)

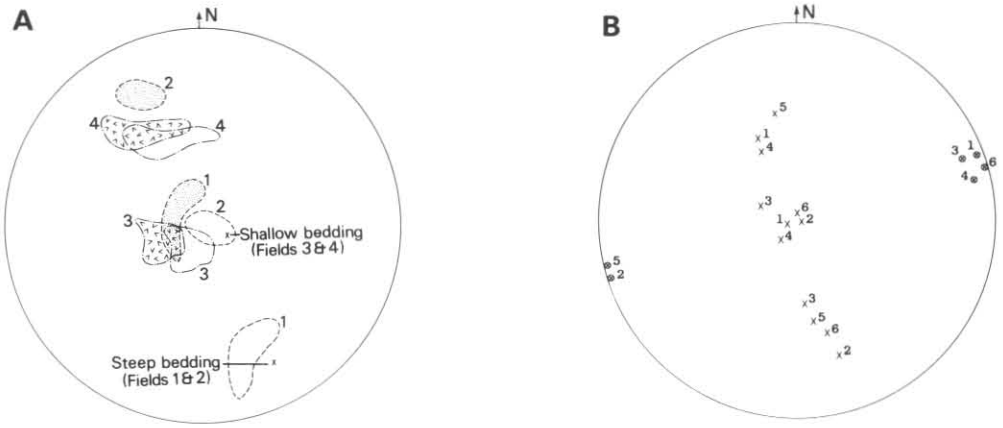

Figure 17. Orientation of conjugate F_2 axial surfaces in relation to bedding. Rotation of bedding values to coincidence (arbitrarily horizontal) results in the close juxtaposition of related folds (fields 1 and 2 related to steeply dipping beds coincide with fields 3 and 4 respectively on rotation). B: Line of intersection of axial surfaces (⊗) related to axial surfaces (×) are coincident before rotation, showing coaxial nature of F_2 and F_3 folds.

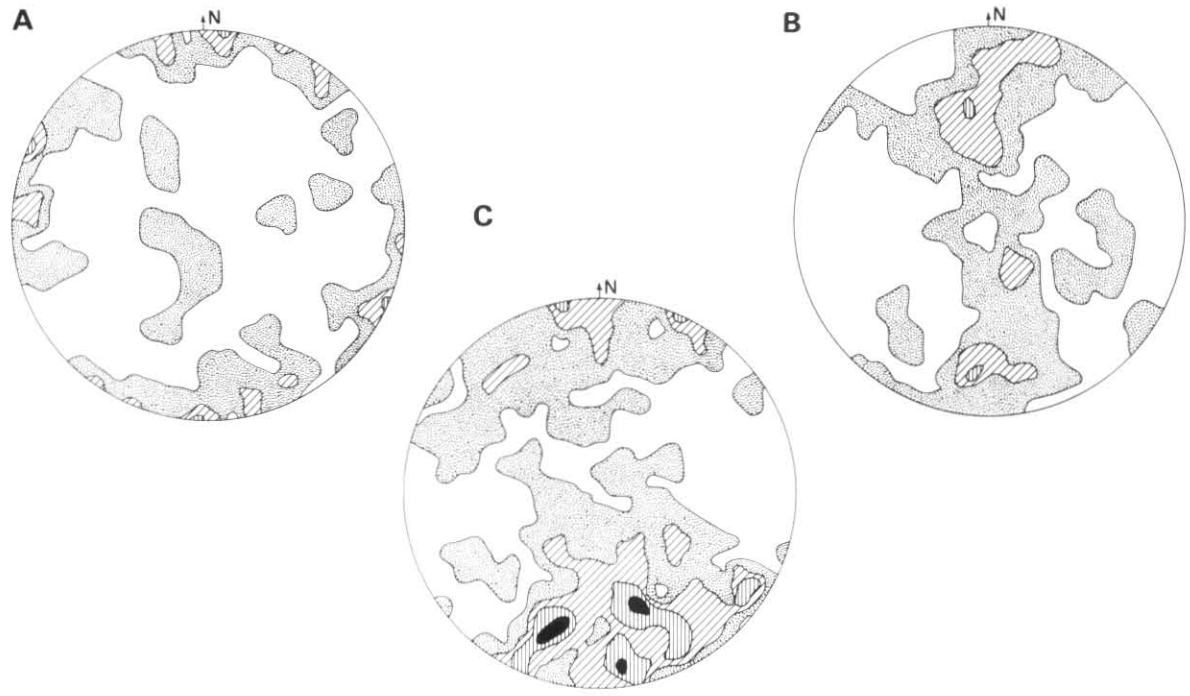

Figure 18. A: Projection of poles to cleavage (lower hemisphere) at Mt Bischoff. 55 values contoured at 1, 5, 9% per 1% area. B: Projection of poles to bedding from east of Mt Bischoff summit (lower hemisphere). 79 values contoured at 0.6, 3.5, 7% per 1% area. C: Projection of poles to bedding from west of Mt Bischoff summit (lower hemisphere). 143 values contoured at 0.35, 2, 3, 4.5% per 1% area. (P.R.W.)

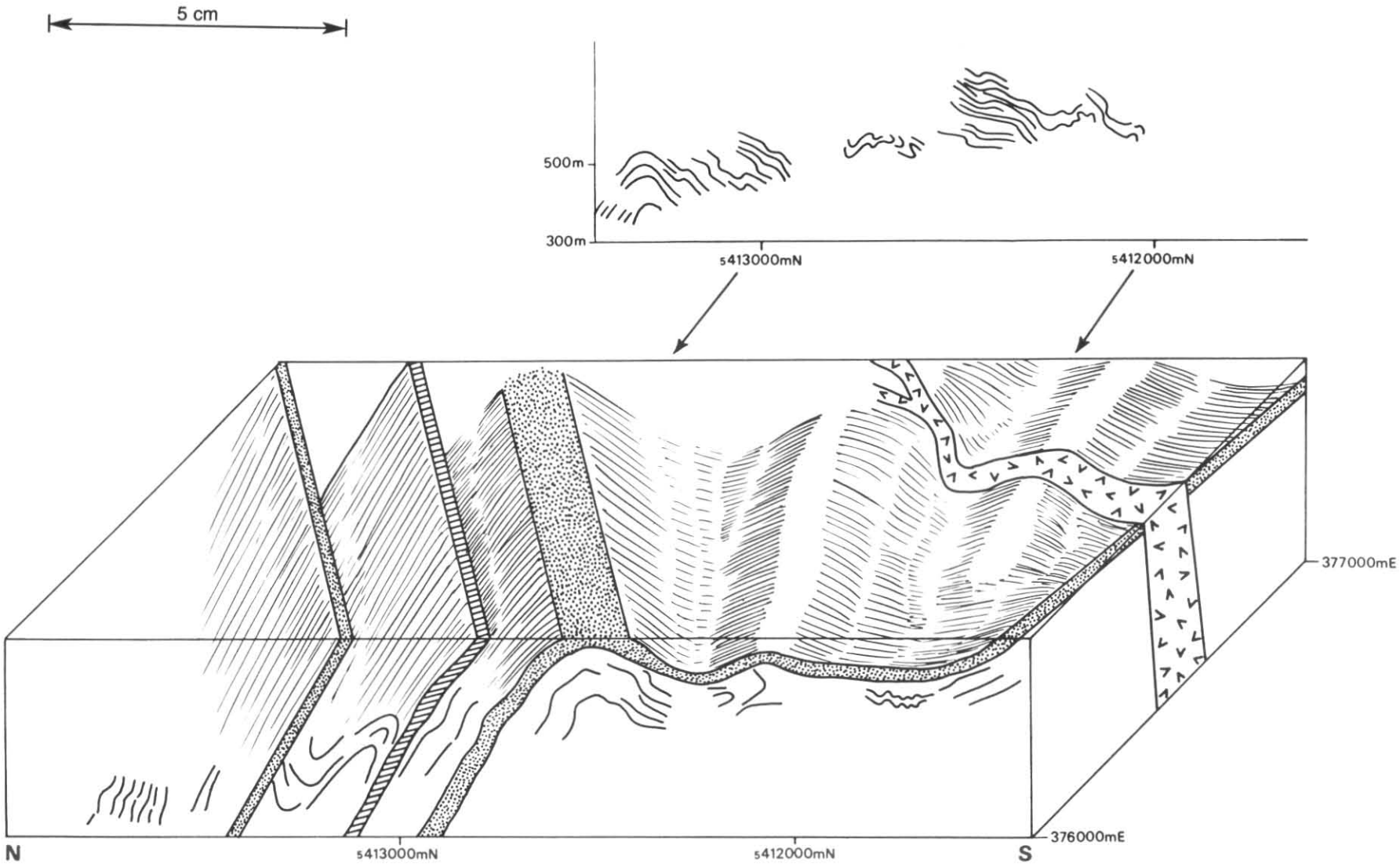

Figure 19. Block diagram showing the geometry of F_3 folds at Mt Bischoff. The structure is transected by a quartz-feldspar porphyry dyke. (P.R.W.)

?Third generation structures

Probable third generation mesoscopic structures are illustrated in Figure 14*f-h*. They are variable in form, as upright flexural slip folds, symmetrical kink bands and single trains of S or Z folds which are probably flexural-slip drag-folds. A moderate cleavage has been developed which overprints pre-existing structures and is consistent in orientation (fig. 18*a*). D_3 folding produced the overall fold geometry of Mt Bischoff shown in Figure 19 along with two measured profile sections. The overall antiformal nature of the structure near the summit of Mt Bischoff is undoubted (*cf.* Groves and Solomon, 1964), but the steep S-facing, southerly-dipping section shown on their cross sections is not confirmed by this study. In particular the southernmost dips shown by Groves and Solomon (1964) are northerly and this study suggests that the enveloping surface of the southern limb of the structure is dipping shallowly north. It is proposed that the overall fold is an antiformal flexure, because the associated cleavage is steeply dipping, but this conclusion can only be proved if drilling data were available in the southernmost area of exposure. The exposed southern section of Mt Bischoff probably represents a broad antiformal crest containing several broad M-folds (see block diagram, fig. 19). Reference to Figure 19 also shows the geometry of the northernmost D_3 fold crest, which has a hinge trace of 230°. The statistical fold hinge direction derived from plots of bedding poles from both the eastern and western cross-sections (fig. 18*b, c*) trends to 268° and 266° respectively. Consequently the D_3 event was also imposed on a shallowly dipping surface and anisotropy caused by several active fabric elements during D_3 produced this discrepancy between fold axis and hinge trace orientations.

?Fourth generation structures

In the open-cut areas, sporadically in the western area and abundantly in the eastern area, a well developed cleavage trending 010-025° is associated with upright flexural slip folds with a half wavelength of about 0.5 m. The fold event is also shown in Figure 18*b* which shows a weaker girdle cutting the N-S girdle indicating folds trending about 035°. This spread is consistent with the broad spread in Figure 18*c*. In thin section the age relationship between the easterly trending cleavage and the NNE-trending cleavage is ambiguous, as both form grain boundary trends and tend to share pressure shadows. Both surfaces have not been studied in a single specimen of phyllite. The form of the spread of bedding, and the consistency of the E-W structures suggests that the NNE-trending event is later. There does not appear to be any macroscopic structure related to the NNE-trending mesoscopic folds.

AGE OF FOLDING IN THE PRECAMBRIAN ROCKS

No large-scale recumbent folding has been reported in Tasmania in rocks younger than the ?Eocambrian-?Early Cambrian sequences, and this observation also applies to the sequences overlying the Mt Bischoff Precambrian rocks. Consequently it is inferred that the recumbent folds (D_1) are Precambrian in age. Groves (1971) reports that the maximum principal stress directions in Mt Bischoff D_2 folds differs from that in the earliest folds in the Cambrian rocks, and this is supported by the current study. It is thus inferred that Mt Bischoff D_2 folds are also Precambrian in age.

However, the major antiformal flexure of Mt Bischoff is coaxial with folds in the Cambrian sequence of the Waratah River and also with folds in Cambrian spilite and argillite/greywacke sequences to the north. Consequently it is postulated that the main Mt Bischoff fold represents a major closure of a fold event which also affected the Cambrian rocks and thus is probably Devonian in age. These are inferred to be the earliest Devonian folds in the region (Seymour, 1980).

The NNE-trending folds are compatible in both style and orientation with folds of the West Coast Range/Valentines Peak trend of Williams, 1979 (shown as D_3 in post-Precambrian rocks on St Valentines Quadrangle), which occur at Mt Pearse and are also present as minor folds in the overlying Cambrian rocks. It is proposed that these folds are of the same age and therefore Devonian.

CONCLUSIONS

The history of deformation of the Mt Bischoff Precambrian rocks, as proposed here, differs substantially from all previous structural interpretations. The inferred antiformal nature of the major D_3 folding, and the inferred recumbent to reclined D_1 event have previously been misinterpreted. In addition, the proposal that the E-W major fold was the earliest folding event (Groves and Solomon, 1964; Groves in Groves *et al.*, 1972) is shown to be incorrect. The complex geometry of fold hinge orientations is caused entirely by the development of conjugate folds on an anisotropic, overturned, dipping surface during D_2, and subsequent rotation of those structures during D_3. Unfortunately, the profile form of D_1 folds cannot be ascertained at this stage, but it is suggested that major D_1 folds may be present between the Waratah River section and Mt Bischoff summit section.

A summary of folding events is as follows:

D_1 produced isoclinal to very tight folds and a good axial surface slaty cleavage in suitable rock types. The major folds were recumbent to reclined;

D_2 produced asymmetric conjugate folds, using bedding and cleavage structures produced during D_1 as active fabric elements. The asymmetry and anisotropy resulted in highly variable hinge line orientations but highly consistent axial surface intersection orientations. Only sporadic cleavage development occurred;

D_3 compression resulted in the formation of the major antiformal flexure defining the Mt Bischoff structure, and also developed an excellent upright crenulation cleavage in suitable rock types. An upright cleavage also developed in sandstone. Anisotropy, caused by the complexity of pre-existing structures, resulted in a large directional divergence between hinge traces and fold axis orientations. The D_2 fold axis (intersection of related axial surfaces) and the D_3 fold axis (statistical axis of bedding rotation) were parallel.

D_4 produced minor folds trending NNE with an associated upright cleavage.

The structural evolution of the Precambrian rocks in the Arthur River in the north-western corner of the Quadrangle is similar, although the early fold events are less well-established there because of difficulties with outcrop.

?Eocambrian-?Early Cambrian rocks

P. R. Williams
P. G. Lennox

West of the Quadrangle boundary, along grid line 24N at CQ742240 a contact is exposed between greywacke of the ?Eocambrian-?Early Cambrian sequence and phyllite of the Proterozoic sequence. The contact is sharp and there is no crushing or distortion of either phyllite or greywacke near the contact. The dominant foliation in the phyllite is locally parallel to the contact. A cleavage in the greywacke about 20° oblique to the contact is parallel to a spaced cleavage in the phyllite. A fault which offsets the contact has a thin mylonite zone associated with it and causes rotation of cleavage in the greywacke. Bedding in the greywacke is parallel to the contact, and beds face away from it. The first bed of the

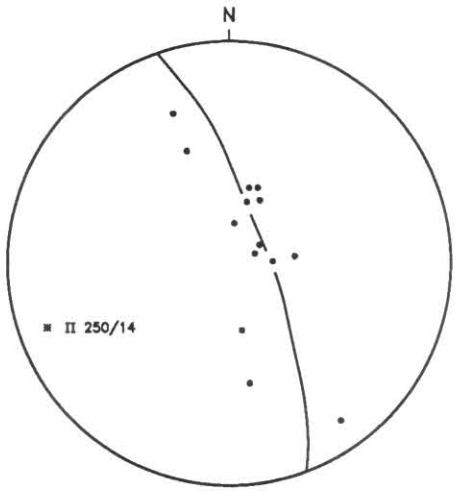

Figure 20. Stereoplot of poles to bedding ?Eocambrian – ?Early Cambrian rocks, Waratah River. Best-fit great circle shown. (P.R.W.)

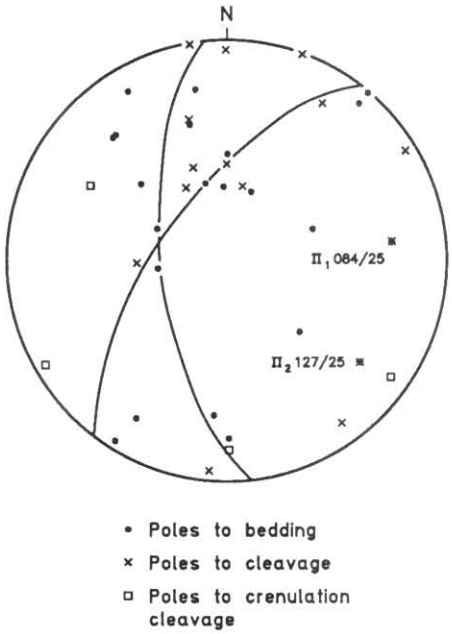

Figure 21. Stereoplot of structural data, ?Eocambrian – ?Early Cambrian sequences south of Mt Bischoff. Best-fit great circles show influence of earlier (π1) and later (π2) folds. (P.R.W.)

?Eocambrian-?Early Cambrian sequence is very muscovite-rich greywacke with abundant sand-sized quartz and phyllite fragments. This is overlain by dark and less weathered greywacke (0.85 m thick) with only quartz and feldspar clasts, and then by thinner graded turbidite beds.

These features are consistent with the contact representing an unconformity. Lack of strong erosion of the phyllite could have been due to the dominant foliation being parallel to the contact, and the contact being below wave base. Any pelagic deposits could have been cleaned off by the first turbidity currents in the area. The absence of fault breccia or mylonite argues against a faulted contact, but definitive structures suggesting either a fault or an unconformity are absent. The observed parallelism of cleavage surfaces in both sequences, and also observed constant orientation of grain alignments in cleavage across the contact, indicate that if there was movement on the contact, it occurred prior to cleavage development in the greywacke. Consequently the contact is a probable unconformity.

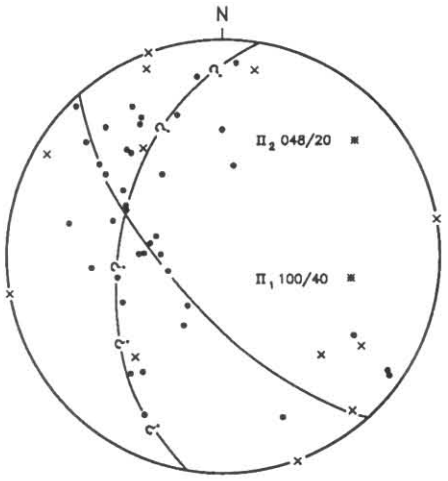

Figure 22. Stereoplot of structural data, ?Eocambrian – ?Early Cambrian rocks, north of ultramafic intrusions and Arthur River. Best-fit great circles show influence of earlier (π1) and later (π2) folds. (P.R.W.)

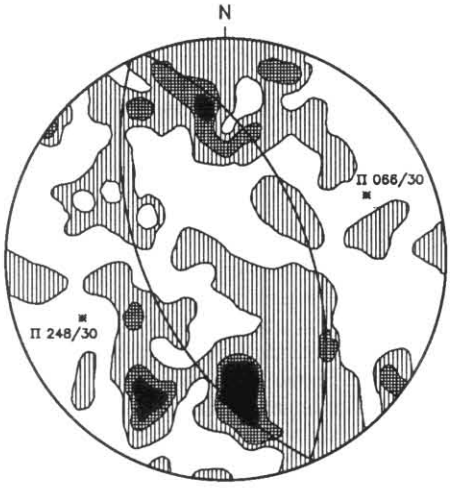

Figure 23. Contoured stereoplot of 54 poles to bedding, ?Eocambrian – ?Early Cambrian rocks between Mt Bischoff and the Deep Gully ultramafics. (P.R.W.)

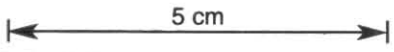

Despite the ambiguous nature of the contact, structures on either side of the contact are significantly different. In the Proterozoic rocks major recumbent to downward-facing folds occur which fold a slaty cleavage, implying that these are F_2 folds. Superimposed on these recumbent structures are three upright crenulation cleavages and associated folds. In the ?Eocambrian-?Early Cambrian sequence there is a single refolded fold, with an axial planar cleavage developed at a low angle to bedding. The dominant cleavages are steeply dipping surfaces related to Devonian folds elsewhere, but a well developed shallowly dipping cleavage surface is present and is axial planar to folds which are folded around the upright structures. The refolded folds are cross-cut by the upright cleavages.

In the sequence of mudstone, sandstone and rare lava overlying the Mt Bischoff Precambrian rocks in the Magnet Tram area [CQ754091], similar overfolds are preserved, producing a shallowly dipping axial plane cleavage cross-cut by two upright cleavage surfaces (trending 090°/270° and 035°/215° in that area). Early, downward-facing folds are also present in the chert sequence on Check Road, west of St Valentines Quadrangle at grid 270 N. There is a well-

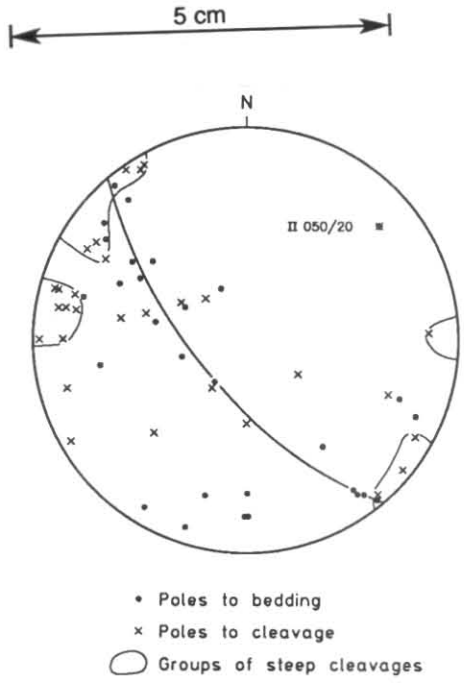

Figure 24. Stereoplot of structural data, ?Eocambrian – ?Early Cambrian rocks, Check Road. (P.R.W.)

developed penetrative cleavage sub-parallel to bedding throughout much of the sequence in this area. Shallowly dipping overturned bedding is present in substantial parts of the section. There is no evidence that the shallow cleavage is only present in fold hinge-zones of later Devonian folds, and therefore these folds are inferred to represent a pre-Devonian deformation event.

Apart from the effects of this early deformation event, there are four sets of upright structures in the area. The earliest of these trends ENE-WSW (070°/250°) and is parallel to the inferred major fold hinge direction of the Mt Bischoff monocline. It comprises shallowly plunging upright structures with only a weakly developed cleavage. It is apparent in the Waratah River sequence adjacent to the Don Hill contact, and is indicated in stereographic projection in Figures 20 and 21.

The next upright cleavage developed on a NE-SW trend, and folding on this trend is apparent from stereographic projections of bedding from sedimentary rocks on Wandle Road north of the ultramafic intrusions. Earlier folds also occur in this area (fig. 22). South of the ultramafic rocks the deformation pattern is simpler, with only the early trends of about 070°/250° being apparent (fig. 23). However in the northern part of the sheet the NE-SW trend is dominant (fig. 24).

Cleavage relationships show that there are folds trending and plunging shallowly SE which affect the earlier cleavages of E-W and NE-SW trend (fig. 21), and that there is a steep cleavage trending east of north which is superimposed on structures of NE-SW trend (fig. 24).

The sequence of Devonian folding episodes and their trends in the ?Eocambrian-?Early Cambrian rocks can be correlated with events elsewhere in north-west Tasmania (E. Williams, 1978). The earliest Devonian folds trend ENE-WSW and include major folds, particularly around Mt Bischoff. They can be correlated with the Loongana/Wilmot trend of E. Williams (1978). The second episode of Devonian deformation (D_2) is represented by dominant structures of NE-SW trend which occur in areas away from the Mt Bischoff Proterozoic rocks, and can be correlated with the Belvoir trend of Seymour (1980) which he considered at the time to be restricted in extent on a regional scale. Clearly it is a more widespread and significant structural trend in north-west Tasmania. In the northern part of the area (north of the Wandle River), the third episode of Devonian deformation (D_3) produced dominant folds and cleavages trending NNE-SSW, and is related to the West Coast Range/Valentines Peak trend (E. Williams, 1978; Seymour, 1980). The final Devonian deformation event (D_4) produced folds and cleavage of NW-SE trend. It can be correlated with the Deloraine-Railton trend of E. Williams (1978). The two later deformation events are not expressed in rocks south of the Wandle River, and it is inferred that the Mt Bischoff Precambrian rocks acted as a competent block during the later deformation events resulting in the protection of surrounding sedimentary rocks from the effects of the deformation.

The deformation which pre-dated the upright folding produced widespread cleavage sub-parallel to bedding. This event has not been detected elsewhere and could be interpreted in two different ways. Either it represents a major structural break between the ?Eocambrian-?Early Cambrian sequences and late Middle Cambrian sequences, or it represents the effects of compression associated with basin rifting. Deformation previously recognised around the edge of the Rocky Cape Block does not include folding (A. V. Brown, pers. comm.), but folding was associated with deformation at the northern margin of the Tyennan Block prior to deposition of the conglomerate units. Northward compression against a NE-trending boundary of the Rocky Cape block with shortening by overthrusting and overfolding could explain these early structures. However, their occurrence in the stratigraphically lower rocks, but not in the higher rocks, implies that this compression was of pre-late Middle Cambrian age, possibly associated with rifting and intrusion of the Bald Hill ultramafic complex, and hence implies significant pre-late Middle Cambrian deformation in the sequences in north-west Tasmania.

In the greywacke sequence of the Hellyer River-Lockwood Creek area, P. G. Lennox has recognised a sequence of three, and possibly four, upright cleavages, overprinting relationships between which were investigated by cutting mutually perpendicular thin sections of oriented samples (e.g. 80-35, 80-40, 80-41). The cleavages were ordered on the basis of bent and disrupted plates of biotite, and kinking and crenulation effects within areas of oriented very fine-grained pale phyllosilicate minerals. The relationships recognised lead Lennox to suggest that the earliest-developed upright cleavage in this area trends NE-SW (i.e. Devonian regional D_2), the next trends N-S (Devonian regional D_3), and the final phase of cleavage development (Devonian regional D_4) may have produced two anastomosing cleavage components trending WNW-ESE and NW-SE. Although such an effect appears to be present in Devonian cleavage development in other parts of the St Valentines Quadrangle (see later discussion), perhaps the possibility should also be considered that the WNW-ESE component indicates the effect of Devonian regional D_1 in this area (D.B.S.). The early deformation which pre-dated the Devonian upright structures in the ?Eocambrian-?Early Cambrian rocks in the Mt Bischoff area was apparently not recognised in the Hellyer River-Lockwood Creek area.

Middle Cambrian rocks

WINTER BROOK AREA

D. B. Seymour

Structural data in the area of Cambrian volcanic and sedimentary rocks surrounding Winter Brook [*c.* DQ150110] has been obtained from only a small number of localities on St Valentines Quadrangle. The area was mapped by Seymour (1980), who obtained a greater density of structural information in the extension of the Winter Brook Cambrian belt several kilometres into the neighbouring Sheffield Quadrangle.

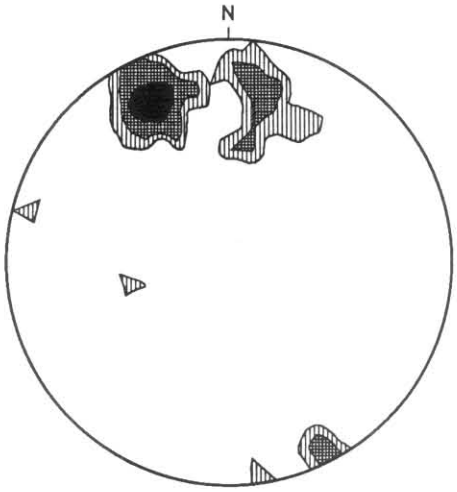

Figure 25. Contoured stereoplot of poles to bedding, pre-Denison Subgroup rocks, Winter Brook area and adjacent areas of the Sheffield Quadrangle (Seymour, 1980). 29 data points, contours at 1, 2, 5 points per 1% area. (D.B.S.)

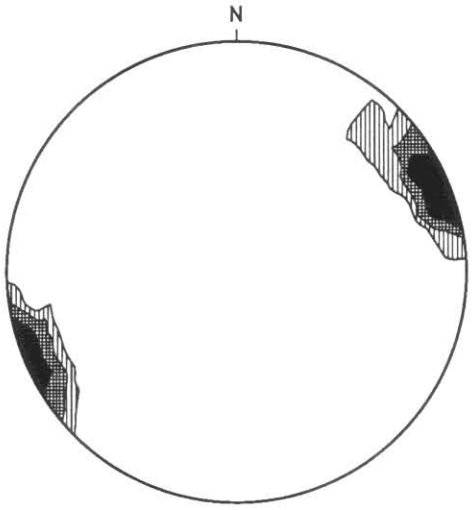

Figure 26. Contoured stereoplot of poles to cleavage, pre-Denison Subgroup rocks, Winter Brook area and adjacent areas of the Sheffield Quadrangle (Seymour, 1980). 52 data points, contours 2, 5, 10 points per 1% area (D.B.S.)

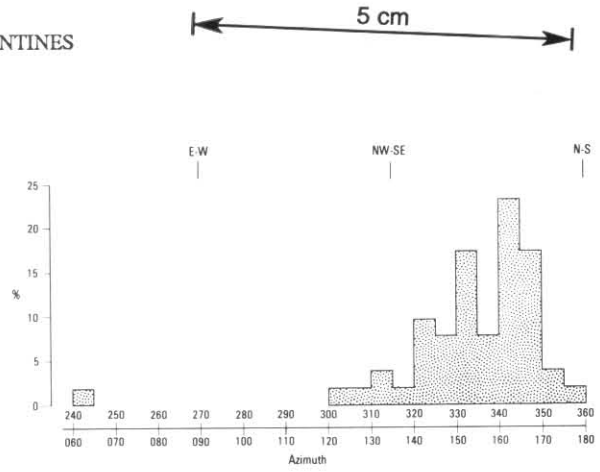

Figure 27. Azimuths of all cleavages, pre-Denison Subgroup rocks, Winter Brook area and adjacent areas of the Sheffield Quadrangle (Seymour, 1980). (D.B.S.)

The data of Seymour (1980) indicate relatively simple structure in the Cambrian rocks in this area, with overall bedding geometry apparently largely unrelated to Devonian structures. Bedding mostly dips steeply SSE or S (fig. 25) with stratigraphic younging in the same direction (based on grading or small-scale cross-lamination). At the small number of localities where bedding dips in the opposite direction (e.g. near DQ192102 on Sheffield Quadrangle), younging is still to the SSE or S. The geological cross-section (Section E-F on the map) suggests the presence of high-angle, angular unconformity between these rocks and the overlying Denison Subgroup correlate in this area. This is particularly apparent around the northern boundary of the small window of Cambrian rocks around DQ150080 to the south of the main Winter Brook belt. Here a close approach to the contact can be achieved from both sides, and steeply dipping compositional layering in the pyroclastic rocks below the contact contrasts with shallowly dipping bedding in the quartzose clastic rocks above. A similar situation exists in the headwaters of a tributary of Winter Brook, near DQ166087 east of the Quadrangle boundary. Perhaps one of the most significant structural aspects of this part of the St Valentines Quadrangle is that the structural relationship of the Denison Subgroup correlate with the rocks immediately underlying it in the Winter Brook area, is apparently the complete opposite of that in the Native Track Tier area to the north, where P. W. Baillie has indicated approximate structural conformity across the contact (see Section E-F on the map).

Most outcrops of Cambrian rocks in the Winter Brook area exhibit a single generation of upright, moderately to strongly developed cleavage. The stereoplot of all field measurements of cleavage in the area (fig. 26) indicates that the dominant trend of this cleavage is NNW-SSE, although the spread in the pattern extends as far as NW-SE. This dominant NNW-SSE cleavage direction is correlated with the Deloraine/Railton trend of E. Williams (1979), shown as D_4 on the St Valentines map. The finer discrimination provided by a 5°-interval histogram of individual strike readings (fig. 27) shows two strong peaks 10° apart but centred on the NNW-SSE direction, as well as some minor peaks closer to NW-SE. Steep to vertical cleavages of NW-SE to NNW-SSE trend developed in the Denison Subgroup correlate immediately north and south of the Winter Brook area are considered to be part of the same generation, the carry-through of cleavages across the contact being particularly obvious around the window of older rocks at DQ150080.

At two localities in Cambrian volcanic rocks east of the St Valentines Quadrangle boundary in the Winter Brook belt, a weakly to moderately developed upright cleavage of N-S trend is present in addition to more strongly developed cleavage of the Deloraine/Railton trend (D_4). This cleavage of N-S trend is correlated with the West Coast Range/Valentines Peak trend (E. Williams, 1979; Seymour, 1980; see table 17 herein), shown as D_3 on St Valentines Quadrangle. It was detected in coarse tuffs and agglomerates in a road cutting at DQ195121, and in an altered ?intermediate lava on the old Devonport Mine track at DQ180094 (Seymour, 1980). At both localities the cleavages are mainly defined by somewhat patchy and zonal development of crystallographic preferred orientations of very fine-grained pale-coloured phyllosilicates. Seymour (1980) suggested that the non-uniform fabric development may have been due to patchiness of earlier hydrothermal alteration in these rocks. Despite this, in thin section the preferred orientations defining the two cleavages appear to be quite critically developed, to the extent that either cleavage can be made virtually invisible by aligning it with the (crossed) polarisers.

Possible overprinting relationships were investigated by examination of horizontally oriented thin sections of oriented samples, in which the largest angle (about 30° in this case) between the cleavage traces is obtained. Overprinting relationships in these rocks generally tend not to be obvious, due to the somewhat patchy and very fine-grained nature of the recrystallisation involved. the criteria used were firstly, that the formation of the later cleavage fabric is associated

with a slight but noticeable asymmetric crenulation of the earlier cleavage fabric; and secondly, that at high magnification, fine-grained phyllosilicates defining the earlier fabric have recrystallised in directions defining the later fabric. Use of these criteria at these two localities seemed to give a consistent result, namely that the cleavage of NW-SE to NNW-SSE trend postdates that of N-S trend. This type of approach using oriented thin sections has been used at a number of localities on St Valentines Quadrangle to investigate structural overprinting relationships.

In some of the pyroclastic rocks in this area, particularly those of ashflow origin, a strong pre-tectonic bedding-parallel foliation of ?compactional origin was apparently present. Where a single tectonic cleavage has developed obliquely to such a primary foliation, it sometimes has a crenulation morphology. An example of this occurs in an ashflow tuff at DQ196103 just east of St Valentines Quadrangle boundary (Seymour, 1980).

The crystal tuffs commonly contain feldspar crystals which were apparently completely altered during pre-tectonic hydrothermal activity. These have in many cases selectively absorbed the tectonic strain, resulting in strongly developed internal preferred orientation of fine-grained phyllosilicates. Again, this fabric is usually constant in orientation from crystal to crystal through the rock, such that in thin section they all go to optical extinction together between crossed polars.

Other tectonic fabric elements present in these rocks include pressure-solution seams, and 'mica beards' (e.g. Williams, 1972; Powell, 1969, 1982) which nucleated on crystals and lithic fragments in tuffs. The beards generally occur as roughly triangular areas of oriented pale phyllosilicates or chlorite projecting from surfaces inclined at moderate to high angles to cleavage, and are best seen in vertical sections perpendicular to cleavage. The phyllosilicates within the beards generally have an overall preferred orientation of [001] traces parallel to the cleavage trace in vertical sections perpendicular to cleavage, while in sections parallel to cleavage a similar preferred orientation commonly defines a lineation which pitches at close to 90° within the cleavage. When the beards are strongly developed they may be the main fabric element responsible for the appearance of cleavage in outcrop and hand specimen. Complementing the beards, and indicating the importance of crack-seal mechanisms in this type of fabric development, quartz crystals and less-altered feldspar crystals in some samples have suffered brittle failure along fractures which have opened and are filled with phyllosilicates with similar preferred orientation to those in the beards on the ends of the grains. Such fractures are usually oriented at high angles to the principal extension direction, but may be controlled by crystal cleavage in feldspar.

MT TOR-TWO HUMMOCKS AREA

D. B. Seymour
P. W. Baillie

Discussion in this section centres on the structure of the four disconnected outcrop areas of Cambrian volcanic and sedimentary rocks underlying the Denison Subgroup correlate in the triangular area roughly bounded by Mt Tor [DQ074128], Two Hummocks [DQ000145], and the point where the Leven River crosses the southern boundary of the Quadrangle [DQ014150]. The available evidence suggests at least local structural conformity across the contact at the base of the Denison Subgroup correlate in this area (see Section C-D on the map), although this relationship is uncertain along the boundary around DQ100060 due to lack of structural data in the basal part of the Denison Subgroup correlate in this vicinity. Apparent structural conformity is particularly evident from bedding data above and below the contact at DQ003145 on Two Hummocks, and near DQ047139 in the Leven River. On the other hand, the apparent asymmetry in limb thicknesses in the large anticlinal structure in the rocks below the contact, outlined by bedding form-lines on Section C-D, suggests a lack of structural conformity on a larger scale, possibly due to low-angle unconformity on the southern flank of this structure. This discrepancy in the cross-section would be reduced if the upper sedimentary part of the Cambrian volcano-sedimentary sequence, beginning at about DQ060109 on Section C-D, belongs more correctly to the Denison Subgroup correlate than to the sequence below. Such an interpretation was indicated following detailed geological mapping in the area by Geopeko Limited (see Rogers, 1976). Nonetheless, large-scale cut-off of the structure in the underlying rocks still appears a distinct possibility if an approximate bedding form-line is traced from DQ045137 around the anticlinal structure south to a point near DQ046121.

A stereoplot of all bedding data from the Cambrian volcanic and sedimentary rocks is shown in Figure 28. Great circle distributions are not particularly obvious on the stereoplot, and the overall structure is apparently not simple. However, there is perhaps a tendency for a distribution of poles to bedding in a band running from NW to SE across the plot (indicative of folding on a NE-SW trend), and a less obvious band running almost E-W across the plot (indicating folding

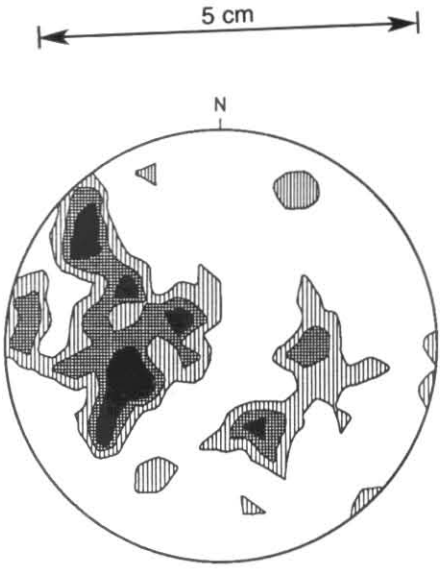

Figure 28. Contoured stereoplot of poles to bedding, pre-Denison Subgroup rocks, Mt Tor – Two Hummocks area. 71 data points, contours 1, 2, 3 points per 1% area. (D.B.S., from data of D.B.S. and P.W.B.)

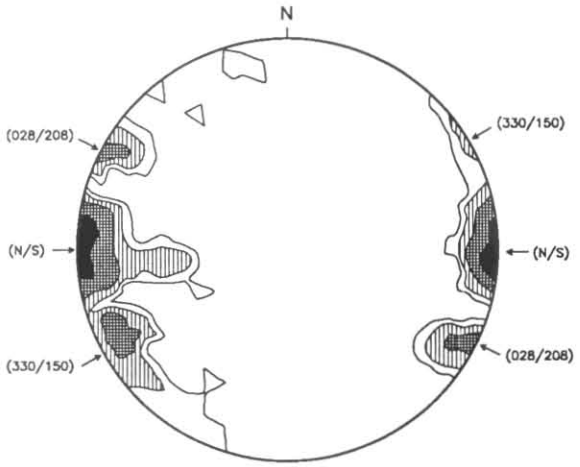

Figure 29. Contoured stereoplot of poles to all cleavages, pre-Denison Subgroup rocks, Mt Tor - Two Hummocks area. Main concentrations indicated, with corresponding trends shown in parentheses. 64 data points. contours 1, 2, 4, 8 points per unit area. (D.B.S., from data of D.B.S. and P.W.B.)

on a N-S trend). Both of these fold trends could be attributed to Devonian deformation (see table 17).

The structural picture is somewhat clearer on examination of cleavages in the area, as virtually all of the characteristics of a stereoplot of poles to all cleavages (fig. 29) can be explained in terms of patterns of Devonian cleavage development. The plot shows three very distinct concentrations. The dominant concentration corresponds to upright cleavage of N-S trend, i.e. the West Coast Range/Valentines Peak trend as re-defined by Seymour (1980), (see table 17), and shown as Devonian regional D_3 on the St Valentines map. The two less dominant concentrations on the plot also represent upright cleavages, distributed about 30° either side of N-S. The cleavage group trending at about 030°/210° belongs to the Belvoir trend of Seymour (1980), shown as Devonian regional D_2 on the St Valentines map. An overprinting relationship between D_2 and D_3 structures is believed to occur in the vicinity of DQ059106 in thinly interbedded crystal tuffs and mudstones, in which an early upright penetrative cleavage trending about 035°/215° (locally close to parallel with bedding) is overprinted by a later upright crenulation cleavage trending N-S (Seymour, 1980). The other group of upright cleavages on the plot, trending at about 150°/330°, is correlated with the Deloraine/Railton trend of E. Williams (1979), identified herein as Devonian regional D_4. Minor folds of this trend occur in road-cuttings at DQ045122. The plot pattern indicates that most D_4 cleavages are steeply NE-dipping rather than vertical (see fig. 29), as is also apparent on the map, suggesting a tendency towards south-westward vergence in D_4 structures in this area. The patterns of the other two cleavage groups on the plot show no such bias.

The three main groups of cleavages are also evident on the 5°-interval histogram of cleavage azimuths (fig. 30). However the finer discrimination of this plot shows a breakdown of the main (D_3) group into two strong peaks about 15° apart and centred on N-S, a similar effect to that observed in the dominant D_4 cleavage pattern in Cambrian rocks in the Winter Brook area (previous section).

ST VALENTINES PEAK AREA

P. G. Lennox
D. B. Seymour

The basic structure of this area is a large upright anticline (half-wavelength about 3 km) and adjacent faulted syncline (see Section A-B on the map). The pattern of bedding form-lines on the geological cross-section suggests structural discordance between the Denison Subgroup correlate and the underlying rocks (as was the case in the Mt Tor-Two Hummocks area), although unrecognised faulting at or near the contact at CQ957222 could also give this impression. P. G. Lennox has reported that actual exposures of the contact

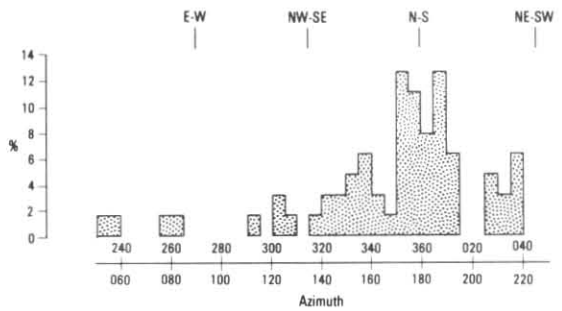

Figure 30. 5°-interval histogram of azimuths of all cleavages, pre-Denison Subgroup rocks, Mt Tor - Two Hummocks area. (D.B.S., from data of D.B.S. and P.W.B.)

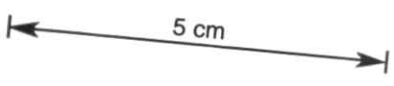

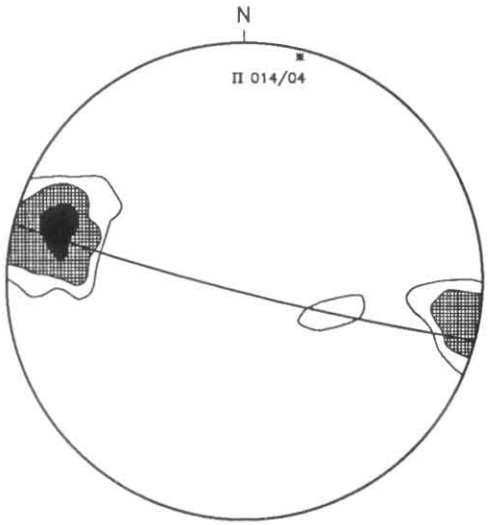

Figure 31. Contoured stereoplot of poles to bedding, Cambrian volcano-sedimentary sequence and Denison Subgroup correlates, Companion Hill - St Valentines area. 162 data points, contours 3.75, 5, 8.5% per 1% area. (P.G.L., re-drawn D.B.S.)

at the base of the Denison Subgroup correlate on both the eastern and western flanks of the belt of underlying rocks show bedding attitudes almost parallel above and below the contact (see Stratigraphy section herein).

A contoured stereoplot of all bedding data in the Denison Subgroup correlates and the underlying Cambrian volcano-sedimentary rocks in the area between Companion Hill and St Valentines Peak indicates that the statistical fold axis is almost horizontal and trending about 015°/195° (fig. 31). This trend presents a correlation problem as it lies half-way between the regional trends of Devonian D_2 and D_3 in the eastern half of St Valentines Quadrangle.

Attempts to clarify the problem by cleavage analysis of the pre-Denison Subgroup rocks are hampered because only a handful of cleavage measurements have been taken in this area. However, in road sections at CQ952213 and in a tributary of the Emu River at CQ948232, steeply eastward-dipping cleavages trending about 025°/205° have been measured (P.G.L.). These cleavages are close in trend to D_2 structures elsewhere in the eastern part of the Quadrangle, and have been identified thus on the map (D.B.S.). Further north at CQ948236 and CQ950241 in the same tributary, P. G. Lennox has measured steeply eastward-dipping cleavages of N-S trend, which have been tentatively correlated with Devonian regional D_3 (D.B.S.). These correlations must be considered as quite interpretive due to the lack of examples of overprinting relationships, and effectively represent a guess (by D.B.S.) that this area was affected by both of the Devonian regional D_2 and D_3 deformation phases. Cleavage development in this area warrants further investigation.

NATIVE TRACK TIER AREA

P. W. Baillie
D. B. Seymour

A considerable amount of structural information has been obtained from the large belt of Cambrian volcanic and sedimentary rocks underlying the Denison Subgroup correlate in the Native Track Tier area, east of the Laurel Creek fault system (P.W.B.). The geological cross-section (see Section E-F on the map) suggests structural conformity across the base of the Denison Subgroup correlate in this area, and also suggests that the structure within the pre-Denison Subgroup rocks is a large symmetrical anticline. Where the contact at the base of the Denison Subgroup correlate has

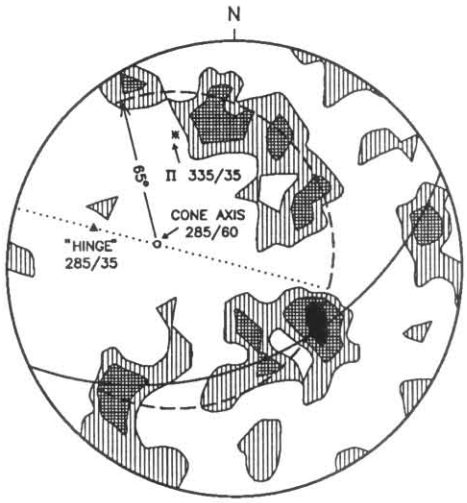

Figure 32. Contoured stereoplot of poles to bedding, pre-Denison Subgroup rocks, Native Track Tier area. Great-circle and conical surface best-fits shown. 70 data points, contours 1, 2, 5, points per 1% area. (D.B.S., from data of P.W.B.)

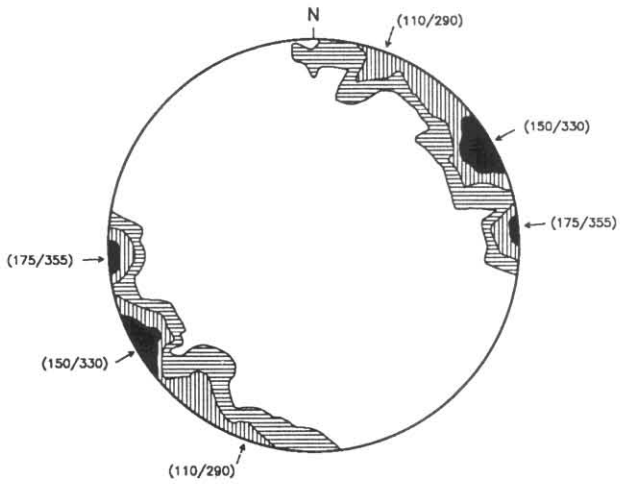

Figure 33. Contoured stereoplot of poles to all cleavage measurements, pre-Denison Subgroup rocks, Native Track Tier area. Main concentrations indicated, with corresponding cleavage trends shown in parentheses. 119 data points, contours 2, 5, 10 points per 1% area. (D.B.S., from data of P.W.B.)

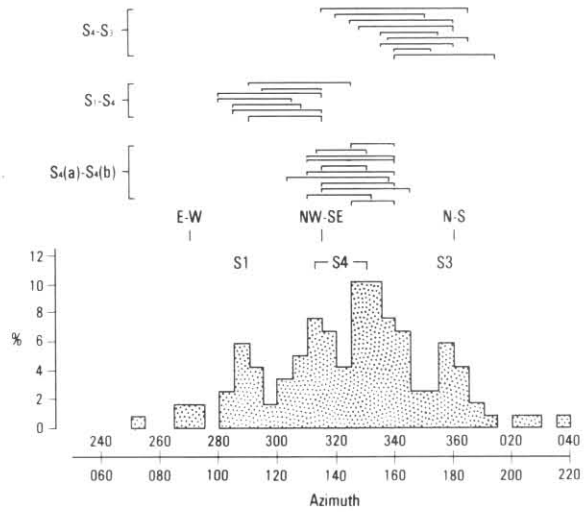

Figure 34. 5°-interval histogram of azimuths of all cleavage measurements, pre-Denison Subgroup rocks, Native Track Tier area. Tie-lines show co-existing cleavages measured in outcrop. (D.B.S., from data of P.W.B.)

actually been observed, either an erosional break or apparent conformity is evident, with no reported occurrences of angular unconformity (P.W.B.; see Stratigraphy section herein).

A stereoplot of all bedding data from the pre-Denison Subgroup rocks in this area (fig. 32) indicates that the fold geometry generally does not fit a simple cylindrical model. The only part of the pattern which may fit a great-circle distribution indicates folding on trends of about 155°/335°, parallel to the most dominant cleavage trend in the area (see below), and correlated with Devonian regional D_4 (Deloraine/Railton trend of Williams, 1979). However, apart from this one possible great-circle fit, the bulk of the pattern of Figure 32 seems to most closely fit a distribution indicating conical folding. The cone axis plunges at 60° to 285°, and assuming that the folding is symmetrical and upright, a fold 'hingeline' can be defined by the intersection of the upright axial surface (trending 105°/285°) with the conically folded bedding surface. This 'hingeline' plunges at 35° to 285°. Moderate westerly plunge is also indicated by the tendency for westward closure in bedding trends on the map, in both the Cambrian volcano-sedimentary sequence and the overlying Denison Subgroup rocks. This dominant upright folding on 105°/285° trend is apparently associated with upright axial plane cleavage development on the same trend (see below), and is also close to parallel with single-phase folds and axial plane cleavage developed in the Gordon Subgroup correlate at Loongana to the south (Loongana trend of Seymour, 1980; see Table 17 herein). All of these structures are now thought to have resulted from the earliest phase of Devonian regional deformation (D_1). The apparent conical geometry of D_1 folds in this area may be a result of interference patterns produced by later cross-folding, as it is apparent from cleavage analysis that D_3 and D_4 have both significantly affected this area (see below).

The stereoplot of all cleavage measurements in the area (fig. 33) shows a number of concentrations, all corresponding to groups of upright cleavages. The most dominant concentration corresponds to upright cleavages trending about 150°/330°, correlated with Devonian regional D_4 (Deloraine-Railton trend of Williams, 1979). A subsidiary concentration representing steep cleavages trending about 130°/310° is only clearly apparent on the south-western side of the plot (indicating a tendency towards steep north-easterly dips) and is also thought to be related to D_4. The second most dominant concentration represents upright cleavages trending almost N-S and is correlated with Devonian regional D_3. The remaining weaker concentration corresponding to upright cleavages trending 110°/290° is interpreted as the expression of D_1 cleavage developed axial planar to the dominant conical folds recognised in the pattern on the bedding stereoplot. The 5°-interval histogram of cleavage azimuths (fig 34) also shows the four peaks clearly defined. The finer discrimination on this plot indicates that the two peaks correlated with D_4 are some 17.5° apart and centred about 7-8° clockwise from NW-SE.

Two cleavages have been measured together in outcrop at a number of localities in the Native Track Tier area (P.W.B.). These coexisting cleavages are indicated by tie-lines on Figure 30. It is notable that at a significant number of localities the two cleavages measured correspond to the two peaks recognised within the D_4 cleavage pattern; these measurements are indicated by the tie-lines labelled $S_{4(a)}$-$S_{4(b)}$ on Figure 34. The other two groups of tie-lines correspond to S_1 and S_4 together, and S_3 and S_4 together. Apparently S_1 and S_3 cleavages were not measured together in outcrop. Overprinting relationships have been suggested at only a small number of localities (P.W.B.). The only observation of probable overprinting of S_1 cleavage occurs in volcanic rocks at DQ161211 in the Leven River, where steeply south-westward dipping cleavage trending NW-SE (S_4)

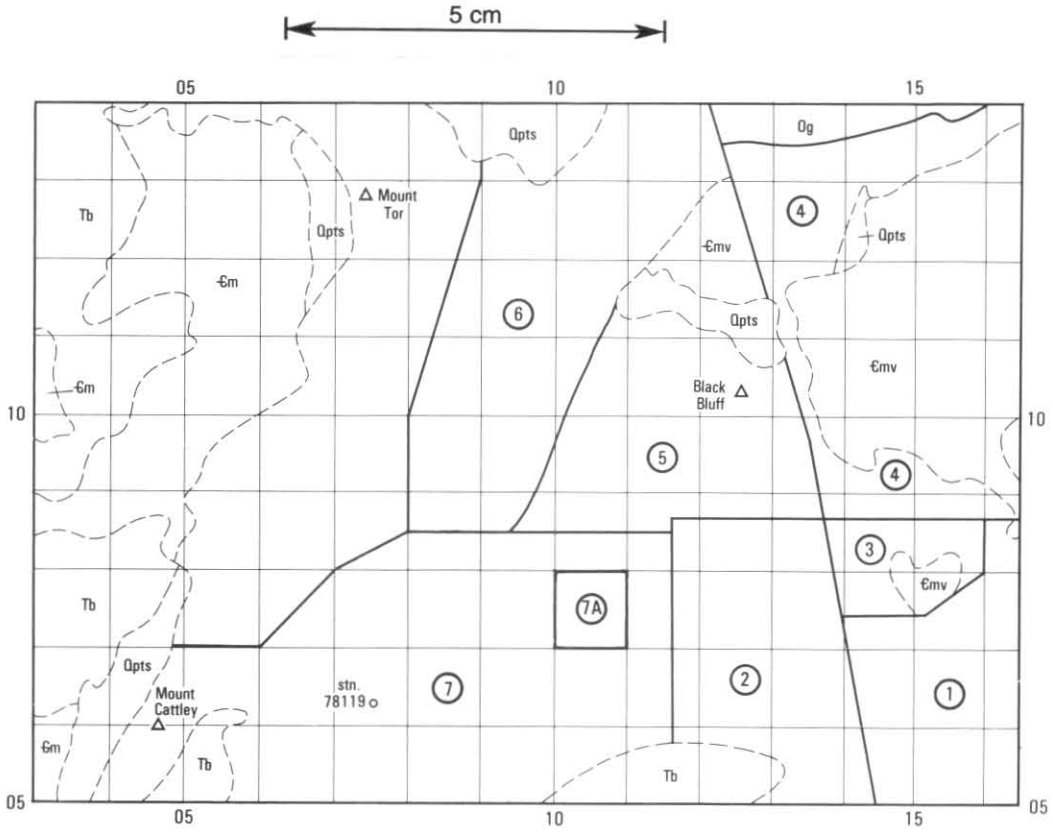

Figure 35. Locality map of south-eastern corner of St Valentines Quadrangle showing sub-areas used in structural analysis of the Denison Subgroup correlate. Symbols as on 1:50 000 geological map, faults not shown. (D.B.S.)

appears to postdate vertical cleavage trending 110°/290° (S_1). In thin bedded siltstones at DQ112205 in the central part of the area, a dominant spaced crenulation cleavage trending 135°/315° and dipping steeply north-east (S_4) apparently overprints a cleavage trending 005°/185° (S_3). A comparable relationship occur in similar rocks at DQ120215 some 1.5 km to the north-east, where minor upright folds trending N-S with vertical axial plane cleavage (F_3/S_3) are apparently transected by a later steep cleavage trending 155°/335° (S_4). However, a contradictory D_3-D_4 relationship was recorded in tuffs and siltstones at DQ110202, where it was considered that steeply west-dipping cleavage trending close to N-S overprints steep cleavage trending 160°/340°.

Minor folds with trends parallel to the more dominant (D_3 and D_4) cleavage trends have been recorded at a number of localities in the volcano-sedimentary sequence in the Native Track Tier area. In the more siliceous sedimentary sequence underlying the Denison Subgroup correlate to the north-west of the Laurel Creek fault system, clusters of shallowly northward and southward-plunging minor D_3 folds occur in association with upright cleavages of the same trend in the vicinity of DQ072218, while D_4 minor folds and cleavages have been recorded at widely separated localities near DQ065209 in the south and near DQ123253 in the Loyetea Peak area in the north.

Denison Subgroup correlate

BLACK BLUFF RANGE AREA

D. B. Seymour

The structural analysis of this area by Seymour (1980) has been considerably revised and refined herein. The bedding geometry of the Denison Subgroup correlates is quite complex due to the interfering fold trends, and an attempt has been made to simplify the analysis by examining bedding data within each of seven sub-areas, shown in Figure 35. The

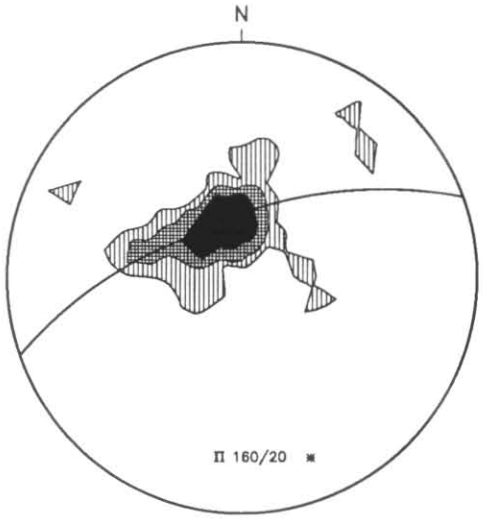

Figure 36. Contoured stereoplot of poles to bedding, Denison Subgroup correlate, Sub-area 1, Black Bluff Range area. 30 data points, contours 1, 2, 4 points per 1% area. Best-fit great circle shown. (D.B.S.)

boundary between Sub-areas 1, 3 and 4 and the remaining sub-areas is drawn along the major fault passing through Paddys Lake, and its possible extension to the south. Cleavage development is generally not strong in these relatively competent rocks, and so the number of cleavage measurements made within each sub-area was small in comparison to the number of bedding measurements. Consequently cleavages are mostly examined *en masse* for the whole area rather than by sub-areas.

Sub-area 1

The stereoplot of bedding data from this sub-area (fig. 36) shows a pattern whose dominant spread indicates a statistical

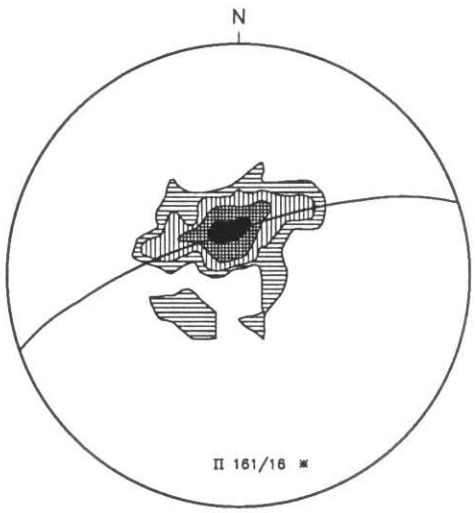

Figure 37. Contoured stereoplot of poles to bedding, Denison Subgroup correlate, Sub-area 2, Black Bluff Range area. 32 data points, contours 1, 2, 4, 8 points per 1% area. Best-fit great circle shown. (D.B.S.)

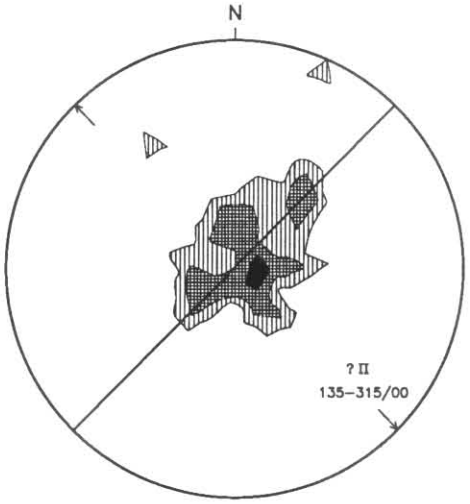

Figure 38. Contoured stereoplot of poles to bedding, Denison Group correlate, Sub-area 3, Black Bluff Range area. 25 data points, contours 1, 2, 4 points per 1% area. Best-fit great circle shown. (D.B.S.)

fold axis which plunges at about 20° to 160°. This fold trend is parallel to the dominant cleavage trend in pre-Denison Subgroup rocks in the Winter Brook area to the north, and it is similarly correlated with the Deloraine/Railton trend of E. Williams (1979), or Devonian regional D_4 herein. The few cleavage measurements made in this sub-area are of more or less N-S trend (Devonian regional D_3) and are therefore probably not related to the dominant folding.

Sub-area 2

Despite being separated from Sub-area 1 by the postulated southward extension of the fault passing through Paddys Lake, the stereoplot of bedding data from Sub-area 2 (fig. 37) has a very similar pattern, with perhaps a more well-defined tendency towards a great-circle distribution. The best-fit great-circle indicates folds plunging at 16° to 161° correlated with Devonian regional D_4. Again, upright cleavages (and minor folds at DQ128081 and DQ136080) measured in the field in this sub-area are of approximately N-S trend and probably belong to D_3.

Sub-area 3

This sub-area includes the surroundings of a triangular inlier of Cambrian volcanic rocks (see fig. 38), and the bedding geometry in the Denison Subgroup correlate here may be somewhat domal. Bedding tends to be shallowly dipping, and the broad elongation of the pattern across the plot suggests folding on NW-SE trends. This apparent trend is some 25° anticlockwise from D_4 cleavage trends in the Winter Brook area and fold trends interpreted as D_4 in Sub-areas 1 and 2. Nonetheless it is still within the full range of structural trends interpreted as due to D_4 in the Black Bluff Range area as a whole (see overall cleavage analysis below).

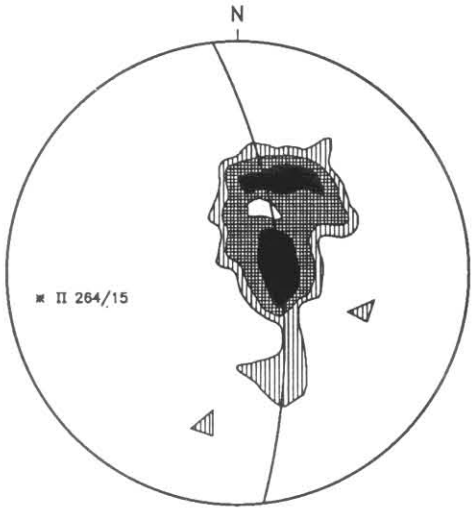

Figure 39. Contoured stereoplot of poles to bedding, Denison Subgroup corelate, Sub-area 4, Black Bluff Range area. 38 data points, contours 1, 2, 4 points per 1% area. Best-fit great circle shown. (D.B.S.)

Sub-area 4

This sub-area takes in the flanks and closure of the broad anticlinal structure enclosing the core of pre-Denison Subgroup rocks surrounding Winter Brook. The great-circle best-fit on the stereoplot of bedding data (fig. 39) indicates a statistical fold axis plunging almost westwards at about 15°. This structural trend is correlated with the group of large open upright folds with horizontal to gently plunging axes trending E-W considered to be the earliest Devonian structures in central northern Tasmania by Jennings (1963), E. Williams (1979), and Seymour (1980). It is therefore considered to be due to Devonian regional D_1. The extra step in correlation taken herein, in comparison with the interpretation of Seymour (1980), is to group this folding on an E-W trend with folding and axial plane cleavage development on trends of about 110°/290° in the Gordon Subgroup correlate at Loongana and in pre-Denison Subgroup rocks in the Native Track Tier area (see table 17). On a regional scale it is also grouped with upright folds and cleavages ranging in trend between about E-W and about 070°/250° in the Precambrian rocks and overlying ?Eocambrian-?Early Cambrian rocks around Mt Bischoff (P.R.W.).

Sub-area 5

Bedding geometry in this sub-area shows a return to the type of structural pattern present in Sub-areas 1 and 2 (see fig. 40). The statistical fold axis (12° to 155°) is within about 5° in trend of that in the other two sub-areas, and the sense of plunge is the same but at a shallower angle. A small but systematic deviation of the pattern from a great-circle distribution suggests that a tendency towards conical folding may be present. The pattern is again interpreted to be largely due to Devonian regional D_4. As was the case in Sub-area 2, many of the upright cleavages measured in this sub-area are of N-S trend (D_3) and are thus probably not related to the dominant folding.

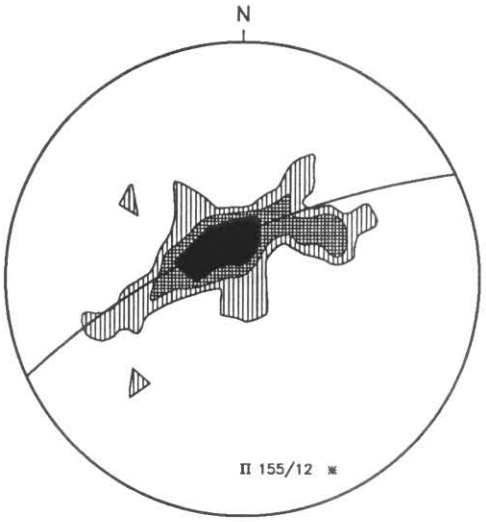

Figure 40. Contoured stereoplot of poles to bedding, Denison Subgroup correlate, Sub-area 5, Black Bluff Range area. 35 data points, contours 1, 2, 4 points per 1% area. Best-fit great circle shown. (D.B.S.)

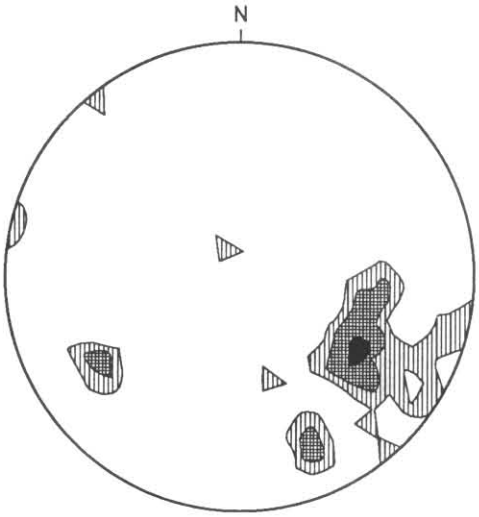

Figure 41. Contoured stereoplot of poles to bedding, Denison Subgroup correlate, Sub-area 6, Black Bluff Range area. 27 data points, contours 1, 2, 4 points per 1% area. (D.B.S.)

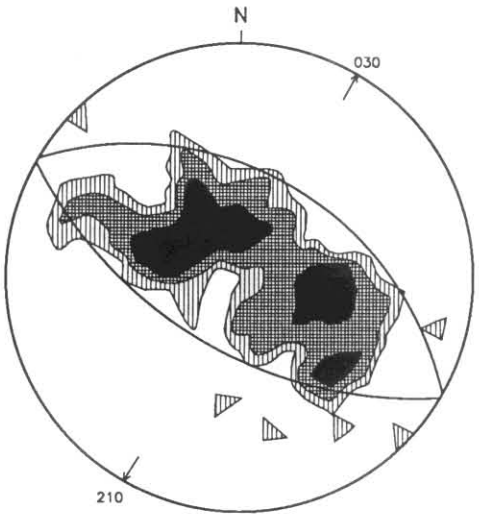

Figure 42. Contoured stereoplot of poles to bedding, Denison Subgroup correlate, Sub-area 7, Black Bluff Range area. 88 data points, contours 1, 2, 4 points per 1% area. Envelope of best-fit great circles shown. (D.B.S.)

Sub-area 6

The stereoplot of bedding data from this sub-area (fig. 41) shows a dominant concentration representing a long NE-trending fold limb with a mean north-westward dip of about 50°. Lack of data in the area to the west of Sub-area 6 precludes showing the corresponding eastward-dipping limb of this structure (see St Valentines map), but the pattern of bedding trends on the map around DQ097125 appears to outline a northward-plunging open syncline (?D_3). A great circle representing part of this structure could possibly be drawn on the stereoplot through the main concentration and the more westerly of the two minor concentrations, and would indicate a northward plunge of about 35°. However, as will be seen, the generally NE-trending fold limb dominating this sub-area may be more closely related to the structural pattern of Sub-area 7.

Sub-area 7

Bedding data from this sub-area form a broad band across the stereoplot, which can be enclosed in an envelope of great circles indicating fold axes plunging at up to about 35° to 030° or 210° (fig. 42). The distribution of the main concentrations on the plot appears to give a strong indication of conical folding, but a conical best-fit would nonetheless still indicate a fold trend similar to that indicated by a cylindrical-fold model. This dominant folding on a 030°/210° trend is correlated with the Belvoir trend of Seymour (1980), see Table 17, and is considered to be due to Devonian regional D_2. Some of the upright cleavages measured in Sub-area 7 are of similar trend (e.g. near DQ087075 and DQ104077) but a considerable number of upright or steeply westward-dipping cleavages of approximately N-S trend (?S_3) were also measured. It thus seems likely that the tendency towards a conical-fold pattern in the bedding geometry of this sub-area is a result of interference between D_2 and D_3.

Some smaller areas within Sub-area 7 yield a more consistent fold plunge. The best example is Sub-area 7A, a kilometre square centred on DQ105075 (see fig. 35). The structural data indicate fairly consistent shallow plunge in directions between about SSW and SW (fig. 43). The great-circle shown is a best-fit to bedding data alone, and yields a statistical fold axis trend a little clockwise from the average trend of minor fold hingelines measured in the field, the latter being about 214°.

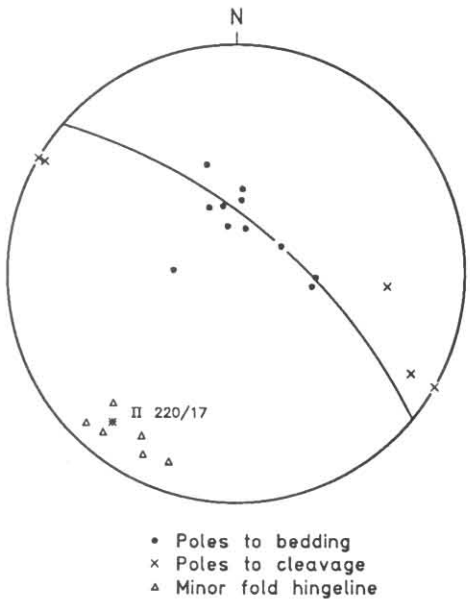

Figure 43. Stereoplot of structural data, Denison Subgroup correlate, Sub-area 7A (part of Sub-area 7), Black Bluff Range area. Great circle best-fit to bedding data shown. (D.B.S.)

5 cm

Minor folds in thin-bedded quartz sandstones at DQ076063 (Station 78119, fig. 44) within Sub-area 7 deviate from the dominant structural trend. The statistical fold axis plunges moderately towards about 283°, while one minor fold hingeline measured plunges at 25° to 265°. This folding may be related to the dominant fold trend in Sub-area 4 (see fig. 39), i.e. Devonian regional D_1.

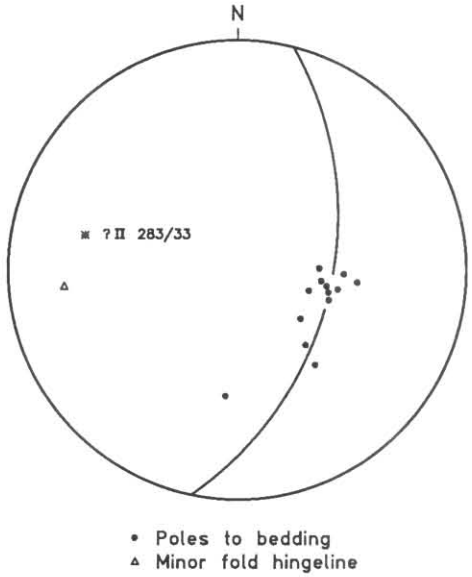

Figure 44. Stereoplot of structural data, Denison Subgroup correlate, Station 78119 (part of Sub-area 7), Black Bluff Range area. Great circle best-fit to bedding data shown. (D.B.S.)

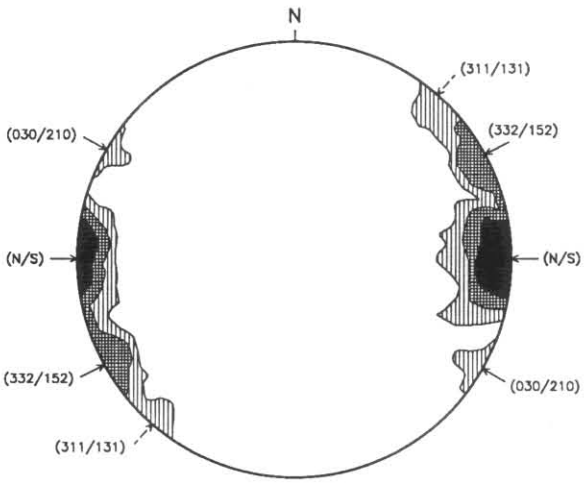

Figure 45. Contoured stereoplot of poles to all cleavage measurements, Denison Subgroup correlate, Sub-areas 1-7, Black Bluff Range area. Main concentrations indicated, with correspponding trends shown in parentheses. 82 data points, contours 2, 5, 10 points per 1% area. (D.B.S.)

Cleavages

All cleavage measurements from the seven sub-areas are plotted together on one stereoplot (fig. 45) and the concentrations in the resultant pattern can be correlated with the major groups of structures in the area. All of the concentrations represent dominantly upright cleavages. The strongest concentration represents cleavages of N-S trend, correlated with Devonian regional D_3. The second-strongest concentration represents cleavage trends of about 150°/330°, and together with a minor concentration some 20° anticlockwise from it is correlated with D_4 (Deloraine/Railton trend of E. Williams, 1979). The small but distinct concentration corresponding to cleavage trends of about 030°/210° derives from Sub-area 7 and is correlated with Devonian regional D_2.

The 5°-interval histogram of cleavage azimuths (fig. 46) again shows a certain amount of breakdown of the concentrations, an effect already noted in other neighbouring areas. The two peaks correlated with D_4 are still evident, as is the peak correlated with D_2, but the group of cleavages centred on N-S (D_3) has apparently broken down into two sub-peaks about 10° apart, a similar effect to that noted in D_3 cleavages in pre-Denison Subgroup rocks in the Mt Tor-Two Hummocks area. The remaining minor peak at about 342° on the histogram was not evident on the stereoplot, but is close to parallel with D_4 fold trends in Sub-areas 1 and 2.

In outcrop, cleavage in the quartz sandstones is often defined mostly by anastomosing cleavage domains spaced about 5-20 mm apart. In thin section the domains are more or less discrete narrow zones up to about 0.5 mm thick, with lower modal quartz content than interdomain areas, and consisting of bunches of discontinuous to semi-continuous dark seams which anastomose around and truncate quartz clasts, the latter having cuspate shapes indicative of pressure dissolution having acted on those faces more or less parallel with cleavage. The seams appear to consist of concentrations of opaque minerals (mostly iron oxides) and fine-grained phyllosilicates.

In some cases, the cleavage is almost solely defined by such domains. However, particularly in the more strongly cleaved and/or more argillaceous rocks, a variably developed tectonite fabric may also be present in the parts of the rock between the domains. This fabric is best seen on vertical sections perpendicular to cleavage, and may be defined by preferred orientation of fine-grained matrix phyllosilicates (including intergrown phyllosilicates + quartz ± iron oxides in 'beard' structures on the clastic grains), and by elongation of clastic quartz grains due to combinations of pressure dissolution of cleavage-parallel faces, passive rotation and intragranular strain. Microfabrics commonly indicate that at least some of the oriented quartz-phyllosilicate intergrowth has formed as extensional fracture infill (crack-seal).

In the coarse siliceous conglomerates, even a single generation of cleavage will anastomose strongly around the pebbles. In the more polymict lithic conglomerates which occur in the basal parts of the Denison Subgroup correlate in places, tectonic strain has commonly been selectively absorbed by the less competent clasts, which are now wrapped around and squeezed between the more rigid quartzose clasts. Argillaceous lithic clasts may develop strong internal preferred orientation of fine-grained

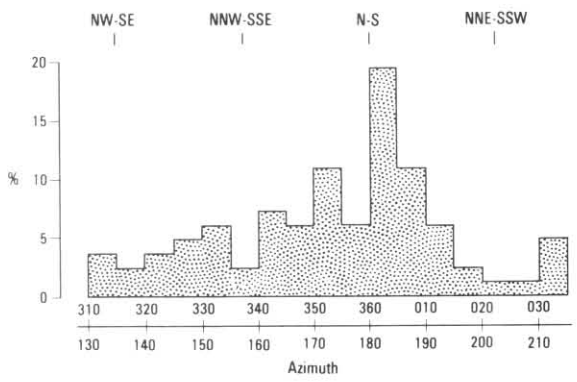

Figure 46. 5°-interval histogram of azimuths to all cleavages, Denison Subgroup correlate, Sub-areas 1-7, Black Bluff Range area. (D.B.S.)

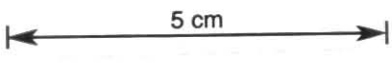

phyllosilicates parallel to the overall rock cleavage. The quartzose clasts may show little apparent internal strain effects but may have well developed triangular 'beard' structures nucleated on them.

These styles of cleavage development, particularly the seam-like cleavages in sandstones, make detection of overprinting relationships very difficult. Nonetheless, in outcrops near DQ112109 and DQ114098 in Sub-area 5, it was considered that the patterns of cleavage seams developed in quartz sandstones indicated the presence of two sets of upright cleavages corresponding in trend to regional D_3 and D_4. A poorly defined overprinting relationship apparent at the first locality indicated that the N-S trending cleavage is the earlier of the two. Similar sets of cleavages have been observed in Denison Subgroup quartz sandstones near DQ172082 and DQ175068 east of St Valentines Quadrangle, but overprinting relationships are obscure at these localities.

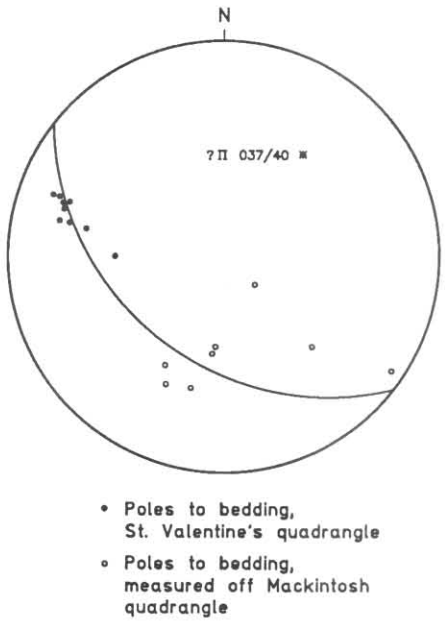

Figure 47. Stereoplot of structural data, Moina Sandstone correlate, Mt Pearse syncline. (P.R.W.)

GRASSTREE RIDGE AND MT PEARSE

P. R. Williams
P. W. Baillie

Little structural data have been obtained from the low outcrops of Moina Sandstone correlates at Grasstree Ridge [c. CQ980130], although the north-east trend of the ridge is probably parallel to the general trend of bedding here. Further to the south-west, similar rocks at Mt Pearse on the southern boundary of the Quadrangle form the easterly-dipping western limb of a major NE-plunging upright open syncline. This structure continues onto the Mackintosh Quadrangle to the south, and bedding data from both the St Valentines and Mackintosh Quadrangles define a statistical fold axis plunging at 40° to 037° (fig. 47). This syncline was included in the West Coast Range/Valentines Peak trend of Williams (1979). However the trend of its axis is close to the 030°/210° trend of structures correlated with Devonian regional D_2 in the south-western part of the Black Bluff Range area on St Valentines Quadrangle (Belvoir trend of Seymour, 1980; see previous section), and it may also correlate with the second set of upright structures (trending NE-SW) recorded by P.R. Williams in the ?Eocambrian-?Early Cambrian rocks of the Mt Bischoff area (see earlier discussion herein). It is therefore considered that the most likely association of the Mt Pearse syncline is with Devonian regional D_2.

ST VALENTINES PEAK AREA

P. G. Lennox
D. B. Seymour

The overall pattern of large upright folds shown on Section A–B in this area is probably largely a result of Devonian regional D_3, although as noted in the discussion of pre-Denison Subgroup structure, the Companion Hill-St Valentines Peak part of the section may have been affected by both D_2 and D_3. Very few cleavage measurements have been made in the Denison Subgroup correlates in this area. In the Moina Sandstone correlate in a tributary of Old Park Creek at CQ968197, P. G. Lennox has noted that a steeply northward-dipping cleavage trending almost ENE-WSW appears to transect a steeply westward-dipping cleavage trending NNE-SSW. These two cleavages fall within the range of trends of Devonian regional D_1 and D_2 respectively, but the apparent overprinting noted by Lennox (which was not definitively proven) contradicts the regional relative age relationship.

NATIVE TRACK TIER AREA

P. W. Baillie
D. B. Seymour

The overall anticlinal structure of the Denison Subgroup correlate in this area (see Section E-F) is considered to be largely a result of Devonian regional D_1. However, bedding trends suggest that the northern limb of this structure has probably been modified by later events. Cleavages and minor folds measured in the various outcrop areas of Denison Subgroup correlates adjacent to Native Track Tier are mostly D_4 structures, and the carry-over of D_4 cleavage across the contact at the base of the Denison Subgroup is particularly obvious around DQ128235 and DQ142293.

Gordon Subgroup correlate

LOONGANA AREA

D. B. Seymour

The Gordon Subgroup carbonate rocks in this area are exposed in an open syncline with a half-wavelength of about 2.5 km, and which is terminated at its western limit by a major NNW-trending steep fault. The exact location, trend and dip of the southern boundary of the limestone are uncertain, but the pattern of bedding form-lines on the geological

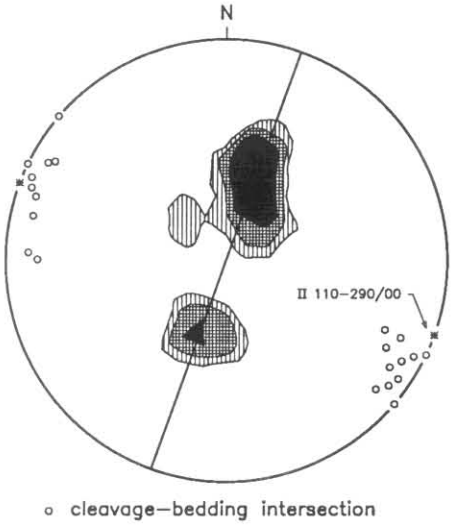

Figure 48. Contoured stereoplot of poles to bedding, Gordon Subgroup correlate, Loongana area. 36 data points, contours 1, 2, 4 points per 1% area. (Excludes Taylors Flats area). (D.B.S.)

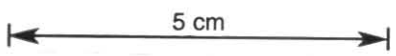

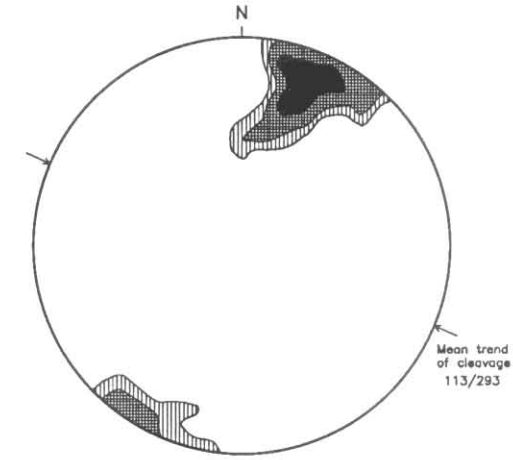

Figure 49. Contoured stereoplot of poles to cleavage, Gordon Subgroup correlate, Loongana area. 29 data points, contours 1, 2, 4 points per 1% area. (Excludes Taylors Flats area). (D.B.S.)

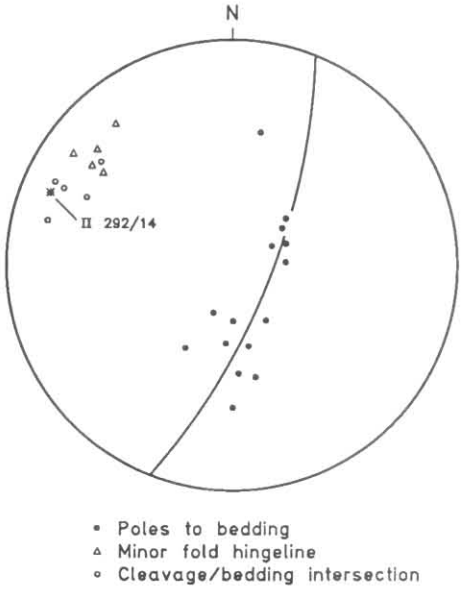

Figure 50. Stereoplot of structural data, Gordon Subgroup correlate, Taylors Flats, Loongana area. (D.B.S.)

cross-section (see Section E-F on the map) strongly suggests a fault relationship with the older rocks to the south.

Analysis of bedding data indicates a statistical fold axis which is horizontal and trending about WNW-ESE (fig. 48). Some data from the western marginal part of the Sheffield Quadrangle is included (Seymour, 1980). The stereoplot of cleavage data (fig. 49) indicates a single generation of cleavage associated with the folding. The cleavages dominantly dip steeply to the SSW, apparently because most measurements are from the northern limb of the syncline and there appears to be an upward-divergent cleavage fan present (see Section E-F). The WNW-ESE structural trend which is dominant in this area is also present in the pre-Denison Subgroup rocks in the Native Track Tier area, and is similarly correlated with Devonian regional D_1 (Loongana-Wilmot trend of Williams, 1979).

Structural data from a small area at Taylors Flats [DQ143143] in the core of the syncline have been considered separately because they indicate shallow westerly plunge (fig. 50). At this locality symmetrical, second-order upright open folds with half-wavelengths of about 100 m are present. The statistical fold axis derived from bedding data has a trend close to parallel with that indicated for the whole Loongana area, and is in approximate agreement with the local average of cleavage/bedding intersections (see fig. 50). However, the average hingeline trend of five small third-order parasitic folds exposed across the closure of a second-order anticline at Taylors Flats deviates by about 18° clockwise from the whole-area trend (fig. 50).

Tectonic fabric elements in the cleaved carbonate rocks in the Loongana area are comparable to those recognised in deformed Gordon Subgroup correlates elsewhere in central northern Tasmania, some of which have been described in detail by Seymour (1975, 1980, 1982*a*, *b*. They include tectonic stylolites (insoluble residue seams resulting from pressure dissolution), pervasive grain-elongation fabrics in very fine-grained micrites, and thin (≤5 mm) calcite fibre-veins whose internal fibre geometry commonly indicates that they have grown by a progressive crack-seal mechanism during a significant part of the strain history of the rock. Fibrous calcite may also form pressure shadows (comparable to phyllosilicate 'beards' in non-carbonate rocks) adjoining large competent grains (e.g. pyrite, quartz). A further important tectonic fabric element in the carbonate rocks is due to intragranular strain expressed mainly as twinning and kinking in coarse calcite spar infilling desiccation vugs ('birdseyes') in dismicrites and forming the cement in sparites.

The tectonic stylolites are assumed to be residue seams consisting of the least soluble components of the bulk rock, namely clays, iron oxides, organic matter and quartz. Their dissolution-related origin is indicated by the common observation of fossil fragments which are truncated against them (e.g. Seymour, 1982*b*). They may not occur in all carbonate lithologies (even when compared at similar strain states) because purity of the bulk rock may be a controlling factor. The work of Seymour (1975) indicated that the first appearance of tectonic grain-elongation fabrics in fine-grained micrite postdates that of tectonic stylolites in the strain history. Thus, at very low strain states (?<15% shortening) cleavage may be defined by tectonic stylolites alone, while at medium to high strains both tectonic stylolites and grain elongation fabrics may be present.

Most of the deformed carbonate rocks at Loongana have well-developed cleavage, commonly with tectonic stylolites with spacing of 5-20 mm, well developed grain elongation fabrics and calcite fibre veins. In some of the more strongly cleaved micrites, well developed down-dip grain elongation lineations are present on the cleavage surfaces. These indicate that the rock fabric is of L-S type in at least some cases, and suggests that the shape of the finite strain ellipsoid is not of purely oblate type.

Some indication of the magnitude of strain associated with cleavage development in the Gordon Subgroup correlate at Loongana was obtained by Seymour (1980) from geometric analysis of the shapes of stromatolites deformed homogeneously with their matrix at Taylors Flats [DQ143143] in the core of the syncline. Cross-sections of the columnar stromatolites are exposed on a sub-horizontal bedding surface at the closure of one of the second-order folds at this locality. A two-dimensional strain ratio for this surface was derived using the methods of Dunnet (1969) and Elliott (1970), and is equivalent to shortening normal to the cleavage of between about 30 and 40%, depending on the assumed type of three-dimensional strain ranging between pure flattening and plane strain (at constant volume).

ST VALENTINES PEAK AREA

P. G. Lennox
D. B. Seymour

The dominant folding on approximately N-S trends in the Gordon Subgroup correlate in this area is probably largely a result of Devonian regional D_3. The structure of the belt of

carbonate rocks has not been studied in great detail because of poor outcrop, but it is apparently faulted against the younger Bell Shale correlate in the south, and faulted in part against Denison Subgroup correlates to the west.

In grey pyritic skarn at DQ015190 in Blythe River upstream of Blythe Road P. G. Lennox has recorded a well developed penetrative upright cleavage trending N-S (?Devonian regional S_3) apparently transected by a spaced upright cleavage which trends NW-SE (?Devonian regional S_4).

GUNNS PLAINS AREA

D. B. Seymour
P. W. Baillie

Only the western marginal part of the synclinal belt of limestone in the Gunns Plains area falls within the St Valentines Quadrangle. The structure of the whole belt has been described by Hughes (1957), whose cross-section shows a large open upright syncline (half-wavelength about 8 km), somewhat asymmetric with the northern limb longer than the southern limb. In his description Hughes states that the syncline axis trends 120°/300°, but a stereoplot of the bedding data on his map indicates that the statistical fold axis is horizontal, and trends 115°/295°. This is within 5° of the dominant statistical structural trend present in the Gordon Subgroup correlate at Loongana, and thus the overall structure at Gunns Plains is similarly assigned to Devonian regional D_1.

Cleavages have been measured at only one locality in the Gunns Plains area on St Valentines Quadrangle, and give an indication that the area may also have been affected by Devonian regional D_4. Thus, in burrowed dolomitic micrites at DQ162253, P.W. Baillie has recorded a dominant steeply SW-dipping cleavage trending 155°/335° (?regional S_4) and an apparently earlier vertical cleavage trending 120°/300°, presumably associated with the main folding and thus identified as regional S_1.

Eldon Group correlates

P. G. Lennox
D. B. Seymour

The internal structure of the fault block of Bell Shale correlates cropping out around CQ980200 and DQ005175 has not been analysed in detail due to lack of data. However, steeply W-dipping cleavages trending almost N-S recorded by P. G. Lennox near CQ981208 are probably Devonian regional S_3, and steeply NE-dipping cleavages which trend approximately NW-SE near CQ975188 are probably S_4. If these correlations are correct the Bell Shale in this area has been affected by at least the last two phases of Devonian deformation.

No structural data have been obtained from the small outcrops identified as Florence Quartzite near CQ955145 on Guildford Road.

Effects of intrusion of the Housetop Granite

As already noted, the shape of the boundaries of the Housetop Granite strongly suggests that joints and other pre-existing structures in the country rocks have controlled the path of intrusion in a number of places, and that stoping was a major mechanism of intrusion. P. G. Lennox has suggested that there may also have been some shouldering aside of the country rocks in the St Valentines Peak area due to the intrusion of the granite, apparently based partly on the belief that the 015°/195° structural trend of the Companion Hill-St Valentines Peak anticline has been warped away from an original N-S trend. However, as noted earlier (D.B.S.) the pattern of structural trends in the area may be due solely to the combined effects of Devonian regional D_2 and D_3 prior to granite intrusion.

Faulting

None of the mapped faults on St Valentines Quadrangle, including those affecting the Parmeener Supergroup correlates in the west of the region, appear to affect the Tertiary rocks. All of the recognised faults appear to be steeply dipping or vertical.

In the west of the map sheet, many of the boundaries of the Parmeener Supergroup correlates against adjacent older rock units are faults (P.R.W., P.G.L.). Near St Valentines Peak an elongate triangular area of Denison Subgroup conglomerate is fault-bounded on all sides against adjacent younger rock units, while just to the south-east apparently all of the boundaries of the Bell Shale correlate against adjoining older rock units are also steep faults (P.G.L.). In the same general area, aeromagnetic anomaly patterns have indicated that the fault shown near DQ013248 on Holloway Creek may be the eastern extension of a NW-trending fault which extends as far west as the Guildford Road-Emu Bay Railway junction at CQ958291 (pers. comm. to P.G.L. by R. G. Gifford, McIntyre Mines). In the Native Track Tier area, P. W. Baillie has brought attention to the fact that the major fault system extending from south-east of Mt Everett to near Loyetea Peak separates Middle Cambrian sequences of significantly different character (see Stratigraphy section).

In the Black Bluff Range area in the south-east of the map sheet, most of the mapped faults trend about NNW-SSE, the principal one being the steep fault passing through Paddys Lake [DQ132104]. This fault may have both west-side-up and dextral components in its total relative movement, and may extend well to the south and off the map sheet, probably passing down the valley of a tributary of the River Lea extending NNW from the abandoned Blacks gold prospect [DQ146053]. Boundary offsets associated with the other more minor faults in this area are consistent with most of them also having west-side-up components in their total relative movements.

REFERENCES

ANDERSON, D. E.; HOPWOOD, T. P. 1963. *The geology of Mt Bischoff.* Aberfoyle Tin Development Partnership.

ANONYMOUS. 1983 *Exploration Licence 33/79, Waratah, Tasmania. Report for the year ended 14 July 1983.* BHP Exploration Department. [TCR 83-2026].

ANONYMOUS. 1984*a*. *Exploration Licence 23/79, Wynyard, Tasmania. Annual report for the year ended 1 December 1983* BHP Exploration Department. [TCR 84-2085].

ANONYMOUS. 1984*b*. *Exploration Licence 33/79, Waratah, Tasmania. Report for the year ended 14 July 1984.* BHP Exploration Department. [TCR 84-2295].

BAILLIE, P. W. 1987a. Completion report : Sub-basalt Drilling Project Hole 1. *Unpub. Rep. Dep. Mines Tasm.* 1987/38.

BAILLIE, P. W. 1987*b*. Completion report : Sub-basalt Drilling Project Hole 2. *Unpub. Rep. Dep. Mines Tasm.* 1987/40.

BAILLIE, P. W. 1987*c*. Completion report : Sub-basalt Drilling Project Hole 4. *Unpub. Rep. Dep. Mines Tasm.* 1987/61.

BAILLIE, P. W.; GREEN, G. R.; COLLINS, P. L. F. 1987. Progress report on the Sub-basalt Drilling Project. *Unpub. Rep. Dep. Mines Tasm.* 1987/44.

BAILLIE, P. W.; GREEN, G. R. 1988a. Completion report : Sub-basalt Drilling Project Hole 6. *Unpub. Rep. Dep. Mines Tasm.* 1988/06.

BAILLIE, P. W.; GREEN, G. R. 1988b. Completion report : Sub-basalt Drilling Project Hole 9. *Unpub. Rep. Dep. Mines Tasm.* 1988/07.

BAILLIE, P. W.; JAGO, J. B. 1985. A new Cambrian fossil locality from Native Track Tier, north-west Tasmania. *Unpubl. Rep. Dep. Mines Tasm.* 1985/15.

BANKS, M. R. 1962. Ordovician System, *in* SPRY, A. H.; BANKS, M. R. The Geology of Tasmania. *J. geol. Aust.* 9:147-176.

BANKS, M. R.; BURRETT, C. F. 1980. A preliminary Ordovician biostratigraphy of Tasmania. *J. geol. Soc. Aust.* 26:363-375.

BARTON, C. M.; BURNS, K. L.; GEE, R. D.; GROVES, G. I.; GULLINE, A. B.; JENNINGS, D. J.; LONGMAN, M. J.; MARSHALL, B.; MATTHEWS, W. L.; MOORE, W. R.; NAQVI, I. H.; THREADER, V. M.; URQUHART, G. 1966. Geological atlas 1 mile series. Zone 7 sheet 44 (8014N). Mackintosh. *Department of Mines, Tasmania.*

BROADBENT, G. 1982. Geology of the Mt Bischoff mine area, *in Sydney Metals Exploration Group Symposium: tin in south-east Australia*. Sydney Metals Exploration Group : Sydney.

BROADHURST, E. 1934. Report on the Stormont, Bell Mount and Black Bluff district. *Unpubl. Rep. Dep. Mines Tasm.* 1934:34-45.

BROOKS, C. 1966. The rubidium-strontium ages of some igneous rocks. *J. geol. Soc. Aust.* 13:457-469.

BROWN, A. V. 1986. Geology of the Dundas-Mt Lindsay-Mt Youngbuck region. *Bull. geol. Surv. Tasm.* 62.

BROWN, A. V.; FORSYTH, S. M. 1984. Chemistry of Tertiary basalt and palynology of interbedded sediments from B.H.P. drill holes, E.L. 33/79. *Unpubl. Rep. Dep. Mines Tasm.* 1984/39.

BROWN, A. V.; MCCLENAGHAN, M. P.; TURNER, M. J.; BAILLIE, P. W.; MCCLENAGHAN, J.; LENNOX, P. G. L.; WILLIAMS, P. R. 1982. Geological atlas 1:50 000 series. Sheet 73(8112N). Huntley. *Tasmania Department of Mines.*

BULL, W. B. 1972. Recognition of alluvial-fan deposits in the stratigraphic record. *Spec. Publ. Soc. econ. Paleont. Mineral.* 16:63-83.

BURNS, K. L. 1962. Barytes and manganese near Guildford. *Tech. Rep. Dep. Mines Tasm.* 7:45-46.

BURRETT, C. F. 1978. *Middle-Upper Ordovician conodonts and stratigraphy of the Gordon Limestone Subgroup, Tasmania.* PhD thesis, University of Tasmania : Hobart.

BURRETT, C. F.; STAIT, B.; SHARPLES, C.; LAURIE, J. 1984. Middle-Upper Ordovician shallow platform to deep basin transect, southern Tasmania, Australia, *in* BRUTON, D. L. (ed). *Aspects of the Ordovician System*:149-157. Universitetsforlaget : Oslo.

CAS, R. A. F.; WRIGHT, J. V. 1984. *Modern and Ancient Volcanic Successions : an approach to analysis of facies, environments of deposition and tectonic setting - course notes.* Department of Earth Sciences, Monash University.

CHAPPELL, K. G. 1971. *Structural geology of Mt Bischoff.* B.Sc. (hons) thesis, University of Tasmania : Hobart.

COLLINS, P. L. F. 1975. The Devonport gold mine, Black Bluff. *Tech. Rep. Dep. Mines Tasm.* 18:10-13.

COLLINS, P. L. F. 1982. Geology and mineralization at Mt Bischoff and Renison Bell. Excursion guide, *in* GREEN, D. C. (ed). *Geology mineralization, exploration - Western Tasmania*: 43-51. Tasmanian Division, Geological Society of Australia : Hobart.

COLLINS, P. L. F. 1983. *Geology and mineralization at the Cleveland mine, western Tasmania.* Ph.D. thesis, University of Tasmania : Hobart

COLLINS, P. L. F.; GULLINE, A. B.; WILLIAMS, E. 1981. Geological atlas 1 mile series. Sheet 44 (8014N). Mackintosh. *Explan. Rep. geol. Surv. Tasm.*

COLLINS, W. J.; BEAM, S. D.; WHITE, A. J. R.; CHAPPELL, B. W. 1982. Nature and origin of A-type granites with particular reference to southeastern Australia. *Contrib. Mineral. Petrology* 80:189-200.

CORBETT, K. D. 1975. The Late Cambrian to Early Ordovician sequence on the Denison Range, southwest Tasmania. *Pap. Proc. R. Soc. Tasm.* 109:111-120.

CORBETT, K. D. 1979. Stratigraphy, correlation and evolution of the Mt Read Volcanics in the Queenstown, Jukes-Darwin and Mt Sedgwick areas. *Bull. geol. Surv. Tasm.* 58.

CORBETT, K. D. 1981. Stratigraphy and mineralization in the Mt Read Volcanics, western Tasmania. *Econ. Geol.* 76:209-230.

CORBETT, E. B.; BANKS, M. R. 1974. Ordovician stratigraphy of the Florentine synclinorium, southwest Tasmania. *Pap. Proc. R. Soc. Tasm.* 107:207-238.

CORBETT, K. D.; BANKS, M. R. 1975. Revised terminology of the Late Cambrian-Ordovician sequence of the Florentine-Denison Range area, and the significance of the 'Junee Group'. *Pap. Proc. R. Soc. Tasm.* 109:121-126.

CREENAUNE, P. J. 1980. *The volcanics of the Heazlewood River complex.* B.Sc. (hons) thesis, University of Tasmania : Hobart.

DUNNETT, D. 1969. A technique of finite strain analysis using elliptical particles. *Tectonophysics* 7:117-136.

EDWARDS, A. B. 1950. The petrology of the Cainozoic basaltic rocks of Tasmania. *Proc. R. Soc. Vict.* 62:97-120.

ELLIOTT, D. 1970. Determination of the finite strain and initial shape from deformed elliptical objects. *Bull. geol. Soc. Am.* 81:2221-2236.

FITCH, R. 1970. *The Mount Bischoff mine area.* Ph.D. thesis, University of Tasmanja : Hobart.

GEE, R. D. 1977. Geological atlas 1 mile series. Zone 7 sheet 28 (8015N). Burnie. *Explan. Rep. geol. Surv. Tasm.*

GEE, R. D.; GULLINE, A. B.; BRAVO, A. P. 1968. Geological atlas 1 mile series. Zone 7 sheet 28 (8015N). Burnie. *Department of Mines, Tasmania.*

GROVES, D. I. 1968. *The cassiterite-sulphide deposits of western Tasmania.* Ph.D. thesis, University of Tasmania.

GROVES, D. I. 1971. The regional significance of the Don Hill fault zone of Mt Bischoff. Tasmania. *Tech. Rep. Dept. Mines Tasm.* 14:7-15.

GROVES, D. I.; SOLOMON, M. 1964. The geology of the Mt Bischoff district. *Pap. Proc. R. Soc. Tasm.* 98:1-22.

GROVES, D. I.; MARTIN, E. L.; MURCHIE, H.; WELLINGTON, H. K. 1972. A century of tin mining at Mt Bischoff. *Bull. geol. Surv. Tasm.* 54.

HARLAND, W. B.; COX, A. V.; LLEWELLYN, P. G.; PICKTON, C. A. G.; SMITH, A. G.; WALTERS, R. 1982. *A Geologic Time Scale* . Cambridge University Press.

HARRIS, W. K. 1968. Tasmanian Tertiary and Quaternary microfloras: summary report. *Pal. Rep. Dep. Mines S. Aust.* 5/68.

HARRIS, W. K. 1973. Tertiary non-marine dinoflagellate cyst assemblages from Australia. *Spec. Pub. geol. Soc. Aust.* 4:159-166.

HENDERSON, Q. J. 1939. Departmental report on the Devonport mine, Black Bluff. *Unpubl. Rep. Dep. Mines Tasm.* 1939:61-64.

HONNOREE, J.; KIRST, P. 1975. Submarine basaltic volcanism: morphometric parameters for discriminating hyaloclastites from hyalotuffs. *Bull. volcanol.* 39:1-25.

HUGHES, T. D. 1957. Loongana. *Miner. Resour. Tasm.* 10:138-141.

HUGHES, T. D. 1960. Magnetite deposits at Loyetea. *Tech. Rep. Dep. Mines Tasm.* 5:98-100.

JACK, R. 1963. Magnetometer survey, Hampshire iron ore deposit. *Tech. Rep. Dep. Mines Tasm.* 8:51-55.

JACK, R. 1964. Drilling results, Hampshire iron ore deposits. *Tech. Rep. Dep. Mines Tasm.* 9:22-23.

JAGO, J. B. 1973. Paraconformable contacts between Cambrian and Junee Group sediments in Tasmania. *J. geol. Soc. Aust.* 20:373-377.

JAGO, J. B. 1976. Late Middle Cambrian agnostid trilobites from the Gunns Plains area, north-western Tasmania. *Pap. Proc. R. Soc. Tasm.* 110:1-18.

JAGO, J. B.; PIKE, G. A.; MILLS, D. 1975. Cambrian stratigraphy of the St Valentines Peak area, north-western Tasmania. *Pap. Proc. R. Soc. Tasm.* 109:85-90.

JENNINGS, I. B. 1958. The Round Mount district. *Bull. geol. Surv. Tasm.* 45.

JENNINGS, I. B. 1963. One mile geological map series. K/55-6-45. Middlesex. *Explan. Rep. geol. Surv. Tasm.*

JENNINGS, I. B. 1979. Geological atlas 1 mile series. Zone 7 Sheet 37. Sheffield. *Explan. Rep. geol. Surv. Tasm.*

JENNINGS, I. B.; BURNS, K. L.; MAYNE, S. J.; ROBINSON, R. G. 1959. Geological atlas 1 mile series. Zone 7 Sheet 37. Sheffield *Department of Mines, Tasmania.*

KNIGHT, C. L. 1953. Mount Bischoff tin mine. *Publs 5th emp. min. metall. Congr.* 1:1185-1193.

KOKELAAR, P. 1986. Magma-water intersections in subaqueous and emergent basaltic volcanism. *Bull. volcanol.* 48:275-289.

LABRECQUE, J. L.; KENT, D. V.; CANDE, S. C. 1977. Revised magnetic planning time scale for Late Cretaceous and Cenozoic time. *Geology.* 5:330-335.

LAMBERT, J. R. 1969. Explanation of Mt Bischoff geology map. Anglo-American Corporation (Australia) Ltd.

LEAMAN, D. E. 1986. *Mount Read Volcanics Project : Interpretation and evaluation report, 1981 West Tasmania aeromagnetic survey.* Department of Mines, Tasmania.

LUCAS, D. S. 1988. *Magnetics of the Tertiary Basalts of north-western Tasmania.* B.Sc. (Hons.) thesis, University of Tasmania : Hobart.

MCCLENAGHAN, M. P. 1985. Granitoids of northeastern Tasmania. *BMR J.* 9:303-312.

MCDOUGALL, I.; LEGGO, P. J. 1965. Isotopic age determinations on granitic rocks from Tasmania. *J. geol. Soc. Aust.* 12:295-332.

MILLS, A. A. 1984. Pillow lavas and the Leidenfrost effect. *J. geol. Soc. Lond.* 141:183-186.

MILLS, D. N. 1971. *The St Valentines Peak granite-metasediment contact zone.* B.Sc.(Hons.) thesis, University of Tasmania : Hobart.

MOORE, J. G. 1975. Mechanism of formation of pillow lava. *Am. Sci.* 63:269-277.

NOLDART, A. J. 1969. Notes on the Hampshire Silver Mine. *Tech. Rep. Dep. Mines Tasm.* 13:40-44.

PARTRIDGE, A. D. 1973. Revision of the spore-pollen zonation in the Bass Basin. *Esso Pal. Rep.* 1973/4.

PARTRIDGE, A. D. 1976. The geological expression of eustasy in the early Tertiary of the Gippsland Basin. *APEA J.* 16:73-79.

PETTERD, W. F. 1910. *Catalogue of the Minerals of Tasmania.* Department of Mines, Tasmania.

PIKE, G. 1964. *Geology of the region around St Valentines Peak, Tasmania.* B.Sc.(Hons.) thesis, University of Tasmania : Hobart.

POLTOCK, R. A. 1985. Cambrian windows in the Black Bluff Range, *in* ROBERTS, P. A. *E.L. 41/83, western 56 sq.km. Relinquishment Report.* Gold Fields Exploration Pty Ltd.

POWELL, C. M. 1969. Intrusive sandstone dykes in the Siamo Slate near Negaunee, Michigan. *Bull. geol. Soc. Am.* 80:2585-2594.

POWELL, C. M. 1982. Overgrowths and mica bears on rounded quartz grains enclosed by cleavage folia, *in* BORRADAILE, G. J.; BAYLY, M. B.; POWELL, C. M. (ed.) *Atlas of deformational and metamorphic rock fabrics.* Springer-Verlag.

RAFTER, T. A.; SOLOMON, M. 1967. Sulphur isotope and oxygen isotope studies of Tasmanian ore deposits. *in: The geology of western Tasmania - A Symposium.* Univ. Tasm. Geology Dept. : Hobart.

RITTMANN, A. 1962. *Volcanoes and their Activity.* Wiley : New York.

ROGERS, M. C. 1976. Loongana area - Tasmania, Progress Report E.L. 2/76. *Geopeko Ltd, King Island, Rept.* K1/76/5.

RUBENACH, M. J. 1973. *The Tasmanian ultramafic-gabbro and ophiolite complexes.* Ph.D. thesis, University of Tasmania : Hobart.

SEYMOUR, D. B. 1975. *Deformation studies of the Gordon Limestone and Moina Sandstone.* B.Sc. (Hons) thesis, University of Tasmania : Hobart.

SEYMOUR, D. B. 1980. *The Tabberabberan Orogeny in northwest Tasmania.* Ph.D. thesis, University of Tasmania : Hobart.

SEYMOUR, D. B. 1982*a*. Finite strain and pressure-solution processes in a deformed limestone *in* BORRADAILE, G. J.; BAYLY, M. B.; POWELL, C. M. (ed.) *Atlas of deformational and metamorphic rock fabrics.* Springer-Verlag.

SEYMOUR, D. B. 1982*b*. Pressure dissolution as a cleavage-forming process in quartz sandstone and limestone, *in* BORRADAILE, G. J.; BAYLY, M. B.; POWELL, C. M. (ed.) *Atlas of deformational and metamorphic rock fabrics.* Springer-Verlag.

STOVER, L. E.; PARTRIDGE, A. D. 1973. Tertiary and Late Cretaceous spores and pollen from the Gippsland Basin, South-eastern Australia. *Proc. R. Soc. Vict.* 86:237-286.

TWELVETREES, W. H. 1913. The Middlesex and Mt Claude mining field. *Bull. geol. Surv. Tasm.* 14.

WEBBY, B. D.; VAN DEN BERG, A. H. M.; COOPER, R. A.; BANKS, M. R.; BURRETT, C. F.; HENDERSON, R. A.; CLARKSON, P. D.; Hughes, C. P.; LAURIE, J.; STAIT, B.; THOMSON, M. R. A.; WEBERS, G. F. 1981. The Ordovician System in Australia, New Zealand and Antarctica: correlation chart and explanatory notes. *I.U.G.S. Publ.* 6.

WESTE, G. 1978. *E.L. 7/74 Moina, Tasmania. Black Bluff - Smiths Plain area. Report on all investigations to September 1978.*

WILLIAMS, E. 1979. *Tasman fold belt system in Tasmania. Explanatory notes for the 1:500 000 structural map of pre-Carboniferous rocks of Tasmania.* (revd ed.) Department of Mines, Tasmania.

WILLIAMS, H.; MCBIRNEY, A. R. 1979. *Volcanology.* Freeman, Cooper.

WILLIAMS, P. F. 1972. 'Pressure shadow' structures in foliated rocks from Bermagui, New South Wales. *J. geol. Soc. Aust.* 18:371-377.

WILLIAMS, P. R.; BROWN, A. V. 1983. An unusual occurrence of ultramafic and rocks north of Mt Bischoff, NW Tasmania. *Pap. Proc. R. Soc. Tasm.* 117:53-58.

WOHLETZ, K. H. 1983. Mechanisms of hydravolcanic pyrochist formation: grain size, scanning electron microscopy and experimental studies. *J. Volcanol. geotherm. Res.* 17:31-63.

WOLFF, G. C. 1978. Excursion 2. The Kara tungsten deposit. *in*: GREEN, D. C.; WILLIAMS, P. R. (ed.), *Geology and mineralization of N.W. Tasmania:*37-38. Geological Society of Australia, Tasmanian Division : Hobart.

APPENDIX A

Economic Geology

METALLIC MINERALS

N. J. Turner
R. S. Bottrill
D. B. Seymour

Mt Bischoff Tin Field

N. J. Turner

Mt Bischoff was the first major mineral resource to be discovered and developed in western Tasmania and was the richest tin deposit in the world during the earlier part of its exploitation, prior to 1900. Most production was from ore bodies held by the Mt Bischoff Tin Mining Company (fig. A1) with minor production coming from the Wheal or Giblin Lode to the west (fig. A2), mainly while the lode was being worked by the Mt Bischoff Extended Tin Mining Company in the period 1907–1919. The tin concentrate from Mt Bischoff was smelted at the Mt Bischoff Tin Mining Company's smelters in Launceston.

Sources of particular importance in the preparation of the following summary were the accounts of the various ore bodies and their geology given by Reid (1923) and the detailed accounts of history, mining, metallurgy and geology in Groves *et al.* (1972).

PRODUCTION AND RESERVES

Up to 1921 the Mt Bischoff Tin Mining Company treated 4.598 million tonnes of open-cut and underground ore for an average recovery grade of 1.17% Sn (Reid, 1923). From 1921 to the end of major hard-rock mining in 1947 the Company and then the Commonwealth and State Governments treated about 0.8 Mt of lower grade ore from the same sources. The Wheal-Giblin Lode and associated workings produced about 0.15 Mt of underground ore, mostly at a recovery grade of 0.94% Sn, in the period to 1918 (Reid, *op. cit.*) and about 0.09 Mt thereafter. About 0.2 million cubic metres of North Valley alluvium, mainly derived from the Waratah River flats (fig. A2) were treated by the Mt Bischoff Tin Mining Company in the period 1928–1942 whilst another 0.556 million cubic metres were treated for 570.167 tonnes of tin in concentrates by Ringarooma Mining Pty Ltd in the period 1972–1976. Altogether about 62 000 t of metallic tin in concentrates were produced from the Mt Bischoff tin field to 1978.

Following a period of detailed prospecting a 4 km^2 area surrounding the old mines was granted as a Retention Licence in 1988 to a joint venture syndicate comprising Comstaff Pty Ltd, Preussag and Metals Exploration Ltd. Geological mapping, trenching, auger and rock-chip sampling, aeromagnetic and ground magnetic studies were followed by diamond, percussion and reverse circulation drilling on 20 × 20 m and 40 × 40 m grids to establish a basis for calculation of ore reserves. Reserves were classified into two ore types namely, dolomite-sulphide lode ore (0.3% Sn cut-off) and quartz porphyry ore (0.2% Sn cut-off). Combined proved, probable and possible reserves of dolomite-sulphide ore are

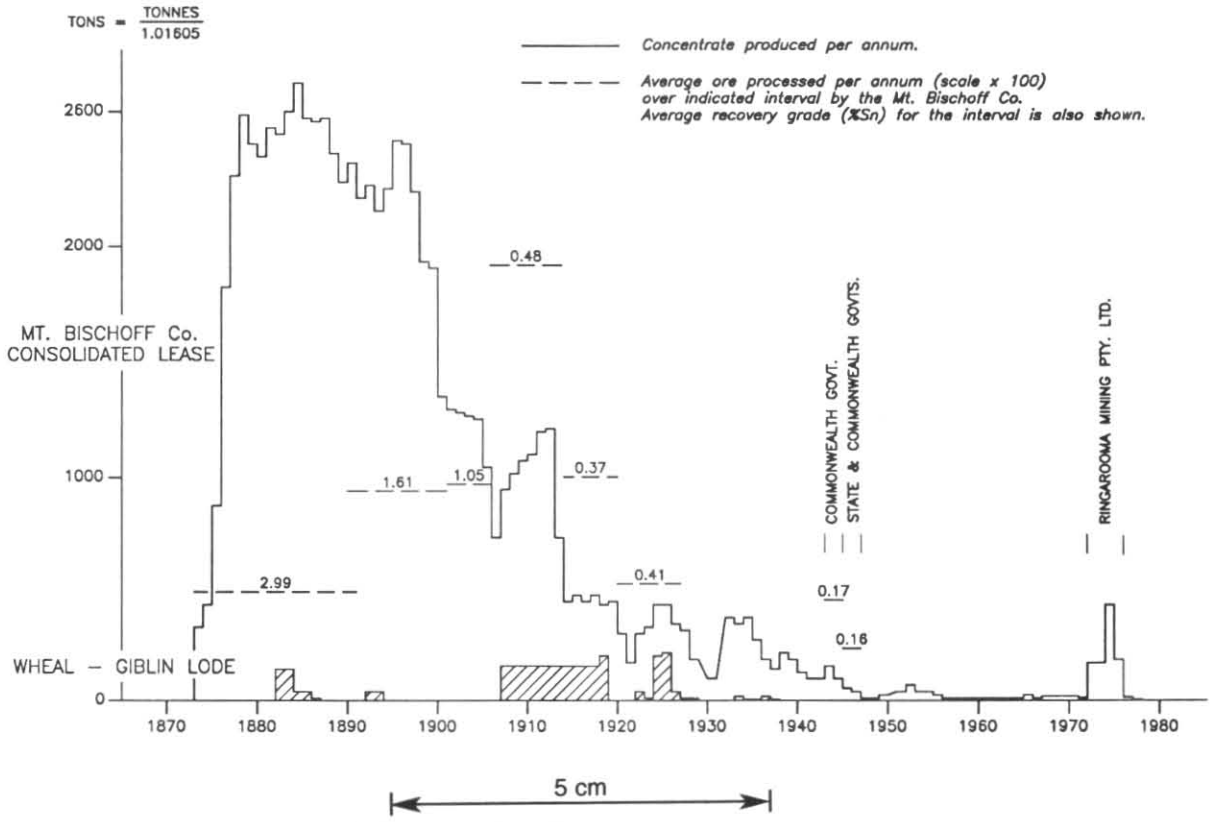

Figure A1. Production history of the Mt Bischoff tine field. Note that concentrate production from the Mt Bischoff Tin Mining Company's consolidated lease was highest prior to 1900, whereas ore production reached its maximum in the years 1907-1914. For the Wheal-Giblin Lode only the annual concentrate production is given and upto 1918 the values are averages for parts of the production periods. After 1947 there was small-scale mining and cleaning up of waste from the previous operations, except for the period of large-scale alluvial mining in 1972-1976. The sources of production data are Reid (1923) and the Reports of the Director of Mines for the years 1918-1978. More detailed data are given by Wellington (in Groves *et. al.*, 1972).

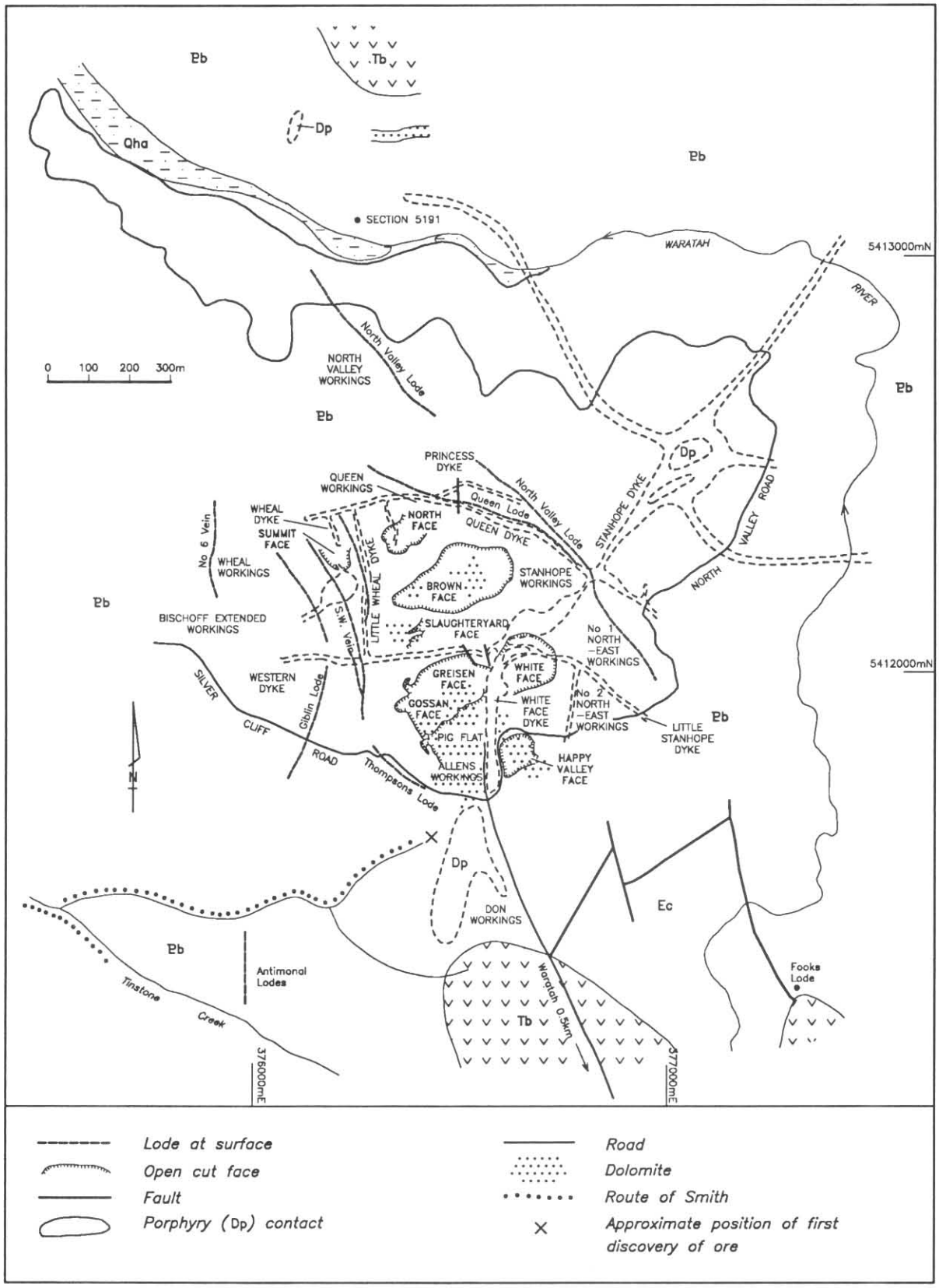

Figure A2. The Mt Bischoff tin field. The alluvial workings were in the tracts of Qha in the lower reaches of the Waratah River and in sub-basalt Teriary sediments at the Don Workings. Sources for the map are Figures 1, 3 and 40 in Martin, Murchie and Groves respectively (in Groves *et al.*, 1972). The symbols indicationg rock type are the same as on the St Valentines map.

about 1.3 million tonnes at 1.00% Sn whilst probable and possible reserves of porphyry ore total about 3.40 Mt at 0.47% Sn.

DISCOVERY

In early December, 1871, James 'Philosopher' Smith prospected what became known as Tinstone Creek on the south-west side of Mt Bischoff. In the bed of the creek he discovered cassiterite which showed little evidence of transport and he sought to trace its origin by following the porphyry boulders which also occurred in the stream (Martin, *in* Groves *et al.*, 1972). He found no cassiterite in the higher reaches of the main stream but found the mineral in abundance in a tributary flowing from the north-east. This stream led him to a source consisting of ore fragments, apparently in blocky eluvium, which was included in the more southerly of Smith's two 80 acre (32 ha) mining lease applications. The southern lease was granted in 1872 and the contiguous northern lease in 1873. Mining commenced at a small scale in December 1872.

Late in 1873 the operation was taken over by the Mt Bischoff Tin Mining Company which Smith had formed that year in conjunction with a group of Launceston businessmen. Development capital was raised through stock issue and bank loans and amounted to 100 000 pounds by 1878 when the Company paid the first of some 40 uninterrupted yearly dividends. Smith had withdrawn from the company in 1876 and dispersed his stock following a disagreement with other board members over the continued employment of the recently appointed mine superintendent H. W. F. Kayser.

ORES

ELUVIUM AND GOSSAN

From the beginning of mining through to 1893 much of the ore mined at Mt Bischoff comprised eluvium and deeply weathered, in situ mineralisation. The average recovered ore grade for the period was very high at almost 3% Sn (fig. A1). This high grade reflects the concentration of cassiterite in the eluvium by natural weathering processes and, to some extent, its concentration in the weathered in situ material or gossan through the removal of other, soluble constituents from the already rich ore. An important additional benefit of these weathered materials was their softness which allowed simple and cheap ore-handling procedures. In particular, it was possible to cheaply excavate the ore then clean it by processing through sluice boxes prior to final ore-dressing. Coarse, hard fragments in the ore were sent directly to the crusher. The combined effects of high grade and cheap handling made the mine very profitable during this early period (see Reid, 1923).

In 1873 W. M. Crosby described the first three metres cut in the North 'Lode' as consisting of a mass of boulders, soft tin-bearing stone and wash-dirt (Martin, *in* Groves *et al.*, 1972). The richest boulders were at the top and there was no sign of a solid, defined lode. Ulrich (1874) identified two types of material in the early Mt Bischoff workings. There was an upper layer of porphyry detritus which varied in thickness from about 0.3 m in parts of the workings to over 10 m in several exploratory shafts. This eluvium was widespread on the south, south-east and east slopes of the mountain and consisted of angular, coarse and fine quartz sand, intermixed with some ferruginous clay and angular or slightly 'waterworn' (?slightly rounded) particles and fragments of porphyry, slate and sandstone. It contained abundant cassiterite ranging from a common value of 0.5–1 lb (0.22–0.45 kg) per panning dish to exceptional values of 6 lb (2.72 kg) per panning dish. The cassiterite grains mostly ranged from very fine to 'the size of a bean' but fragments up to many pounds in weight were also present.

The in situ, deeply weathered materials in the earliest workings comprised highly ferruginous and easily disaggregated porphyry containing small quartz veins and enclosing veins and irregular patches of ferruginous tin ore as well as disseminated tin ore ranging in size from dust to 'pea size' (Ulrich, *op. cit.*). Later mining showed that gossans were extensively developed on the pyrrhotite-rich ores and included indigenous and exotic types (Groves, *in* Groves *et al.*, 1972). At Brown Face gossan extended to a depth of 60 m. Chemical weathering of pyrrhotite resulted either in development of friable limonitic crusts containing cassiterite or, with complete removal of Fe and S, in the formation of cassiterite-quartz sand. Intercalated sandy layers of quartz, cassiterite and other minerals, including tourmaline and talc occurred in the upper parts of Brown Face and White Face. These layers were thought to be alluvial by some early workers but actually represented disaggregated, weathered ore (Reid, 1923). Cassiterite in some of the layers was sufficiently clean to be sent directly to the smelter.

PRIMARY ORE

Underground production of primary ore from the Wheal-Giblin Lode began in 1882 and was in progress on the Mt Bischoff Tin Mining Company leases by 1888. Primary ore also became the principal product of surface workings as the eluvial and gossan ore was worked out. The primary ore is subdivided into three main classes by Groves (*in* Groves *et al.*, 1972) namely, stratabound deposits due to dolomite replacement, quartz-carbonate-fluorite fissure lodes and topazised zones in quartz-feldspar porphyry intrusions. Reid (1923) distinguished the North and Summit ore bodies as a fourth class comprising joint fillings and impregnations in slate and quartzite. Most ore was derived from the dolomite replacement deposits with substantially less coming from altered prophyry and even less from the fissure lodes.

Replacement Deposits

These occur in the lower part of a dolomite horizon in the Precambrian sequence of predominantly quartzose lithicwacke and phyllite which underlies Mt Bischoff. They provided most of the ore that was mined, a large part of it being in gossan form, and comprised the three biggest ore bodies of Brown Face, White Face and Slaughteryard Face as well as Gossan and Happy Valley Faces. The primary ore consists of pyrrhotite with arsenopyrite, pyrite, sphalerite, chalcopyrite, siderite, fluorite, silicates and cassiterite with minor stannite and wolframite. Cassiterite was the only economic mineral and Brown Face had an average grade of 2% Sn (Reid, 1923).

Topazised Porphyry

A network of porphyry dykes and sills intrudes the Precambrian rocks at Mt Bischoff and extends east and north to the Waratah River. Breccias probably related to faulting and possibly to high vapour pressures associated with porphyry emplacement occur along some of the lines of intrusion (Groves, *in* Groves *et al.*, 1972). The intrusive rocks have an age of 349± 54 Ma, similar to the 353± Ma age of the Meredith Granite (Brooks, 1966) which crops out about 8 km south-west of Mt Bischoff. Relatively unaltered porphyry consists of phenocrysts up to 5 mm across of bipyramidal quartz and lath-shaped, almost pure orthoclase with sporadic, smaller grains of muscovite in a fine-grained groundmass of intergrown quartz and sericitised feldspar (Groves in Groves *et al.*, 1972). In the mine area the porphyry displays variable alteration to topazite containing abundant topaz together with pyrrhotite or pyrite, intermittent arsenopyrite and sphalerite and insignificant proportions of original feldspar. Cassiterite is disseminated in the altered porphyry and also occurs on joint surfaces. Intensely altered parts of the Stanhope, Queen

and Western dykes were developed for ore at (?recovery) grades of 0.2–0.25% Sn (Reid, 1923).

Fissure Lodes

Quartz-carbonate-fluorite veins occupy generally NNW-trending, vertical to steeply dipping fractures which transect country rock and porphyry intrusions. They contain varying proportions of cassiterite, wolframite and silicates together with stannite, galena, jamesonite and bismuthinite. The principal ore-producing structures were the Queen, North Valley and Wheal-Giblin Lodes and Thompsons Lode which was still being worked in 1962 (Noldart, 1963). The Queen Lode was 0.3–1.5 m wide and to 1921 it was worked along a length of 335 m and to a depth of 107 m for grades of 3–20% Sn (Reid, 1923). The North Valley Lode was also 0.2–1.5 m wide and was worked along a length of about 550 m. The Wheal-Giblin Lode pinched and swelled along strike and down dip, ranging in thickness from 0.2–2.4 m and averaging about 0.6 m. It was worked along a length of 610 m and to a depth of 305 m. It produced 0.133 million tonnes of ore at 0.94% Sn recovery grade whilst being worked by the Mt Bischoff Extended Tin Mining Company and small tonnages of richer ore at earlier times. Fooks Lode [CQ772113] which contains cassiterite with abundant fluorite, sphalerite, pyrite and jamesonite lies outside the main zone of Sn-mineralisation which is bounded by a radius of one kilometre from Mt Bischoff peak (Groves, *in* Groves *et al.*, 1972).

Similarly remote lode Sn may also occur in Section 5191 [CQ766136].

Genesis

Most Mt Bischoff ore occurred in hydrothermally altered dolomite in close proximity to tin-bearing hydrothermally altered, quartz-orthoclase porphyry intrusions. Subordinate ore occurred in late, cross-cutting fractures.

Paragenetic sequences and fluid inclusions (Halley, 1987) indicate that the dolomite experienced an early high temperature (400–600°C) phase of alteration during which chondrodite, serpentinite, pyrrhotite and arsenopyrite were formed from fluids with 30–36 mass% NaCl. Isotopic values of –1 to about 0 are equivocal but consistent with the sulphur associated with this stage of alteration being magmatic in origin and the alteration may have accompanied the emplacement of the porphyry intrusions. The main hydrothermal stage in the dolomite occurred at about 350°C and was caused by fluids with about 2mol NaCl, 1.5 mol CO_2 and 0.3 m CH_4. During this stage cassiterite bearing assemblages formed which included quartz, phlogopite, talc, Mg-Fe carbonates, pyrrhotite, sellaite, topaz and fluorite with arsenopyrite, pyrite, chalcopyrite, stannite, fluobarite, phenakite and isokite as minor phases.

The most intense alteration in the porphyry intrusions occurred at the same temperature as the main alteration in the country rock (Halley, *op. cit.*).

Increasing intensity of alteration in the porphyry is marked by sequential alteration of the orthoclase phenocrysts by sericite, siderite, then pyrrhotite or pyrite intergrown with quartz, topaz, fluorite and cassiterite. Intensity of alteration varies both along and across the porphyry intrusions with maximum alteration in the centre. This pattern suggests that the intrusions contained the major fluid conduits. Lateral zonation seems to suggest that the conduits were confined to the mine area.

Sulphur isotope values of +2, +3 suggest that the hydrothermal fluid which caused the main alteration phase was of non-magmatic origin. Halley (*op.cit.*) suggests that water derived from other sources entered the cooling granite body at depth and, in the process of being heated, the water leached metals from the already enriched (by magmatic processes) roof zone of the granite. The vapour-rich, metalliferous fluid then found its way up the existing network of porphyry intrusions. Since carbonate replacement had already largely occurred in the ore zone during the early phase of alteration, it seems likely that the mechanism of cassiterite precipitation was boiling.

Fissure lode ores display temperatures of formation of fluorite and quartz in the range 170–380°C with the majority in the range 200–250°C (Groves and Solomon, 1969). The structural relationships of these ores show that they formed late in the mineralising period.

ALLUVIAL DEPOSITS

Tertiary

Cassiterite occurs in the basal units of sub-basaltic sediments of Tertiary age in the district around Mt Bischoff but production from these sources has been minor.

At the Don Workings near the southern end of Mt Bischoff the basal Tertiary unit comprises 6–9 m of boulders of brecciated wall-rock, indurated sandstone and porphyry together with abundant large boulders of conglomerate containing rounded to subangular pebbles of porphyry, indurated slate, quartz and quartzite (Reid, 1923). The deposit was worked by open cut and unsuccessful attempts were made to develop underground workings. Similar cassiterite bearing, basal Tertiary material occurs on the eastern side of the Waratah River about 3 km north-east of Mt Bischoff at the

Bischoff-Taylor prospect. Before 1900 a series of bores were drilled through the basalt cover south of Waratah to test the underlying Tertiary sediments but no significant deposits of cassiterite were discovered.

Quaternary

Alluvium in the Waratah River flats has been worked at various times during the history of the Mt Bischoff tin field. Dredging in 1927–1928 returned grades of about 1.2 kg per cubic metre but handling was made difficult by the presence of numerous large boulders in the alluvium (Murchie, *in* Groves *et al.*, 1972). Production was maintained to World War II and the deposits were worked again by Ringarooma Mining Pty Ltd in the period 1972–1976.

Ag-Pb-Zn deposits near Mt Bischoff

N. J. Turner

Scattered fissure vein lodes containing argentiferous galena and sphalerite occur around Mt Bischoff. The largest lode was extensively worked at the Magnet Mine some 5 km west of Mt Bischoff, outside the St Valentines quadrangle. Other lodes are very small.

In St Valentines quadrangle the largest deposit was at Silver Cliffs [CQ750140]. It produced a little over 160 tonnes of ore (Nye, 1923) from two veins of 0.6–1.2 m width. The veins probably occupied faults and had trends of 35° and 352° with steep esasterly dips. Mineralisation consisted of banded galena, jamesonite, sphalerite, pyrite and minor boulangerite in a gangue of quartz and siderite (Groves and Solomon, 1964). Galena also occurs in narrow veins at the Persic Mine [CQ751137] but little, if any, ore was produced (Nye, *op. cit.*). Veins containing Pb-Zn(-?Sn) mineralisation occur in the old mineral section 5191 at CQ766136 (Groves, *in* Groves *et al.*, 1972) whilst the small Antimonial Lodes south-west of Mt Bischoff [CQ755155] are probably genetically related to the Ag-Pb-Zn lodes because they contain abundant

jamesonite. The Antimonial Lodes also contain sulphantimonides, stibnite, berthierite and boulangerite. Jamesonite occurs in Fooks Lode.

The Ag-Pb-Zn deposits form a 'halo' around the Mt Bischoff Sn mineralisation and are related to the same mineralising event (Groves, *in* Groves *et al.*, *op. cit.*).

Scheelite-magnetite deposits – Housetop region

N. J. Turner

DEPOSITS AND PRODUCTION

In the northern part of the St Valentines quadrangle the open-pit mining of scheelite in skarn units has been in progress since 1977, initially at Kara No. 1 and then at Bobs Bonanza [CQ977257] then returning to Kara No. 1 [CQ974258]. Tasminex N.L. developed the deposits which have been operated by Tasmania Mines Ltd since 1985–1986.

To June 1988, a total of 1.03 million tonnes of ore had been mined giving 2454 tonnes of WO_3 in concentrates (Director of Mines, Annual Reports, 1977–1988) which also contain 1–1.5% molybdenum. Overall the avera recovery grade of WO_3 is 0.24% which is substantially lower than the in-ground ore grade of about 0.8% cited by Tasminex N.L. (Annual Report, 1985). Scheelite reserves equivalent to several years of operation remain at Kara No. 1 with further reserves at Kara North [CQ972267], locality L5 [CQ379277], Eastern Ridge [CQ978263] and elsewhere. At locality L5 there are in-ground grades of up to 3.47% WO_3 (Collins, 1986).

Magnetite in the skarn units was a cause of early interest in their economic potential. At Kara No. 1 a magnetite concentrate is produced during scheelite extraction and is stockpiled. Sales have been limited to about 36 000 tonnes though the prospects for further sales appear good. Reserves of magnetite are present in the other scheelite-bearing skarn units and there are magnetite-rich skarn units which are poor in scheelite. The latter include Kara No. 2 [DQ026254] which contains possible magnetite reserves of 200 000 tons at 45% Fe (Jack, 1963, 1964). Magnetite bearing skarn occurs at Suttons [DQ006274] and as rubble outcrop in an area [CQ979304] near Hampshire shown as Tertiary basalt on the St Valentines map. Magnetite skarn also occurs along the south-east edge of the Housetop Granite at DQ111266 on Redwater Creek (Hughes, 1960; Ruxton, 1984), near DQ090250 at the Laurel Creek West prospect and around DQ106254 near Peak Hill Farm (Ruxton, *op. cit.*). The latter locality is shown as Tertiary basalt on St Valentines map. Each of the skarns in the south-east of the Housetop region is of low tonnage potential and contains low metal values.

MINERALISATION

The western skarn units are favourably developed in a stratigraphic interval that is transitional between the siliceous Denison Group and overlying limestone of the Gordon Group (Collins, 1986, after Wolff, 1978 and Tasmania Mines Ltd. unpublished). Around Kara No. 1 the skarn units occupy a pendant (fig. A3) in the roof zone of a biotite-hornblende granite that is an extension of the magnetite series Housetop granite. At Kara No. 2 the skarn is a pendant (Jack, 1964) within the main mass of the granite whilst at Redwater Creek the skarn forms a skin at the Gordon subgroup-granite contact (Ruxton, 1984). The Housetop Granite has a K-Ar age of 353-370 Ma and a Rb-Sr age of 367±10 Ma (McDougall, pers.com., after McDougall and Leggo, 1965).

Scheelite ore at Kara No. 1 occurs in an irregularly shaped skarn blanket draped 15–25 m above the granite (Collins, *op. cit.*). The ore is underlain by a poorly mineralised quartz-epidote zone and Denison Group rocks (Moina Sandstone) are preserved against the granite. Skarn minerals include garnet, diopside, magnetite, amphibole and vesuvianite forming mainly magnetite rich or grossular-andradite rich lithologies. Scheelite is widespread but ore grades occur either within magnetite-amphibole skarn or in adjacent garnet skarn. Minor tin in silicates occur above the scheelite rich zone and may reflect either metal zoning in

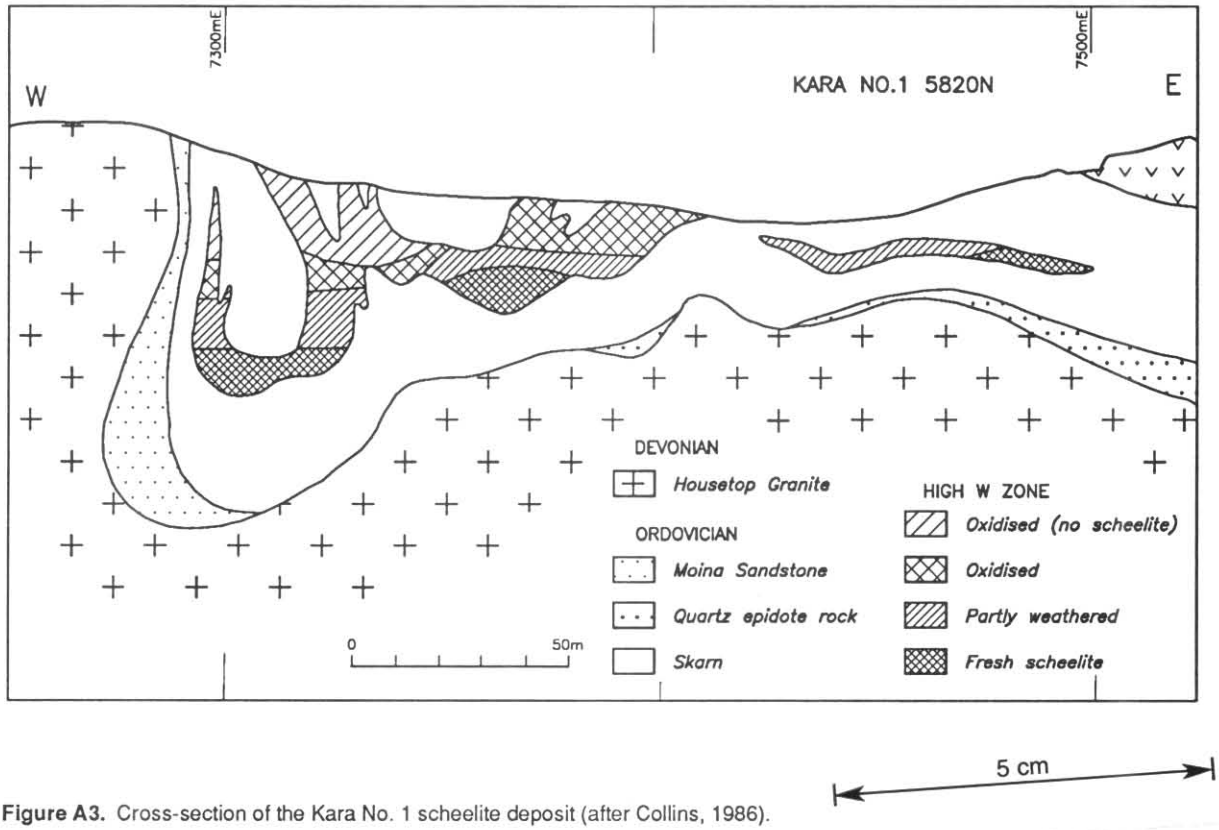

Figure A3. Cross-section of the Kara No. 1 scheelite deposit (after Collins, 1986).

Table A1
WHOLE ROCK ANALYSES (mass%)

Sample	SiO_2	Al_2O_3	Fe_2O_3	MgO	CaO	CO_2	SO_3	Total
R886/A1	41.44	2.30	1.32	3.47	39.51	8.97	0.10	97.11
T & H1	29.20	3.11	0.72	3.42	44.46	18.62	2.50	102.03
T & H3	68.00	4.50	2.20	0.40	21.60	2.60	n.d.	99.30
851468	46.60	1.70	1.40	4.30	40.70	3.80	0.40	98.90
R886/A8	52.08	2.37	0.78	2.67	41.14	0.62	0.03	99.69
Com. Mins	48.77	0.66	0.43	0.06	48.02	1.68	n.d.	99.62

Table A2
CALCULATED MINERAL CONSTITUTION (from Table A1)

Sample	Wollastonite	Diopside	Calcite	Feldspar(An)	Quartz	Pyrrhotite	Haematite	Total
R886/A1	44.93	22.21	20.39	6.78	2.24	0.11	1.21	97.87
T & H1	29.08	21.89	42.32	9.68	-3.18	2.74	-2.02	97.02
T & H3	32.67	2.56	5.91	15.81	40.88	0.00	2.20	97.97
851468	58.92	27.52	8.64	4.32	-1.40	0.44	0.96	96.57
R886/A8	73.06	17.09	1.41	7.35	0.73	0.03	0.75	96.57
Comm. Mins	94.80	0.38	3.82	2.32	-2.03	0.00	0.43	99.73

Table A3
SAMPLE DESCRIPTIONS

R886/A1	Bulk ore sample
T & H1	Wollastonite-bearing band (Thomas and Henderson, 1943)
T & H3	Siliceous band (Thomas and Henderson, 1943)
851468	Bulk ore sample
R886/A8	Wollastonite-concentrate produced from R886/A1
Comm. Mins	Commercial wollastonite product (Commercial Minerals)

Notes on Tables A1 to A3: Whole rock analyses and calculated proportions of constituent minerals for samples from the Tasmania Mines Ltd prospect near CQ396289. Calculations of the mineral proportions were based on electron microprobe determinations of the average compositions of wollastonite, diposide, calcite and feldspar in the rocks sampled. An example of a commercial wollastonite product (Comm. Mins) is included for comparative purposes. Its mineralogical composition was determined on the basis of the same data used for the other samples.

the skarn or a later, weathering effect. Much of the WO_3 in the upper part of the deposit is in secondary hydrous minerals (e.g. anthoinite) and is not presently recovered during processing.

Around Kara No. 2 the skarn minerals include andradite, diopside, epidote, clinozoisite, vesuvianite and chlorite (Jack, 1963). Scheelite is very minor, a little tin is present and there are magnetite rich zones. At Redwater Creek there is magnetite skarn, wrigglite and garnet-biotite-actinolite skarn with maximum values of 760 ppm WO_3 and 430 ppm Sn (Ruxton, *op. cit.*).

Tin and silver deposits – Housetop region

N. J. Turner
D. B. Seymour

TIN DEPOSITS

Many small, abandoned, alluvial tin workings are scattered through the area that is underlain by the Housetop Granite and are notably common around Lake Kara [DQ032309]. Some prospects, such as Crane's (DQ026325], were in sub-basalt Tertiary alluvium (Blake, 1957).

Tin bearing greisen veins traverse aplitic intrusions in the Housetop Granite at DQ033322, immediately NW of the old Crane's timber mill (Blake, 1957). However, Crane's prospect was the alluvial prospect at DQ026325. A hard rock prospect to the north of this alluvial prospect is shown as Crane's on the St Valentines map. About 3 km to the east of Crane's prospect is Clark's where several lodes carrying erratic tin distributions were prospected (Blake, *op. cit.*). One of the lodes in this vicinity was called the Kaolin lode.

Minor sericite-chlorite-quartz greisenisation occurs in the 'Redwater Granite' which is a belt of porphyritic and fine grained variants in the normally medium to coarse grained pink, biotite adamellite in the south-east of the Housetop Granite (Ruxton, 1984). Associated metal values are low. The belt of variant granitoids underlies an area about 2 km wide to the north of the Redwater Granite prospect [DQ101274] shown on St Valentines map. Ruxton (*op. cit.*) infers that the rocks occupy a position near the top of the Housetop Granite and cites the presence of tourmaline-quartz veins and tourmaline-quartz-feldspar pegmatite clots (?miarolitic cavity fills) in support of this view.

HAMPSHIRE SILVER MINE

The old Hampshire Silver Mine [CQ983297] produced a relatively small, but unknown, quantity of ore in the period 1877–1888 (Noldart, 1969). A fissure-vein lode was worked which had a thickness of about 0.45 m in granite but became thin and poorly mineralised in the adjacent hornfels. Gangue minerals in the lode were quartz and hornblende (Rowe, 1886, in Noldart, *op. cit.*) whilst the principal ore mineral was native silver (Petterd, 1910). Other minerals in the lode included galena, arsenopyrite, argenite, bismite, bismutite, erythrite, manganite, molybdenite, smaltite, sphalerite, strontianite, vanadinite and wulfenite.

Table A4
*CONSTRUCTION MATERIAL SITES IN THE ST VALENTINES QUADRANGLE**

AMG Ref.	Locality	Occupier	Mining Lease	Rock Type	Rock Unit	Status	Reserves
DQ026107	Black Marsh Road	APPM		gravel	Cm	F	medium
DQ008140	Black Marsh Road	APPM		gravel	Cmv	O	medium
DQ008143	Black Marsh Road	APPM		gravel	Cmv	A	nil
CQ944209	Guildford Road	APPM		gravel	Cm	A	medium
CQ953228	Black Pit Road	APPM		gravel	Cm	O	medium
CQ960224	Black Pit Road	APPM		gravel	Odc	O	medium
CQ947219	Guildford Road	APPM		gravel	Cm	A	nil
CQ949225	Guildford Road	APPM		gravel	Cm	A	nil
CQ807221	Bells Plain	APPM		chert	Ech	O	medium
CQ800236	Bells Plain	APPM		chert	Ech	O	medium
DQ142294	South Riana Road			gravel	Em	A	nil
DQ144296	South Riana Road	DMR		gravel	Odc	A	nil
CQ944242	Guildford Road	APPM		gravel	TB	A	medium
DQ006152	Leven Road	APPM		gravel	Tb	A	medium
CQ951174	Guildford Road	APPM		basalt	Tb	A	nil
CQ987252	Kara Road			limestone	Og	O	small
CQ984250	Kara Road			limestone	Og	O	small
DQ142293	South Riana Road			gravel	Odc	O	nil
DQ097243	Loyetea Road			gravel	Odm	A	nil
DQ097242	Loyetea Road			gravel	Odc	O	small
DQ086219	Loyetea Road			gravel	Cm	A	small
DQ072225	Laurel Creek			granite		A	small
CQ807219	Bells Plain	DMR		chert	Ech	O	medium
CQ811271	Parrawe	Associated Forest Holdings	927P/M	basalt	Tb	F	vast
CQ974292	Hampshire	Assoiciated Forest Holdings	929P/M	basalt	Tb	F	vast

Rock units: Refer to St Valentines map
Status: F = fully operational, O = occasional use, A = abandoned
Reserves: nil = <1 000 tonnes, small = 1 000-10 000 tonnes, medium = 10 000-1 000 000 tonnes
large = 1 000 000-1 000 000 000 tonnes, vast = >1 000 000 000 tonnes

* *Source:* Tasmania Department of Mines Construction Materials Register.

Gold deposits

R. S. Bottrill

Two small gold mines are known on the St Valentines sheet area: Golden Cliff [DQ153060] and Blacks Mine [DQ146053]. These form part of the western extremity of the Moina mining field, predominately of Devonian veins in Moina Sandstone or equivalents, closely associated with the Housetop and Dalcoath granites. No production is officially recorded.

GOLDEN CLIFF

This mine was discovered in about 1893 (Twelvetrees, 1913). About half a ton of ore was mined from a tunnel in the junction of two veins, and assayed about 32 g/t Au. Visible gold in iron-stained cavities in quartz probably derived from decomposed pyrite (*op.cit.*).

The lode is probably closely related to the Deep Creek Fault, a NNW-trending fault parallel to the Kauri Fault at Blacks mine, and the Bismuth Creek Fault at Moina. A Devonian granite association is thus suggested, as for Blacks mine, and most mineralisation in the Moina district.

BLACKS MINE

This mine, also known as the Lea River mine, was first worked in about 1895-1896, and work continued up to at least 1913 (Twelvetrees, 1913). A visit by Conder in 1903 was reported by Twelvetrees (*op. cit.*), who quoted the existence of stockpiles containing several hundreds of tons of ore assaying up to 22 g/t Au, averaging 8 g/t for ten samples. This suggests that at least several kilograms (about a hundred oz) of gold may have been recovered. Twelvetrees (*op. cit.*) describes numerous workings, including shafts (to about 20 m), crosscuts and adits (to about 70 m), all in sandstone and quartzite. Broadhurst (1934) described a number of workings in nearby alluvium, and suggested that little work had been undertaken on the lodes since Twelvetrees' visit.

Geopeko explored the group of prospects in 1980–1983, renaming them Mariner 6. The area was gridded and surveyed with geophysics (Dighem and IP) and geochemistry (soil and rock chip); grab samples from the dumps assayed up to 68 g/t Au, with minor Bi, Sn, Cu, Pb and Zn but a drillhole collared in 1981 provided disappointing results (Pemberton, 1983).

Pemberton (1983) described the lodes as being a stockwork of pyritic, hematitic and quartz rich veins in a shallow anticline in the Owen Conglomerate. He suggested an association with Devonian granites, based on gravity surveys and contact metamorphic assemblages in nearby rocks, with the Kauri Fault zone probably providing a fluid conduit. Twelvetrees (1913) noted the common presence of visible gold in both hematite and quartz.

Broadhurst (1934) described the alluvial workings as gold-bearing wash overlying limonite-cemented gravels, and pyritic sands. He found some pyrite nodules to assay about 7.5 g/t Au, and thought they represented original lode material. The alluvium is Tertiary and sub-basaltic, and no anomalous gold was found by Geopeko (Pemberton, 1983).

Volcanogenic base-metal prospects

D. B. Seymour

The pre-Denison Subgroup sequences in the eastern half of St Valentines quadrangle display lithological similarities with sequences in the Mt Read Volcanics. The Hellyer and

Que River volcanogenic massive sulphide (VMS) deposits are only some 10 km south of the quadrangle and the rocks in St Valentines quadrangle are being actively explored by companies for other VMS deposits (e.g. Rogers, 1976; Weste, 1978; Poltock, 1985). The Department of Mines is currently completing a stratigraphic drilling programme to outline areas of Mt Read Volcanics under the Tertiary basalt to aid exploration planning.

Narrow veins of barite in acid pyroclastics at DQ010138 near Two Hummocks may have significance in respect of VMS mineralisation (Rogers, 1976). The veins are subvertical, trend 035° and are located in possible faults (Rogers, *op. cit.*; Burns, 1962).

NON-METALLIC MINERALS

C. A. Bacon
R. S. Bottrill

Wollastonite

R. S. Bottrill
C. A. Bacon

On the eastern side of Wollastonite Creek at CQ396289 there is a deposit of wollastonite in Gordon Subgroup strata metamorphosed by the Housetop Granite. The deposit is currently being prospected by Tasmania Mines Ltd.

Thomas and Henderson (1943) and Hughes (1950) reported briefly on the deposit. Longman (1961) described the host sequence as comprising fine alternating bands of calcium silicate rocks (containing wollastonite as a prominent constituent), recrystallised limestones and quartzites ranging in thickness from 0.2–0.6 m and dipping 10–15°W. The rocks are part of a roof pendant in the granite and are limited in depth.

The rocks contain wollastonite intergrown intimately with varying proportions of diopside, calcite, quartz, feldspars, pyrrhotite and minor accessories (Bottrill and Bacon, in prep.). The wollastonite comprises between 20 and 70 vol.% of various samples (tables A1-A3), with a prismatic to fibrous texture and between 0.05 and 1 mm in size. It is commonly poikiloblastic, with fine inclusions of calcite, diopside and other phases, between about 5 and 50 μm in size (plate A1). The feldspars range from An_1 to An_{100}, and diopside may contain a few per cent of Al_2O_3 and FeO. Accessories include pyrite, chalcopyrite, sphene, epidote, leucoxene, zircon and amphibole.

There is little or no quartz coexisting with calcite, indicating complete reaction to wollastonite. The diopside indicates some original dolomite, pyrrhotite original pyrite, and the feldspars probably some original kaolinitic layers. The textures and mineralogies are compatible with an origin by hornfelsing of mixed carbonate and siliciclastic sediments by a nearby granite intrusion.

Longman (*op.cit.*) estimated open-cut reserves of one million tons at 30% wollastonite with the possibility of increasing the grade to 37% by selective mining to exclude dark coloured chert. Recent mineral processing tests by the Department of Mines Laboratories, Launceston, have produced concentrates with grades of greater than 70% wollastonite from selected parts of the deposit having natural grades of 45% wollastonite.

Slate

C. A. Bacon

Slate was discovered on the bank of the Arthur River [at CQ755289] by Henry Hellyer in 1827 and the deposit was held under two leases by J. Kirkup and one lease by C. C. Plante for a period from 1920. However, there has been no production from the deposit. The slate comprises flat-lying, evenly laminated siltstone and mudstone with erratic pebbles. It is a varved interval within the Carboniferous Wynyard Tillite and contains the annelid fossil, *Tasmanadia twelvetreesii* (Gulline, 1967). Colours range from pale olive green to dark bluish green and black and the layers are perfectly parallel (Chapman, 1929). Hellyer found that the slate was of the best quality, splitting in parallel thicknesses to the size of Ladies, Countesses or Duchesses (Bacon, 1987). However, commercial applications are limited because parts of the deposit are quite soft.

Gravel and aggregates

C. A. Bacon

Gravel and weathered rock is obtained from a number of pits within the St Valentines Quadrangle (table A4) and used for road construction (road base coarse, unsealed road surfacing and sealed road surfacing) and for aggregate in concreting. The gravels are derived from weathered Middle Cambrian sequences of volcanics and sedimentary rocks (€m) and Middle Cambrian volcanics (€mv), and also from conglomerate and sandstone sequences within the Denison Subgroup and correlates.

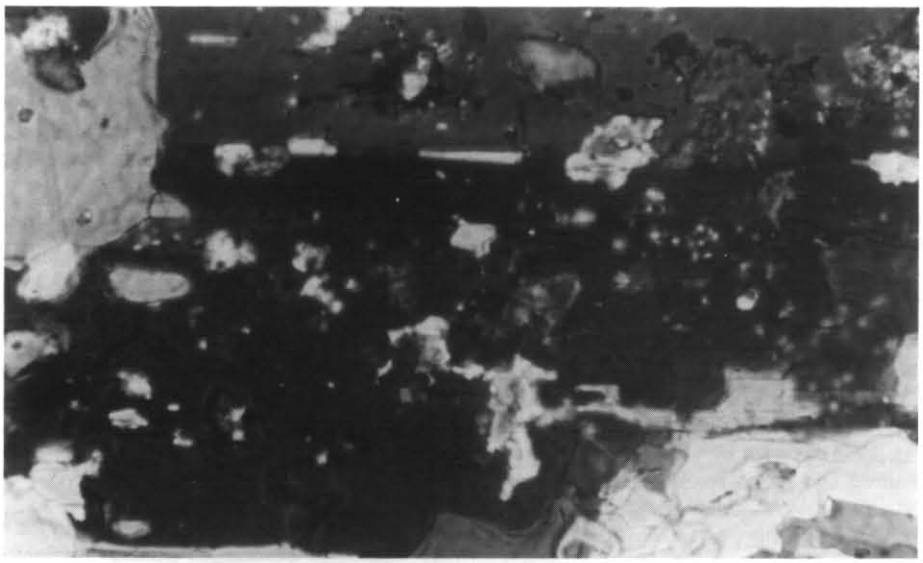

Plate A1. Photomicrograph of a twinned wollastonite crystal (crossed polars) surrounded by calcite. It is richly poikiloblastic, with inclusions of calcite and diopside. Field of view 690 × 460 μm.

5 cm

Limestone is quarried at two pits on Kara Road from the Ordovician Gordon Subgroup and chert from the Crimson Creek Formation is quarried on Bells Plain. Basalt and gravel derived from basalt is quarried at a number of localities, and is used both in road construction and as coarse aggregate for concreting. Two leases, 927P/M and 929P/M are both held by Associated Forest Holdings for the quarrying of basalt rock for use in concrete manufacture.

REFERENCES

BACON, C. A. 1987. Industrial minerals in Tasmania - Slate. *Unpubl. Rep. Dep. Mines Tasm.* 1987/15.

BLAKE, F. 1957. Crane's tin prospect, Upper Natone. *Tech. Rep. Dep. Mines Tasm.* 2:22–24.

BOTTRILL, R. S.; BACON, C. A. 1988. Wollastonite in Tasmania. *Unpubl. Rep Dep. Mines Tasm.* 1988/29.

BROADHURST, E. 1934. Report on the Stormont, Bell Mount and Black Bluff District. *Unpubl. Rep. Dep. Mines Tasm.* 1934:32-45.

BROOKS, C. 1966. The rubidium-strontium ages of some Tasmanian igneous rocks. *J. geol. Soc. Aust.* 13:457–469.

BURNS, K. L. 1962. Barytes and manganese near Guildford. *Tech. Rep. Dep. Mines Tasm.* 45–46.

CHAPMAN, F. 1929. On some remarkable annelid remains from Arthur River, N.W. Tasmania. *Pap. Proc. R. Soc. Tasm.* 1928:1-5.

COLLINS, P. L. F. 1986. The Kara Tungsten Mine, in Tin and tungsten deposits in western Tasmania. *IGCP Project 220, Excursion B1 Guidebook.*

GROVES, D. I.; SOLOMON, M. 1969. Fluid inclusion studies at Mt Bischoff, Tasmania. *Trans. Instn Min. Metall.* 78B:1–11.

GROVES, D. I.; MARTIN, E. L.; MURCHIE, H.; WELLINGTON, H. K. 1972. A century of tin mining at Mt Bischoff. *Bull. geol. Surv. Tasm.* 54.

GULLINE, A. B. 1967. The first proved Carboniferous deposits in Tasmania. *Aust. J. Sci.* 29:332–333.

HALLEY, S. W. 1987. *Genesis of the Mt Bischoff tin deposit.* Ph.D. thesis, A.N.U. : Canberra.

HUGHES, T. D. 1950. Limestone at Hampshire. *Unpubl. Rep. Dep. Mines Tasm.* 1950:160.

JACK, R. 1963. Magnetometer survey, Hampshire iron ore deposit. *Tech. Rep. Dep. Mines Tasm.* 8:50–54.

JACK, R. 1964. Drilling results, Hampshire iron ore deposits. *Tech. Rep. Dep. Mines Tasm.* 9:22–23.

LONGMAN, M. J. 1961. Wollastonite at Limestone Creek near Hampshire. *Tech. Rep. Dep. Mines Tasm.* 6:11–15.

MCDOUGALL, I.; LEGGO, P. J. 1965. Isotopic age determinations on granitic rocks from Tasmania. *J. geol. Soc. Aust.* 12:296–332.

NOLDART, A. J. 1962. Notes on Thompson's Lode, Mt Bischoff. *Tech. Rep. Dep. Mines Tasm.* 7:18–21.

NOLDART, A. J. 1969. Notes on the Hampshire Silver Mine. *Tech. Rep. Dep. Mines Tasm.* 13:40–44.

NYE, P. B. 1923. The silver-lead deposits of the Waratah district. *Bull. geol. Surv. Tasm.* 33.

PEMBERTON, J. 1982. *Progress Report on EL 10/74, Black Bluff, Tasmania, June 1981 to June 1982.* Geopeko Ltd. [TCR 82-1880]

PETTERD, W. F. 1910. *Catalogue of the minerals of Tasmania.* Department of Mines, Tasmania.

POLTOCK, R. A. 1985. Cambrian windows in the Black Bluff Range, *in:* ROBERTS, P. A. *EL 41/83, western 56 sq.km. Relinquishment Report. Gold Fields Exploration Pty Ltd.* [TCR 85-2506]

REID, A. M. 1923. The Mt Bischoff tin field. *Bull. geol. Surv. Tasm.* 34.

ROGERS, M. C. 1976. *Loongana area – Tasmania, Progress Report EL 2/76. Geopeko Ltd, King Island, Rept. No. K1/76/5.* [TCR 76-1184]

RUXTON, P. A. 1984. *EL 8/77 – Riana. Progress report on exploration during the period 2.9.83 - 1.3.84. The Shell Company of Australia Ltd, Metals Division. 08-2264.* [TCR 84-2142]

TASMINEX N.L. 1985. Annual report.

THOMAS, D. E.; HENDERSON, Q. J. 1943. Wollastonite at Hampshire. *Unpubl. Rep. Dep. Mines Tasm.* 1943:178-180.

TWELVETREES, W. H. 1913. The Middlesex and Mt Claude Mining Field. *Bull. geol. Surv. Tasm.* 14.

ULRICH, G. H. F. 1874. *The Mt Bischoff tin mines.* Mt Bischoff Tin Mining Company : Launceston.

WESTE, G. 1978. *EL 7/74 Moina, Tasmania. Black Bluff – Smiths Plain area. Report on all investigations to September 1978. Comalco.* [TCR 78-1306]

WOLFF, G. C. 1978. The Kara tungsten deposit, *in:* GREEN, D. C.; WILLIAMS, P. R. (ed.), *Geology and Mineralisation of N.W. Tasmania.* Abstracts:37–38. Geological Society of Australia (Tasmanian Division) : Hobart.

APPENDIX B

Petrology of the Tertiary basalt

J. L. Everard

INTRODUCTION

The most extensive and voluminous region of Tertiary basalt in Tasmania lies east of Waratah, largely coinciding with the St Valentines Quadrangle, but has received little previous attention from petrologists.

In December 1986, thirty-nine surface specimens of basalt (EV1-39), largely from eastern and central parts of the quadrangle, were collected by the author from mainly roadside outcrop or near outcrop, so as to obtain an areally representative suite of samples. All these samples have been studied petrographically and chemically analysed. A further forty or so samples were collected, mostly by P. W. Baillie and P. G. Lennox, during mapping, but only three have been analysed. In addition, two of the Tasmanian Tertiary basalts described and analysed by Edwards (1950) are from the St Valentines Quadrangle; the analyses were quoted by Joplin (1963) and are also reproduced here (analyses Nc15, Oc37).

Samples from the western part of the St Valentines Quadrangle and adjoining areas of the Mackintosh Quadrangle to the south were mostly obtained from drill core. Forty-one analysed samples were taken by P. W. Baillie from six holes drilled by the Department of Mines as part of the Sub-Basalt Drilling Project (SBDP) (Baillie, 1987*a-c*; Baillie and Green, 1988*a, b*, unpublished data). A further 18 analysed samples, collected by A. V. Brown from six of the holes (WY1, WA1-4, WA6) drilled by B.H.P. near the Murchison Highway, were tabulated by Brown and Forsyth (1984) and are also quoted here.

Sample and drill hole localities are given in Table B1 and Figure B1.

All 103 chemical analyses, including trace elements, are quoted in Table B2. Surface samples (EV1-39) are all of fairly fresh rocks, with H_2O <4% (commonly <2%) and $CO_2 \leq 0.31\%$. The samples from the SBDP series holes are more altered, probably due to the effects of groundwater, and in particular samples SBDP 5/248.7 and 9/115.5 should be treated with caution. Samples from the WA and WY series holes are more altered still, and only WY2/272 and WA1/96 are reasonably fresh rocks.

CIPW and Rittmann norms (table B3) were calculated from major elements, assuming $Fe_2O_3/FeO = 0.15$ as recommended by Brooks (1976), and recalculated to 100%.

The petrography of more than 130 thin sections is summarised in Table B4, with selected rocks described in more detail below.

About 250 electron probe microanalyses from 13 selected samples, obtained at the University of Tasmania, are given in Table B5.

NOMENCLATURE AND CLASSIFICATION

Igneous rocks may be named either according to their chemical composition or according to their modal composition (i.e. mineralogy). The chemical scheme of nomenclature discussed here is based on a total alkali/silica diagram, as recommended by the I.U.G.S. Subcommission on the Systematics of Igneous Rocks (Le Maitre, 1984). Before plotting, all analyses were recalculated to 100% major elements (SiO_2, TiO_2, Al_2O_3, ΣFeO, MnO, MgO, CaO, Na_2O, K_2O, P_2O_5) on a H_2O^- and CO_2 free basis, with all iron as FeO, to minimise spurious differences due to alteration. In Figure B2 recalculated total alkalis ($Na_2O^* + K_2O^*$) are plotted against recalculated silica (SiO_2^*) for all 103 analyses of Tertiary basaltic rocks from this area.

The basalt field, defined as $SiO_2^* = 45$ to 52%, $Na_2O^* + K_2O^* < 5\%$ (Le Maitre, *ibid.*), includes a large majority of these rocks. Fourteen analyses with more than 52% SiO_2 are, strictly speaking, basaltic andesites, whilst those with plot nos. 1, 7, 11, 59, 60 and 61 are more undersaturated than basalt *sensu stricto* and are more properly termed basanites. A further two, plot nos. 26 and 34, have a high total alkali content and just fall within the trachybasalt field; the former could be termed a potassic trachybasalt and the latter a hawaiite.

The line of dividing tholeiites and alkali olivine basalts (Macdonald and Katsura, 1964) obliquely cuts through the trend shown by these analyses in the total alkali-silica plot (Figure B2) and clearly there is a gradation between the two types. In this study, the quantity

$$\Delta^* = (Na_2O^* + K_2O^*) - 0.37\ SiO_2^* + 14.43$$

is used as a measure of alkalinity, as defined by major elements. Graphically, it is simply the vertical distance of a point in Figure B2 above the line of Macdonald and Katsura (1964); tholeiites which plot below the line will have a negative value.

The Nb:Y ratio has also been used to quantify alkalinity (e.g. Pearce and Cann, 1973; Floyd and Winchester, 1975); generally the ratio exceeds 1 in alkali basalt, as opposed to tholeiite. A plot of Δ^* against Nb/Y (fig. B3) shows a good correlation and general agreement between these criteria of alkalinity.

The Tertiary basaltic rocks of the St Valentines Quadrangle and adjacent areas range widely in chemistry, from quartz-normative tholeiite, through olivine-normative tholeiite and transitional basalt to alkali-olivine basalt and basanite. Although tholeiites are the most abundant, and data for the more alkaline types is comparatively sparse, there appears to be a continuous gradation between the various types (fig. B2, B3).

For the purposes of this study, the analyses are rather arbitrarily divided into five groups, based on major and trace element chemistry and CIPW norms:

(a) strongly alkaline basalt, including basanite (12 analysed samples. These are all olivine (*ol*) and nepheline (*ne*) normative, with $\Delta^* > 1.5$ and generally high Nb/Y and total alkali contents and low silica ($SiO_2^* > 47\%$).

The four most undersaturated analysed samples form a basanite subgroup; these are sample EV1 and three from hole SBDP4 (plot numbers 1, 59, 60, 61). Petrographically, these rocks lack plagioclase and are akin to rocks termed olivine nephelinite from elsewhere in Tasmania (e.g. Sutherland, 1969, 1976; Brown and McClenaghan, 1982). Sample EV7 (plot no. 7) is transitional to this subgroup.

(b) alkaline basalt (9 analysed samples). These include the remainder of the *ol-ne* normative analyses, with $\Delta^* > 0$ and generally Nb/Y>1.

(c) transitional basalt (29 analysed samples). These samples have hypersthene (*hy*) and *ol* in the norm, but have Δ^* and Nb/Y ratios that cannot be unequivocally assigned to either the tholeiitic or alkaline magma types.

(d) tholeiite (35 analysed samples). These samples are also *ol-hy* normative but with lower Δ^* (<0) and Nb/Y (<1) ratios.

(e) quartz tholeiite (18 analysed samples), *q-hy* normative, with the lowest Δ^* and Nb/Y values. All of these analyses are from drill core, but similar rocks probably occur at the surface in the western part of the quadrangle.

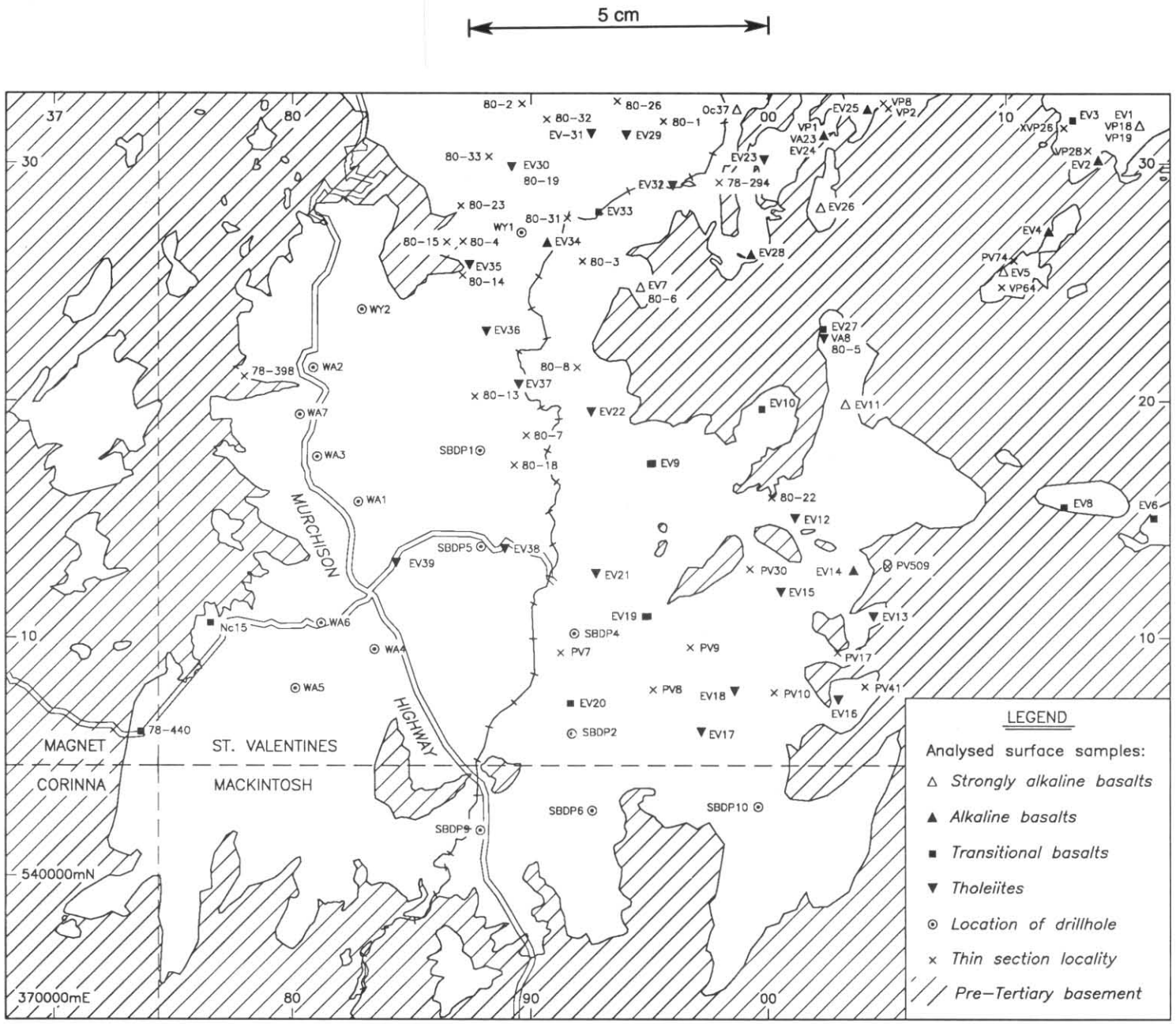

Figure B1. Tertiary basalt sample localities, St Valentines Quadrangle.

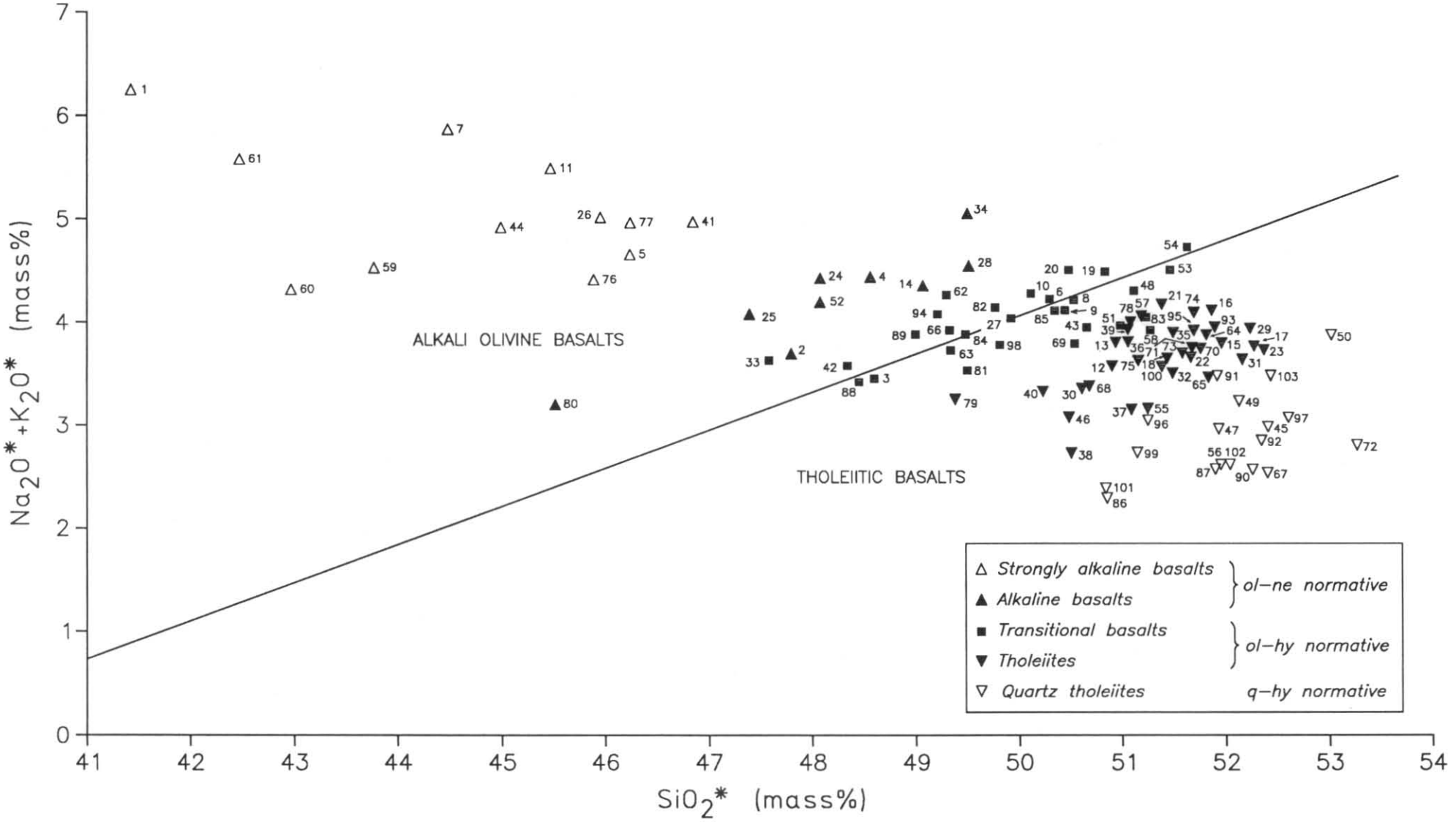

Figure B2. Alkali-silica diagram for Tertiary basaltic rocks, St Valentines Quadrangle.

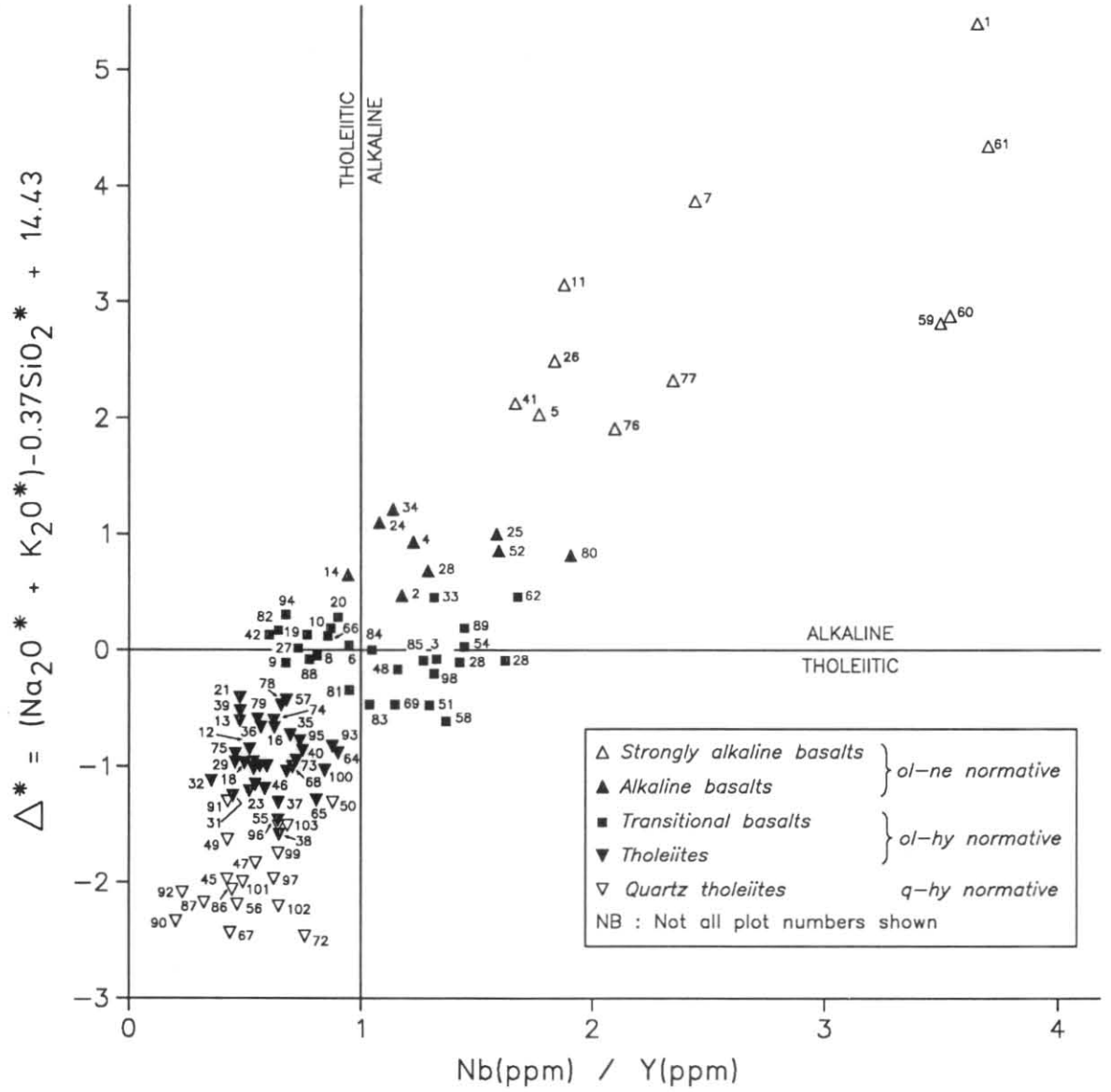

Figure B3. Alkalinity of Tertiary basaltic rocks, St Valentines Quadrangle.

5 cm

Modal schemes of nomenclature are less convenient for fine-grained volcanic rocks such as these, because of the difficulty of accurately estimating the abundance of, and sometimes even identifying, the constituent minerals. For these rocks, it is assumed that the Rittmann norms (table B3) are good approximations to the mode, enabling the quartz (Q) – alkali-feldspar (A) – plagioclase (P) – feldspathoid (F) classification recommended by the I.U.G.S. (Streckeisen, 1967, 1980) to be applied (fig. B4). Again, a big majority of analyses fall in the basalt field (fields 9 and 10), with those with more than 52% SiO_2 marginally qualifying as mela-andesite. Three analyses (SBDP2/282.0, 293.0 and Nc15) have colour indices of less than 35 vol% because of their high feldspar content and thus qualify as leucobasalt.

The twelve analyses assigned to the strongly alkaline group *(a)* above have higher feldspathoid (F) contents and largely fall into the phonolitic tephrite/phonolitic basanite field (field 13). The most undersaturated sample, EV1, is a tephritic phonolite (field 12) in this classification system.

SPATIAL DISTRIBUTION OF MAGMA TYPES

Despite the large number of analyses, only a vague relationship between the spatial distribution of the basalts and their chemistry can be discerned. Alkaline or strongly alkaline types predominate in the north-eastern and central northern parts of the quadrangle or in places near basement highs (e.g. EV7, EV11, EV14) where the basalt is probably thinner. Surface samples from the west and south-west are usually tholeiitic. Notable exceptions to this generalisation are samples EV23, EV34, and a very coarse, titanaugite-bearing and presumably alkaline sample (not analysed) from Goderich Road (HR17, tables B2, B4). There also appears to be a tendency for samples from drill holes in the western part of the quadrangle to be transitional or more alkaline at depth (table B1).

Thus, on the current data, there are indications that the volcanism becomes more tholeiitic and less alkaline with time and from the north-east to the south-west of the quadrangle. Possibly a more detailed, flow-by-flow sampling of basalt from a particular drill hole would provide a better picture of any temporal changes in the nature and chemistry of the lavas.

Table B1
TERTIARY BASALT SPECIMEN LOCALITIES

Field No. or drill hole and depth (m)	Reg.No.	Analysis No.	Plot No.	Thin Section*	Locality	Grid Ref.	Chemical Type†	Collector
EV1	000501	880671	1	P	Hilltop, 3.5 km SSE of South Riana	DQ156310	B	JLE
EV2	000502	870699	2	C	South Riana Road, Lowana Creek	DQ139302	A	JLE
EV3	000503	870700	3	C	Loyetea Road, near Drury Creek	DQ128319	R	JLE
EV4	000504	870701	4	P	Loyetea Road, Loyetea	DQ121272	A	JLE
EV5	000505	870702	5	C	Track to Laurel Creek, near Peak Hill Farm	DQ099250	AA	JLE
EV6	000506	870703	6	P	Track S of Leven Cave	DQ163154	R	JLE
EV7	000507	870704	7	C	Guildford Road, northern gravel pit	CQ944242	AA	JLE
EV8	000508	870705	8	C	talus, Loongana Rd	DQ125156	R	JLE
EV9	000509	870706	9	C	Guildford Rd, southern gravel pit	CQ952175	R	JLE
EV10	000510	870707	10	C	Old Park Road	CQ998198	R	JLE
EV11	000511	870708	11	C	Blythe Road, west of Mt Everett	DQ034202	AA	JLE
EV12	000512	870709	12	C	Leven Road, north-east of Two Hummocks	DQ007150	T	JLE
EV13	000513	870710	13	C	Leven Rd, 3 km WSW of Mt Tor	DQ050114	T	JLE
EV14	000514	870711	14	C	Leven Rd, 1 km north of bridge	DQ043132	A	JLE
EV15	000515	870712	15	C	Black Marsh Rd/Wattle Park Road junction	DQ007122	T	JLE
EV16	000516	870713	16	P	Black Marsh Rd, 2.5 km north-west of Mt Cattley	DQ028077	T	JLE
EV17	000517	870714	17	C	Sawyer's Flats	CQ974063	T	JLE
EV18	000518	870715	18	C	Middlesex Rd, 2 km S of Medway River	CQ988079	T	JLE
EV19	000519	870716	19	C	Racecourse Rd, SE of Talbots Lagoon	CQ950110	R	JLE
EV20	000520	870717	20	P	Racecourse Rd, crest	CQ919074	R	JLE
EV21	000521	870718	21	C	Wey Road, W of Talbots Lagoon	CQ928128	T	JLE
EV22	000522	870719	22	C	Wey Rd, 3.5 km WSW of St Valentines Peak	CQ926196	T	JLE
EV23	000523	870720	23	C	Upper Natone Road, near Wollastonite Creek	CQ998303	T	JLE
EV24	000524	870721	24	C	Upper Natone Road, Osborne Creek	DQ023315	A	JLE
EV25	000525	870722	25	P	Upper Natone Road, Tittie Gee Creek	DQ043327	A	JLE
EV26	000526	870723	26	P	1 km W of Tiffs Mistake	DQ023278	AA	JLE
EV27	000527	870724	27	C	Quarry Blythe Road	DQ023231	R	JLE
EV28	000528	870725	28	C	Kara Road	CQ991261	A	JLE
EV29	000529	870726	29	C	Talunah Road, near transmission line	CQ940313	T	JLE
EV30	000530	870727	30	P	Lockwood Creek Rd, East Cam River	CQ892299	T	JLE
EV31	000531	870728	31	C	Talunah Road, St Joseph's River	CQ926313	T	JLE
EV32	000532	870729	32	C	New road cutting, 2.5 km south-west of Hampshire	CQ960293	T	JLE
EV33	000533	870730	33	C	4 km north-east of Goodwood	CQ929280	R	JLE
EV34	000534	870731	34	C	Emu Bay Railway, 1.5 km north of Goodwood	CQ906262	A	JLE
EV35	000535	870732	35	C	Basils Rd, 2.5 km WNW of Goodwood	CQ874257	T	JLE
EV36	000536	870733	36	C	Bunkers Rd, 2.5 km south-west of Goodwood	CQ879234	T	JLE
EV37	000537	870734	37	C	Railway crossing near Shooter's Hill	CQ895209	T	JLE
EV38	000538	870735	38	C	Guildford Road, Hellyer River.	CQ890139	T	JLE
EV39	000539	870736	39	C	Guildford Rd, 1.5 km north-east of Fingerpost	CQ844134	T	JLE
V1	1980-1	-	-	C	Talunah Road, 2.5 km west of Hampshire	CQ956318	-	PGL
V2	1980-2	-	-	C	Talunah Road, south-east of Gotopeak Hill	CQ897327	-	PGL
V3	1980-3	-	-	C	Basils Road, crossroads	CQ922259	-	PGL
V4	1980-4	-	-	C	Basils Road spur	CQ872267	-	PGL
V6	1980-5	-	-	C	Quarry, Blythe Road	DQ024232	-	PGL
V7	1980-6	-	-	C	Guildford Road, northern gravel pit	CQ944243	-	PGL
V12	1980-7	-	-	C	Bunkers Road, 1 km south of Wey River	CQ899186	-	PGL
V13	1980-8	-	-	C	Bunkers Road, south of Companion Reservoir	CQ920215	-	PGL
V30	1980-13	-	-	C	Hellyer River, west of Shooters Hill	CQ877203	-	PGL
V31	1980-14	-	-	C	Basils Road, 3 km west of Goodwood	CQ871253	-	PGL
V32	1980-15	-	-	C	Basils Road spur	CQ866266	-	PGL
V37	1980-18	-	-	C	Hellyer River, 5 km north of Guildford	CQ894173	-	PGL
V40	1980-19	-	-	C	Lockwood Creek Road, East Cam River	CQ893300	-	PGL
V45	1980-22	-	-	C	Upper Blythe River	DQ003162	-	PGL
V55	1980-23	-	-	C	Lockwood Creek, near fork	CQ871282	-	PGL
V62	1980-26	-	-	C	St Josephs River, 4.5 km WNW of Hampshire	CQ938329	-	PGL
V85	1980-31	-	-	C	Emu Bay Railway, 3 km north of Goodwood	CQ915277	-	PGL
V86	1980-32	-	-	C	Branch of East Cam River	CQ907319	-	PGL
V87	1980-33	-	-	C	Near end of Lockwood Creek Road	CQ883303	-	PGL
VA8	-	791080	40	C	Quarry, Blythe Road	DQ024231	T	PWB
VA23	-	850090	41	-	Upper Natone Road, Osborne Creek	DQ023315	AA	PWB
VP1	78-1	-	-	C	Upper Natone Road, Osborne Creek	DQ023315	-	PWB
VP8	78-8	-	-	C	Near Upper Natone Road	DQ049327	-	PWB
VP18	78-19	-	-	C	Hilltop 3.5 km SSE of South Riana	DQ156310	-	PWB
VP19	78-20	-	-	C	Hilltop 3.5 km SSE of South Riana	DQ156310	-	PWB
VP26	78-27	-	-	C	Loyetea Road	DQ125316	-	PWB
VP28	78-29	-	-	C	South Riana Road	DQ136307	-	PWB
VP64	78-791	-	-	C	Laurel Creek, near Peak Hill Farm	DQ099250	-	PWB
PV7	-	-	-	C	3.5 km south of Guildford	CQ913094	-	PWB
PV8	-	-	-	C	South of Richards Ridge	CQ952079	-	PWB
PV9	-	-	-	C	1 km south-east of Richards Ridge	CQ968097	-	PWB
PV10	-	-	-	C	May Day Road	DQ003078	-	PWB
PV17	-	-	-	C	Black Marsh Road	DQ030095	-	PWB
PV30	-	-	-	C	South-west of The Hummocks	CQ993130	-	PWB
PV41	-	-	-	C	Cattley Creek	DQ045086	-	PWB
PV74	-	-	-	C	Peak Hill Farm	DQ104261	-	PWB
WA46	78-398	-	-	C	Sheffield Plain	CQ780208	-	PRW
CR32	78-440	781006	42	-	Corinna Road, 6 km south-west of Waratah	CQ739060	R	PLFC
HR17	-	-	-	C	Goderich Road (exact locality unknown)	-	-	PRW
GV33	78-294	-	-	C	Emu River near Hampshire	CQ980292	-	GRG
-	-	Nc15	43	-	'Northern end of Waratah township'	-	T	ABE
-	-	Oc37	44	-	North of Hampshire (Coastview Hill?)	-	AA	ABE
SBDP1/	-	-	-	-	6 km NNW of Guildford	CP87981797	-	-
125.3	101624	871834	45	C			Q	PWB
171.4	101625	871835	46	C			T	PWB
224.5	101626	871836	47	C			Q	PWB
245.6	101627	871837	48	C			R	PWB

Table B1
TERTIARY BASALT SPECIMEN LOCALITIES (continued)

Field No. or drill hole and depth (m)	Reg.No.	Analysis No.	Plot No.	Thin Section*	Locality	Grid Ref.	Chemical Type†	Collector
SBDP2/	-	-	-	-	Racecourse Road, 7 km south of Guildford	CP91810601	-	-
101.5	101628	872167	49	C			Q	PWB
145.0	101629	872168	50	C			Q	PWB
190.0	101630	872169	51	C			R	PWB
238.0	101631	872170	52	C			A	PWB
282.0	101632	872171	53	C			R	PWB
293.0	101633	872172	54	P			R	PWB
SBDP4/	-	-	-	-	Snipeford Marsh, 2.5 km SSE of Guildford	CP91891021	-	-
107.9	101639	872226	55	C			T	PWB
129.1	101640	872227	56	C			Q	PWB
160.9	101641	872228	57	C			T	PWB
206.0	101642	872229	58	C			R	PWB
251.1	101643	872230	59	C			B	PWB
255.8	101644	872231	60	C			B	PWB
269.1	101645	872232	61	P			B	PWB
341.0	101646	872233	62	C			R	PWB
366.0	101647	872234	63	C			R	PWB
SBDP5/	-	-	-	-	3 km WNW of Guildford	CP88011389	-	-
6.4	101658	872673	64	C			T	PWB
61.0	101659	872674	65	C			T	PWB
81.4	101660	872675	66	C			R	PWB
116.7	101661	872676	67	C			Q	PWB
159.3	101662	872677	68	C			T	PWB
173.3	101663	872678	69	C			R	PWB
219.5	101664	872679	70	C			T	PWB
237.0	101665	872680	71	C			T	PWB
248.7	101667	872682	73	P			T	PWB
280.8	101666	872681	72	C			Q	PWB
SBDP6/	-	-	-	-	Upper Hatfield River	CP92640273	-	-
75.8	101688	874881	74	C			T	PWB
108.0	101689	874882	75	C			T	PWB
177.0	101690	874883	76	P			AA	PWB
202.8	101691	874884	77	C			AA	PWB
SBDP9/	-	-	-	-	4.5 km south-east of Mt Pearse	CP87910191	-	-
115.5	101650	872455	78	C			T	PWB
129.0	101651	872456	79	C			T	PWB
213.5	101652	872457	80	C			A	PWB
237.6	101653	872458	81	C			R	PWB
SBDP10/	-	-	-	-	Leven R., 3 km WSW of Mt Cattley	CP99630302	-	-
39.5	101694	874885	82	C			R	PWB
128.3	101695	874886	83	C			R	PWB
152.7	101696	874887	84	C			R	PWB
201.5	101697	874888	85	C			R	PWB
WY1	-	-	-	-	2 km NNW of Goodwood	CQ895268	-	-
WY2/	-	-	-	-	3 km SSE of Parrawe	CQ830238	-	-
137.5	-	830774	86	C			Q	AVB
175	-	830773	87	C			Q	AVB
218	-	830772	88	C			R	AVB
272	85-0049	830771	89	C			R	AVB
WA2/	-	-	-	-	Bells Plain	CQ809215	-	-
113	-	830767	90	C			Q	AVB
154	-	830768	91	C			Q	AVB
186	-	830769	92	C			Q	AVB
WA7	-	-	-	-	Belmont Plain	CQ80401945	-	-
WA3/	-	-	-	-	Belmont Plain	CQ811177	-	-
163.5	-	830758	93	C			T	AVB
196	85-0048	830759	94	C			R	AVB
WA1/	-	-	-	-	4 km north of Fingerpost	CQ829158	-	-
96	-	830774	95	C			T	AVB
144	-	830773	96	C			Q	AVB
179	-	830772	97	C			Q	AVB
221	85-0050	830771	98	C			R	AVB
WA6/	-	-	-	-	Waratah Rd, 2.5 km from Fingerpost	CQ815106	-	-
150	-	830762	99	C			Q	AVB
11197.5	-	830763	100	C			T	AVB
WA4/	-	-	-	-	White Marsh, 2.5 km south of Fingerpost	CQ835096	-	-
105	-	830757	101	C			Q	AVB
140	-	830755	102	P			Q	AVB
197.5	-	830756	103	C			Q	AVB
WA5	-	-	-	-	4 km south-east of Waratah	CQ804096	-	-

* C - covered thin section, P - polished thin section (probe mount)

† Q - quartz-normative tholeiite, T - olivine-normative tholeiite, R - transitional basalt, A - alkaline basalt, AA - Strongly alkaline basalt, B - basanite (see text).

Note: holes WY1, WA7, WA5 were not sampled.

PETROGRAPHY

The Tertiary basalts vary widely in their phenocryst mineralogy, grain size and groundmass texture.

Olivine is by far the commonest phenocryst mineral, occurring in about 90% of studied samples, and in almost all cases represents the low-pressure liquidus phase. Although point counting was not attempted, olivine abundance in thin sections is estimated visually as abundant (>10%), common (5-10%), sparse (<5%), or absent. In rocks with alkaline affinities, olivine is either euhedral (e.g. plate B3) or somewhat embayed (plate B4), probably due to the effects of decompression on the liquidus temperature during ascent of the magma, and commonly grades in size downward to groundmass olivine. In the most strongly undersaturated rocks (basanite) many phenocrysts are anhedral (e.g. plate B2) and highly magnesian (Fo_{90}) and, as discussed later, are probably xenocrysts. In rocks with tholeiitic affinities olivine phenocrysts are usually embayed and occasionally skeletal (e.g. plate B12), probably largely due to reaction with the melt caused by the incongruent melting behaviour of olivine, in addition to any effect due to decompression. Even quartz-normative tholeiite samples generally contain olivine phenocrysts. In tholeiite samples, olivine is not present in the groundmass, except in a few rapidly quenched rocks with intersertal texture, in which olivine granules and plagioclase lie in a quartz-normative black glass (e.g. SBDP5/248.7, probe analysis 254, table B5). Rocks in which olivine phenocrysts are sparse or absent are usually transitional or tholeiitic basalts with low Mg#(100Mg/Mg+Fe) and Ni, which have probably lost olivine by crystal fractionation (e.g. EV12, SBDP2/287.0, SBDP2/293.0, WY2/175, WA2/186). However, a few phenocryst-poor alkaline rocks also have these characteristics (e.g. EV11, EV24).

Olivine phenocrysts are completely fresh in only a few samples, and commonly show incipient to complete alteration to pale to dark orange brown, poorly crystalline 'iddingsite', or less commonly dirty-green chloritic 'bowlingite'.

Plagioclase occurs as a phenocryst phase in about 20% of samples, including alkaline basalt (EV14, EV34), transitional basalt (e.g. EV20, EV3) and olivine-normative tholeiite samples (e.g. EV16, SBDP4/160.9). Typically it occurs as rather sparsely distributed narrow oblongs or laths which grade in size down to the much more abundant groundmass plagioclase (e.g. plate B9). Samples EV7, EV11 and EV24 (all alkaline or strongly alkaline basalt) contain more equant, anhedral plagioclase fragments which are sometimes inclusion-ridden (sieve texture), suggesting disequilibrium, and are probably xenocrysts. Sample PV30, from near the Two Hummocks, is unique in the size (<6 mm) and abundance of plagioclase phenocrysts (plate B16).

Clinopyroxene phenocrysts are also found in about 20% of samples, but their mode of occurrence is more variable. Only rarely do they rival or exceed olivine in abundance and size (V6, PV41, HR17). Most commonly they are rather sparsely distributed, small equant euhedra and subhedra, often clustered in glomerocrysts (plate B3). Occasionally they are found in large composite glomerocrysts with olivine, frequently surrounding a central core of orthopyroxene (e.g. plate B10). In EV1, rare augite anhedra appear to be derived from disaggregation of spinel lherzolite nodules. The clinopyroxene phenocrysts, where present, are colourless (augite) in tholeiitic to transitional basalts, and tend to be pinkish-purple (titanaugite) in more alkaline samples. Significantly, they are often accompanied by plagioclase microphenocrysts, suggesting that both minerals formed together at about the same stage of crystallisation, after olivine phenocrysts. In most (80%) of samples, apparently only olivine had crystallised before the magma was erupted.

The four most undersaturated, strongly alkaline basanites (EV1, SBDP4/269.1, 4/255.8, 4/251.1) all have a very fine to almost glassy groundmass lacking plagioclase but containing nepheline, alkali feldspar, augite and opaque minerals. In the remaining basalts plagioclase, augite or titanaugite, and opaques are almost invariably present, and olivine, alkali feldspar and apatite may occur, particularly in the more alkaline rocks. There is no relationship between grain size and chemistry, and the groundmass is described according to the typical size of plagioclase laths as very fine (< 100 μm), fine (100-200 μm), medium-grained (200-500 μm) or coarse (>500 μm).

The groundmass texture is largely a result of the cooling history, particularly the rapidity of cooling, of the lava and again has little or no relationship to chemistry; occasionally several types of texture can be found in a single thin section. It is described as ophitic (augite frequently completely surrounding plagioclase laths), subophitic (augite partly surrounding plagioclase laths), intergranular (augite and/or olivine interstitial to plagioclase) or intersertal (substantial amounts of interstitial, usually black, glass).

The petrography of all samples is summarised in Table B4. Selected samples, representative of all chemical and textured types, are described in more detail below.

Basanite

EV1 (very fine to glassy) [DQ156310] - Plate B1

This specimen, the most undersaturated rock collected, consists of anhedral-granular nodules of spinel lherzolite (<100 mm), (described later) and rather sparsely distributed phenocrysts of olivine and subordinate clinopyroxene, set in a very fine, almost glassy groundmass. The olivine phenocrysts vary widely in size, from up to 2 mm to tiny granules, and are typically anhedral and often embayed, indicating resorption by the groundmass. Most are too magnesian (Fo_{89-90}) to be in equilibrium with the bulk rock composition, but are compositionally similar to the olivine in the lherzolite nodules. They are probably either fragments of disrupted nodules or genetically related xenocrysts. Likewise, the much rarer clinopyroxene phenocrysts are also anhedral, embayed, and compositionally similar to that in the nodules. However, a few euhedral to subhedral olivine phenocrysts are more iron rich (Fo70-72, table B5, analyses 1, 3) and are probably cognate.

The groundmass varies slightly between different thin sections, but is always very fine and sometimes almost glassy. Equant blebs (typically 10-20 μm) of titanomagnetite are dispersed throughout the rock, or clustered into granular aggregates. Sometimes narrow laths and almost acicular microlites (typically ≤50 μm) of clinopyroxene are discernible, and may be aligned, suggesting a flow lamination. Very finely acicular crystallites may be apatite. Electron probe microanalyses (table B5, analyses 11-13) suggest that the very fine, low birefringence material is predominantly alkali feldspar and nepheline. Plagioclase is apparently absent.

Many sections contain rounded to ellipsoidal or more elongate amygdales, usually <500 μm across of zeolites (low birefringence, patchy, uneven extinction). The rock is slightly altered, particularly with partial iddingsitisation of olivine.

Samples VP18 and VP19 from the same locality are very similar but more altered.

SBDP4/269.1 (very fine) - Plate B2

This rock also consists of olivine phenocrysts set in a very fine-grained groundmass. The larger phenocrysts (<3 mm, typically 500 μm-1 mm) are anhedral, embayed, too magnesian (Fo_{90}) to be cognate, and are probably xenocrysts. The smaller phenocrysts, which grade in size into the groundmass, may be euhedral or subhedral, and are more iron-rich and therefore probably cognate.

The groundmass consists of olivine granules, abundant elongate clinopyroxene microlites (≤100 μm), titanomagnetite blebs, very finely acicular apatite, and a very fine low birefringence mesostasis, probably mainly alkali feldspar and nepheline. Small (≤400 μm) equidimensional amygdales contain a zeolite, possibly gonnardite (table B5, analyses 58-60).

Samples SBDP4/255.8 and SBDP4/251.1 are chemically and petrographically very similar, but more altered; the latter contains no fresh olivine.

Table B2
CHEMICAL ANALYSES OF TERTIARY BASALTS

Field No.	EV1	EV2	EV3	EV4	EV5	EV6	EV7	EV8	EV9	EV10	EV11	EV12	EV13	EV14	EV15	EV16	EV17	EV18	EV19	EV20
Analysis No.	880671	870699	870700	870701	870702	870703	870704	870705	870706	870707	870708	870709	870710	870711	870712	870713	870714	870715	870716	870717
Plot No.	1	2	3	4	5	6	7	8	9	10	11	12	13	14	15	16	17	18	19	20
SiO_2	39.67	46.03	46.61	47.48	45.61	49.53	43.65	49.24	50.13	49.85	44.37	50.30	50.50	48.51	51.33	51.64	51.44	50.69	50.22	50.33
TiO_2	2.27	1.66	1.60	1.72	2.06	1.71	2.47	1.75	1.73	1.74	2.43	1.77	1.59	1.79	1.67	1.71	1.46	1.58	1.75	1.65
Al_2O_3	11.25	13.64	13.82	14.04	14.19	14.36	14.25	14.44	14.20	14.36	13.56	14.43	14.32	14.36	13.91	14.32	13.99	14.11	14.60	14.30
Fe_2O_3	6.80	1.89	3.04	1.70	2.19	1.91	2.91	3.81	3.07	1.74	4.71	3.80	2.09	3.04	3.65	1.88	3.46	3.31	3.49	1.68
FeO	7.80	9.07	7.46	8.85	8.76	9.50	9.04	7.92	8.57	9.90	9.62	8.38	9.01	9.42	7.63	8.82	7.27	8.16	7.56	9.16
MnO	0.19	0.17	0.16	0.16	0.18	0.16	0.19	0.15	0.18	0.17	0.20	0.16	0.17	0.19	0.17	0.16	0.16	0.17	0.17	0.15
MgO	13.51	10.90	11.66	10.18	10.99	8.42	10.02	8.01	8.60	8.23	8.13	7.72	8.74	8.71	7.87	7.74	8.70	8.38	7.60	8.66
CaO	7.91	9.17	8.27	9.11	9.74	8.60	9.33	8.10	8.78	9.05	8.88	8.83	8.90	8.53	8.92	9.10	8.32	8.64	8.96	9.17
Na_2O	4.03	2.48	2.19	3.09	3.16	3.45	4.18	3.36	3.46	3.49	3.79	3.10	3.17	3.46	3.10	3.49	3.02	3.15	3.50	3.58
K_2O	1.94	1.07	1.12	1.24	1.44	0.69	1.58	0.74	0.64	0.78	1.57	0.44	0.62	0.83	0.66	0.62	0.71	0.45	0.94	0.92
P_2O_5	1.03	0.36	0.33	0.34	0.50	0.32	0.75	0.27	0.30	0.31	0.74	0.26	0.22	0.30	0.23	0.24	0.19	0.21	0.32	0.24
H_2O	4.20	3.39	3.47	2.38	1.30	1.10	2.10	1.99	0.90	0.64	1.68	1.31	0.98	1.24	1.31	0.80	1.36	1.38	1.40	0.69
CO_2	0.35	0.10	0.09	0.06	0.05	0.08	0.14	0.07	0.05	0.31	0.16	0.03	0.02	0.05	0.31	0.03	0.15	0.17	<0.01	0.03
Total S	<0.10	0.05	<0.05	<0.05	<0.05	<0.05	<0.05	<0.05	<0.05	<0.05	<0.05	<0.05	<0.05	<0.05	<0.05	<0.05	<0.05	<0.05	<0.05	<0.05
Total	100.95	99.98	99.82	100.35	100.17	99.83	100.61	99.85	100.61	100.57	99.84	100.53	100.33	100.69	100.51	100.55	100.23	100.40	100.51	100.56
*100Mg/Mg+Fe	66.3	67.2	69.8	66.5	67.4	60.3	63.5	58.8	60.6	59.2	54.3	57.0	61.9	59.2	59.3	59.8	62.9	57.3	55.9	59.1
†Chemical Type	B	A	R	A	AA	R	AA	R	R	R	AA	T	T	A	T	T	T	T	R	R
Trace elements (ppm)																				
Sc	12	21	19	23	24	20	19	18	23	19	15	22	21	20	20	17	21	23	21	22
V	155	190	195	220	220	185	230	165	195	190	190	190	180	180	185	175	160	175	200	180
Cr	400	400	450	430	420	320	310	300	320	290	210	250	350	280	340	330	330	320	270	320
Co	54	51	54	53	54	51	53	52	52	56	62	62	49	58	48	47	50	50	45	51
Ni	290	220	210	170	260	130	210	130	195	180	140	190	180	185	150	140	165	185	99	170
Cu	25	63	51	56	100	56	63	46	71	68	60	69	67	68	64	57	60	68	49	64
Zn	155	99	94	96	110	125	120	120	120	120	160	135	120	130	115	115	105	115	105	110
Ga	21	12	18	17	16	20	21	18	19	20	24	21	19	19	19	19	19	18	20	19
Rb	16	25	36	30	34	16	31	14	11	17	28	7	15	19	18	14	20	8	20	17
Sr	1450	590	460	600	680	390	840	350	350	360	920	290	360	360	310	330	270	290	360	320
Y	26	22	18	22	26	20	25	21	22	23	24	23	25	22	24	24	22	22	22	21
Zr	330	140	125	135	180	125	240	120	125	130	270	110	115	130	125	120	105	105	130	110
Nb	95	26	24	27	46	19	61	17	15	20	45	12	12	21	13	15	12	11	17	19
Mo	20	7	3	5	4	4	8	4	3	3	4	3	3	5	4	3	3	3	3	3
Sn	<4	<4	<4	<4	<4	<4	4	<4	<4	<4	4	<4	<4	<4	<4	<4	<4	<4	<4	<4
Ba	210	125	125	125	260	58	115	48	58	40	210	<9	210	43	65	35	49	48	61	100
La	65	6	24	13	27	<6	36	<6	<6	<6	35	<6	12	15	<6	9	7	<6	7	<6
Ce	120	69	82	61	82	62	110	56	54	54	110	39	46	66	56	63	49	49	50	39
Nd	63	19	15	17	24	15	30	15	15	10	32	14	14	15	15	10	15	13	10	18
W	420	220	71	87	52	68	47	41	57	58	37	85	49	66	145	60	210	110	88	130
Pb	7	5	4	6	<4	<4	<4	<4	<4	<4	<4	<4	<4	<4	5	<4	8	<4	<4	<4
Th	<4	6	4	<4	<4	<4	<4	<4	<4	<4	<4	<4	<4	<4	<4	<4	<4	<4	<4	<4
U	<5	<5	5	5	<5	<5	<5	<5	<5	<5	<5	<5	<5	<5	<5	<5	<5	<5	<5	5

* atomic proportions, Fe recalculated to $Fe_2O_3/FeO = 0.15$ (Brooks 1976.)
† A – alkaline basalt, AA – strongly alkaline basalt, B – basanite, R – transitional basalt, Q – quartz tholeiite, T – tholeiite (see text)
Analyses by Department of Mines Analytical Laboratories, Launceston
Analysts: R. Roby, M. Frith

Table B3

CIPW AND RITTMAN NORMS OF TERTIARY BASALTS

Field No.	EV1	EV2	EV3	EV4	EV5	EV6	EV7	EV8	EV9	EV10	EV11	EV12	EV13	EV14	EV15	EV16	EV17	EV18	EV19	EV20
Analysis No.	880671	870699	870700	870701	870702	870703	870704	870705	870706	870707	870708	870709	870710	870711	870712	870713	870714	870715	870716	870717
CIPW NORMS (mass%)																				
or	7.52	6.55	6.91	7.50	8.62	4.13	9.50	4.48	3.77	4.60	9.50	2.66	3.71	4.95	3.95	3.65	4.25	2.72	5.60	5.43
ab	-	21.24	19.26	22.29	13.30	29.56	8.43	29.14	29.39	29.66	14.81	26.52	27.03	29.04	26.53	29.66	25.93	27.02	29.91	30.32
an	7.15	23.77	25.57	21.22	20.56	21.97	15.75	22.67	21.46	21.32	15.68	24.38	23.18	21.43	22.31	21.65	22.87	23.32	21.61	20.30
lc	3.49	-	-	-	-	-	-	-	-	-	-	-	-	-	-	-	-	-	-	-
ne	19.26	0.30	-	2.39	7.44	-	14.92	-	-	-	9.77	-	-	0.28	-	-	-	-	-	-
di	21.64	17.03	12.04	18.37	20.26	15.62	21.42	13.68	16.65	17.79	20.13	14.94	16.22	15.85	17.11	18.03	14.51	15.33	17.39	19.33
hy	-	-	10.00	-	-	6.89	-	10.49	7.69	3.35	-	19.21	13.38	-	20.48	13.76	23.10	19.24	5.63	0.10
ol	31.13	24.82	20.23	22.04	22.59	15.56	21.14	13.23	14.85	17.03	20.89	6.00	10.83	21.94	3.75	7.39	4.05	6.68	13.67	18.76
mt	2.77	2.15	2.03	2.03	2.09	2.19	2.28	2.23	2.19	2.20	2.72	2.29	2.10	2.36	2.12	2.03	2.03	2.16	2.07	2.06
il	4.49	3.26	3.16	3.33	3.96	3.29	4.78	3.41	3.29	3.32	4.72	3.39	3.04	3.43	3.20	3.27	2.81	3.03	3.36	3.14
ap	2.54	0.87	0.80	0.83	1.20	0.78	1.79	0.66	0.71	0.73	1.79	0.61	0.52	0.71	0.54	0.57	0.45	0.50	0.75	0.57
Total	99.99	99.99	100.00	100.00	100.02	99.99	100.01	99.99	100.00	100.00	100.01	100.00	100.01	99.99	99.99	100.01	100.00	100.00	99.99	100.01
mol % an (plagioclase)	100.00	51.3	55.6	47.3	59.3	41.2	63.8	42.3	40.8	41.8	49.9	46.4	44.7	39.0	44.2	40.8	45.4	44.9	40.5	38.7
RITTMANN NORMS (vol.%)																				
Quartz	-	-	-	-	-	-	-	-	-	-	-	-	-	-	-	-	-	-	-	-
Sanidine	13.9	4.9	5.5	6.7	8.5	-	10.3	-	-	0.3	11.4	-	-	0.9	-	-	-	-	1.8	1.7
Plagioclase	7.3	51.4	51.0	50.7	39.5	60.6	28.6	61.6	59.4	59.9	35.3	58.7	58.6	60.1	57.5	59.6	57.8	58.0	60.1	58.6
Nepheline	19.8	-	-	1.2	6.5	-	14.3	-	-	-	9.1	-	-	-	-	-	-	-	-	-
Clinopyroxene*	27.6(T)	21.5(A)	24.8(S)	20.2(D)	22.5(D)	25.9(S)	24.3(T)	26.6(S)	27.8(S)	25.5(A)	22.6(T)	35.0(P)	31.9(S)	20.0(A)	38.4(P)	33.8(S)	38.0(P)	35.7(P)	26.5(S)	24.5(A)
Olivine	25.9	18.2	14.9	17.2	18.4	9.5	17.0	7.8	8.9	10.3	15.7	2.3	6.0	14.8	0.4	3.0	0.9	2.8	7.7	11.5
Magnetite	2.8	1.6	1.4	1.6	1.7	1.7	2.1	1.8	1.7	1.8	2.5	1.7	1.6	1.9	1.6	1.6	1.5	1.6	1.7	1.7
Ilmenite	0.3	1.6	1.7	1.5	1.8	1.6	1.8	1.7	1.6	1.5	1.9	1.7	1.5	1.7	1.5	1.5	1.4	1.5	1.6	1.4
Apatite	2.4	0.8	0.7	0.8	1.1	0.7	1.7	0.6	0.6	0.7	1.7	0.6	0.5	0.7	0.5	0.5	0.4	0.5	0.7	0.5
Total	100.0	100.0	100.0	100.0	100.0	100.0	100.1	100.1	100.0	100.0	100.2	100.0	100.1	100.1	99.9	100.0	100.0	100.1	100.1	99.9

* (D) – diopside, (A) – augite, (T) – titanaugite, (S) – sub-calcic augite, (P) – pigeonite

All norms calculated from major elements, Fe redistributed so that $Fe_2O_3/FeO=0.15$ (Brooks, 1976), normalised to 100% anhydrous.

Table B2
CHEMICAL ANALYSES OF TERTIARY BASALTS (continued)

Field No.	EV21	EV22	EV23	EV24	EV25	EV26	EV27	EV28	EV29	EV30	EV31	EV32	EV33	EV34	EV35	EV36	EV37	EV38	EV39
Analysis No.	870718	870719	870720	870721	870722	870723	870724	870725	870726	870727	870728	870729	870730	870731	870732	870733	870734	870735	870736
Plot No.	21	22	23	24	25	26	27	28	29	30	31	32	33	34	35	36	37	38	39
SiO_2	51.31	50.92	51.58	47.21	46.56	45.25	49.26	48.88	51.07	50.17	51.56	50.74	46.07	48.16	50.95	50.14	49.99	48.82	50.13
TiO_2	1.60	1.58	1.68	1.93	1.85	2.04	1.79	1.92	1.54	1.65	1.55	1.59	1.90	1.79	1.60	1.63	1.58	1.60	1.60
Al_2O_3	14.30	14.11	14.42	13.51	14.11	14.46	13.49	13.37	14.50	13.97	14.28	14.91	14.14	13.94	13.97	14.12	14.03	15.09	13.97
Fe_2O_3	1.47	3.83	5.80	3.53	2.07	2.74	2.79	3.25	1.72	2.82	1.99	2.82	2.26	1.31	2.22	3.22	4.04	3.72	2.62
FeO	9.70	7.06	5.39	9.56	9.42	9.64	8.90	8.19	8.53	9.04	8.88	8.35	9.37	10.33	8.38	8.03	6.64	6.94	8.45
MnO	0.17	0.16	0.13	0.22	0.18	0.21	0.16	0.21	0.16	0.17	0.17	0.16	0.17	0.17	0.16	0.16	0.15	0.14	0.15
MgO	8.22	8.56	8.08	8.69	10.45	9.09	9.26	9.56	7.39	9.32	7.94	7.73	10.65	8.14	8.88	8.40	9.30	9.03	9.32
CaO	8.82	8.79	8.06	9.07	9.39	9.56	9.03	8.75	8.92	8.62	8.82	8.85	8.54	8.25	8.79	8.77	9.08	8.75	8.05
Na_2O	3.64	3.17	3.00	3.56	2.93	3.10	3.26	3.53	3.33	2.82	2.98	2.98	2.21	3.25	3.19	3.18	2.68	2.35	3.30
K_2O	0.54	0.49	0.69	0.78	1.07	1.84	0.73	0.95	0.54	0.52	0.62	0.49	1.31	1.67	0.68	0.58	0.44	0.31	0.59
P_2O_5	0.21	0.25	0.23	0.47	0.39	0.76	0.29	0.42	0.22	0.28	0.23	0.21	0.41	0.39	0.31	0.28	0.28	0.23	0.24
H_2O	0.78	0.66	1.53	1.42	1.62	1.96	1.16	1.59	0.88	1.14	1.11	1.30	3.49	2.67	1.16	1.47	1.68	2.60	1.75
CO_2	0.02	0.13	0.13	0.11	0.05	0.10	0.07	0.04	0.24	0.13	0.10	0.19	0.05	0.04	0.06	0.10	0.06	0.13	0.07
Total S	<0.05	<0.05	<0.05	<0.05	<0.05	<0.05	<0.05	<0.05	<0.05	<0.05	<0.05	<0.05	<0.05	<0.05	<0.05	<0.05	<0.05	<0.05	<0.05
Total	100.78	99.71	100.72	100.06	100.09	100.75	100.19	100.66	99.04	100.65	100.23	100.32	100.57	100.11	100.35	100.08	100.13	99.71	100.24
100Mg/Mg+Fe	60.1	62.2	60.6	58.0	65.2	60.3	62.1	63.5	59.7	62.0	60.1	59.0	65.4	58.9	63.4	60.9	64.7	64.0	63.6
Chemical Type	T	T	T	A	A	AA	R	A	T	T	T	T	R	A	T	T	T	T	T
Trace elements (ppm)																			
Sc	20	20	19	19	23	17	22	18	23	21	18	24	17	19	18	17	16	17	18
V	180	165	165	200	210	185	210	195	175	195	175	170	200	175	170	170	165	160	165
Cr	340	340	290	310	370	220	360	320	320	360	310	270	350	260	360	300	350	330	310
Co	51	48	43	56	56	54	52	50	58	55	49	50	57	51	57	48	49	50	49
Ni	135	135	160	180	240	180	190	220	175	180	170	140	230	155	160	165	170	210	170
Cu	50	47	52	65	89	67	62	62	64	59	63	54	66	64	43	57	44	56	67
Zn	130	120	115	135	115	130	110	115	115	130	115	115	110	120	120	115	110	115	155
Ga	18	18	19	21	19	19	19	19	19	18	19	20	21	19	19	18	18	16	19
Rb	13	10	14	16	26	33	19	21	13	19	15	11	41	66	19	10	10	9	12
Sr	310	310	270	600	560	860	340	420	300	320	290	270	690	350	330	330	350	320	290
Y	23	21	21	25	22	25	22	24	24	24	22	22	22	22	20	21	20	20	23
Zr	105	110	105	160	140	210	125	135	110	115	105	105	160	145	115	115	110	115	105
Nb	11	12	11	27	35	46	16	31	11	13	10	8	29	25	14	12	13	13	11
Mo	4	4	7	4	4	7	3	4	4	4	4	3	4	6	4	5	3	5	8
Sn	<4	<4	<4	<4	<4	<4	<4	<4	<4	<4	4	<4	<4	<4	<4	<4	<4	<4	5
Ba	33	73	<9	105	135	125	41	120	27	9	17	18	58	68	55	41	69	34	10
La	<6	<6	<6	29	16	38	<6	11	6	<6	12	<6	18	14	15	9	<6	<6	<6
Ce	42	51	42	84	72	84	45	73	47	45	50	47	62	60	59	69	52	52	51
Nd	14	14	11	28	20	27	15	20	10	11	14	13	17	17	16	15	11	17	9
W	260	175	76	68	42	34	47	37	30	48	42	37	42	34	55	31	39	59	100
Pb	4	7	5	<4	<4	5	<4	<4	5	<4	<4	<4	<4	<4	<4	4	<4	<4	<4
Th	<4	<4	<4	<4	<4	<4	<4	<4	<4	<4	<4	<4	<4	<4	6	<4	<4	<4	<4
U	<5	<5	<5	<5	<5	<5	<5	<5	<5	<5	<5	<5	<5	<5	<5	<5	<5	<5	<5

Analyses by Department of Mines Analytical Laboratories, Launceston
Analysts R. Roby, M. Frith

Table B3
CIPW AND RITTMANN NORMS OF TERTIARY BASALTS (continued)

Field No.	EV21	EV22	EV23	EV24	EV25	EV26	EV27	EV28	EV29	EV30	EV31	EV32	EV33	EV34	EV35	EV36	EV37	EV38	EV39
Analysis No.	870718	870719	870720	870721	870722	870723	870724	870725	870726	870727	870728	870729	870730	870731	870732	870733	870734	870735	870736
CIPW NORMS (mass%)																			
or	3.18	2.96	4.13	4.66	6.43	11.03	4.36	5.66	3.25	3.07	3.71	2.96	7.97	10.15	4.07	3.48	2.66	1.89	3.54
ab	30.83	27.20	25.97	25.57	20.16	13.30	27.88	28.70	28.81	24.07	25.51	25.51	19.26	25.99	27.28	27.36	23.15	20.53	28.38
an	21.07	23.12	24.15	18.89	22.58	20.39	20.28	18.04	23.51	24.11	23.98	26.22	25.61	19.00	21.96	22.92	25.46	30.73	21.94
lc	-	-	-	-	-	-	-	-	-	-	-	-	-	-	-	-	-	-	-
ne	-	-	-	2.76	2.72	7.21	-	0.83	-	-	-	-	-	1.21	-	-	-	-	-
di	17.42	15.86	12.14	19.46	17.99	18.52	18.88	18.74	16.55	14.00	15.24	13.84	12.45	16.70	16.32	15.86	15.13	10.24	13.93
hy	9.91	18.85	27.54	-	-	-	4.62	-	18.25	20.63	24.29	22.57	5.69	-	15.83	15.13	22.80	28.30	14.22
ol	11.93	6.36	0.42	21.32	23.42	21.46	17.65	21.17	4.13	8.07	1.58	3.23	22.06	20.27	8.71	9.28	5.04	2.57	12.20
mt	2.12	2.04	2.06	2.48	2.20	2.36	2.22	2.16	1.97	2.23	2.07	2.12	2.26	2.26	2.02	2.13	2.02	2.04	2.12
il	3.04	3.04	3.25	3.73	3.56	3.92	3.43	3.69	3.00	3.17	2.98	3.06	3.71	3.48	3.07	3.14	3.08	3.15	3.10
ap	0.50	0.59	0.54	1.13	0.94	1.82	0.68	1.01	0.54	0.66	0.54	0.50	0.99	0.94	0.73	0.68	0.68	0.57	0.57
Total	100.00	100.02	100.00	100.00	100.00	100.01	100.00	100.00	100.01	100.01	100.00	100.01	100.00	100.00	99.99	99.98	100.02	100.02	100.00
mol% an (plagioclase)	39.2	44.5	46.9	33.7	51.4	59.1	40.7	37.2	43.5	48.6	47.0	50.7	55.6	40.8	43.1	44.1	50.9	58.5	42.2
RITTMANN NORMS (vol.%)																			
Quartz	-	-	0.9	-	-	-	-	-	-	-	0.5	-	-	-	-	-	-	-	
Sanidine	-	-	-	0.9	4.5	12.4	0.4	2.6	-	-	-	-	7.2	12.2	-	-	-	-	-
Plagioclase	59.8	56.3	59.1	55.3	51.1	38.7	56.5	55.7	60.3	56.2	58.0	59.7	50.7	50.2	57.9	58.6	55.8	58.1	58.8
Nepheline	-	-	-	1.5	1.6	6.4	-	-	-	-	-	-	-	-	-	-	-	-	-
Clinopyroxene	30.3(S)	35.7(P)	36.3(P)	21.7(D)	19.9(D)	20.4(D)	28.2(A)	22.2(A)	35.6(P)	35.7(P)	37.9(P)	36.3(P)	21.5(S)	18.5(D)	34.0(S)	32.9(S)	38.6(P)	37.5(P)	30.2(P)
Olivine	6.4	4.0	-	15.9	18.6	16.6	11.0	15.2	0.7	4.3	-	0.4	16.1	14.7	4.4	4.8	2.0	0.8	7.3
Magnetite	1.7	1.5	1.5	2.1	1.7	2.0	1.7	1.8	1.5	1.6	1.5	1.5	1.6	1.9	1.5	1.6	1.4	1.3	1.6
Ilmenite	1.4	1.8	1.7	1.6	1.7	1.8	1.5	1.6	1.5	1.6	1.5	1.6	2.0	1.6	1.5	1.5	1.6	1.7	1.5
Apatite	0.5	0.7	0.5	1.1	0.9	1.7	0.6	0.9	0.5	0.6	0.5	0.5	0.9	0.9	0.7	0.6	0.6	0.5	0.5
Total	100.1	100.0	100.0	100.1	100.0	100.0	99.9	100.0	100.1	100.0	99.9	100.0	100.0	100.0	100.0	100.0	100.0	99.9	99.9

Table B2
CHEMICAL ANALYSES OF TERTIARY BASALTS (continued)

Field No.	VA8	VA23	CR32	-	-
Analysis No.	791080	850090	781006	Nc15	Oc37
Plot No.	40	41	42	43	44
SiO_2	49.1	46.13	46.6	48.40	44.12
TiO_2	1.8	2.27	1.6	1.88	2.30
Al_2O_3	14.0	13.24	13.9	15.59	13.94
Fe_2O_3	2.1	2.45	1.2	5.12	2.60
FeO	9.3	10.76	10.5	6.29	8.98
MnO	0.18	0.19	0.17	0.14	0.14
MgO	8.8	9.03	9.8	6.52	11.43
CaO	9.1	9.07	8.9	7.95	9.40
Na_2O	2.6	3.76	2.8	2.69	2.83
K_2O	0.66	1.13	0.64	1.09	1.99
P_2O_5	0.29	0.64	0.38	0.36	0.55
H_2O^+	1.5	1.32	2.80	2.40	0.10
H_2O^-	0.87	nd	0.30	1.74	1.94
CO_2	0.05	0.06	nd	tr	tr
SO_3	nd	0.02	0.11	tr	-
F	0.08	nd	nd	nd	nd
Total	100.40	100.07	99.7	100.17	100.32
100Mg/Mg+Fe	61.4	58.5	63.1	54.8	67.1
Chemical type	T	AA	R	T	AA
Trace elements (ppm)					
Li	10	nd	6	nd	nd
Sc	nd	18	19	nd	nd
V	nd	200	198	nd	nd
Cr	461	270	294	nd	nd
Co	nd	58	69	nd	nd
Ni	203	175	226	nd	nd
Cu	58	54	60	nd	nd
Zn	126	145	124	nd	nd
Ga	19	23	nd	nd	nd
As	nd	10	nd	nd	nd
Rb	13	25	8	nd	nd
Sr	308	710	312	nd	nd
Y	24	24	18	nd	nd
Zr	135	210	114	nd	nd
Nb	18	40	11	nd	nd
Mo	nd	4	nd	nd	nd
Ag	nd	<5	nd	nd	nd
Sn	nd	<4	nd	nd	nd
Ba	111	260	210	nd	nd
La	nd	41	nd	nd	nd
Ce	nd	96	nd	nd	nd
Nd	nd	37	nd	nd	nd
W	nd	nd	nd	nd	nd
Pb	71	12	nd	nd	nd
Bi	nd	7	nd	nd	nd
Th	nd	<4	nd	nd	nd
U	nd	<5	nd	nd	nd

Analyses by Department of Mines Analytical Laboratories, Launceston
Analysts: R. Roby, M. Frith

Table B3
CIPW AND RITTMANN NORMS OF TERTIARY BASALTS (continued)

Field No.	VA8	VA23	CR32	-	-
Analysis No.	791080	850090	781006	Nc15	Oc37
CIPW NORMS (mass%)					
or	4.01	6.79	3.89	6.73	11.98
ab	22.47	20.26	24.58	23.82	7.47
an	25.12	16.13	24.30	28.46	19.80
ne	-	6.50	-	-	9.17
di	15.53	20.70	15.41	8.44	19.43
hy	18.76	-	4.01	22.18	-
ol	7.73	21.21	21.44	3.55	24.16
mt	2.19	2.51	2.31	2.19	2.22
il	3.48	4.38	3.14	3.73	4.45
ap	0.71	1.53	0.92	0.90	1.32
Total	100.00	100.01	100.00	100.00	100.00
mol% an (plagioclase)	51.3	42.9	48.2	53.0	71.4
RITTMANN NORMS (vol.%)					
Quartz	-	-	-	-	-
Sanidine	-	5.8	-	3.8	13.6
Plagioclase	56.3	43.8	57.5	60.9	31.3
Nepheline	-	5.6	-	-	8.3
Clinopyroxene	35.7(P)	23.3(T)	23.6(A)	29.7(P)	21.7(T)
Olivine	4.0	16.2	14.7	1.0	20.1
Magnetite	1.5	2.2	1.7	1.6	1.8
Ilmenite	1.8	1.7	1.6	2.1	2.0
Apatite	0.7	1.4	0.9	0.8	1.2
Total	100.0	100.0	100.0	99.9	100.0

Strongly alkaline basalt

EV7 (very fine, intergranular to glassy) [CQ944242]

This rock is the most undersaturated of its group and is transitional in both chemistry and texture to basanite. It contains abundant but small (usually ≤500 μm but rarely ≤2 mm) euhedra and anhedra of olivine, sometimes embayed and often clumped in glomerocrysts, set in a very fine, intergranular groundmass in which narrow plagioclase microlites (~100 μm), olivine granules, pinkish titanaugite granules, opaque blebs (5-50 μm) and very finely acicular apatite are resolvable. The low birefringence mesostasis is presumably composed mainly of alkali feldspar and nepheline. Rare oblong phenocrysts (≤2 mm) of plagioclase (?labradorite) are typically clumped in glomerocrysts, as may be corroded or inclusion-ridden (sieve texture), and are probably xenocrystal. A few rounded to irregularly shaped amygdales (≤500 μm) filled with low birefringence, polycrystalline zeolite are present. The rock is fresh with only slight iddingsitisation of the margins and fractures of a few olivine phenocrysts.

Sample V7 from the same locality is nearly identical, and contains a rounded corroded xenocryst (1 mm across) of recrystallised, finely granular olivine.

EV5 (fine, intergranular) [DQ699250] - Plates B3, B4

The rock contains abundant equant euhedral or subhedral, sometimes embayed phenocrysts of olivine (≤1 mm) and subordinate, smaller pinkish titanaugite phenocrysts. Both grade in size down to the fine intergranular groundmass of plagioclase laths (100-200 μm × 5-20 μm), titanaugite and olivine granules, angular and more or less equant opaques, and low birefringence mesostasis. There is a strong flow lamination, defined by alignment of plagioclase laths, which envelops olivine phenocrysts. A single corroded, well rounded quartz xenocryst (500 μm) is surrounded by a reaction corona 150 μm wide of fine, radiating, elongate to acicular (?)clinopyroxene (plate B4). The rock is fairly fresh with incipient to partial alteration of some olivine phenocrysts. Samples VP64 and VP74 from the same vicinity (Peak Hill Farm) are nearly identical.

Sample EV11, from about 8 km to the south-west, is a similar fine-grained basalt, but contains very few olivine phenocrysts, but abundant olivine granules (50-200 μm). Corroded quartz xenocrysts with reaction rims are also present and rare anhedral plagioclase fragments may also be xenocrysts. The rock is more altered and contains vesicles lined with limonitic material (?goethite), sometimes with an inner core of calcite. Samples V62 (80-26) and VP1 (analysis VA23, 850090), from quite different localities, are similar phenocryst-poor rocks containing abundant olivine granules in a somewhat finer groundmass.

EV26 (medium-fine, intergranular) [DQ023278]

Olivine phenocrysts (Fo_{79-83}) are typically euhedral or subhedral, 500 μm-2 mm across and often clumped in glomerocrysts. The medium-fine groundmass consists of unoriented narrow plagioclase laths (200-500 μm) and intergranular pale pink, titanaugite, olivine (Fo_{55-67}), equant titanomagnetite (50-200 μm) and alkali feldspar (biaxial negative). There is very little obvious alteration, but interstitial zeolite (scolecite or thomsonite?) was identified by electron microprobe.

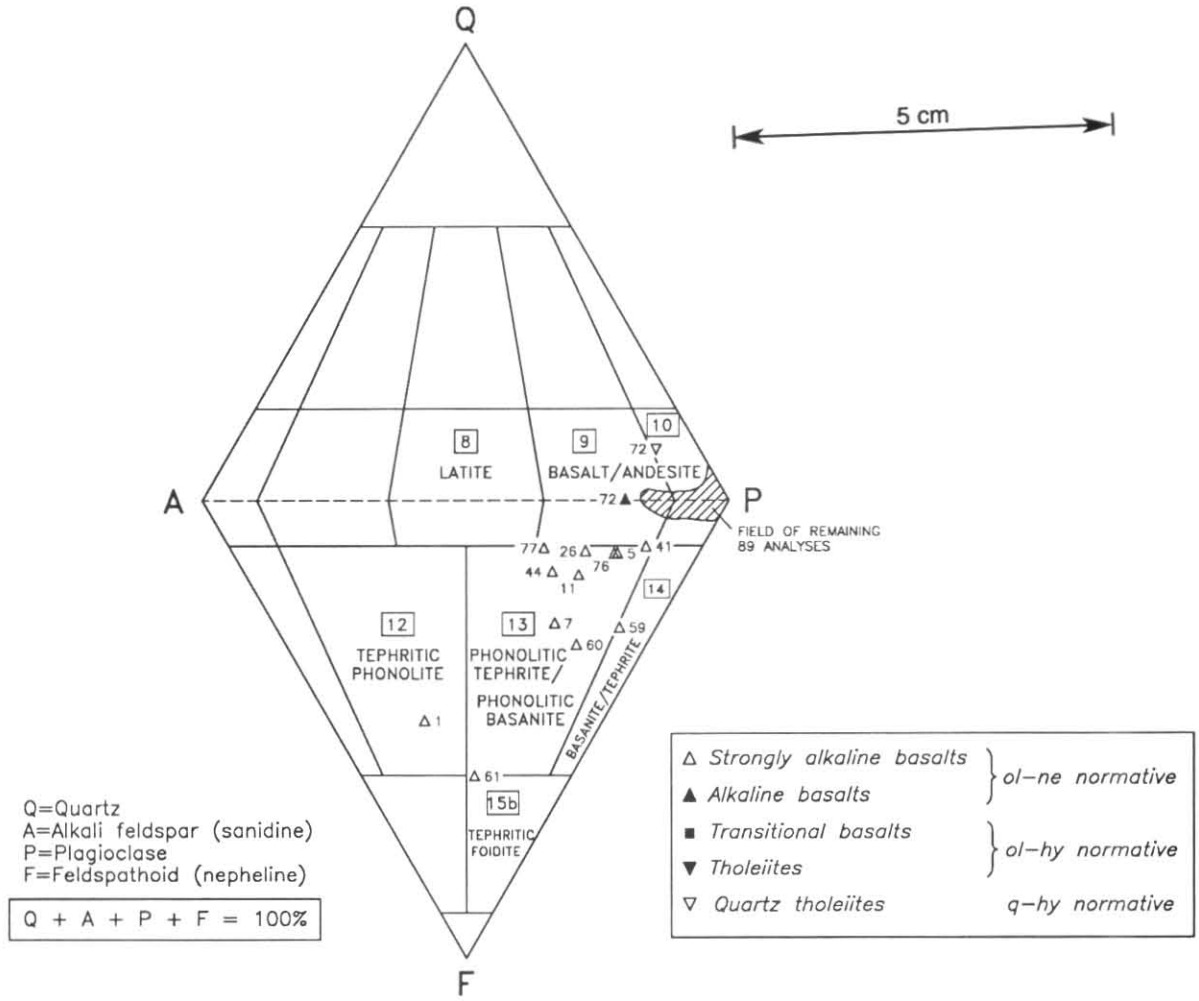

Figure B4. Modal classification of Tertiary basaltic rocks (Rittmann norms)

SBDP6/1770 (coarse, intersertal) - Plate B5

Abundant olivine phenocrysts (Fo_{84-74}) lie in a coarse, intersertal groundmass containing about 30% black glass. The phenocrysts are up to 3 mm but typically 500 μm, equant, euhedral or more often subhedral and clustered in glomerocrysts, and, rarely, slightly embayed. The coarse groundmass consists of elongate plagioclase (typically 500 μm-2 mm × 200-150 μm) fine, freshly nucleated granular titanaugite granules (50-200 μm) and black glass, in which may sometimes be discerned very narrow opaque needles and titanaugite crystallites. The glass has an almost phonolitic composition (table B5, analyses 99-102). The rock is very fresh.

SBDP6/202.8 (fine, glassy)

The thin section is of a glassy basalt clast from a breccia (hyalotuff). Abundant euhedral phenocrysts (typically 50 μm-1.5 mm) and glomerocrysts of fresh olivine are set in a groundmass of black to brown, partly altered glass, containing rather sparse narrow plagioclase laths (≤200 μm) and titanaugite and olivine granules. The rock contains more glass and the groundmass minerals are sparser and finer than in SBDP6/177.0 and was quenched at an earlier stage of crystallisation. Amygdales filled with zeolites and veinlets of calcite are present.

Alkaline basalt

SBDP9/213.5 (very fine, intergranular) - Plate B6

This basalt is transitional to the previously described, more strongly alkaline group. Its high Mg number (69.3) suggests that it has crystallised from an unfractionated, primary magma. In thin section the rock consists of abundant euhedral or slightly embayed olivine phenocrysts (≤1 mm) which grade down in size to granules (20 μm or less). The groundmass consists of small, aligned plagioclase laths (≤100 μm), olivine granules, euhedral augite granules (≤100 mm) and a very fine mesostasis of opaques, pinkish titanaugite and probably alkali feldspar.

EV28 (very fine, intergranular) [CQ991261]

Fairly common but rather small (≤1 mm, typically about 500 μm), sometimes embayed euhedra and anhedra of olivine, sometimes clumped in glomerocrysts, lie in a very fine intergranular groundmass in which plagioclase (<100 μm), augite granules (10-30 μm), both equant and elongate opaques, finely acicular apatite and probable alkali feldspar can be identified.

Sample SBDP2/238.0 contains more abundant, larger (≤3 mm), often deeply embayed olivine phenocrysts in an identical groundmass. Both samples are fairly fresh, with only peripheral alteration of olivine.

EV24 (medium-fine, intergranular) [DQ023315]

Olivine phenocrysts (≤1.5 mm) are rare in this sample. There are also rare equidimensional anhedra (500 μm) of plagioclase, probably xenocrysts. The groundmass is slightly coarser than in EV24 and has a medium-fine, intergranular texture, consisting of aligned plagioclase laths (typically 200-300 μm), olivine granules (≤200 μm), interstitial colourless augite, opaques and alkali feldspar.

EV4 (medium-coarse, intergranular) [DQ121272] - Plate B7

This is a fresh, medium-coarse alkali-olivine basalt, containing abundant euhedral to subhedral olivine phenocrysts (≤1 mm; up to Fo_{85}) which are often clumped in glomerocrysts. There are also rare xenocrysts of polycrystalline quartz (≤1.5 mm), surrounded by a reaction corona of outwardly radiating, elongate (?) clinopyroxene. The groundmass is intergranular, containing narrow plagioclase laths (typically 500 μm long), granules of olivine (Fo_{53-72}), almost colourless augite, interstitial alkali feldspar and generally elongate opaques (100-300 μm), mainly ilmenite. Very finely acicular apatite is a common but inconspicuous accessory mineral.

This is the main type of alkali olivine basalt in the north-eastern part of the quadrangle near South Riana. Sample EV2 is nearly identical

Table B2
CHEMICAL ANALYSES OF TERTIARY BASALTS (continued)

Hole No.	SBDP1				SBDP2						SBDP4								
Depth (m)	125.3	171.4	224.5	245.6	101.5	145.0	190.0	238.0	282.0	293.0	107.9	129.1	160.9	206.0	251.1	255.8	269.1	341.0	366.0
Analysis No.	871834	871835	871836	871837	872167	872168	872169	872170	872171	872172	872226	872227	872228	872229	872230	872231	872232	872233	872234
Plot No.	45	46	47	48	49	50	51	52	53	54	55	56	57	58	59	60	61	62	63
SiO_2	51.38	48.19	49.93	49.71	50.54	51.59	48.62	46.63	48.75	49.27	49.55	50.38	50.25	48.99	41.69	40.57	40.89	47.78	47.17
TiO_2	1.51	1.57	1.55	1.75	1.60	1.52	1.79	2.18	2.05	2.18	1.68	1.56	1.60	1.72	2.62	2.51	2.52	1.90	1.97
Al_2O_3	14.11	13.83	13.61	13.43	14.13	14.34	14.24	12.86	15.18	15.73	13.78	13.95	13.78	13.55	11.25	10.74	10.56	13.37	13.93
Fe_2O_3	1.97	4.66	6.00	3.69	5.12	5.13	3.46	2.31	3.36	3.35	3.55	4.27	3.03	3.27	5.69	6.43	4.13	2.61	3.08
FeO	8.54	6.98	5.39	7.12	6.49	5.72	7.01	9.90	6.68	6.92	7.17	6.91	8.52	7.27	7.54	6.94	8.97	8.17	7.62
MnO	0.16	0.16	0.15	0.14	0.14	0.16	0.15	0.17	0.15	0.15	0.15	0.17	0.15	0.16	0.22	0.20	0.20	0.15	0.18
MgO	8.10	9.40	8.20	8.96	6.77	6.61	7.05	9.83	6.46	5.51	8.16	7.89	8.21	8.76	10.90	11.20	11.96	9.74	8.21
CaO	9.28	7.89	8.75	8.26	9.30	8.69	9.17	8.79	7.76	7.72	9.77	9.48	8.68	8.06	10.69	11.41	11.09	8.84	9.67
Na_2O	2.69	2.23	2.41	3.14	2.71	3.01	2.83	2.84	2.75	2.82	2.70	2.39	3.43	2.79	3.65	3.24	4.57	2.92	2.51
K_2O	0.25	0.72	0.45	1.05	0.44	0.79	0.95	1.21	1.52	1.69	0.29	0.17	0.56	0.96	0.67	0.82	0.80	1.21	1.05
P_2O_5	0.20	0.25	0.28	0.35	0.21	0.23	0.34	0.47	0.38	0.40	0.21	0.20	0.21	0.31	0.85	0.96	0.93	0.46	0.49
H_2O^+	1.70	3.42	2.51	2.32	1.99	1.86	2.78	2.29	2.50	2.77	1.95	2.07	1.12	3.29	3.79	3.99	2.98	2.41	2.74
CO_2	0.11	0.18	0.17	0.13	0.27	0.26	0.92	0.16	0.54	0.38	0.46	0.29	0.18	0.26	0.14	0.28	0.29	0.11	0.67
Total S	<0.05	<0.05	<0.05	<0.05	<0.05	<0.05	<0.05	<0.05	0.11	<0.05	<0.05	<0.05	<0.05	<0.05	<0.05	<0.05	0.05	<0.05	<0.05
Total	100.00	99.48	99.40	100.05	99.71	99.91	99.31	99.64	98.19	98.89	99.42	99.73	99.72	99.39	99.70	99.29	99.94	99.67	99.29
$100Mg/Mg+Fe^{II}$	61.4	63.0	60.6	63.5	55.2	56.4	58.5	62.4	57.4	52.9	61.4	59.8	59.6	63.4	63.5	64.0	65.6	65.2	61.5
Chemical type	Q	T	Q	R	Q	Q	R	A	R	R	T	Q	T	R	B	B	B	R	R
Trace elements (ppm)																			
Sc	24	16	15	18	21	20	19	20	18	15	22	19	20	19	17	17	19	22	18
V	160	155	155	185	155	145	170	195	195	175	165	145	150	165	210	195	195	180	170
Cr	370	340	300	390	300	280	230	290	50	69	280	270	280	250	320	390	400	320	300
Co	47	53	51	45	50	45	47	56	35	34	48	48	49	45	57	63	60	50	48
Ni	150	165	185	155	175	140	160	230	44	54	175	165	170	130	250	320	310	215	195
Cu	54	56	56	44	60	54	57	73	40	38	46	60	66	48	65	76	78	57	54
Zn	110	110	115	105	125	120	125	135	120	120	115	115	125	105	140	140	140	110	115
Ga	18	18	19	18	19	18	20	21	22	22	17	18	18	18	20	21	20	19	20
As	12	15	<10	14	13	<10	11	<10	16	19	14	<10	15	<10	17	22	16	15	23
Rb	5	13	7	25	7	18	18	19	38	35	6	8	12	22	15	24	24	19	14
Sr	270	240	290	380	240	280	390	640	610	370	300	270	300	350	930	1160	920	610	620
Y	21	17	20	19	21	17	20	20	23	23	20	19	19	19	24	24	23	19	19
Zr	96	105	92	125	99	100	115	185	160	155	105	100	99	125	250	240	240	135	140
Nb	9	10	11	22	9	15	26	32	33	29	13	9	13	26	84	85	85	32	31
Mo	4	2	2	3	22	15	17	11	10	13	2	2	2	3	4	5	6	3	3
Ag	5	7	7	6	5	5	<5	8	<5	7	<5	<5	5	<5	12	12	8	<5	<5
Sn	4	<4	<4	<4	54	11	7	4	4	6	<4	<4	4	<4	<4	<4	<4	<4	<4
Ba	<9	52	22	110	<9	52	110	77	1300	310	<9	<9	26	99	340	330	320	155	210
La	6	<6	<6	14	<6	7	15	15	12	19	7	<6	<6	23	50	68	50	11	11
Ce	42	48	54	57	41	52	60	76	74	73	43	45	53	62	125	140	130	69	70
Nd	13	12	14	18	14	10	20	17	19	20	12	12	12	20	31	34	34	20	17
Ta	<9	<9	<9	<9	<9	<9	<9	9	<9	<9	<9	<9	<9	<9	<9	<9	<9	<9	<9
W	400	640	470	120	380	260	155	110	210	270	48	53	42	35	34	30	36	33	36
Pb	<4	<4	<4	<4	10	6	4	7	4	<4	<4	6	5	6	<4	<4	<4	<4	6
Bi	6	13	5	<5	5	7	6	<5	<5	<5	7	<5	<5	<5	9	9	6	<5	6
Th	<4	<4	<4	<4	<4	<4	4	<4	<4	<4	<4	5	4	6	5	4	5	<4	6
U	<5	<5	<5	5	<5	<5	<5	<5	<5	5	<5	<5	<5	<5	<5	<5	<5	<5	<5

Analyses by Department of Mines Analytical Laboratories, Launceston
Analysts: R. Roby, M. Frith

Table B3
CIPW AND RITTMANN NORMS OF TERTIARY BASALTS (continued)

Hole No.	SBDP1				SBDP2						SBDP4								
Depth (m)	125.3	171.4	224.5	245.6	101.5	145.0	190.0	238.0	282.0	293.0	107.9	129.1	160.9	206.0	251.1	255.8	269.1	341.0	366.0
Analysis No.	871834	871835	871836	871837	872167	872168	872169	872170	872171	872172	872226	872227	872228	872229	872230	872231	872232	872233	872234
CIPW NORMS (mass%)																			
Q	1.39	-	1.24	-	1.42	1.14	-	-	-	-	-	2.07	-	-	-	-	-	-	-
or	1.54	4.42	2.78	6.37	2.66	4.78	5.90	7.38	9.51	10.44	1.77	1.06	3.36	5.96	4.13	5.13	4.90	7.38	6.49
ab	23.23	19.77	21.20	27.29	23.65	26.10	25.08	23.84	24.50	25.00	23.57	20.86	29.56	24.68	8.59	3.82	0.14	25.43	22.21
an	26.14	26.78	25.95	19.97	25.85	23.93	24.47	19.31	25.93	26.45	25.46	27.60	20.89	22.60	12.97	13.06	6.18	20.43	24.69
ne	-	-	-	-	-	-	-	0.49	-	-	-	-	-	-	12.86	13.62	21.64	-	-
di	15.89	10.17	14.09	16.09	16.64	15.41	17.09	18.30	9.85	8.96	18.91	15.92	17.66	13.93	29.92	32.59	36.12	17.59	18.01
hy	26.41	27.82	28.87	11.73	23.95	23.09	14.98	-	20.27	20.92	21.97	26.81	11.13	19.05	-	-	-	2.18	9.37
ol	-	5.06	-	12.23	-	-	6.04	22.93	2.96	0.90	2.46	-	11.61	7.58	21.67	21.76	21.25	20.09	12.04
mt	2.02	2.25	2.15	2.06	2.19	2.03	2.03	2.36	1.96	2.00	2.06	2.13	2.19	2.04	2.54	2.57	2.51	2.09	2.09
il	2.92	3.12	3.05	3.41	3.12	2.96	3.56	4.26	4.09	4.34	3.29	3.05	3.10	3.42	5.21	5.04	4.97	3.71	3.90
ap	0.47	0.61	0.68	0.85	0.52	0.57	0.85	1.13	0.94	0.99	0.52	0.50	0.50	0.75	2.10	2.40	2.29	1.11	1.20
Total	100.01	100.00	100.01	100.00	100.00	100.01	100.00	100.00	100.01	100.00	100.01	100.00	100.00	100.01	99.99	99.99	100.00	100.01	100.00
mol%an (plagioclase)	51.5	56.1	53.6	40.8	50.7	46.4	47.9	43.3	49.9	49.9	50.4	55.5	39.9	46.3	58.7	76.3	97.8	43.1	51.2
RITTMANN NORMS (vol.%)																			
Quartz	2.6	-	2.4	-	2.8	2.5	-	-	-	0.6	0.2	3.3	-	-	-	-	-	-	-
Sanidine	-	0.6	-	4.2	-	0.6	2.8	7.5	9.2	10.6	-	-	-	3.3	2.8	4.8	6.0	6.9	4.6
Plagioclase	55.4	55.5	54.6	54.1	56.9	59.0	57.5	48.5	56.2	56.9	55.2	54.0	58.5	54.8	27.0	20.6	7.1	50.8	53.3
Nepheline	-	-	-	-	-	-	-	-	-	-	-	-	-	-	11.5	11.9	19.7	-	-
Clinopyroxene	38.8(P)	37.6(P)	39.4(P)	30.6(S)	36.8(P)	34.4(P)	33.5(S)	22.8(A)	29.6(P)	27.2(P)	41.2(P)	39.3(P)	31.7(S)	34.1(P)	35.3(T)	38.8(T)	44.8(T)	24.6(A)	30.5(S)
Olivine	-	2.5	-	7.1	-	-	2.3	16.4	0.5	-	-	-	6.1	3.8	18.2	18.6	17.7	13.4	7.2
Magnetite	1.4	1.5	1.4	1.6	1.5	1.5	1.5	1.8	1.4	1.5	1.4	1.4	1.7	1.5	2.1	2.1	2.4	1.6	1.5
Ilmenite	1.5	1.7	1.6	1.6	1.6	1.5	1.7	1.9	2.2	2.4	1.6	1.6	1.4	1.7	1.1	0.9	-	1.7	1.9
Apatite	0.4	0.6	0.6	0.8	0.5	0.5	0.8	1.1	0.8	0.9	0.5	0.5	0.5	0.7	2.0	2.3	2.2	1.0	1.1
Total	100.1	100.0	100.0	100.0	100.1	100.0	100.1	100.0	99.9	100.1	100.1	100.1	99.9	99.9	100.0	100.0	99.9	100.0	100.1

Table B2
CHEMICAL ANALYSES OF TERTIARY BASALTS (continued)

Hole No.	SBDP5										SBDP6				SBDP9			
Depth (m)	6.4	61.0	81.4	116.7	159.3	173.3	219.5	237.0	248.7	280.8	75.8	108.0	177.0	202.8	115.5	129.0	213.5	237.6
Analysis No.	872673	872674	872675	872676	872677	872678	872679	872680	872682	872681	874881	874882	874883	874884	872455	872456	872457	872458
Plot No.	64	65	66	67	68	69	70	71	73	72	74	75	76	77	78	79	80	81
SiO_2	50.86	50.38	47.68	51.01	48.18	48.72	51.30	51.09	50.93	48.13	51.01	50.73	44.57	44.53	49.85	47.46	44.05	47.54
TiO_2	1.77	1.68	1.81	1.51	1.60	1.81	1.59	1.55	1.55	1.55	1.56	1.53	2.02	2.28	1.44	1.44	2.12	1.95
Al_2O_3	14.00	13.83	13.26	14.36	13.99	13.48	14.20	13.98	13.90	13.40	13.94	14.25	13.06	14.03	14.08	15.51	12.69	12.93
Fe_2O_3	2.35	1.57	2.59	3.35	2.90	3.77	1.91	1.60	1.61	5.24	1.31	1.64	2.71	2.20	3.63	2.70	3.87	2.66
FeO	7.94	9.06	9.45	6.96	8.37	8.01	8.93	9.44	9.42	5.83	9.59	9.61	9.31	8.78	8.02	8.84	7.92	8.82
MnO	0.15	0.15	0.16	0.15	0.15	0.16	0.17	0.14	0.16	0.13	0.15	0.16	0.16	0.16	0.16	0.16	0.17	0.17
MgO	8.17	7.70	9.39	8.31	8.96	8.74	8.48	8.66	8.75	7.59	8.52	8.39	10.73	8.41	8.16	8.87	12.71	9.89
CaO	9.01	9.33	8.42	9.29	7.71	8.09	8.74	8.56	8.61	6.21	8.41	9.22	9.98	10.57	8.39	7.98	9.83	8.55
Na_2O	2.90	2.98	3.07	2.28	2.39	2.82	3.21	3.07	3.09	1.55	3.06	3.13	2.96	2.51	3.14	2.52	2.33	2.58
K_2O	0.92	0.40	0.72	0.21	0.84	0.83	0.52	0.64	0.59	1.01	0.99	0.48	1.32	2.26	0.78	0.62	0.76	0.81
P_2O_5	0.31	0.27	0.32	0.22	0.23	0.33	0.23	0.25	0.25	0.22	0.23	0.19	0.54	0.72	0.27	0.25	0.68	0.36
H_2O^+	1.65	1.67	2.20	1.92	4.28	3.04	1.10	0.91	1.39	8.20	0.92	1.16	2.58	2.96	0.63	3.29	3.04	3.04
CO_2	0.07	0.09	0.15	0.32	0.11	0.15	0.25	0.15	0.15	0.63	0.07	0.26	0.13	0.35	1.48	0.21	0.17	0.52
Total S	<0.05	<0.05	<0.05	<0.05	<0.05	<0.05	<0.05	0.05	<0.05	0.05	<0.05	<0.05	<0.05	<0.05	<0.05	<0.05	<0.05	<0.05
Total	100.10	99.11	99.22	99.89	99.71	99.95	100.63	100.09	100.40	99.74	99.76	100.75	100.07	99.76	100.03	99.85	100.34	99.82
100Mg/Mg+Fe	62.2	59.8	61.7	62.8	62.3	60.8	61.7	61.7	62.0	59.3	61.5	60.5	64.9	61.3	59.4	61.4	69.3	64.1
Chemical type	T	T	R	Q	T	R	T	T	T	Q	T	T	AA	AA	T	T	A	R
Trace elements (ppm)																		
Sc	23	21	25	19	17	18	20	20	18	21	23	26	23	21	19	20	19	19
V	180	150	175	140	165	160	145	150	145	135	180	195	220	230	140	155	210	170
Cr	350	260	310	300	320	290	300	320	320	260	410	360	430	300	330	320	460	280
Co	42	47	57	46	47	50	48	51	46	43	49	52	54	50	50	51	55	59
Ni	97	155	220	135	135	155	125	145	155	130	190	190	230	150	190	210	360	250
Cu	35	55	66	49	41	52	46	51	53	48	53	60	63	66	64	70	100	82
Zn	120	120	120	105	110	120	110	115	120	110	94	95	95	100	115	125	120	125
Ga	18	19	19	17	18	18	19	17	18	17	15	15	16	17	18	19	17	19
As	14	11	<10	<10	12	<10	18	17	14	<10	<10	10	11	14	13	<10	13	21
Rb	16	11	15	6	22	18	15	17	17	24	23	7	28	29	19	14	16	14
Sr	360	340	340	280	290	310	310	300	310	270	320	290	870	840	290	280	710	350
Y	20	21	22	18	17	20	20	20	17	17	24	24	21	23	18	18	22	21
Zr	125	120	125	95	105	120	96	99	96	93	125	110	175	210	105	105	160	120
Nb	18	17	19	8	12	23	12	14	12	13	15	11	44	54	12	10	42	20
Mo	2	2	<2	2	2	2	2	3	3	2	3	2	4	6	3	<2	4	2
Ag	<5	10	5	5	<5	6	6	<5	<5	<5	<3	<3	3	<3	6	<5	<5	<5
Sn	<4	<4	<4	<4	<4	4	<4	<4	6	<4	7	<4	<4	<4	5	<4	9	17
Ba	105	56	165	17	70	52	59	250	<9	160	165	260	350	380	55	57	160	58
La	30	15	11	<6	45	57	38	74	9	10	16	<6	23	29	11	11	31	12
Ce	52	55	60	50	130	120	120	175	60	57	62	51	82	95	50	54	91	56
Nd	13	19	16	18	32	29	32	52	20	11	15	10	26	29	15	16	25	17
Ta	<9	<9	<9	<9	<9	<9	<9	<9	<9	<9	<7	<7	<7	<7	<9	<9	<9	<9
W	29	31	25	28	14	20	33	26	36	28	25	15	18	17	29	37	38	25
Pb	7	<4	6	5	<4	5	<4	4	5	4	<4	<4	<4	<4	<4	6	<4	5
Th	4	<4	<4	5	<4	4	4	6	4	<4	<4	<4	<4	<4	4	<4	<4	<4
U	5	<5	<5	<5	<5	<5	<5	<5	<5	<5	5	5	<5	8	<5	<5	<5	<5

Analyses by Department of Mines Analytical Laboratories, Launceston
Analysts: R. Roby, M. Frith

Table B3

CIPW AND RITTMANN NORMS OF TERTIARY BASALTS (continued)

Hole No.	SBDP5										SBDP6				SBDP9			
Depth (m)	6.4	61.0	81.4	116.7	159.3	173.3	219.5	237.0	248.7	280.8	75.8	108.0	177.0	202.8	115.5	129.0	213.5	237.6
Analysis No.	872673	872674	872675	872676	872677	872678	872679	872680	872682	872681	874881	874882	874883	874884	872455	872456	872457	872458
CIPW NORMS (mass%)																		
Q	-	-	-	3.03	-	-	-	-	-	6.23	-	-	-	-	-	-	-	-
or	5.55	2.42	4.42	1.30	5.19	5.07	3.07	3.83	3.54	6.61	5.90	2.84	8.03	13.86	4.72	3.83	4.66	4.95
ab	24.93	25.93	26.86	19.77	21.28	24.75	27.37	26.27	26.44	14.53	26.20	26.70	12.47	9.44	27.20	22.13	16.21	22.72
an	22.87	23.80	20.94	29.09	26.22	22.45	23.00	22.70	22.57	29.40	21.66	23.57	18.97	21.09	22.52	30.31	22.60	22.16
ne	-	-	-	-	-	-	-	-	-	-	-	-	7.20	6.83	-	-	2.25	-
di	16.73	17.92	16.39	13.63	10.10	13.79	15.67	15.16	15.50	2.52	15.59	17.37	22.97	23.12	14.95	7.48	18.67	15.83
hy	19.85	22.12	5.89	27.76	25.30	17.83	19.21	20.26	19.52	34.66	17.05	15.58	-	-	14.58	19.08	-	13.67
ol	3.94	1.81	18.85	-	5.94	9.49	6.04	6.10	6.75	-	7.98	8.43	22.80	17.25	10.35	11.48	27.55	13.68
mt	1.96	2.06	2.33	1.96	2.22	2.26	2.06	2.12	2.12	2.23	2.09	2.15	2.32	2.15	2.22	2.25	2.26	2.23
il	3.42	3.28	3.54	2.94	3.18	3.56	3.04	2.98	2.98	3.26	3.00	2.92	3.94	4.49	2.81	2.84	4.15	3.85
ap	0.75	0.66	0.78	0.54	0.57	0.80	0.54	0.59	0.59	0.57	0.54	0.45	1.32	1.77	0.66	0.61	1.65	0.90
Total	100.00	100.00	100.00	100.02	100.00	100.00	100.00	100.01	100.01	100.01	100.01	100.01	100.02	100.00	100.01	100.01	100.00	99.99
mol% an (plagioclase)	46.4	46.4	42.4	58.1	53.7	46.1	44.2	44.9	44.6	65.6	43.8	45.4	58.9	67.8	43.8	56.3	58.2	49.4
RITTMANN NORMS (vol.%)																		
Quartz	-	0.5	-	4.2	-	-	-	-	-	7.3	-	-	-	-	-	-	-	-
Sanidine	2.3	-	0.5	-	1.7	1.6	-	-	-	4.9	3.1	-	8.1	16.7	0.6	-	1.9	1.8
Plagioclase	55.6	56.8	56.5	54.5	56.3	55.8	58.2	57.6	57.3	50.8	55.5	57.7	36.9	33.3	58.8	61.9	47.6	52.7
Nepheline	-	-	-	-	-	-	-	-	-	-	-	-	6.1	5.9	-	-	0.9	-
Clinopyroxene	37.5(P)	39.1(P)	26.5(S)	38.0(P)	35.2(P)	33.1(P)	35.9(P)	36.4(P)	36.2(P)	33.2(P)	34.2(P)	34.8(S)	25.8(D)	25.7(D)	31.4(S)	26.7(P)	21.2(D)	32.4(S)
Olivine	0.8	-	12.3	-	3.1	5.3	2.3	2.4	2.9	-	3.7	4.0	18.4	13.2	5.4	7.6	23.4	8.8
Magnetite	1.4	1.5	1.8	1.2	1.6	1.7	1.6	1.6	1.6	1.4	1.6	1.6	1.9	1.7	1.8	1.6	1.5	1.6
Ilmenite	1.6	1.6	1.7	1.6	1.7	1.8	1.5	1.5	1.5	1.9	1.4	1.4	1.6	1.9	1.4	1.6	2.0	1.9
Apatite	0.7	0.6	0.7	0.5	0.5	0.7	0.5	0.5	0.5	0.5	0.5	0.4	1.2	1.6	0.6	0.6	1.6	0.8
Total	99.9	100.1	100.0	100.0	100.1	100.0	100.00	100.00	100.0	100.0	100.0	99.9	100.0	100.0	100.0	100.0	100.1	100.0

Table B2
CHEMICAL ANALYSES OF TERTIARY BASALTS (continued)

Hole No.	SBDP10			
Depth (m)	39.5	128.3	152.7	201.5
Analysis No.	874885	874886	874887	874888
Plot No.	82	83	84	85
SiO_2	48.80	48.96	46.95	48.88
TiO_2	1.70	1.77	1.70	1.78
Al_2O_3	13.89	13.24	12.85	13.19
Fe_2O_3	2.39	3.29	2.95	3.41
FeO	9.70	7.95	8.62	8.82
MnO	0.16	0.15	0.16	0.16
MgO	8.73	8.55	9.55	8.73
CaO	8.55	7.79	8.40	8.08
Na_2O	3.34	2.68	2.57	2.89
K_2O	0.72	1.19	1.10	1.10
P_2O_5	0.30	0.32	0.29	0.35
H_2O^+	1.70	3.08	3.48	2.72
CO_2	0.19	0.16	0.96	0.23
Total S	<0.05	<0.05	<0.05	<0.05
Total	100.17	99.13	99.58	100.34
$100Mg/Mg+Fe^{II}$	59.8	61.3	63.1	59.8
Chemical Type	R	R	R	R
Trace elements (ppm)				
Sc	24	21	17	22
V	185	180	185	200
Cr	340	330	340	340
Co	53	46	55	48
Ni	185	185	260	200
Cu	63	62	59	65
Zn	125	110	100	94
Ga	17	16	16	16
As	<10	<10	<10	14
Rb	13	25	19	20
Sr	360	330	330	390
Y	23	24	22	22
Zr	130	150	135	135
Nb	15	25	23	28
Mo	3	4	2	3
Ag	<3	<3	<3	<3
Sn	<4	<4	<4	<4
Ba	130	185	185	350
La	11	14	11	14
Ce	55	76	72	70
Nd	13	19	19	13
Ta	<7	<7	<7	<7
W	15	12	16	15
Pb	<4	<4	<4	<4
Bi	5	6	<5	<5
Th	<4	<4	<4	<4
U	6	<5	8	5

Analyses by Department of Mines Laboratories, Launceston
Analysts: R. Roby, M. Frith

Table B3
CIPW AND RITTMANN NORMS OF TERTIARY BASALTS (continued)

Hole No.	SBDP10			
Depth (m)	39.5	128.3	152.7	201.5
Analysis No.	874885	874886	874887	874888
CIPW NORMS (mass%)				
or	4.30	7.38	6.85	6.67
ab	28.80	23.65	22.89	25.17
an	21.17	21.52	21.35	20.34
ne	-	-	-	-
di	16.36	13.62	16.70	15.19
hy	4.81	20.13	8.84	13.30
ol	18.23	7.24	16.98	12.67
mt	2.32	2.19	2.28	2.35
il	3.28	3.50	3.39	3.47
ap	0.73	0.78	0.73	0.85
Total	100.00	100.01	100.01	100.01
mol% an (plagioclase)	40.9	46.2	46.8	43.2
RITTMANN NORMS (vol.%)				
Quartz	-	-	-	-
Sanidine	-	6.1	5.8	5.2
Plagioclase	5.92	51.6	49.9	52.1
Nepheline	-	-	-	-
Clinopyroxene	25.3(S)	34.7(P)	29.3(S)	31.1(S)
Olivine	11.4	3.5	11.0	7.4
Magnetite	1.9	1.6	1.7	1.8
Ilmenite	1.6	1.8	1.6	1.7
Apatite	0.7	0.7	0.7	0.8
Total	100.1	100.0	100.0	100.1

and VP28 is similar but with more strongly coloured, pinkish and therefore more titaniferous, augite. Sample V87 (80-33) from the Lockwood Creek area well to the west is a similar, more altered, titanaugite bearing variety, containing occasional glomerocrysts (≤5 mm) of titanaugite and minor olivine.

EV14 (fine, intergranular, with plagioclase microphenocrysts) [DQ043132]

In addition to embayed phenocrysts of olivine (≤4 mm) this sample also contains abundant narrowly oblong phenocrysts of plagioclase (≤1.5 mm) which grade down in size to the fine intergranular groundmass. The groundmass consists of plagioclase (typically 100-200 μm), colourless augite, minor olivine, alkali feldspar and opaques. Minor patches of brown to brown-green alteration may be derived from devitrified glass.

Sample EV34, from a completely different part of the quadrangle, is nearly identical. Similar olivine-plagioclase-phyric basalts were termed Waratah Type by Edwards (1950), but his group probably includes transitional to tholeiitic basalt as well.

EV25 (coarse, subophitic) [DQ043327] - Plate B8

No meaningful distinction between phenocrysts and groundmass can be made in this coarse, subophitic basalt. The rock consists of equant rounded olivine crystals (100-500 μm), pale to deep pink-purple titanaugite platelets (50 μm-1 mm) and plagioclase laths (typically 500 μm × 50 μm), with minor opaques (both ilmenite and titanomagnetite), possible interstitial alkali feldspar and, in places, black incipiently crystalline interstitial glass.

Sample V68 is a similar subophitic, titanaugite bearing rock, but is slightly finer and more altered. This type of basalt corresponds to the Deloraine type of Edwards (1950).

Transitional basalt

EV9 (very fine, intergranular) [CQ952175]

Common euhedral or sometimes embayed olivine phenocrysts (mostly 500 μm-1 mm) and glomerocrysts lie in a slightly altered, very fine intergranular groundmass in which plagioclase laths (mostly about 100 μm), tiny augite granules and opaques are resolvable. Some olivines are incipiently altered to iddingsite around their margins and there are a few amygdales (≤500 μm) filled with orange-brown limonite, but otherwise the rock is fairly fresh. Chemically, this rock has tholeiitic affinities.

Samples SBDP4/341.0 and 4/366.0 are texturally very similar very-fine to fine-grained basalts, but with more alkaline affinities. In addition to altered olivine phenocrysts, the latter contains rare, small (≤200 μm) euhedral augite phenocrysts and microphenocrysts. Samples SBDP5/81.4 and SBDP10/201.5 are also texturally similar.

EV6 (fine intergranular/intersertal) [DQ163154]

This rather fine-grained transitional basalt is somewhat unusual in containing small amounts (5%) of black glass in addition to augite and olivine granules interstitial to plagioclase laths (mostly ≤200 μm). Euhedral or embayed olivine phenocrysts (500 μm-1 mm) are common.

Samples SBDP5/173.3, WA1/221 and WA3/196 are similar, but lack glass (intergranular texture) and are more altered, the latter containing 10-15% secondary calcite in the groundmass.

Table B2
CHEMICAL ANALYSES OF TERTIARY BASALTS (continued)

Hole No.	WY2				WA2			WA3		WA1				WA6		WA4		
Depth (m)	137.5	175	218	272	113	154	186	163.5	196	96	144	179	221	150	197.5	105	140	197.5
Analysis No.	830770	830764	830765	830766	830767	830768	830769	830758	830759	830774	830773	830772	830771	830762	830763	870757	830755	830756
Plot No.	86	87	88	89	90	91	92	93	94	95	96	97	98	99	100	101	102	103
SiO_2	46.53	48.33	43.96	47.08	48.84	49.39	47.01	49.21	45.72	50.56	46.71	49.05	46.63	47.10	48.62	47.06	48.01	49.85
TiO_2	1.56	1.50	1.62	1.91	1.45	1.62	1.38	1.75	1.73	1.73	1.51	1.55	1.79	1.52	1.55	1.38	1.49	1.45
Al_2O_3	13.05	13.31	13.20	13.11	13.68	13.26	12.88	13.54	13.36	14.04	13.38	13.64	12.62	13.22	13.53	13.27	13.17	13.64
Fe_2O_3	3.43	1.68	0.79	1.65	2.54	1.00	0.68	2.98	1.09	1.23	4.15	3.42	3.05	3.31	3.14	3.28	3.76	1.77
FeO	7.51	8.72	10.38	8.87	7.94	9.79	9.59	7.45	10.21	9.37	6.65	6.75	7.84	7.77	7.79	7.85	6.49	8.43
MnO	0.15	0.17	0.16	0.16	0.15	0.15	0.15	0.13	0.16	0.15	0.20	0.16	0.15	0.14	0.14	0.16	0.13	0.14
MgO	8.55	6.88	9.26	10.84	7.65	7.50	6.48	7.39	7.47	7.80	7.65	6.47	8.86	9.50	8.47	9.81	8.77	7.74
CaO	8.62	9.94	7.97	8.41	8.81	8.92	8.91	8.57	9.07	8.86	8.17	9.32	9.04	7.01	7.85	7.56	8.09	8.59
Na_2O	1.91	2.15	2.13	2.44	2.26	2.51	2.11	2.65	2.96	2.86	2.03	2.56	2.49	1.83	2.53	1.85	2.10	2.76
K_2O	0.36	0.30	0.97	1.29	0.17	0.82	0.47	1.11	0.83	0.98	0.77	0.33	1.06	0.72	0.86	0.39	0.34	0.57
P_2O_5	0.26	0.23	0.32	0.44	0.20	0.25	0.19	0.32	0.38	0.31	0.30	0.29	0.38	0.25	0.40	0.24	0.25	0.28
H_2O^+	3.54	2.14	2.11	2.36	2.17	1.26	1.57	2.16	1.11	0.94	3.63	2.14	3.03	4.49	3.17	3.53	3.22	1.88
H_2O^-	3.81	1.50	1.30	0.78	3.24	0.91	0.50	1.39	0.23	0.68	3.29	2.95	1.17	2.24	1.32	2.59	3.18	1.45
CO_2	0.20	2.70	2.38	0.21	0.11	1.59	7.16	1.03	5.32	0.07	0.70	0.73	1.05	0.15	0.23	0.18	0.17	0.87
SO_3	<0.05	1.05	4.03	0.17	<0.05	<0.05	<0.05	0.07	0.14	0.09	<0.05	<0.05	<0.05	0.18	<0.05	0.07	0.10	0.11
Total	99.36	100.60	100.58	99.72	99.21	98.97	99.08	99.75	99.78	99.67	99.14	99.36	99.16	99.43	99.60	99.22	99.27	99.53
100Mg/Mg+Fe	62.0	57.6	62.8	67.9	60.2	58.7	56.2	59.6	57.5	60.1	59.8	57.1	62.9	64.1	61.7	64.8	64.2	61.0
Chemical type	Q	Q	R	R	Q	Q	Q	T	R	T	Q	Q	R	Q	T	Q	Q	Q
Trace elements (ppm)																		
Sc	17	18	15	18	18	19	18	16	18	19	16	18	15	13	18	16	17	17
V	150	130	140	160	130	145	130	145	140	150	135	135	155	125	140	130	125	130
Cr	230	210	230	270	240	230	230	250	210	260	250	230	270	210	240	240	230	250
Co	47	43	46	49	38	46	39	39	46	43	41	43	42	43	45	47	38	40
Ni	200	155	190	210	160	155	155	115	175	115	160	125	230	165	180	190	140	145
Cu	44	41	40	39	47	43	38	29	51	36	29	36	43	40	47	25	54	38
Zn	110	115	110	100	110	115	105	105	125	105	105	105	99	115	115	110	110	110
As	>10	>10	>10	>10	>10	>10	>10	>10	>10	>10	>10	>10	>10	>10	>10	>10	>10	>10
Rb	11	12	16	26	7	20	15	25	13	22	21	10	25	20	19	12	10	21
Sr	260	270	570	470	250	280	230	370	420	360	280	350	470	240	350	250	330	340
Y	20	18	18	20	19	21	17	17	19	19	20	19	19	17	20	16	20	19
Zr	96	87	110	145	84	105	80	125	105	120	100	92	120	92	110	93	95	96
Nb	9	6	14	29	4	9	4	15	13	14	13	12	25	11	17	8	13	13
Ba	120	83	105	220	60	110	105	200	180	180	125	105	280	115	180	110	145	160
Pb	<4	<4	<4	<4	<4	<4	<4	<4	5	<4	<4	<4	<4	<4	<4	10	23	15

Analyses by Department of Mines Analytical Laboratories, Launceston
Analyst: J. Furst

Table B3
CIPW AND RITTMANN NORMS OF TERTIARY BASALTS (continued)

Hole No.	WY2				WA2			WA3		WA1				WA6		WA4		
Depth (m)	137.5	175	218	272	113	154	186	163.5	196	96	144	179	221	150	197.5	105	140	197.5
Analysis No.	870770	870764	870765	870766	870767	870768	870769	870758	870759	830774	830773	830772	830771	830762	830763	870757	830755	830756
CIPW NORMS (mass%)																		
Q	1.28	2.68	-	-	2.84	0.15	2.96	-	-	-	0.66	2.80	-	0.49	-	0.15	1.96	0.38
or	2.31	1.89	6.31	7.91	1.06	5.07	3.07	6.91	5.25	5.90	5.01	2.07	6.67	4.60	5.37	2.48	2.19	3.54
ab	16.55	19.51	19.84	21.46	20.45	22.31	19.85	23.65	26.94	24.75	18.84	23.24	22.47	16.82	22.64	16.90	19.26	24.50
an	28.94	27.70	25.97	21.85	28.52	23.61	27.04	22.91	22.28	23.04	27.52	26.51	21.47	27.91	24.29	28.87	27.59	24.33
ne	-	-	-	-	-	-	-	-	-	-	-	-	-	-	-	-	-	-
di	12.96	19.35	12.45	14.99	13.76	17.32	17.05	16.06	19.22	16.13	12.07	17.24	19.29	6.57	11.49	8.06	11.45	15.16
hy	31.84	23.13	12.13	7.96	27.85	25.54	24.45	22.19	1.92	20.07	29.80	22.26	10.06	37.62	26.80	37.38	31.79	26.49
ol	-	-	16.74	18.92	-	-	-	1.94	17.59	3.94	-	-	13.29	-	3.17	-	-	-
mt	2.22	2.10	2.35	2.06	2.10	2.16	2.17	2.04	2.31	2.06	2.19	2.02	2.16	2.23	2.15	2.23	2.06	2.02
il	3.24	3.06	3.39	3.77	2.94	3.23	2.92	3.50	3.52	3.35	3.14	3.15	3.62	3.13	3.10	2.83	3.07	2.91
ap	0.66	0.59	0.83	1.09	0.50	0.61	0.50	0.80	0.97	0.75	0.78	0.73	0.97	0.64	0.99	0.61	0.64	0.68
Total	100.00	100.01	100.01	100.01	100.02	100.00	100.01	100.00	100.00	99.99	100.01	100.02	100.00	100.01	100.00	100.01	100.01	100.01
mol% an (plagioclase)	62.2	57.2	55.2	49.0	56.8	49.9	5 6.2	47.7	43.8	46.7	57.9	51.8	47.4	61.0	50.3	61.7	57.5	48.3
RITTMANN NORMS (vol. %)																		
Quartz	2.1	4.1	-	-	4.0	1.4	4.4	0.4	-	-	1.6	4.2	-	1.1	-	0.7	2.9	1.6
Sanidine	-	-	4.4	7.8	-	1.7	-	5.1	1.7	3.1	1.6	-	5.4	1.1	2.1	-	-	-
Plagioclase	52.4	53.3	52.9	48.0	54.6	53.9	54.4	53.2	57.4	55.4	54.8	56.2	49.5	53.4	55.4	53.3	53.6	57.0
Nepheline	-	-	-	-	-	-	-	-	-	-	-	-	-	-	-	-	-	-
Clinopyroxene	41.7(P)	39.3(S)	26.9(S)	26.6(S)	38.1(P)	39.3(P)	37.9(P)	37.3(P)	25.9(A)	36.9(P)	38.2(P)	36.0(P)	33.1(S)	40.6(P)	37.9(P)	42.5(P)	39.9(P)	37.9(P)
Olivine	-	-	11.6	13.2	-	-	-	-	10.7	0.7	-	-	7.9	-	0.6	-	-	-
Magnetite	1.3	1.4	1.7	1.5	1.3	1.5	1.4	1.5	1.8	1.5	1.5	1.4	1.6	1.4	1.5	1.4	1.3	1.5
Ilmenite	1.7	1.5	1.8	1.9	1.5	1.6	1.5	1.7	1.6	1.6	1.7	1.6	1.7	1.8	1.6	1.6	1.7	1.5
Apatite	0.6	0.5	0.8	1.0	0.5	0.6	0.5	0.7	0.9	0.7	0.7	0.7	0.9	0.6	0.9	0.6	0.6	0.6
Total	99.8	100.1	100.1	100.0	100.0	100.0	100.1	99.9	100.0	99.9	100.1	100.1	100.1	100.0	100.0	100.1	100.0	100.1

Table B4
SUMMARY OF PETROGRAPHY

Sample	Chemistry Type*	Mg No.	Phenocrysts	Groundmass Grain size†	Texture	Flow lamination	Alteration and comments
EV1	B	66.3	*olivine*, ≤500 μm, rarely ≤2 mm, usually anhedral *augite*, rare, anhedral *spinel lherzolite* nodules present	vf	almost glassy, no plagioclase, augite microlites	strong to none	slightly altered
EV2	A	67.2	*olivine* abundant, ≤3 mm, to groundmass	mc	intergranular, titanaugite present	none	very fresh, similar to EV4
EV3	R	69.8	*olivine* abundant, ≤3 mm, *plagioclase* ≤1.5 mm, grading to groundmass	c	intergranular	none	slightly altered
EV4	A	66.5	*olivine* abundant, ≤1 mm, often in glomerocrysts *quartz xenocrysts*, polycrystalline, reaction coronas	mc	intergranular	moderate	fresh
EV5	AA	67.4	*olivine* abundant, ≤1 mm, euhedral *titanaugite* sparse, equant granules ≤250 μm *quartz xenocryst* 500 μm with reaction corona	f	intergranular	strong	nearly fresh
EV6	R	60.3	*olivine* abundant, 500 μm-1 mm, resorbed to euhedral	f	intergranular/ intersertal, about 5% black glass	none	slightly altered
EV7	AA	63.5	*olivine* abundant, ≤500 μm, euhedral to anhedral, *plagioclase* rare, oblongs ≤2 mm, corroded, xenocrystal ?	vf	intergranular, almost glassy	none	fresh; some zeolite amygdales
EV8	R	58.8	*olivine* abundant, ≤3 mm, embayed or euhedral	m	ophitic, titaniferous augite present	none	moderately altered
EV9	R	60.6	*olivine* common, 500 μm-1 mm, some embayed	vf	intergranular	none	slightly altered; sparse amygdales
EV10	R	59.2	*olivine* abundant, ≤3 mm plagioclase laths ≤2 mm, grading to groundmass	mc	intergranular	none	very fresh
EV11	AA	54.3	*olivine* rare, small (≤500 μm) *plagioclase* rare, anhedral, ≤500 μm *quartz xenocrysts* very rare, with reaction coronas	f	intergranular	strong	slightly altered; elongate calcite amygdales
EV12	T	57.0	none	m	intergranular, minor (?) glass	strong	minor inter stitial brown limonitic alteration (? of glass)
EV13	T	61.9	*olivine* common, ≤2 mm, often deeply embayed	m	intersertal/ intergranular	none	fresh
EV14	A	59.2	*olivine* abundant, ≤4 mm, embayed *plagioclase* ≤1.5 mm, grading to groundmass	f	intergranular	weak	fresh, similar to EV34
EV15	T	59.3	*olivine* rather sparse and small, mostly ≤ 1 mm, mostly fresh	m	subophitic/ intergranular	none	interstitial amber coloured altered (?) glass
EV16	T	59.8	*olivine* abundant, 500 μm-2 mm, embayed *plagioclase* oblongs ≤1 mm, grading to groundmass	f	intergranular, very minor (?) glass	none	fresh; rare pale brown altered (?) glass
EV17	T	62.9	*olivine* rather sparse and small, ≤1 mm, well rounded	m	subophitic, about 5% altered brown (?) glass	none	moderately altered
EV18	T	57.3	*olivine* rather sparse, 500 μm- 2 mm, embayed, partly altered	f	intergranular	strong	moderately altered
EV19	R	55.9	*olivine* sparse, ≤2.5 mm *plagioclase* laths ≤2 mm, grading to groundmass *orthopyroxene-augite-olivine* glomerocrysts ≤5 mm	m	intergranular	weak	moderately altered
EV20	R	59.1	*olivine* abundant, small ≤500 μm *plagioclase* laths 500 μm-2 mm, grading to groundmass, *orthopyroxene augite-olivine* glomerocrysts ≤4 mm	m	intergranular	none	fresh
EV21	T	60.1	*olivine* sparse, ≤2 mm, euhedral to deeply embayed	f	intergranular	moderate	nearly fresh, similar to EV18

Table B4
SUMMARY OF PETROGRAPHY (continued)

Sample	Chemistry Type*	Mg No.	Phenocrysts	Groundmass Grain size†	Texture	Flow lamination	Alteration and comments
EV22	T	62.2	*olivine* common, 500 μm-1 mm, embayed partly altered	f	intergranular/ intersertal, minor brown altered glass	none	moderately altered
EV23	T	60.6	*olivine* abundant, small (500 μm-1 mm) completely altered *augite* rare, euhedral, ≤1.5 mm, *orthopyroxene-augite* glomerocrysts ≤500 μm, rare	f	subophitic/ intergranular	none	moderately altered
EV24	A	58.0	*olivine* rare 1.5 mm, *plagioclase* rare anhedral, 500 μm, xenocrystal ?	mf	intergranular	strong	patchy alteration
EV25	A	65.2	none	c	subophitic, titanaugite present	none	very fresh
EV26	AA	60.3	*olivine* abundant, 500 μm-2 mm, often glomerocrystal	mf	intergranular	none	very fresh, but zeolites present
EV27	R	62.1	*olivine* abundant, 500 μm-1 mm, *plagioclase* laths ≤2 mm, grading to groundmass *augite-olivine* glomerocrysts ≤1 mm	mc	inergranular	none	slightly altered
EV28	A	63.5	*olivine* common, ≤1 mm	vf	intergranular	none	moderate alteration
EV29	T	59.7	*olivine* sparse, 500 μm-1 mm	m	subophitic, about 5% interstitial black glass	none	slightly altered
EV30	T	62.0	*olivine* abundant, ≤3 mm, typically 500 μm-1 mm embayed to skeletal	c	intersertal, about 30% black glass	none	slight patchy alteration of olivine and glass
EV31	T	60.1	*olivine* common, 500 μm-2 mm, deeply embayed, sometimes glomerocrystal	mf	intergranular, minor interstital (?)glass	none	slightly altered, brown (?) altered glass
EV32	T	59.0	*olivine* rather sparse, 500 μm-1 mm, almost completely altered, *plagioclase* common, oblong, 1-1.5 mm	f	intergranular	moderate	moderately altered
EV33	R	65.4	*olivine* common ≤500 μm	mf	intergranular, titanaugite present	none	slightly altered
EV34	A	58.9	*olivine* abundant, ≤3 mm, often embayed, *plagioclase* laths, ≤1 mm, grading to groundmass, *augite* ≤500 μm sparse, often glomerocrystal	f	intergranular	moderate	fresh, zeolite amygdales present, resembles EV14
EV35	T	63.4	*olivine* common, ≤2.5 mm, deeply embayed, sometimes glomerocrystal	mf	intergranular, minor interstitial (?)glass	none	slightly altered, brown (?) altered glass
EV36	T	60.9	*olivine* rather sparse, small 200 μm-500 μm, embayed, mostly altered	f	intergranular, minor interstitial (?) glass	weak	moderately altered; brown (?) altered glass
EV37	T	64.7	*olivine* rather sparse, ≤4 mm, usually 500 μm-2 mm, mostly altered	mc	intergranular	none	abundant interstitial brown limonitic alteration
EV38	T	64.0	*olivine* abundant, ≤2 mm, often deeply embayed, a few altered	m	intergranular	weak	slightly altered, some small limonitic amygdales
EV39	T	63.6	*olivine* common ≤1 mm, mostly altered	f	subophitic	strong	moderately altered
V1 (80-1)			*olivine* common ≤1.5 mm, *plagioclase* oblongs up to 2 mm × 400 μm, common	mf	intergranular/ intersertal, minor green glass	none	slightly altered
V2 (80-2)			*olivine* common, ≤1 mm, often deeply embayed	mf	intersertal, about 40% black glass	none	moderately altered
V3 (80-3)			*olivine* common, 500 μm-1.5 mm, *plagioclase* laths common, ≤1 mm, grading to groundmass	m	intergranular	weak	moderately altered
V4 (80-4)			*olivine* common, ≤1 mm, mostly altered	f	intersertal/ intergranular	none	moderately altered
V6 (80-5)			*augite* ≤1 mm, often glomerocrystal, *plagioclase* ≤3 mm, grading to groundmass	c	intergranular	none	slightly altered
V7 (80-6)			*olivine* abundant, small (mostly ≤50 μm) glomerocrysts ≤4 mm corroded, *granular olivine xenocryst*	vf	intergranular, almost glassy	none	identical to EV7 (same locality)

Table B4
SUMMARY OF PETROGRAPHY (continued)

Sample	Chemistry Type*	Mg No.	Phenocrysts	Groundmass Grain size†	Texture	Flow lamination	Alteration and comments
V12(80-7)			*olivine* common, ≤1-4 mm, almost completely altered	m	intergranular/ intersertal	none	strongly altered
V13(80-8)			*olivine* sparse, 500 μm-1.5 mm completely altered	m	ophitic	none	strongly altere
V30(80-13)			none	m	intersertal, about 40% black glass; resorbed olivine	none	fresh; amygdales of calcite and chlorite
V31(80-14)			*olivine* sparse, ≤1.5 mm, embayed *augite* rare, ≤500 μm	vf	intergranular	weak	moderately altered
V32(80-15)			*olivine* sparse, ≤1 mm, embayed often altered	mf	intergranular/ intersertal	none	moderately altered
V37(80-18)			*olivine* common, 500 μm-1 mm, embayed	m	subophitic/ intersertal, about 20% glass	none	slightly altered
V40(80-19)			*olivine* common, 500 μm-1 mm, embayed	c	intersertal, about 40% glass, resorbed olivine	none	sparse alteration of olivine
V45(80-22)			none	f	intergranular	strong	slightly altered
V55(80-23)			*olivine* common, 500 μm-1 mm	m	intersertal, about 25% glass	none	slightly altered
V62(80-26)			*olivine* rare, small, ≤500 μm, sometimes glomerocrystal	f	intergranular	none	slightly altered similar to EV11
V85(80-31)			*olivine* common, 500 ≤-1 mm, *plagioclase* common, ≤1 mm	mf	intergranular	weak	slightly altered, similar to V1
V86(80-32)			*olivine* sparse, ≤500 μm, partly altered	mf	intergranular/ subophitic, minor black glass	none	moderately altered
V87(80-33)			*olivine* abundant, 500 μm-1 mm *titanaugite* sparse 500 μm-1 mm, often glomerocrystal	c	intergranular, titanaugite present	none	moderately altered alkali basalt
VA8	T	61.4	*olivine* common, ≤2 mm *orthopyroxene-augite-olivine* glomerocrysts ≤3 mm *plagioclase* laths ≤1 mm, grading to groundmass	c	intergranular	none	moderately altered, similar to EV27
VP1(VA23)	AA	58.5	*olivine* rare, small, ≤500 μm	vf	intergranular	weak	fresh; similar to EV1
VP8			*olivine* ≤1 mm, grading to groundmass	mc	subophitic, titan- augite present	none	slightly altered, similar to EV25
VP18,VP19			*olivine* ≤1 mm, usually anhedral, *spinel lherzolite* nodules present	vf	almost glassy, no plagioclase, augite microlites	strong to none	very similar to EV11 (same locality)
VP26			*olivine* 500 μm-1 mm, euhedral	m	intergranular/ intersertal, pink glass(?)	none	fresh(?); poor slide
VP28			*olivine* abundant, 500 μm-1 mm	m	intergranular	none	slightly altered, similar to EV2,EV4
VP 64			*olivine* abundant, 500 μm-1 mm	f	intergranular/ intersertal, almost glassy	moderate	fresh; very similar to EV5
PV 7			*olivine* sparse, ≤1 mm, *augite- olivine* glomerocrysts ≤2 mm, *plagioclase* laths ≤1 mm, grading to groundmass	f	intergranular	none	slightly altered
PV 8			*olivine* sparse, ≤1 mm, partly altered	f	intergranular to finely subophitic	strong	moderately altered, similar to EV18
PV 9			*olivine* sparse, 500-200 μm, embayed, mostly altered	f	intergranular	moderate	moderately altered, similar to EV18
PV10			*olivine* common, ≤2 mm, sometimes embayed	m	intergranular	none	moderately altered, interstital limonite, similar to EV38
PV17			*olivine* common, 500 μm-1.5 mm	mf	intersertal, about 20% black glass	none	fairly fresh; some interstitial limonite

Table B4
SUMMARY OF PETROGRAPHY (continued)

Sample	Chemistry Type*	Mg No.	Phenocrysts	Groundmass Grain size†	Texture	Flow lamination	Alteration and comments
PV30			*plagioclase* common, oblong, ≤6 mm *augite* sparse, ≤500 μm, euhedral	vf	glassy, sparse plagioclase laths	weak	strongly altered, amygdaloidal groundmass
PV41			*augite* abundant, ≤1 mm, euhedral, grading to groundmass, *olivine* sparse, ≤1 mm, euhedral, grading to groundmass	vf	glassy, augite granules, plagioclase microlites	none	fresh; zeolite and calcite amygdales present
PV74			*olivine* abundant, 500 μm-2 mm, *augite* microphenocrysts rare, ≤200 μm	vf	intergranular/ intersertal	moderate	slightly altered; very similar to EV5
WA46			*olivine* common, 500 μm-1 mm euhedral	f	intersertal, about 40% black glass	none	fresh; similar to SBDP5/ 237.0
HR17			*titanaugite* abundant, ≤2 mm, grading to groundmass, *olivine* sparse, ≤500 μm	vc	intergranular	none	slightly altered
GV33			*olivine* abundant, 500 ≤-3 mm, euhedral *augite* rare, ≤500 μm, euhedral	f	intersertal to glassy	strong	slightly altered, round amygdales present
SBDP1/125.3	Q	61.4	*olivine* common 500 μm-1 mm, completely altered	m	intergranular	none	strongly altered
171.4	T	63.0	*olivine* common, 500 μm-2 mm, largely altered	mc	subophitic	none	very altered
224.5	Q	60.6	*olivine* sparse, 500 μm-1 mm, completely altered	mf	ophitic	none	very altered; abundant goethitic amygdales
245.6	R	63.5	*olivine* common, 500 μm-1 mm, *plagioclase* laths ≤700 μm, grading to groundmass	m	intergranular	none	moderately altered
SBDP2/101.5	Q	55.2	*olivine* sparse, ≤1.5 mm, mostly altered *plagioclase* xenocryst, 2 mm	mf	subophitic/ intergranular	none	moderately altered
145.0	Q	56.4	*olivine* common, 1-4 mm, embayed, almost completely altered	m	ophitic	none	strongly altered, abundant interstitial alteration
190.0	R	58.5	*olivine* common, 500 μm-2 mm altered, *augite* 300 μm-1 mm, clumped in groundmass, *plagioclase* oblongs 500 μm-1.5 mm	mf	intergranular	none	altered
238.0	A	62.4	*olivine* abundant, ≤3 mm, often deeply embayed	vf	intergranular	none	slight alteration
282.0	R	57.4	none	c	equigranular-consertal	none	moderately altered
293.0	R	52.9	none	c	equigranular- consertal	none	moderately altered
SBDP4/107.9	T	61.4	*olivine* common 1-3 mm, completely altered *plagioclase* ≤500 μm, sparse	f	intergranular	none	strongly altered
129.1	Q	59.8	*olivine* common, ≤1 mm, completely altered	m	subophitic/ ophitic	none	strongly altered; limonitic amygdales, calcite veinlets
160.9	T	59.6	*olivine* common 500 μm-1 mm, embayed; sometimes glomerocrystal, *plagioclase* rare, 500 μm-1.5 m oblong to irregular	f	subophitic	strong	slightly altered; flow elongated amygdales present
206.0	R	63.4	*olivine* common, 500 μm-2 mm, altered *augite* sparse, 100-500 μm, glomerocrystal with olivine, *plagioclase* rare, ≤ 500 μm	m	intergranular	moderate	altered
251.1	B	63.5	*olivine* common, ≤2.5 mm, completely altered	vf	altered, chloritic	none	similar to SBDP4/269.1, very altered
255.8	B	64.0	*olivine* common, ≤1.5 mm, subhedral to anhedral	vf	altered, chloritic	none	similar to SBDP4/269.1 partly altered
269.1	B	65.6	*olivine* common, ≤3 mm, usually anhedral, to euhedral	vf	olivine granules, augite microlites, no plagioclase	none	fairly fresh
341.0	R	65.2	*olivine* common, 500 μm-1.5 mm, partly altered	vf	intergranular	none	slightly altered

Table B4
SUMMARY OF PETROGRAPHY (continued)

Sample	Chemistry Type*	Mg No.	Phenocrysts	Groundmass Grain size†	Texture	Flow lamination	Alteration and comments
61.0	T	59.8	*olivine* common, 200 μm-1.5 mm, rounded, embayed, *plagioclase* phenocrysts rare, ≤0.5 mm	f	intergranular	none	moderately altered
81.4	R	61.7	*olivine* sparse, small, ≤500 μm, resorbed	vf	intergranular	none	slightly altered
116.7	Q	62.8	*olivine* (?)common, 500 μm-2 mm, completely altered	mc	subophitic	none	strongly altered; interstital limonitic material
159.3	T	62.3	*olivine* common 500 μm-2 mm, completely altered	c	intergranular	none	strongly altered
173.3	R	60.8	*olivine* common, 500 μm-2 mm, partly altered	f	intergranular	none	moderately altered
219.5	T	61.7	*olivine* common, 500 μm-1 mm, embayed to skeletal	m	subophitic, minor black glass	none	fresh but amygdaloidal, yellow brown isotopic filling
237.0	T	61.7	*olivine* common, ≤1 mm, euhedral to deeply embayed *black glassy fragments* (≤3 mm) with very fine plagioclase laths	f	intersertal, about 30% black glass	none	fresh but amygdaloidal, yellow brown isotropic filling
248.7	T	62.0	*olivine* common, 500 μm-2 mm, deeply embayed to skeletal	f	intersertal/ intergranular about 25% black glass	none	very fresh; sparse amygdales
280.8	Q	59.3	none	vf	glassy (hyalotuff)	none	very altered
SBDP6/75.8	T	61.5	*olivine* common, ≤3.5 mm, often deeply embayed	f	ophitic, with about 10% black glass	none	very fresh, but vesicular to amygdaloidal
108.0	T	60.5	*olivine* common, ≤3 mm, deeply embayed to skeletal	f	ophitic, with about 10% black glass	none	very fresh, but vesicular to amygdaloidal
177.0	AA	64.9	*olivine*, very abundant, typically 500 μm-1 mm	c	intersertal, about 30% black glass	none	fresh
202.8	AA	61.3	*olivine*, abundant, 500 μm-1.5 mm	f	glassy, sparse small (≤200 μm) plagioclase	none	zeolite amygdales, calcite veinlets
SBDP9/115.5	T	59.4	*olivine* rather sparse, 500 μm-2 mm partly altered	mf	ophitic	none	much green brown alteration; carbonate veinlets
129.0	T	61.4	*olivine* common, 500 μm-1 mm, largely altered	f	ophitic	none	moderately altered
213.3	A	69.3	*olivine* abundant, ≤1 mm, euhedral	vf	intergranular, very fine mesostasis	moderate	fresh
237.6	R	64.1	*olivine* common, 1-3 mm, partly altered	mc	intergranular/ intersertal, minor black glass	none	moderately altered
SBDP10/39.5	R	59.8	*olivine* common, ≤3 mm, embayed	m	intergranular	weak	fresh
128.3	R	61.3	*olivine* abundant, ≤2 mm, largely altered	m	intergranular	none	altered
152.7	R	63.1	*olivine* abundant ≤2 mm, partly altered	mc	intergranular	none	moderately altered
201.5	R	59.8	*olivine* sparse, small mostly ≤500 μm, resorbed	vf	intergranular	none	slightly altered
WY2/137.5	Q	62.0	*olivine* (?), sparse, small, completely altered	f	intergranular	none	strongly altered
175	Q	57.6	none	m	subophitic	none	abundant, irregular limonitic amygdales
218	R	62.8	*olivine* common, 500 μm-1 mm, partly altered	m	ophitic, titaniferous augite present	none	moderately altered
272	R	67.9	*olivine* common, 500 μm-2 mm, partly altered	mc	intergranular, titanaugite present	none	moderately altered
WA2/113	Q	60.2	*olivine* (?) sparse, ≤1 mm, completely altered	m	subophitic/ intergranular	none	strongly altered, abundant irregular limonitic amygdales
154	Q	58.7	*olivine* common, 500 μm-2 mm, embayed to skeletal	f	ophitic	none	fresh; sparse amygdales, often with calcite
186	Q	56.2	none	mf	intergranular/ subophitic	none	abundant (15%) carbonate in groundmass

Table B4
SUMMARY OF PETROGRAPHY (continued)

Sample	Chemistry Type*	Mg No.	Phenocrysts	Groundmass Grain size†	Texture	Flow lamination	Alteration and comments
WA3/163.5	T	59.6	*olivine* abundant, ≤5 mm, typically 500 μm-2 mm, often embayed	c	intergranular	none	moderately altered; calcite veinlets present
196	R	57.5	*olivine* common, 500 μm-1 mm	f	intergranular	weak	10-15% secondary calcite in groundmass
WA1/96	T	60.1	*olivine* common, 1-2.5 mm, embayed to rarely skeletal	mc	intergranular, minor (2%) black glass	none	slightly altered; vesicular
144	Q	59.8	*olivine* abundant, 500 μm-2 mm, mostly altered	mf	subophitic	moderate	moderately altered
179	Q	57.1	*olivine* sparse, 500 μm-2 mm, embayed, completely altered	f	intergranular	weak	strongly altered; limonitic amygdales
221	R	62.9	*olivine* abundant, mostly ≤400 μm	f	intergranular	none	slightly altered
WA6/150	Q	64.1	none	mf	subophitic/ intergranular	none	strongly altered; abundant limonitic amygdales
197.5	T	61.7	*olivine* sparse, small 200 μm-1 mm, partly altered	vf	intergranular	strong	moderately altered; calcite veinlets present
WA4/105	Q	64.8	*olivine* sparse, 500 μm-1 mm, almost completely altered	m	subophitic/ ophitic	none	strongly altered; abundant limonitic amygdales
140	Q	64.2	*olivine* rare, ≤3 mm, usually completely altered	mc	subophitic	none	strongly altered; interstitial limonite, calcite
197.5	Q	61.0	*olivine* sparse, 500 μm-2 mm, embayed, partly altered	f	intergranular	weak	moderately altered; limonitic amygdales

* Q – quartz-normative tholeiite, T – olivine-normative tholeiite, R – transitional basalt, A – alkaline basalt, AA – strongly alkaline basalt, B – basanite (see text).

† vf – very fine (plagioclase laths typically ≤100 μm), f – fine (100-200 μm), m – medium (200-500 μm), c – coarse (>500 μm).

EV8 (medium-grained, ophitic) [DQ125186]

Abundant, partly iddingsitised, sometimes embayed or euhedral olivine phenocrysts (≤3 mm) lie in a medium-grained ophitic groundmass of plagioclase laths (200-400 μm), largely enclosed by pale pink titaniferous augite platelets that may be optically continuous for 2-3 mm. Opaque grains are usually elongate (150-400 μm) and probable interstitial alkali feldspar are also present.

Sample WY2/218 has a similar well-developed ophitic texture.

SBDP10/39.5 (medium-grained, intergranular).

Abundant, typically embayed or rarely skeletal phenocrysts of fresh olivine (≤3 mm, typically about 1 mm) lie in a weakly flow-laminated, medium-grained intergranular groundmass of plagioclase laths (200-400 μm), augite granules, opaques and alkali feldspar.

Similar medium-fine to medium-coarse intergranular textures are the most common texture of transitional basalt (e.g. samples EV3; SBDP10/128.3; SBDP10/152.7; SBDP9/237.6). Sample SBDP4/206.0 is slightly unusual in containing composite olivine-augite glomerocrysts and rare plagioclase microphenocrysts (≤500 μm) in addition to olivine phenocrysts. Samples EV33 and WY2/272, contain pinkish titanaugite (rather than colourless augite), consistent with the slightly alkaline affinities indicated by their chemistry.

EV20 (medium-grained, intergranular, with plagioclase) microphenocryst [CQ919074] - Plates B9, B10

This sample is a very fresh specimen of a characteristic olivine-plagioclase-phyric type of basalt, termed Waratah Type by Edwards (1950). It contains abundant but small (≤500 μm), generally euhedral olivine phenocrysts (Fo_{71-79}) and lath-like microphenocrysts (500 μm-2 mm) of plagioclase (An_{63-65}), both of which grade in size down to the intergranular groundmass of plagioclase (An_{55-58}), augite, olivine (Fo_{66-73}), opaques and interstitial purplish isotropic glass.

A notable feature is the presence of rounded to ellipsoidal orthopyroxene-augite-olivine glomerocrysts up to 4 mm across. Usually they contain at their core a single anhedral or subhedral grain of orthopyroxene (En_{82-85}). In some glomerocrysts, the surrounding augite is a single, optically continuous, but twinned crystal, with a few olivine inclusions and a mottled sieve-texture suggesting incipient melting. In others, the outer zone is a polycrystalline anhedral-granular aggregate of equant (typically 200 μm) olivine, augite and sometimes elongate plagioclase laths. The orthopyroxene cores probably represent a high-pressure phenocryst phase, which on ascent of the magma has reacted with the melt to form the augite-olivine outer zone.

Samples EV10, EV19, EV27, SBDP2/190.0, V3 and V85 are similar olivine-plagioclase-phyric basalts, differing somewhat in grain size and degree of alteration. Samples SBDP1/245.6, V1 and PV7 contain minor green glass or devitrified glass. Not all of the above thin sections contain orthopyroxene-augite-olivine glomerocrysts.

SBDP2/293.0 (coarse, equigranular-consertal) - Plate B11

This coarse equigranular feldspar-rich rock is unusual in totally lacking olivine. It consists of interlocking subhedral crystals of plagioclase, (500 μm-1.5 mm), alkali feldspar and pinkish titaniferous augite, with also common equant, angular opaques (50-100 μm) including both ilmenite and titanomagnetite, and minor very fine acicular apatite. Augite is partly altered to a fine brown aggregate.

Sample SBDP2/282.0, from the same interval of core, is a similar olivine-free, feldspar-rich rock, also with a coarse, interlocking (consertal) texture.

Tholeiite

SBDP5/237.0 (fine, intersertal)

This fine, intersertal basalt contains about 10% olivine phenocrysts, including equant, polygonal euhedra (≤1 mm) and slightly to deeply

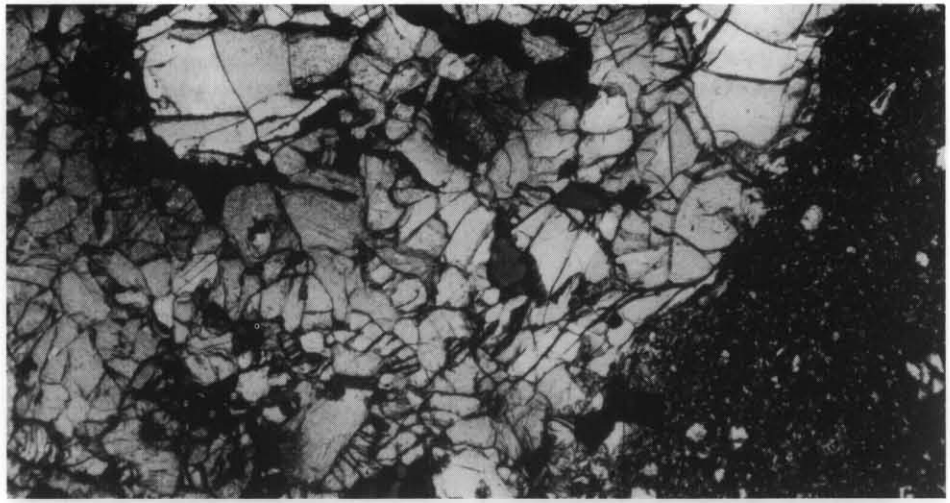

Plate B1. Sample EV1 Basanite. Part of a granoblastic spinel-lherzolite nodule, within a very fine groundmass. Plane polarised light, field of view 4.3 × 2.3 mm.

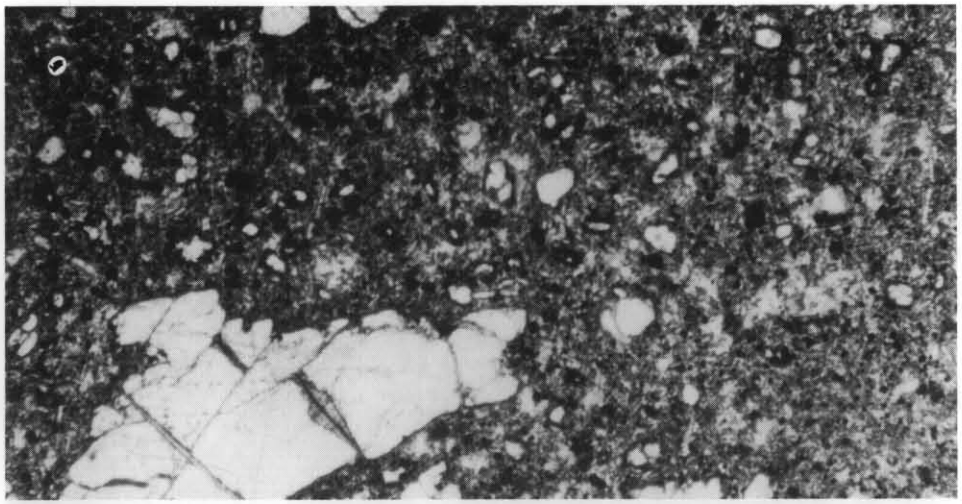

Plate B2. Sample SBDP4/269.1 Basanite showing an embayed, anhedral olivine phenocryst and smaller olivine granules within a very fine groundmass. Plane polarised light, field of view 4.3 × 2.3 mm.

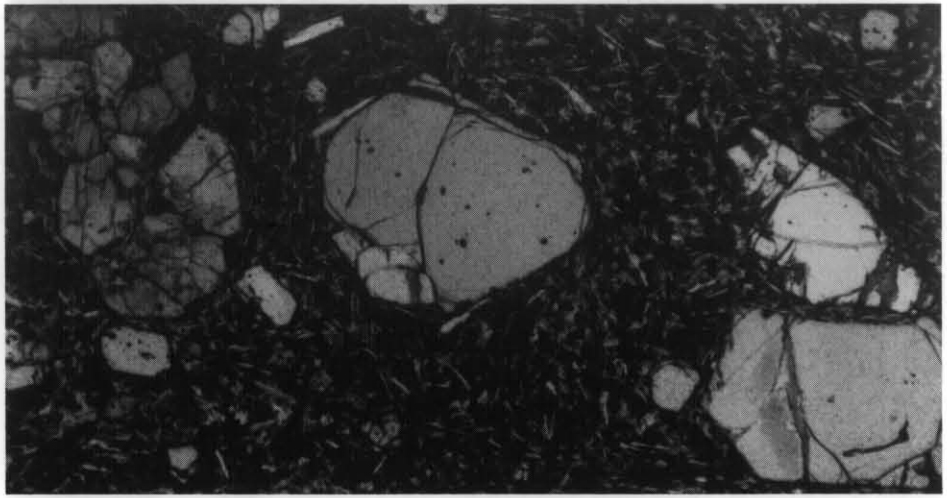

Plate B3. Sample EV5. Strongly alkaline basalt showing a euhedral olivine phenocryst (centre) and a titanaugite glomerocryst (left) within a fine intergranular groundmass. Plane polarised light, field of view 4.3 × 2.3 mm.

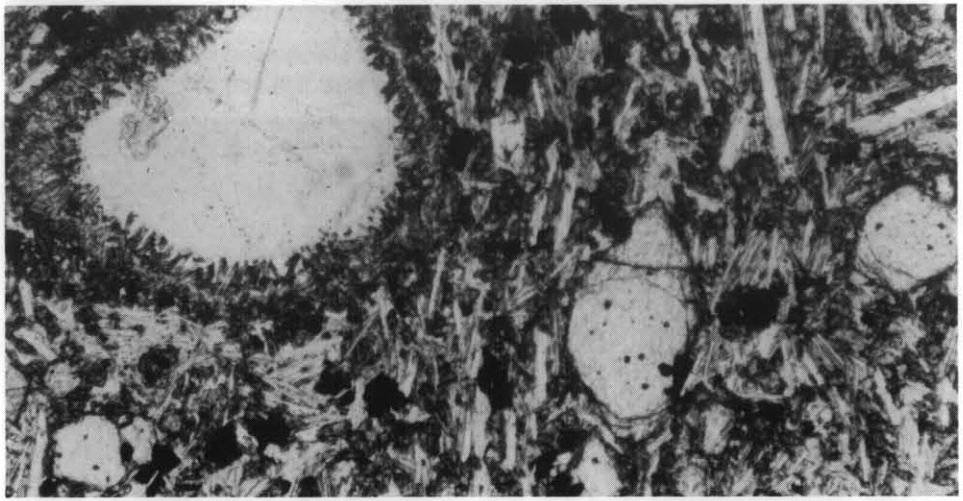

Plate B4. Sample EV5. Close up of groundmass; also showing an embayed quartz xenocryst with a reaction corona of ?clinopyroxene. Plane polarised light, field of view 1.7 × 0.9 mm.

5 cm

Plate B5. Sample SBDP6/177.0. Strongly alkaline basalt consisting mainly of olivine phenocrysts (colourless), plagioclase laths, titanaugite granules (grey) and black glass. Coarse intersertal texture. Plane polarised light, field of view 4.3 × 2.3 mm.

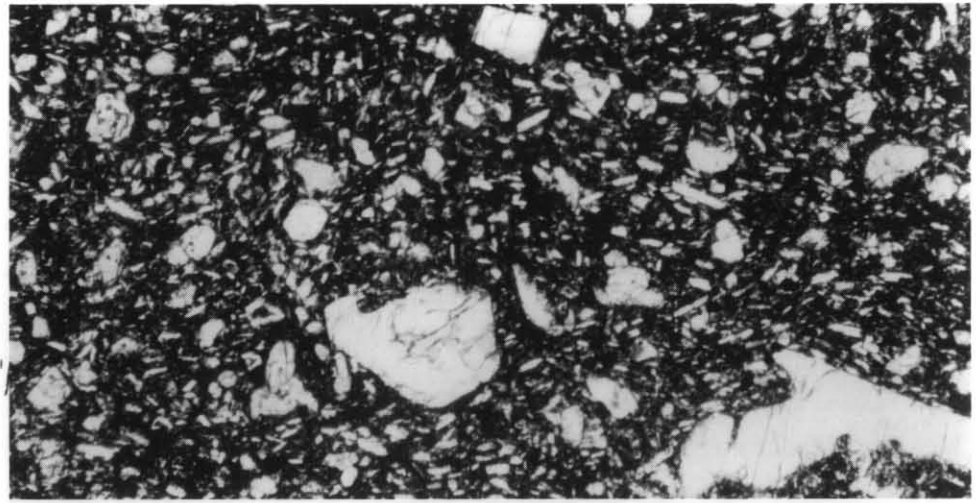

Plate B6. Sample SBDP9/213.5. Strongly alkaline basalt, possible primary magma. Olivine phenocrysts and granules, small plagioclase laths, and a very fine mesostasis. Plane polarised light, field of view 4.3 × 2.3 mm.

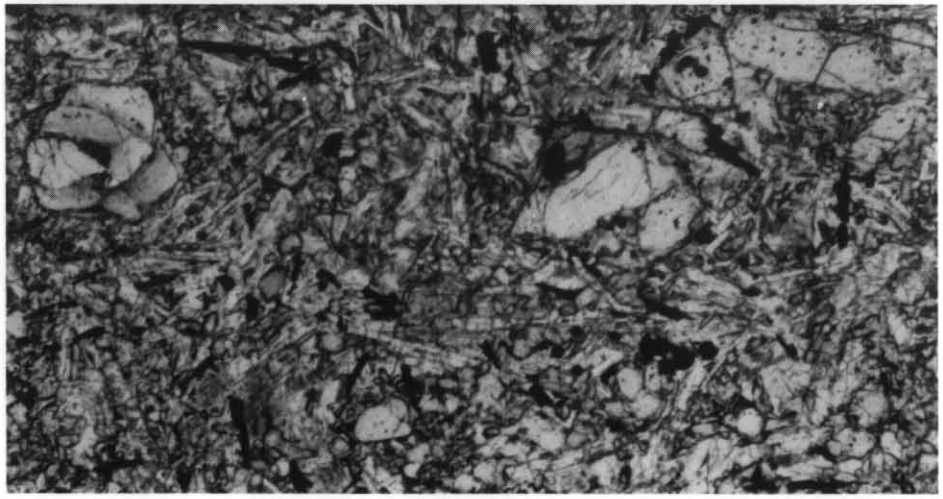

Plate B7. Sample EV4. Alkaline basalt showing euhedral to subhedral olivine phenocrysts within a medium-coarse intergranular groundmass. Plane polarised light, field of view 4.3 × 2.3 mm.

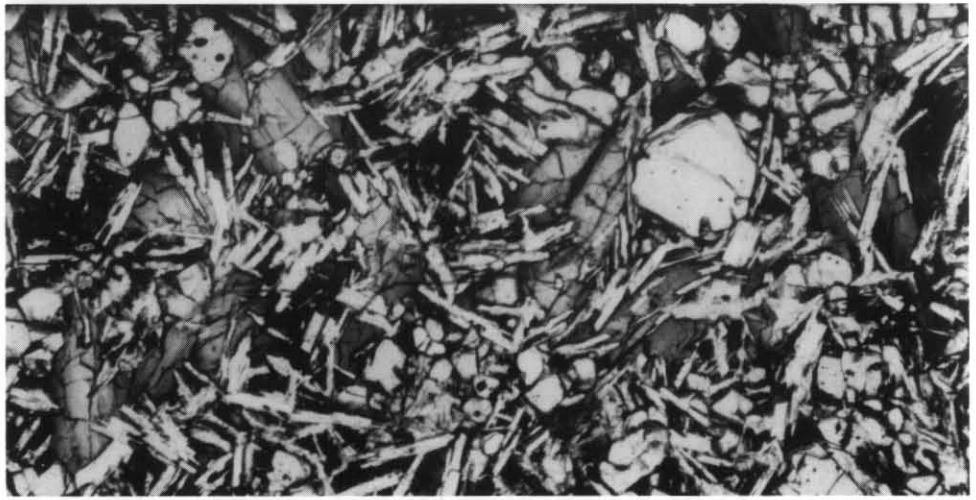

Plate B8. Sample EV25. Alkaline basalt, showing olivine grains (colourless), and a coarse subophitic intergrowth of titanaugite (grey) and plagioclase. Plane polarised light, field of view 4.3 × 2.3 mm.

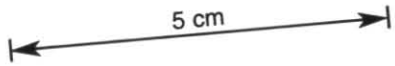

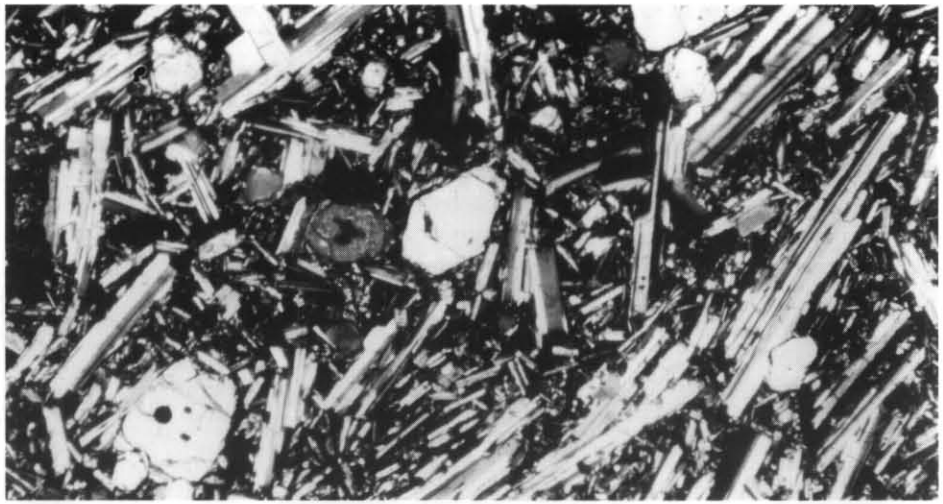

Plate B9. Sample EV20. Transitional basalt. Small euhedral phenocrysts and plagioclase microphenocrysts, grading into medium-grained, intergranular groundmass. Crossed nicols, field of view 4.3 × 2.3 mm.

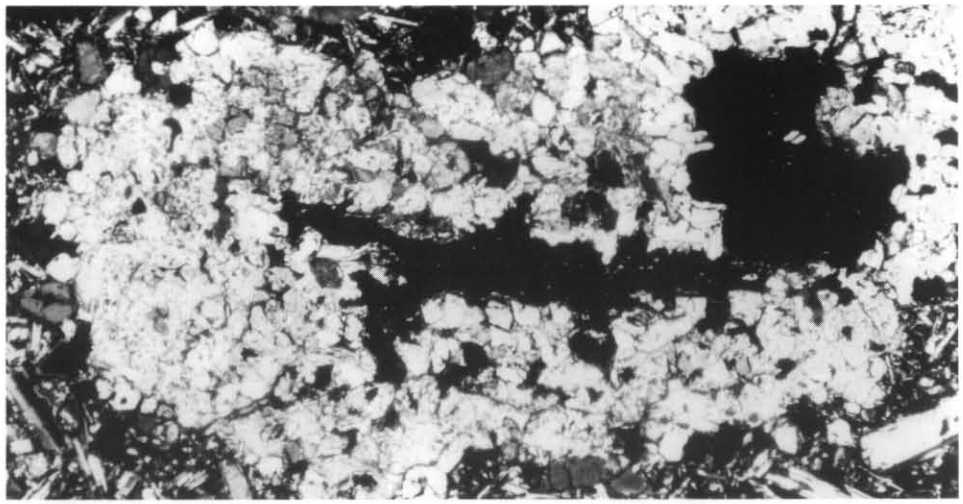

Plate B10. Sample EV20. Glomerocryst with core of orthopyroxene (in extinction) and mantle of granular clinopyroxene and olivine. Crossed nicols, field of view 4.3 × 2.3 mm.

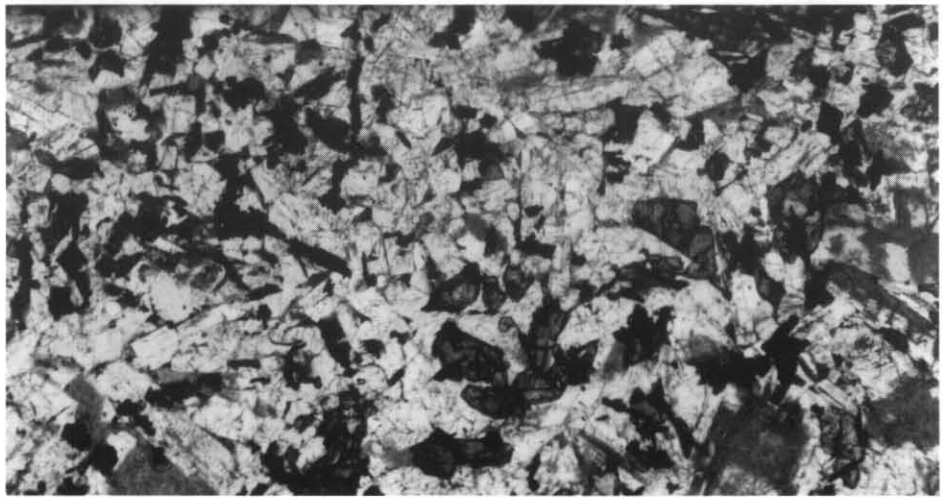

Plate B11. Sample SBDP2/282.0 (2/293.0 is similar). Transitional basalt, consisting of augite (grey), plagioclase and alkali feldspar (paler) and opaque minerals. Equigranular-consertal texture. Plane polarised light, field of view 4.3 × 2.3 mm.

Plate B12. Sample EV21. Tholeiite, showing deeply embayed olivine phenocryst (in extinction) and fine intergranular groundmass. Crossed nicols, field of view 4.3 × 2.3 mm.

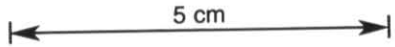

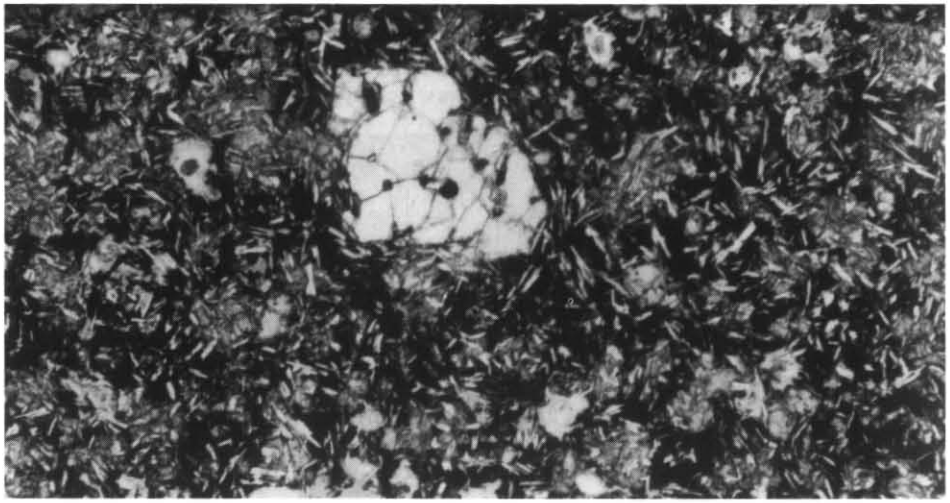

Plate B13. Sample SBDP6/75.8. Tholeiite, showing embayed olivine phenocryst and fine groundmass with minor black glass. Plane polarised light, field of view 4.3 × 2.3 mm.

Plate B14. Sample WA4/140. Quartz-normative tholeiite, consisting of coarse subophitically intergrown augite and plagioclase, and ilmenite. Plane polarised light, field of view 4.3 × 2.3 mm.

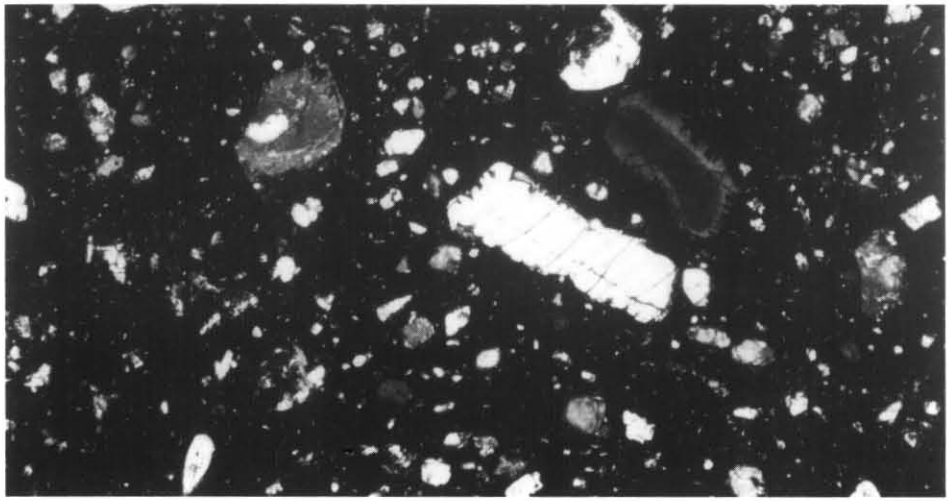

Plate B15. Sample J124 (PV41). Phenocrysts of augite and subordinate olivine within a very fine groundmass. Plane polarised light, field of view 4.3 × 2.3 mm.

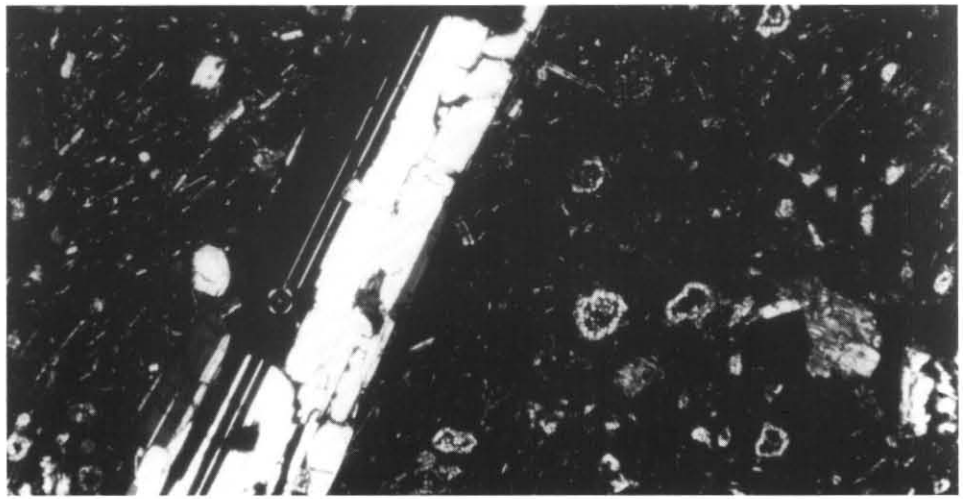

Plate B16. Sample PV30. Large plagioclase phenocryst (left), small augite phenocrysts (right), limonitic amygdales and a very fine groundmass. Crossed nicols, field of view 4.3 × 2.3 mm.

embayed, rarely skeletal, subhedra. The groundmass consists of small plagioclase laths (≤200 μm, but mostly 100 μm or less), rather sparse olivine granules (typically 20-50 μm, but ranging upward to the phenocrysts) and rare augite granules with about 30% black glass rich in minute opaque specks. Within the groundmass are a few irregular but well defined, more glassy patches several mm across, in which elongate to acicular (≤700 μm) microlites of both plagioclase and clinopyroxene lie in black glass. These more glassy patches probably represent gaps within the crystal mush in which, at the time of quenching, the remaining interstitial liquid had been concentrated.

Also within the groundmass are irregular, discontinuous patches of pale yellow isotopic material, probably an amygdaloidal filling.

Sample WA46 is similar but both olivine phenocrysts and groundmass plagioclase are smaller.

EV21 (fine, intergranular) [DQ928128] - Plate B12

This fine, intergranular basalt contains sparsely distributed, deeply embayed to almost skeletal olivine phenocrysts (≤2 mm) in a fresh, slightly flow laminated groundmass in which plagioclase laths (100-200 μm) augite granules, opaques and untwinned interstitial (?)alkali feldspar can be distinguished. Very minor interstitial pale brown isotropic or amorphous material may be altered glass.

Sample EV18 is similar but more altered, EV22 contains more brown (?)altered glass, and EV36 is slightly coarser and more altered. The unanalysed samples PV8 and PV9 from the same vicinity are also very similar.

EV16 (fine, intergranular, with plagioclase microphenocrysts) [DQ028077]

This is also a fine intergranular basalt, but differs in containing rather common oblong plagioclase microphenocrysts (≤1 mm, grading to groundmass) in addition to abundant, euhedral to deeply embayed or skeletal olivine phenocrysts (500 μm-2 mm). The groundmass consists predominantly of plagioclase laths (≤200 μm) and clinopyroxene granules (mostly 15-50 μm), which electron probe microanalyses show include pigeonite as well as augite. Opaques and interstitial (?) alkali feldspar and minor pale yellow-brown (?)glass are also present.

Samples SBDP4/107.9 and SBDP5/61.0 are similar but more altered rocks. Sample EV32 contains particularly abundant, large (1-1.5 mm) oblong plagioclase phenocrysts, some of which form composite glomerocrysts with iddingsitised olivine.

SBDP4/160.9 (fine, subophitic)

As well as common, embayed olivine phenocrysts (500 μm-1 mm) and glomerocrysts, this sample contains a few plagioclase microphenocrysts, either as subhedral oblongs (500 μm-1.5 mm) or irregular, equant, anhedra, sometimes with sieve texture suggesting resorption. The groundmass is subophitic consisting of aligned narrow plagioclase laths (100-200 μm) partly enveloped by augite (≤400 μm), with also generally equant opaques and possible alkali feldspar. Minor interstitial khaki-brown alteration may have been glass.

Sample EV39 is similar but lacks plagioclase microphenocrysts, whilst in EV23 the subophitic texture is poorly developed and rare augite phenocrysts and orthopyroxene-augite glomerocrysts are present.

SBDP6/75.8 (fine, ophitic) - Plate B13

Common large olivine phenocrysts (≤3.5 mm, typically about 1 mm) are characteristically deeply embayed. The groundmass consists largely of more or less equant clots (100-400 μm), of usually optically continuous augite, riddled with inclusions of plagioclase laths, usually ≤100 μm. Between the clots is black opaque-rich glass surrounding similar plagioclase laths. Vesicles and a few amygdales are present.

Sample SBDP6/108.0 is practically identical, SBDP9/115.5 is much coarser (plagioclase laths 150-300 μm) and SBDP9/129.0 contains less olivine and glass and is more altered. All have a well-developed ophitic texture.

EV12 (medium-fine, intergranular) [DQ007150]

This sample is unusual in containing no olivine phenocrysts. It is intergranular, consisting of aligned plagioclase laths (150-300 μm) augite granules, small generally elongate opaques (typically 100 μm long), alkali feldspar and minor interstitial orange-brown alteration possibly derived from glass.

Samples EV31 and EV35 contain abundant embayed olivine phenocrysts (≤2.5 mm) in a similar but not flow laminated groundmass.

EV13 (medium-grained, intersertal/intergranular) [DQ050114]

Abundant deeply embayed phenocrysts of olivine (≤2 mm) lie in a groundmass of plagioclase laths (200-500 μm), intergranular augite (50-150 μm) and about 10% black glass.

Sample EV38 is a similar but intergranular rock, with opaque grains, alkali feldspar and very little glass.

SBDP5/6.4 (medium-grained, intergranular, with plagioclase microphenocrysts)

This is an olivine-augite-plagioclase-phyric basalt, resembling EV20 and other transitional basalts described above. Olivine phenocrysts are fairly common, mostly 500 μm-1 mm (rarely ≤3 mm) across and partly altered to green-brown chloritic material ('bowlingite'). Augite grains are much smaller (≤500 gm) and characteristically clumped into glomerocrysts (≤2 mm), sometimes accompanied by olivine. Plagioclase microphenocrysts (≤1 mm) grade downward in size to the medium-grained (150-400 μm) groundmass.

SBDP5/219.5 (medium-grained, subophitic)

Common, well rounded to embayed or skeletal olivine phenocrysts (500 μm-1 mm) and glomerocrysts lie in a medium-grained, subophitic groundmass of plagioclase laths (150-300 μm), partly surrounded by augite platelets (≤500 μm), with very narrowly elongate to acicular opaques (100-400 μm long) and interstitial black glass. Numerously irregularly shaped amygdales, typically only 500 μm-1 mm long but sometimes interconnected, are filled with a clear, isotropic, cryptocrystalline or amorphous pale yellow material.

Sample EV29 is similar but finely vesicular rather than amygdaloidal. Samples EV15 and EV17 contain relatively few olivine phenocrysts; the latter is rather altered. SBDP1/171.4 is a medium-coarse, strongly altered basalt, also with a subophitic texture.

EV30 (coarse, intersertal) [CQ892299]

This rather unusual rock contains abundant, large (≤3 mm, typically 500 μm-1 mm), often embayed olivine phenocrysts in a groundmass of plagioclase laths (typically 500 μm × 50 μm), olivine granules (typically 50 μm but grading in size upward to phenocrysts) and abundant (30%) black glass. Narrowly elongate crystallites of incipiently crystallised plagioclase and (?) clinopyroxene and very fine opaque specks are common within the glass, which has a granophyric composition (table B5, analyses 233,234). Patches of yellow-orange limonitic alteration, chiefly of glass, are present.

WA3/163.5 (coarse, intergranular)

Abundant, very large (≤5 mm, typically 500 μm-2 mm) embayed olivine phenocrysts lie in a coarse, intergranular groundmass of mainly plagioclase laths (400 μm-1 mm) and anhedral equant augite granules (50-200 μm × 20-40 μm), but a few are more equant and polygonal. Minor orange-brown iddingsite occurs as an alteration of both olivine and interstitial material, and a few calcite veinlets are present.

Samples EV37, SBDP5/159.3 and WA1/96 are similar but more altered coarse or medium-coarse intergranular tholeiites.

Quartz tholeiite

SBDP5/248.7 (fine, intersertal/intergranular)

Euhedral or deeply embayed to skeletal phenocrysts (typically 500 μm-2 mm) of olivine (Fo_{79-83}) are common, and grade downward in size to more iron-rich granules (typically 50 μm). The groundmass also contains plagioclase laths (100-300 μm) and abundant (25%) black glass. Augite is absent. The rock is very fresh, but contains scattered irregular vesicles and amygdales (500 μm-1 mm) filled with pale amber-yellow, clear, isotropic (?)limonitic alteration.

WA1/179 (fine, intergranular)

Rather sparsely distributed, embayed phenocrysts of former olivine (500 μm-2 mm) have been completely altered to orange-brown, fibrous, birefringent 'iddingsite'. The fine, intergranular groundmass has a flow lamination defined by orientation of plagioclase laths (100-200 μm) and flattening of large (1-7 mm) amygdales filled with fine-grained brown limonite and less commonly calcite. Interstitial

augite, opaques, possible alkali feldspar and brown limonitic alteration (?often glass) are also present.

WA2/154 (fine-grained, ophitic)

Fresh olivine phenocrysts (500 μm-2 mm) are common and typically embayed to skeletal. Small plagioclase laths (50-20 μm) pervade the groundmass. They are either completely enveloped by roughly equidimensional clots of augite (≤500 μm), or lie within the black glass which forms about 20% of the rock. Texturally, this rock is similar to the ophitic olivine-normative tholeiites SBDP6/75.8 and SBDP6/108.0, but contains more glass. A few amygdales of calcite or yellowish-green fine-grained isotropic material are present.

WA4/140 (coarse, subophitic) - Plate B14

Olivine phenocrysts (≤3 mm) are rare and usually completely altered. The groundmass consists of plagioclase laths (25-600 μm) partly enveloped by augite platelets (≤50 μm), abundant elongate to acicular ilmenite (200-400 μm) and much fine-grained pale yellow interstitial alteration.

The remaining quartz-tholeiite samples are mostly of fairly altered rocks, and vary considerably in grain size, texture, abundance of olivine phenocrysts and degree of alteration. Many samples contain an interstitial brown to yellow-brown or yellow-green limonitic alteration, sometimes associated with secondary calcite, which may form an almost interconnected network of amygdales. Sample WA2/186 contains about 15% secondary carbonate in the groundmass.

Sample SBDP2/101.5 contains an anhedral xenocryst (2 mm) of feldspar (?plagioclase, but not twinned), with a clear core and narrow rim, and inclusion-ridden, sieve-textured mantle.

In the groundmass of sample SBDP4/129.1 is a diffuse, crescent shaped zone about 5 mm long, consisting of very fine plagioclase laths (30-150 μm) and minor interstitial black glass, surrounded by a medium-grained (200-400 μm) subophitic groundmass. The finer zone may represent a melted and partly digested plagioclase xenocryst.

Miscellaneous samples

Three unanalysed samples have unusual textures unlike any described above, and are thus worthy of special note.

PV41 (very fine, with abundant augite phenocrysts) [DQ045086] - Plate B15

This rock contains abundant, euhedral to subhedral phenocrysts of colourless to very pale yellow augite (biaxial positive) and subordinate colourless olivine. Both minerals occur as generally equant subhedra and euhedra, up to one millimetre across, but grading down to much smaller granules. The groundmass is dark grey to black and very fine, but rather sparse, small plagioclase laths (≤50 μm), augite and olivine granules and opaque blebs can be resolved from the mesostasis which probably includes alkali feldspar and nepheline. A few irregular amygdales filled with calcite and zeolites are present.

A similar sample (J124) was collected from nearby (Cattley Creek, DQ04086) by J. Pemberton, who, on the basis of field relationships, considers it to be the site of a Tertiary feeder (pers. comm.). Both samples texturally resemble EV7, a strongly alkaline, very fine-grained basalt from Guildford Road, but differ in containing mainly augite rather than merely olivine phenocrysts. Chemically, they are probably also similar strongly undersaturated alkaline basalt or basanite.

HR17 (very coarse, intergranular, with titanaugite phenocrysts)

This sample is from Goderich Road (exact locality not recorded) from the western part of the quadrangle. It is a very coarse grained alkali-olivine basalt, containing common phenocrysts of pinkish-purple titanaugite (≤1.5 mm) and subordinate olivine (500 μm-1 mm), both of which grade in size down to the groundmass, and may be clumped in glomerocrysts. The groundmass also contains plagioclase laths (0.5-3 mm), generally more or less equant and angular opaques (typically 50-200 μm) very finely acicular apatite and interstitial perthitic alkali feldspar. There is no flow lamination and the rock is relatively fresh with only patchy development of brown iddingsite and green chlorite around mafic minerals.

This sample is probably a particularly coarse example of the Hampshire textural type (titanaugite porphyry) of Edwards (1950), but does not appear to be a common rock type in this area.

PV30 (very fine, with common large plagioclase phenocrysts) [CQ993130] - Plate B16

From near the Two Hummocks, this sample is most unusual in containing no olivine phenocrysts, but common plagioclase (labradorite) phenocrysts. They are mostly oblong (≤6 mm long, but typically 3 mm × 500 μm) or more equant and polygonal, and euhedral or slightly embayed. There are also sparsely distributed small euhedral phenocrysts of augite (≤500 μm). The groundmass is very fine and altered, but rather sparse narrow laths (≤200 μm) and microlites of plagioclase, and opaque blebs, are resolvable. Numerous limonitic amygdales are present.

MINERAL CHEMISTRY

The composition of the constituent minerals of thirteen relatively unaltered samples, selected to include as large a range of chemical and textural types as possible, was studied by electron microprobe. Results are presented in Table B5 and discussed below.

Olivine (fig. B5)

Eleven of the samples studied contain olivine, as phenocrysts and sometimes also as smaller granules in the groundmass. Phenocryst olivine is usually rather magnesian, but is commonly zoned and may have iron-rich rims (e.g. EV4/105) similar in composition to groundmass olivine.

The composition of olivine in equilibrium with magma of the same composition as the whole rock can be calculated, assuming $Fe_2O_3/FeO = 0.15$ (Brooks, 1976) using an iron-magnesium olivine-liquid distribution coefficient of 0.3 (Roeder and Emslie, 1970):

$$KD = X^{ol}_{FeO} X^{liq}_{MgO} / X^{liq}_{FeO} X^{ol}_{MgO} = 0.3$$

The most magnesian analysed olivine composition in each sample is plotted against the calculated equilibrium olivine composition in Figure B5. Several of the olivine phenocrysts in sample EV1 (probe analyses 2, 4, 5) are too magnesian (Fo_{88-90}) to have been in equilibrium with the bulk rock at any stage of crystallisation and are therefore probably xenocrysts. They are compositionally similar to the olivine in the spinel lherzolite nodules (analyses 17-21) and, together with the augite phenocryst (analysis 6), originated from their disaggregation. On the other hand, analyses 1 and 3, of more euhedral phenocrysts, may be cognate.

Similarly, four out of the five analyses from SBDP4/269.1 are highly magnesian (Fo_{88-90}) and are probably also xenocrysts.

In the remaining samples, the olivine phenocrysts are probably cognate, and directly crystallised from the magma in relatively shallow magma chambers.

Groundmass olivine is almost invariably more iron-rich, and the molar forsterite content (Fo) may be as low as 53 (analyses EV4/113, EV6/159). At this stage, crystallisation of olivine phenocrysts and augite would have generated an iron enriched melt, which has been quenched to glass in a few samples (SBDP6/177.0; EV30; SBDP5/248.7).

Of the minor elements, Ni is detectable (>0.30% approximately) in only a few, generally more magnesian olivine phenocrysts, whilst Mn increases with the iron content of olivine. The trend displayed by Ca is less marked; it also tends to increase with iron content and is higher in groundmass olivine. However, this may be at least partly due to low pressure during crystallisation, which favours incorporation of Ca into the olivine lattice (e.g. Simkin and Smith, 1970).

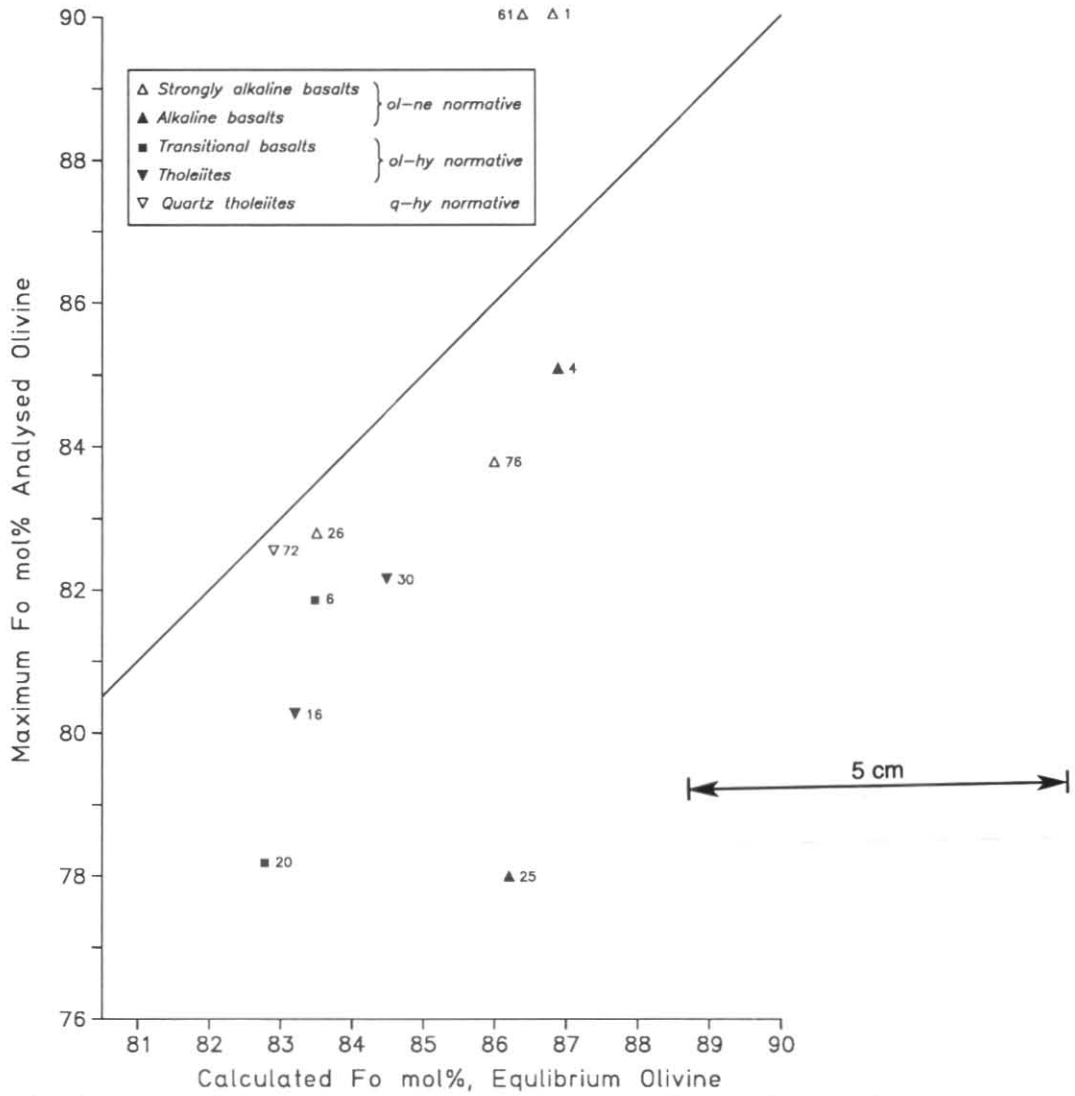

Figure B5. Electron probe microanalyses of olivines from Tertiary basalts *vs* theoretical equilibrium olivine compositions

● *From transitional basalts*
⊙ *From glomerocrysts in transitional basalts*
▼ *From tholeiites*

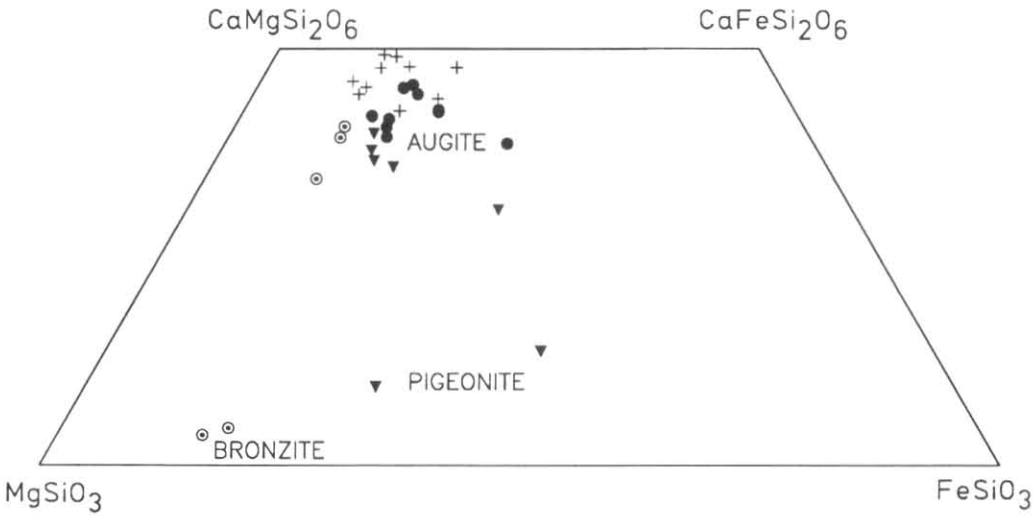

Figure B6. Microanalyses of pyroxenes from Tertiary basalts

Pyroxenes (fig. B6)

Except for a few glassy rocks quenched at an early stage of crystallisation (e.g. EV30; SBDP5/248.7), augite is a major constituent in these basalts. Calcium-poor pyroxenes such as pigeonite and orthopyroxene are much rarer, and *hy* (hypersthene) in the CIPW norms of the tholeiitic and transitional types is largely represented by partly resorbed olivine.

The pyroxene analyses in Table B5 have been converted to formulae, assuming all iron is Fe^{II} and a total oxygen number of 6. For many analyses, it would be possible to estimate the relative Fe^{III} and Fe^{II} content by recalculating the total number of cations to 4. This procedure however cannot be followed if the cation total is less than 4, and is very sensitive to analytical error. Accordingly, this has not been done in Table B5.

The Ca:Mg:Fe cation ratios are projected on to the pyroxene quadrilateral in Figure B6. Some distortions are present as the presence of non-quadrilateral components involving Al,Ti,Cr,Fe^{III} and Na is not allowed for, but the diagram shows several essential features.

Pyroxenes from the alkaline basalt and basanite are all fairly magnesian, calcic clinopyroxenes (augites and salites). They plot in a fairly tight cluster and no clear differentiation trend of iron-enrichment is apparent. Their most interesting features are their minor element contents, particularly TiO_2 which may be up to 3.5% in the pinkish titanaugites of sample EV25. TiO_2 is strongly correlated with Al_2O_3 (up to 6.9%), suggesting that $CaTiAl_2O_6$ is an important component (up to 10 mol%). However, not all the Al_2O_3 present can be accounted for by this component, and a few mole per cent of $CaAl_2SiO_6$ (calcium - Tschermak's pyroxene) or similar hypothetical components are also commonly present. Cr_2O_3 tends to be detectable (<0.20%) in the more magnesian analyses, probably representing strong partitioning of Cr into

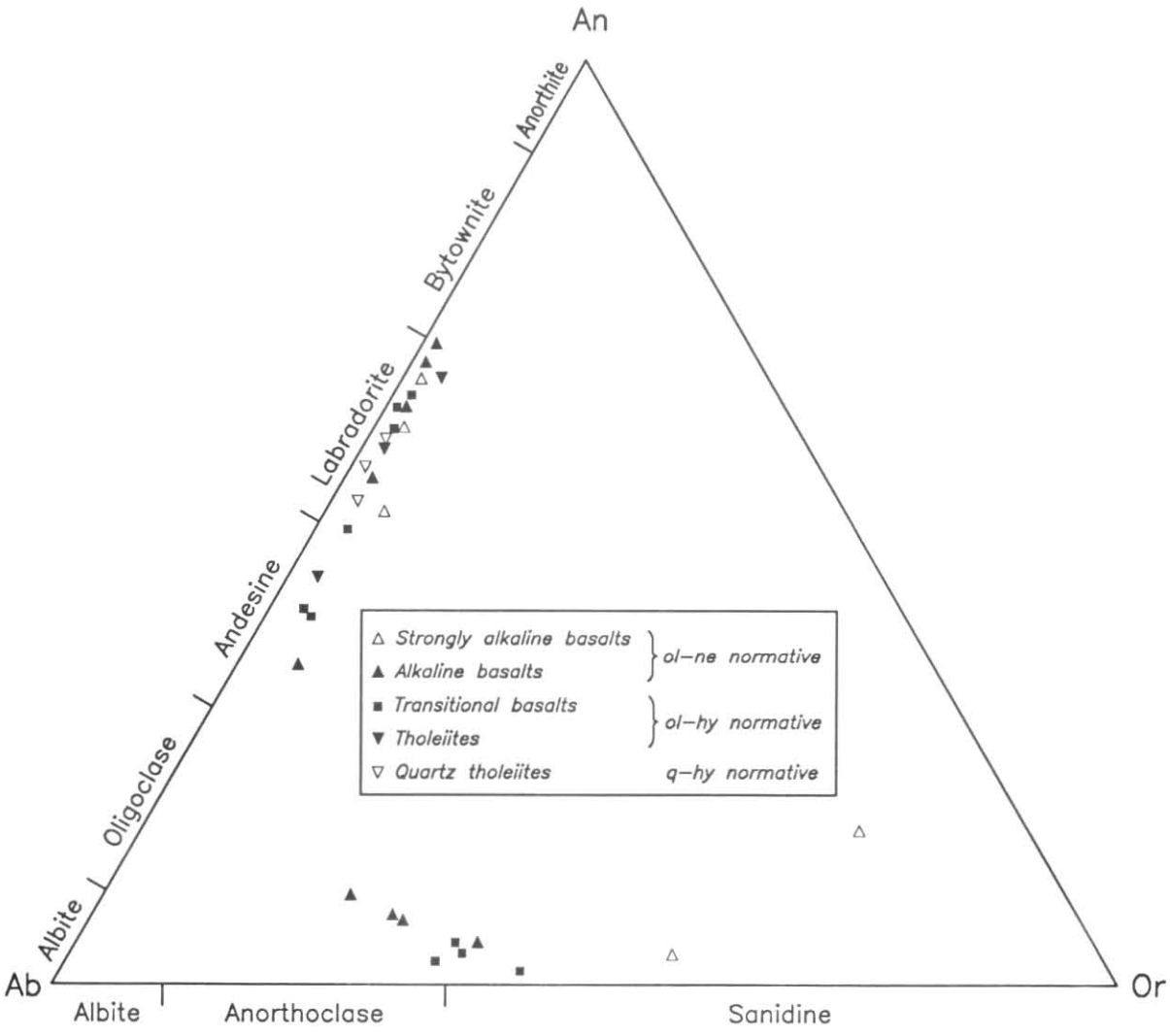

Figure B7. Microanalyses of feldspars from Tertiary basalts

early-formed, magnesian augite, rather than any control by bulk rock composition or crystal lattice substitutions. Small quantities of Na_2O are usually present, but do not seem to vary systematically. There are too many other factors involved for any correlation with Al or Fe^{III} (jadeite or acmite components) to be detected. K_2O and P_2O_5 probably represent impurities; the latter has been subtracted as apatite before cation calculation.

Analyses 6 and 7, from sample EV1, are similar to clinopyroxene from the spinel-lherzolite nodules, and are probably fragments of disrupted nodules or related xenocrysts.

Pyroxenes from transitional basalts samples (EV6, EV20, SBDP2/293.0) are intermediate in CaO, TiO_2 and Al_2O_3 content between pyroxenes from alkaline basalt and tholeiite. Analysis 160 (sample EV6) has anomalously high TiO_2 and ΣFeO, may therefore include some iron-titanium oxide impurity, and is dubious. Again, data are insufficient to establish any differentiatation trend.

The orthopyroxene-clinopyroxene-olivine glomerocrysts present in several samples were described from sample EV20 (see petrography section) and analysed (table B5, analyses 162-177). All the constituent minerals are too iron-rich for the glomerocrysts to be xenoliths derived from the mantle, and probably they are cognate. The orthopyroxene is a bronzite (Fs_{82-85}), clinopyroxene is more magnesian and less titaniferous than in the groundmass and the associated olivine (Fo_{76-78}) is compositionally similar to phenocryst olivine. The orthopyroxene cores of the glomerocrysts probably represent the high pressure liquidus phase, formed at pressures (>7 kb) sufficient to suppress the incongruent melting of $MgSiO_3$. Some of the surrounding clinopyroxene and olivine could be of cumulate origin, but there is textural evidence suggesting reaction of the orthopyroxene with the melt at lower pressures.

Augite from the tholeiitic basalts is less calcic and has lower TiO_2 and Al_2O_3 contents than from alkaline or transitional basalts. There is a strong suggestion of a trend of increasing iron and decreasing calcium with differentiation, similar to the trend observed in slowly cooled tholeiitic intrusions (e.g. Brown, 1957; McDougall, 1961; Everard, 1987). In the groundmass of sample EV16, augite is accompanied by pigeonite (analyses 222, 223). No groundmass orthopyroxene has been found, but by analogy with tholeiitic intrusions it would be expected to be restricted to more magnesian compositions of En>70 mol%.

Overall, the general characteristics of pyroxenes in these rocks are similar to those of mafic intrusives, but because of more rapid cooling, differentiation trends are poorly developed and more iron-rich members are apparently absent.

Feldspars (fig. B7)

Plagioclase is present and usually abundant in all samples, except in the four basanite samples. In thin section, plagioclase crystals are often strongly zoned, and compositionally range from An_{70} to at least An_{34}, both extremes being found in sample EV4 (table B5). Most analyses are labradorite, although andesine appears to predominate in strongly fractionated sample SBDP2/293.0. Plagioclase microphenocrysts, where present, tend to be slightly more calcic than groundmass plagioclase (samples EV20, EV16, table B2). The normative plagioclase composition (table B3) is usually more sodic than the actual analyses, largely because part of the albite component is found in alkali feldspar. A few percent orthoclase component is found in plagioclase, and is generally greater in more sodic compositions. Nearly all analyses contain a few tenths of a percent FeO, probably due to minute inclusions of iron oxides; this is common in volcanic calcic plagioclase (Smith, 1974*b*). Consistently slightly low cation totals (>5.000) appears to be due to excess Si, either as a vacancy-coupled substitution for Al, or as minute inclusions of silica.

Interstitial alkali feldspar has been analysed only in a few K_2O-rich samples, either with alkaline affinities (EV1, EV26, EV4) or strongly fractionated transitional basalt (SBDP2/293.0). In the basanite EV1, highly potassic sanidine is abundant in the very fine groundmass, but the analysis (table B5, analyses 11) contains appreciable MgO, CaO and TiO_2 and may not be reliable, possibly including intergrown clinopyroxene. Sanidine also occurs in sample EV26 (analysis 76). The remaining analyses (EV4, 124-127; SBDP2/293.0, 198-201) straddle the sanidine/ anorthoclase boundary at Or_{37}. The alkali feldspar is too fine-grained to determine optically and may be sanidine-anorthoclase cryptoperthite.

Nepheline

Nepheline occurs in the groundmass of the basanite samples and possibly in some of the alkaline basalt samples, but because of its very fine grain size, uncontaminated analyses are difficult to obtain, even with the electron microprobe. It appears to contain about 15 mol% $KAlSiO_4$ (kalsilite). The high Si cation numbers (>1) and low Al (<1) in the formulae are typical of nepheline analyses, and are probably coupled with vacancies in the Na+K sites (e.g. Deer *et al.*, 1963, p.240).

Iron-titanium oxides

Opaque accessory minerals are common in all samples, but are sometimes very fine crystallites that have only incipiently formed out of black glass. At least two minerals are present: a more titaniferous (about 50% TiO_2) phase, probably ilmenite, and a less titaniferous phase (23-29% TiO_2), probably titanomagnetite. Ilmenite has not been recorded from the more alkaline basalt and basanite, which contain titanomagnetite alone; possibly this is related to the presence of titaniferous clinopyroxene in these rocks (e.g. Carmichael *et al.*, p.273). On the limited data available, ilmenite is the more common phase in tholeiites.

The temperature and oxygen fugacity at the time of crystallisation can be calculated from the compositions of coexisting ilmenite and titanomagnetite (Buddington and Lindsley, 1964). These minerals are also important in understanding the magnetic properties of basalts (e.g. Lucas, 1988). There is much scope for further work on these aspects of the basalts.

Zeolites

Gonnardite (analyses 58-60) from sample SBDP4/269.1 and scolecite or thomsonite (analyses 82, 83) from sample EV26 were tentatively identified from electron probe microanalyses. Reliable identification of zeolites is best done by X-ray diffraction (table 2, p. 33).

Glass

The composition of interstitial glass in quenched samples, whilst very variable, is interesting in indicating the results of extreme differentiation of various magma types. Glass from a strongly alkaline basalt (SBDP6/177.0, probe analyses 99-102) has a *ne*-normative, phonolitic composition, and is very enriched in alkalis (up to 15%), whilst silica has increased only modestly to 52-56%. In contrast, glass derived from differentiation of initially tholeiitic compositions (probe analyses 233, 234, 254) have dacitic compositions with only 5-7% alkalis but up to 65% SiO_2. In both cases, total FeO is very enriched relative to MgO.

Table B5
ELECTRON PROBE MICROANALYSES OF TERTIARY BASALTS
Sample EV1 (880671)

	phenocrysts					groundmass										
	olivine					augite	augite			alkali feldspar			nepheline	titanomagnetite		
	1	2	3	4 (core)	5	6	7	8	9	10	11	12	13	14	15	16
SiO_2	37.58	41.28	37.39	41.19	40.87	52.55	52.87	52.04	51.93	52.12	66.87	43.77	44.09	-	-	-
TiO_2	-	-	-	-	-	0.33	0.23	1.25	1.38	0.99	0.23	-	-	23.15	23.16	23.88
Al_2O_3	-	-	-	-	-	5.67	4.81	1.98	1.90	3.45	18.85	33.30	31.99	-	-	0.20
Cr_2O_3	-	-	-	-	-	0.80	0.78	-	-	-	-	-	-	0.38	0.49	0.36
ΣFeO	25.11	10.50	26.49	9.70	10.95	2.31	2.34	7.05	7.09	6.75	-	1.17	1.80	75.12	74.86	73.94
MnO	0.36	-	0.62	-	-	-	-	-	-	-	-	-	-	0.60	0.76	0.67
NiO	-	-	-	0.34	0.35	-	-	-	-	-	-	-	-	-	-	-
MgO	36.69	48.22	35.08	48.76	47.84	15.43	15.81	13.92	14.08	13.59	0.44	0.53	1.63	0.74	0.73	0.94
CaO	0.26	-	0.42	-	-	21.80	22.17	22.85	22.92	21.05	2.81	-	0.29	-	-	-
Na_2O	-	-	-	-	-	1.10	0.99	0.67	0.69	1.82	1.39	16.28	15.45	-	-	-
K_2O	-	-	-	-	-	-	-	-	-	0.23	9.41	4.96	4.75	-	-	-
P_2O_5	-	-	-	-	-	-	-	0.24	-	-	-	-	-	-	-	-
Total	100.00	100.00	100.00	99.99	100.01	99.99	100.00	100.00	99.99	100.00	100.00	100.01	100.00	99.99	100.00	99.99
(O)	(4)	(4)	(4)	(4)	(4)	(6)	(6)	(6)	(6)	(6)	(8)	(4)	(4)	(4)	(4)	(4)
Si	0.993	1.012	0.996	1.008	1.006	1.900	1.914	1.914	1.930	1.928	3.015	1.059	1.082	-	-	-
Ti	-	-	-	-	-	0.009	0.006	0.035	0.039	0.028	excl.	-	-	0.636	0.636	0.655
Al	-	-	-	-	-	0.242	0.205	0.087	0.083	0.151	1.002	0.949	0.925	-	-	0.009
Cr	-	-	-	-	-	0.023	0.022	-	-	-	-	-	-	0.011	0.014	0.011
Fe^{III}	-	-	-	-	-	-	-	-	-	-	-	-	-	0.717	0.911	0.671
Fe^{II}	0.555	0.215	0.590	0.199	0.225	0.070	0.220	0.220	0.209	-	excl	excl	1.577	1.376	1.583	
Mn	0.008	-	0.014	-	-	-	-	-	-	-	-	-	-	0.019	0.023	0.021
Ni	-	-	-	0.007	0.007	-	-	-	-	-	-	-	-	-	-	-
Ca	0.007	-	0.012	-	-	0.845	0.860	0.913*	0.913	0.834	0.136	-	0.008	-	-	-
Na	-	-	-	-	-	0.078	0.070	0.048	0.050	0.131	0.122	0.764	0.735	-	-	-
K	-	-	-	-	-	-	-	-	-	0.011	0.541	0.153	0.149	-	-	-
P	-	-	-	-	-	-	-	excl*	-	-	-	-	-	-	-	-
Cation total	3.008	2.988	3.004	2.993	2.993	3.999	4.001	4.018	4.015	4.041	4.815	2.925	2.899	3.001	3.000	3.001
$Mg/Mg+Fe^{II}$	0.723	0.891	0.702	0.900	0.886	0.922	0.923	0.779	0.780	0.782	-	-	-	-	-	-

* apatite subtracted

1. euhedral phenocryst; 2. enhedral phenocryst; 5. inclusion in cpx(6)

Table B5 a
ELECTRON PROBE MICROANALYSES
Sample EV1(880671) - continued

	Nodule A																					
	olivine					orthopyroxene						clinopyroxene					spinel					
	17	18	19	20	21	22	23	24	25	26	27	28	29	30	31	32	33	34	35	36	37	38
SiO_2	41.22	41.25	41.07	40.88	41.13	56.15	56.34	56.35	56.25	56.44	56.11	52.74	52.94	53.02	53.38	53.32	-	-	-	-	-	-
TiO_2	-	-	-	-	-	-	-	-	-	-	-	0.18	0.28	0.28	0.23	0.20	-	-	-	-	-	-
Al_2O_3	-	-	-	-	-	3.69	3.31	3.61	3.56	3.37	3.45	5.06	5.29	4.75	3.98	4.18	57.34	57.18	56.84	56.07	57.03	56.93
Cr_2O_3	-	-	-	-	-	0.20	0.21	0.21	0.19	-	0.19	0.78	0.78	0.70	0.64	0.48	11.08	10.94	10.94	11.00	10.99	10.74
ΣFeO	9.96	9.89	9.63	9.82	9.93	6.34	6.38	6.06	6.42	6.25	6.43	2.43	2.36	2.27	2.45	3.04	11.19	10.72	11.18	14.31	11.15	11.45
NiO	-	-	0.35	0.36	0.31	-	-	-	-	-	-	-	-	-	-	-	-	0.45	0.31	-	0.41	0.35
MgO	48.82	48.86	48.95	48.94	48.63	33.30	33.40	33.37	33.25	33.56	33.48	15.85	15.69	15.82	16.82	16.88	20.40	20.71	20.73	18.62	20.42	20.53
CaO	-	-	-	-	-	0.32	0.36	0.39	0.34	0.37	0.34	22.21	21.85	22.40	21.75	21.06	-	-	-	-	-	-
Na_2O	-	-	-	-	-	-	-	-	-	-	-	0.76	0.80	0.77	0.75	0.68	-	-	-	-	-	-
K_2O	-	-	-	-	-	-	-	-	-	-	-	-	-	-	-	0.15	-	-	-	-	-	-
Total	100.00	100.00	100.00	100.00	100.00	100.00	100.00	99.99	100.01	99.99	100.00	100.01	99.99	100.01	100.00	99.99	100.01	100.00	100.00	100.00	100.00	100.00
(O)	(4)	(4)	(4)	(4)	(4)	(6)	(6)	(6)	(6)	(6)	(6)	(6)	(6)	(6)	(6)	(6)	(4)	(4)	(4)	(4)	(4)	(4)
Si	1.008	1.009	1.005	1.002	1.008	1.932	1.940	1.937	1.936	1.941	1.933	1.909	1.912	1.917	1.929	1.928	-	-	-	-	-	-
Ti	-	-	-	-	-	-	-	-	-	-	-	0.005	0.008	0.008	0.006	0.005	-	-	-	-	-	-
Al	-	-	-	-	-	0.150	0.134	0.146	0.144	0.137	0.140	0.216	0.225	0.203	0.170	0.178	1.746	1.739	1.730	1.731	1.738	1.735
Cr	-	-	-	-	-	0.005	0.006	0.006	0.005	-	0.005	0.022	0.022	0.020	0.018	0.014	0.226	0.223	0.224	0.228	0.225	0.219
Fe^{III}	-	-	-	-	-	-	-	-	-	-	-	-	-	-	-	-	0.028	0.037	0.046	0.041	0.037	0.046
Fe^{II}	0.204	0.202	0.197	0.201	0.204	0.183	0.184	0.174	0.185	0.180	0.185	0.074	0.071	0.069	0.074	0.092	0.214	0.194	0.196	0.273	0.204	0.202
Ni	-	-	0.007	.007	.006	-	-	-	-	-	-	-	-	-	-	-	-	0.009	0.006	-	0.009	0.007
Mg	1.780	1.781	1.786	1.788	1.775	1.708	1.714	1.709	1.706	1.720	1.719	0.855	0.845	0.853	0.906	0.910	0.786	0.797	0.798	0.727	0.787	0.791
Ca	-	-	-	-	-	0.012	0.013	0.015	0.013	0.014	0.013	0.861	0.846	0.868	0.842	0.816	-	-	-	-	-	-
Na	-	-	-	-	-	-	-	-	-	-	-	0.053	0.056	0.054	0.053	0.047	-	-	-	-	-	-
K	-	-	-	-	-	-	-	-	-	-	-	-	-	-	-	0.007	-	-	-	-	-	-
Cation total	2.992	2.992	2.995	2.998	2.993	3.990	3.991	3.987	3.989	3.992	3.995	3.995	3.985	3.992	3.998	3.997	3.000	2.999	3.000	3.000	3.000	3.000
$Mg/Mg+Fe^{II}$	0.897	0.898	0.901	0.899	0.897	0.903	0.903	0.907	0.902	0.905	0.903	0.921	0.922	0.926	0.924	0.908	0.786	0.804	0.803	0.727	0.794	0.797
Cr/Cr+Al	-	-	-	-	-	-	-	-	-	-	-	-	-	-	-	-	0.115	0.114	0.114	0.116	0.114	0.112

Table B5 a
ELECTRON PROBE MICROANALYSES
Sample EV1 (880671) - continued

	Nodule B olivine			orthopyroxene			cpx	spinel
	39	40	41	42	43	44	45	46
SiO_2	41.20	40.86	40.97	55.94	56.05	56.36	53.51	-
TiO_2	-	-	-	-	-	-	0.47	-
Al_2O_3	-	-	-	3.68	3.53	3.31	2.75	57.14
Cr_2O_3	-	-	-	0.26	0.25	0.21	0.83	10.87
ΣFeO	9.88	9.85	9.88	6.60	6.52	6.18	2.24	10.99
NiO	-	0.34	0.35	-	-	-	-	0.37
MgO	48.92	48.95	48.80	33.04	33.24	33.62	16.67	20.63
CaO	-	-	-	0.47	0.41	0.31	22.81	-
Na_2O	-	-	-	-	-	-	0.72	-
K_2O	-	-	-	-	-	-	-	-
Total	100.00	100.00	100.00	99.99	100.00	99.99	100.00	100.00
O	4	4	4	6	6	6	6	4
Si	1.007	1.002	1.004	1.929	1.932	1.939	1.941	-
Ti	-	-	-	-	-	-	0.013	-
Al	-	-	-	0.150	0.144	0.134	0.118	1.739
Cr	-	-	-	0.007	0.007	0.006	0.024	0.222
Fe^{III}	-	-	-	-	-	-	-	0.039
Fe^{II}	0.202	0.202	0.203	0.190	0.188	0.178	0.068	0.198
Ni	-	0.007	0.007	-	-	-	-	0.008
Mg	1.783	1.788	1.783	1.699	1.708	1.724	0.901	0.794
Ca	-	-	-	0.018	0.015	0.011	0.887	-
Na	-	-	-	-	-	-	0.050	-
K	-	-	-	-	-	-	-	-
Cation total	2.992	2.999	2.997	3.993	3.994	3.992	4.002	3.000
$Mg/Mg+Fe^{II}$	0.898	0.899	0.898	0.899	0.901	0.906	0.930	0.800
Cr/Cr+Al	-	-	-	-	-	-	-	0.113

GEOCHEMISTRY AND PETROGENESIS

The variations in the chemistry of the Tertiary basalts of this area are of two, essentially unrelated kinds, reflecting two different, essentially independent physical processes that occurred at different stages and pressure-temperature regimes during the evolution of the basalts:

(a) differences in MgO and Mg#(100 Mg/Mg + Fe), Ni and, rarely, Cr are caused by crystal fractionation, principally of olivine and, much more occasionally, of pyroxene. This process probably occurred mainly within relatively shallow crustal magma chambers, but there is some evidence that some fractionation occurred at greater depths. On the other hand, *in situ* gravitational settling of olivine within some thick and slowly cooled basalt flows is likely, and has been documented from elsewhere (e.g. Fuller, 1939; Mathews, *et al.*, 1964; Everard, 1987).

(b) much more profound differences in chemistry, affecting a wide range of major and trace elements, are due to processes that occurred in the upper mantle during the generation of batches of primary magma that subsequently rose, differentiated and were extruded to form the basalts. It is postulated that the more undersaturated basalt and basanite flows, low in SiO_2 and high in alkalis and incompatible elements, evolved from primary magmas that were generated by relatively low amounts of partial melting, whilst the transitional basalt and tholeiite flows which are relatively low in alkalis and incompatible elements, were generated by larger amounts of partial melting. Some further variation, usually slight but occasionally very marked, is probably attributable to chemical heterogeneities within the upper mantle source.

Fractionation of olivine and pyroxene

Primary basaltic magmas (i.e. the direct results of partial melting of the upper mantle, unmodified by crystal fractionation) will have compositions in equilibrium with mantle olivine of about Fo_{88-90} (e.g. Ringwood, 1966; Carter, 1970). Adopting a value of 0.3 for the Fe/Mg liquid-olivine distribution coefficient (Roeder and Enslie, 1970), as defined above, implies Mg#(100 Mg/Mg + Fe^{II}) of 68.8 to 73.0. On this basis, only two of the analysed basalts, EV3 and SBDP9/213.5 (table B2), respectively transitional and strongly alkaline basalts, are possible primary magmas. The remainder have lower Mg# and are likely to have fractionated appreciable amounts of Mg-rich mafic minerals, such as olivine or pyroxene, at some stage of their evolution.

The presence of ultramafic xenoliths with upper mantle mineralogy indicates that the host magma rose rapidly to the surface, without any opportunity for crystal fractionation within the crust, and has been considered to be suggestive of a primary host magma (e.g. Frey *et al.*, 1978; Irving and Green, 1976). However, the only nodule-bearing sample collected in the present study, the basanite EV1 from near South Riana, has a slightly lower Mg# of 66.3, suggesting a small amount of fractionation, probably of olivine, occurred within the mantle, before incorporation of the spinel-lherzolite nodules. (If allowance is made for contamination of the analysis by nodule debris, this conclusion is still more valid). Similar fractionated, but nodule-bearing basalts have been reported from Andover, Tasmania (Sutherland, 1974) and Mt Leura, Victoria (Irving and Green, 1976), and high pressure fractionation was also invoked for these rocks (Frey, *et al.*, 1978).

Spinel-lherzolite nodules are usually found at or near volcanic feeders, and their apparent absence elsewhere in the flood basalts of the St Valentines Quadrangle is not surprising.

A third criteria proposed for the identification of primary magmas is high compatible trace element content, particularly of Ni (e.g. Frey, *et al.*, 1978). These elements partition strongly into liquidus or near-liquidus phases such as olivine, and will therefore be rapidly depleted in the melt by any crystal fractionation. Sato (1977) suggests Ni values in primary magmas should be about 240-390 ppm, but since partition coefficients are temperature and composition dependent (Frey *et al.*, 1978), a qualitative approach may be all that can be justified. Of the two candidates for primary magmas identified in this study, sample SBDP9/213.5 contains the highest Ni value of the suite, 360 ppm, whilst sample EV3 has only a moderately high value of 210 ppm.

If olivine is the only phase involved, it is possible in principle to calculate the amount of crystal fractionation the remaining samples have undergone, and therefore the composition of the parental primary magma of each. Assumptions made in this study are parental magmas with Mg#70.8 (in equilibrium with olivine of Fo_{89}), equilibrium fractional crystallisation with each newly crystallised increment of olivine in equilibrium with the melt assuming $K_D = 0.3$ as above, and a constant oxygen fugacity maintaining a Fe_2O_3/FeO ratio of 0.15 (implying an effective total Fe/Mg K_D of 0.2643). These assumptions are arbitrary but probably realistic, and provide the basis for a simple model in which the amount of olivine fractionation and composition of parental magma for each sample can be visually estimated from a plot of recalculated MgO* against recalculated total iron, ΣFeO* (fig. B8). Note that olivine fractionation causes a rapid depletion in MgO, but only very slightly affects ΣFeO*. According to this model, the majority of samples are derived from primary

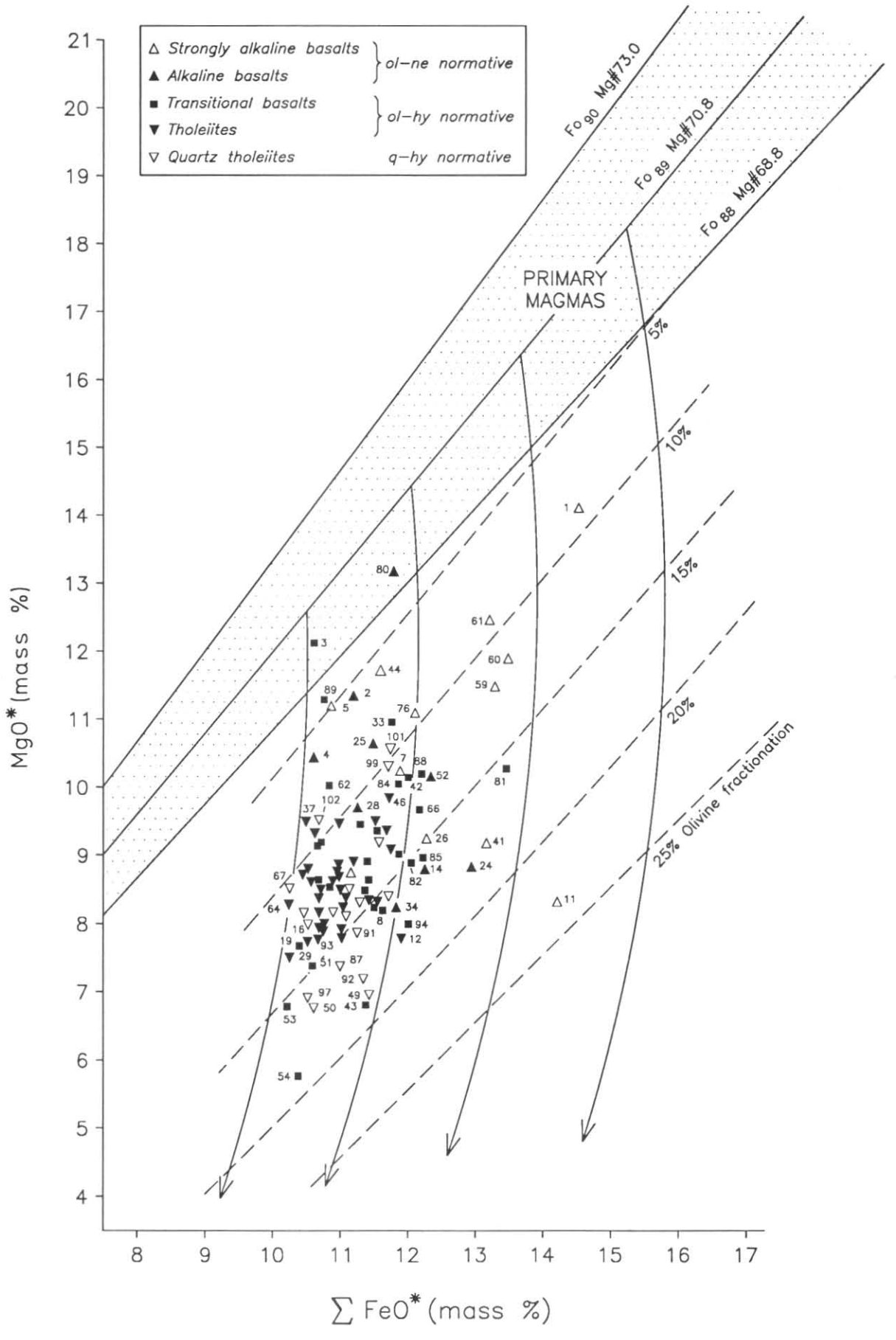

Figure B8. MgO* *vs* FeO* diagram of Tertiary basaltic rocks

Table B5 b
ELECTRON PROBE MICROANALYSES
Sample SBDP4/269.1 (872232)

	phenocrysts olivine					groundmass olivine			augite		zeolite (gonnardite?)			nepheline		titanomagnetite
	47 core	48 rim	49 core	50 rim	51	52	53	54	55	56	57	58	59	60	61	62
SiO_2	41.02	41.14	41.16	39.90	41.08	40.30	36.92	39.31	52.65	49.03	49.10	43.98	43.11	45.50	43.64	-
TiO_2	-	-	-	-	-	-	-	-	1.02	2.18	2.13	-	-	-	-	23.26
Al_2O_3	-	-	-	-	-	-	-	-	1.48	4.79	4.57	25.06	24.11	27.70	33.71	0.54
Cr_2O_3	-	-	-	-	-	-	-	-	-	-	-	-	-	-	-	1.13
ΣFeO	9.71	10.72	9.67	14.53	9.94	13.35	26.64	17.90	7.26	7.45	7.13	0.49	1.15	-	0.90	71.23
MnO	0.36	-	-	-	-	0.23	-	-	-	-	-	-	-	0.60	0.76	0.68
NiO	0.32	0.37	0.40	-	0.45	-	-	-	-	-	-	-	-	-	-	-
MgO	48.95	47.78	48.77	45.57	48.54	45.95	35.46	42.06	14.08	13.02	13.15	1.06	1.86	0.42	-	3.15
CaO	-	-	-	-	-	0.17	0.51	0.26	23.01	23.21	23.31	5.14	4.54	5.02	0.24	-
Na_2O	-	-	-	-	-	-	-	-	0.51	0.31	0.62	6.62	7.52	7.73	16.66	-
K_2O	-	-	-	-	-	-	-	0.14	-	-	-	0.13	0.18	0.10	4.84	-
Total	100.00	100.01	100.00	100.00	100.01	100.00	100.01	100.00	100.01	99.99	100.01	82.48	82.47	86.47	99.99	99.99
H_2O by difference	-	-	-	-	-	-	-	-	-	-	-	17.52	17.53	13.53	-	-
(O)	(4)	(4)	(4)	(4)	(4)	(4)	(4)	(4)	(6)	(6)	(6)	(10)	(10)	(10)	(4)	(4)
Si	1.004	1.011	1.008	0.998	1.007	1.004	0.985	1.002	1.954	1.832	1.834	3.007	2.976	2.964	1.049	-
Ti	-	-	-	-	-	-	-	-	0.028	0.061	0.060	-	-	-	-	0.626
Al	-	-	-	-	-	-	-	-	0.065	0.211	0.201	2.020	1.962	2.127	0.955	0.023
Cr	-	-	-	-	-	-	-	-	-	-	-	-	-	-	-	0.032
Fe^{III}	-	-	-	-	-	-	-	-	-	-	-	-	-	-	-	0.694
Fe^{II}	0.199	0.220	0.198	0.304	0.204	0.278	0.594	0.382	0.225	0.233	0.223	0.028	0.066	-	excl.	1.437
Mn	-	-	-	-	-	0.005	0.011	0.007	-	-	-	-	-	-	-	0.021
Ni	0.006	0.007	0.008	-	0.009	-	-	-	-	-	-	-	-	-	-	-
Mg	1.786	1.750	1.779	1.699	1.774	1.706	1.410	1.598	0.779	0.725	0.732	0.108	0.191	0.040	-	0.168
Ca	-	-	-	-	-	0.005	0.015	0.007	0.915	0.929	0.933	0.377	0.336	0.350	0.006	-
Na	-	-	-	-	-	-	-	-	0.037	0.022	0.045	0.878	1.007	0.781	0.777	-
K	-	-	-	-	-	-	-	excl	-	-	-	0.011	0.016	0.066	0.148	-
Cation total	2.995	2.988	2.993	3.001	2.994	2.998	3.015	2.996	4.003	4.013	4.028	6.429	6.554	6.328	2.935	3.001
Mg/Mg+Fe	0.900	0.888	0.900	0.848	0.897	0.860	0.703	0.807	0.776	0.757	0.767	-	-	-	-	-

Table B5 c
ELECTRON PROBE MICROANALYSES
Sample EV26 (870723)

	phenocrysts				groundmass																
	olivine				olivine			augite		plagioclase				alkali feldspar		titanomagnetite				scolecite/thomsonite?	
	63	64	65	66	67	68	69	70	71	72	73	74	75	76	77	78	79	80	81	82	83
SiO_2	39.33	39.11	39.47	39.16	36.36	35.64	35.06	49.13	45.38	53.53	55.80	53.79	52.59	64.75	53.45	0.42	-	-	-	46.71	42.81
TiO_2	-	-	-	-	-	-	-	1.42	3.77	0.17	-	-	-	0.34	-	28.85	28.06	28.64	28.13	-	-
Al_2O_3	-	-	-	-	-	-	-	3.71	7.32	28.87	28.14	29.44	28.58	19.67	28.31	1.67	2.65	2.64	1.97	24.84	22.53
Cr_2O_3	-	-	-	-	-	-	-	0.21	0.20	-	-	-	-	-	-	-	-	-	-	-	-
ΣFeO	19.06	18.52	16.48	16.32	29.72	34.75	37.53	9.97	8.96	0.75	0.35	0.41	0.89	0.43	0.66	66.67	66.34	65.72	67.22	-	-
MnO	-	-	-	-	0.47	0.54	0.73	-	-	-	-	-	-	-	-	0.77	0.79	0.78	0.74	-	-
NiO	-	-	-	0.35	-	-	-	-	-	-	-	-	-	-	-	-	-	-	-	-	-
MgO	41.38	42.13	43.92	43.93	33.05	28.56	26.11	14.46	11.72	-	-	-	-	-	-	1.62	2.15	2.22	1.93	1.24	0.96
CaO	0.23	0.24	0.13	0.23	0.39	0.50	0.56	20.74	21.79	10.71	10.39	11.92	12.50	0.71	1.48	-	-	-	-	10.65	10.34
Na_2O	-	-	-	-	-	-	-	0.37	0.50	4.84	4.60	4.08	3.51	4.49	12.79	-	-	-	-	-	-
K_2O	-	-	-	-	-	-	-	-	-	0.95	0.72	0.37	1.07	9.62	3.32	-	-	-	-	0.70	0.58
P_2O_5	-	-	-	-	-	-	-	-	0.35	0.17	-	-	0.86	-	-	-	-	-	-	-	-
Total	100.00	100.00	100.00	99.99	99.99	99.99	99.99	100.01	99.99	99.99	100.00	100.01	100.00	100.01	100.01	100.00	99.99	100.00	99.99	84.14	77.22
H_2O (by difference)	-	-	-	-	-	-	-	-	-	-	-	-	-	-	-	-	-	-	-	15.86	22.78
(O)	(4)	(4)	(4)	(4)	(4)	(4)	(4)	(6)	(6)	(8)	(8)	(8)	(8)	(8)		(4)	(4)	(4)	(4)	(10)	(10)
Si	1.005	0.998	0.997	0.992	0.985	0.991	0.990	1.846	1.724	2.452	2.516	2.437	2.447	2.951		excl	-	-	-	3.093	3.095
Ti	-	-	-	-	-	-	-	0.040	0.108	excl	-	-	-	excl		0.789	0.758	0.773	0.763	-	-
Al	-	-	-	-	-	-	-	0.164	0.328	1.559	1.496	1.572	1.567	1.056		0.072	0.112	0.112	0.084	1.938	1.920
Cr	-	-	-	-	-	-	-	0.006	0.006	-	-	-	-	-		-	-	-	-	-	-
Fe^{III}	-	-	-	-	-	-	-	-	-	-	-	-	-	-		0.350	0.373	0.342	0.391	-	-
Fe^{II}	0.407	0.395	0.348	0.346	0.673	0.808	0.886	0.313	0.285	excl	excl	excl	excl	excl		1.677	1.619	1.630	1.636	-	-
Mn	-	-	-	-	0.011	0.013	0.018	-	-	-	-	-	-	-		0.024	0.024	0.024	0.023	-	-
Ni	-	-	-	0.007	-	-	-	-	-	-	-	-	-	-		-	-	-	-	-	-
Mg	1.576	1.602	1.654	1.658	1.335	1.183	1.099	0.810	0.664	-	-	-	-	-		0.088	0.115	0.119	0.104	0.122	0.104
Ca	0.006	0.007	0.004	0.006	0.011	0.015	0.017	0.835	0.868*	0.515*	0.502	0.578	0.566*	0.035		-	-	-	-	0.756	0.801
Na	-	-	-	-	-	-	-	0.027	0.037	0.430	0.402	0.358	0.317	0.397		-	-	-	-	-	-
K	-	-	-	-	-	-	-	-	-	0.055	0.041	0.021	0.063	0.559		-	-	-	-	0.059	0.054
P	-	-	-	-	-	-	-	-	excl*	excl*	-	-	excl*	-		-	-	-	-	-	-
Cation total	2.994	3.002	3.003	3.009	3.015	3.010	3.010	4.041	4.020	5.011	4.957	4.966	4.960	4.998		3.000	3.001	3.000	3.001	5.909	5.974
Mg/Mg+Fe	0.795	0.802	0.826	0.828	0.665	0.594	0.554	0.721	0.700	-	-	-	-	-	-	-	-	-	-	-	-
an										51.5	53.1	60.4	59.8	3.5							
ab										43.0	42.5	37.4	33.5	40.0							
or										5.5	4.4	2.2	6.7	56.5							

* apatite subtracted

77 - approximately 55% alkali feldspar + 45% nepheline

Table B5 d
ELECTRON PROBE MICROANALYSES
Sample SBDP6/177.0 m (874883)

	phenocrysts				groundmass														
	olivine				olivine		augite			plagioclase			titanomagnetite			glass			
	84	85	86 rim	87 core	88	89	90	91	92	93	94	95	96	97	98	99	100	101	102
SiO_2	39.72	37.67	38.31	39.59	37.90	38.32	47.85	47.15	42.29	53.14	52.29	52.34	-	0.94	-	55.83	52.34	52.54	53.07
TiO_2	-	-	-	-	-	-	2.43	3.34	5.77	-	-	-	25.68	25.52	25.23	0.61	0.96	0.89	1.05
Al_2O_3	-	-	-	-	-	-	6.52	6.24	11.91	29.76	30.18	29.62	4.41	4.66	4.19	23.09	21.39	21.45	21.22
Cr_2O_3	-	-	-	-	-	-	0.30	-	-	-	-	-	-	-	-	-	-	-	-
ΣFeO	15.82	23.50	21.87	15.46	23.80	21.62	6.56	9.97	9.92	0.42	0.37	0.87	64.58	64.19	66.19	3.44	4.32	3.59	6.49
MnO	0.27	0.24	0.25	-	-	0.31	-	-	-	-	-	-	0.58	0.64	0.57	-	-	-	-
MgO	44.05	38.22	39.18	44.73	37.87	39.34	13.22	10.60	7.08	-	-	0.72	4.75	4.04	3.82	0.78	1.07	0.60	1.88
CaO	0.13	0.36	0.40	0.21	0.43	0.42	23.13	21.25	19.98	12.22	13.19	12.44	-	-	-	3.38	4.23	4.05	4.12
Na_2O	-	-	-	-	-	-	-	1.20	2.24	4.01	3.65	3.62	-	-	-	5.23	10.32	9.55	5.68
K_2O	-	-	-	-	-	-	-	-	0.23	0.44	0.32	0.38	-	-	-	6.52	3.95	5.03	4.85
P_2O_5	-	-	-	-	-	-	-	0.26	0.58	-	-	-	-	-	-	0.97	1.43	2.06	1.42
SO_3	-	-	-	-	-	-	-	-	-	-	-	-	-	-	-	-	-	0.25	-
Cl	-	-	-	-	-	-	-	-	-	-	-	-	-	-	-	0.14	-	-	0.22
Total	99.99	99.99	100.01	99.99	100.00	100.01	100.00	100.01	100.00	99.99	100.00	99.99	100.00	99.99	100.00	99.99	100.01	100.01	100.00
(O)	(4)	(4)	(4)	(4)	(4)	(4)	(6)	(6)	(6)	(8)	(8)	(8)	(4)	(4)	(4)				
Si	1.001	0.988	0.996	0.996	0.994	0.995	1.781	1.790	1.626	2.413	2.379	2.405	-	excl	-				
Ti	-	-	-	-	-	-	0.068	0.095	0.167	-	-	-	0.673	0.678	0.666				
Al	-	-	-	-	-	-	0.286	0.279	0.540	1.593	1.619	1.604	0.181	0.194	0.174				
Cr	-	-	-	-	-	-	0.009	-	-	-	-	-	-	-	-				
Fe^{III}	-	-	-	-	-	-	-	-	-	-	-	-	0.473	0.450	0.494				
Fe^{II}	0.334	0.515	0.475	0.325	0.522	0.469	0.204	0.317	0.319	excl	excl	excl	1.409	1.446	1.449				
Mn	0.006	0.005	0.005	-	-	0.007	-	-	-	-	-	-	0.017	0.019	0.017				
Mg	1.655	1.494	1.517	1.677	1.479	1.522	0.733	0.600	0.406	-	-	excl	0.247	0.213	0.200				
Ca	0.004	0.010	0.011	0.006	0.012	0.012	0.922	0.850*	0.792*	0.595	0.643	0.612	-	-	-				
Na	-	-	-	-	-	-	-	0.088	0.167	0.353	0.322	0.323	-	-	-				
K	-	-	-	-	-	-	-	-	0.011	0.025	0.019	0.022	-	-	-				
P	-	-	-	-	-	-	excl	- *	excl*	-	-	-	-	-	-				
Cation total	3.000	3.012	3.004	3.004	3.007	3.005	4.003	4.019	4.028	4.979	4.982	4.966	3.000	3.000	3.000				
Mg/Mg+Fe	0.832	0.744	0.761	0.838	0.739	0.764	0.782	0.654	0.560	-	-	-	-	-	-				
an										61.1	65.4	63.9							
ab										36.3	32.7	33.7							
or										2.6	1.9	2.3							

* - apatite subtracted

Table B5
ELECTRON PROBE MICROANALYSES
Sample EV4(870701)

	phenocrysts olivine							groundmass olivine				augite			
	103	104 core	105 rim	106 core	107 rim	108 core	109 rim	110	111	112	113	114	115	116	117
SiO_2	39.03	39.91	36.10	39.98	38.15	38.30	38.35	37.64	36.37	36.51	34.87	50.17	51.21	52.45	51.61
TiO_2	-	-	-	-	-	-	-	-	-	-	-	1.64	1.21	1.09	1.09
Al_2O_3	-	-	-	-	-	-	-	-	-	-	-	2.94	3.31	2.11	2.87
Cr_2O_3	-	-	-	-	-	-	-	-	-	-	-	-	0.94	-	0.81
ΣFeO	18.15	14.80	31.87	14.26	21.02	20.71	22.29	25.39	31.62	28.78	39.32	11.73	6.30	6.81	6.09
MnO	0.21	-	0.42	-	0.24	0.27	0.21	0.23	0.34	0.38	0.65	-	-	-	-
MgO	42.40	45.11	31.38	45.88	40.38	40.52	38.88	36.48	31.41	33.98	24.82	12.35	15.29	15.71	15.35
CaO	0.21	0.19	0.24	0.18	0.22	0.20	0.26	0.27	0.27	0.35	0.34	20.78	21.58	21.83	21.80
Na_2O	-	-	-	-	-	-	-	-	-	-	-	0.40	0.27	-	0.38
K_2O	-	-	-	-	-	-	-	-	-	-	-	-	-	-	-
SO_2	-	-	-	-	-	-	-	-	-	-	-	-	-	-	-
Total	100.00	100.01	100.01	100.00	100.01	100.00	99.99	100.01	100.01	100.00	100.00	100.01	100.01	100.00	100.00
(O)	(4)	(4)	(4)	(4)	(4)	(4)	(4)	(4)	(4)	(4)	(4)	(6)	(6)	(6)	(6)
Si	0.995	1.000	0.987	0.999	0.988	0.990	0.998	0.995	0.993	0.984	0.993	1.895	1.891	1.933	1.905
Ti	-	-	-	-	-	-	-	-	-	-	-	0.047	0.034	0.030	0.030
Al	-	-	-	-	-	-	-	-	-	-	-	0.131	0.144	0.092	0.125
Cr	-	-	-	-	-	-	-	-	-	-	-	-	0.025	-	0.024
Fe^{III}	-	-	-	-	-	-	-	-	-	-	-	-	-	-	-
Fe^{II}	0.387	0.310	0.729	0.298	0.455	0.448	0.561	0.722	0.649	0.936	0.370	0.195	0.210	0.188	
Mn	0.004	-	0.010	-	0.005	0.006	0.005	0.005	0.008	0.009	0.016	-	-	-	-
Mg	1.612	1.685	1.280	1.698	1.558	1.561	1.508	1.437	1.277	1.365	1.053	0.695	0.841	0.863	0.844
Ca	0.006	0.005	0.007	0.005	0.006	0.006	0.007	0.008	0.008	0.010	0.010	0.841	0.854	0.862	0.862
Na	-	-	-	-	-	-	-	-	-	-	-	0.029	0.019	-	0.027
K	-	-	-	-	-	-	-	-	-	-	-	-	-	-	-
Cation total	3.004	3.000	3.013	3.000	3.012	3.011	3.003	3.006	3.008	3.017	3.008	4.008	4.003	3.990	4.005
$Mg/Mg+Fe^{II}$	0.806	0.845	0.637	0.851	0.774	0.777	0.757	0.719	0.639	0.678	0.529	0.652	0.812	0.804	0.818
an															
ab															
or															

Table B5 e
ELECTRON PROBE MICROANALYSES
Sample EV4 (870701 – continued)

	groundmass (continued) plagioclase						alkali feldspar				ilmenite				
	118	119	120	121	122	123	124	125	126	127	128	129	130	131	132
SiO_2	53.57	59.96	52.55	54.56	52.61	51.18	65.83	66.55	65.94	64.98	-	-	-	-	-
TiO_2	-	-	-	-	-	-	-	-	-	0.19	49.72	50.37	50.38	50.96	49.97
Al_2O_3	29.46	25.37	29.92	28.53	28.92	30.86	20.64	19.88	20.30	20.98	-	0.20	-	-	-
Cr_2O_3	-	-	-	-	-	-	-	-	-	-	-	-	-	-	-
ΣFeO	0.41	0.25	0.42	0.48	1.94	0.51	-	-	0.25	0.37	47.43	46.29	46.91	46.46	47.54
MnO	-	-	-	-	-	-	-	-	-	-	0.63	0.60	0.76	0.68	0.64
MgO	-	-	-	0.19	0.98	0.18	-	-	-	-	2.22	2.31	1.96	1.90	1.85
CaO	12.20	6.90	12.67	11.12	11.32	13.85	1.49	0.90	1.42	1.96	-	0.24	-	-	-
Na_2O	4.06	6.57	3.97	4.74	3.99	3.22	7.21	6.34	7.13	7.58	-	-	-	-	-
K_2O	0.30	0.95	0.27	0.38	0.25	0.20	4.83	6.33	4.97	3.94	-	-	-	-	-
SO_3	-	-	0.20	-	-	-	-	-	-	-	-	-	-	-	-
Total	100.00	100.00	100.00	100.00	100.01	100.00	100.00	100.00	100.01	100.00	100.00	100.01	100.01	100.00	100.00
(O)	(8)	(8)	(8)	(8)	(8)	(8)	(8)	(8)	(8)	(8)	(3)	(3)	(3)	(3)	(3)
Si	2.429	2.678	2.394	2.476	2.440	2.340	2.929	2.968	2.941	2.904	-	-	-	-	-
Ti	-	-	-	-	-	-	-	-	-	excl	0.924	0.935	0.939	0.951	0.932
Al	1.574	1.335	1.606	1.526	1.581	1.663	1.082	1.045	1.067	1.105	-	0.006	-	-	-
Cr	-	-	-	-	-	-	-	-	-	-	-	-	-	-	-
Fe^{III}	-	-	-	-	-	-	-	-	-	-	0.151	0.124	0.122	0.098	0.136
Fe^{II}	excl	excl	excl	excl	excl	excl	-	-	-	excl	0.830	0.831	0.851	0.866	0.850
Mn	-	-	-	-	-	-	-	-	-	-	0.013	0.013	0.016	0.014	0.014
Mg	-	-	-	excl	excl	excl	-	-	-	-	0.082	0.085	0.072	0.070	0.068
Ca	0.593	0.330	0.619	0.541	0.562	0.678	0.071	0.043	0.068	0.094	-	0.006	-	-	-
Na	0.357	0.569	0.350	0.417	0.359	0.286	0.622	0.548	0.616	0.225	-	-	-	-	-
K	0.017	0.054	0.016	0.022	0.015	0.012	0.274	0.360	0.283	0.657	-	-	-	-	-
Cation total	4.970	4.966	4.985	4.982	4.957	4.979	4.978	4.964	4.975	4.985	2.000	2.000	2.000	1.999	2.000
$Mg/Mg+Fe^{II}$	-	-	-	-	-	-	-	-	-	-	-	-	-	-	
an	61.3	34.6	62.8	55.2	60.1	69.5	7.3	4.5	7.0	9.6	-	-	-	-	-
ab	36.9	59.7	35.6	42.6	38.4	29.3	64.3	57.6	63.8	67.4	-	-	-	-	-
or	1.8	5.7	1.6	2.3	1.6	1.2	28.3	37.9	29.2	23.0	-	-	-	-	-

Table B5 f
ELECTRON PROBE MICROANALYSES
Sample EV25 (870722)

	olivine				augite					plagioclase				ilmenite		titanomagnetite	
	133	134	135	136	137	138	139	140	141	142	143	144	145	146	147	148	149
SiO_2	38.45	37.81	38.28	38.48	51.91	46.63	47.11	52.27	52.11	53.30	52.23	51.53	53.08	-	-	-	-
TiO_2	-	-	-	-	0.95	3.49	3.18	1.16	1.22	-	-	-	-	50.27	50.35	26.37	24.98
Al_2O_3	-	-	-	-	2.61	6.93	5.25	2.32	2.39	29.29	30.29	30.69	29.64	0.23	-	1.83	1.65
Cr_2O_3	-	-	-	-	0.44	-	-	-	0.25	-	-	-	-	-	-	-	-
ΣFeO	20.38	23.00	21.02	21.56	5.78	8.56	11.30	6.56	6.84	0.47	0.48	0.40	0.48	46.95	47.26	69.75	71.44
MnO	0.25	0.23	0.25	-	-	-	-	-	-	-	-	-	-	0.57	0.66	0.70	0.67
MgO	40.65	38.58	40.08	39.60	15.58	12.21	10.68	15.18	15.09	0.47	-	-	0.23	1.82	1.72	1.35	1.26
CaO	0.27	0.38	0.37	0.36	22.42	21.88	21.81	22.22	22.10	12.04	12.93	13.66	12.36	-	-	-	-
Na_2O	-	-	-	-	0.31	0.29	0.67	0.28	-	2.96	3.86	3.51	3.92	-	-	-	-
K_2O	-	-	-	-	-	-	-	-	-	1.49	0.21	0.21	0.29	-	-	-	-
Total	100.00	100.00	100.00	100.00	100.00	99.99	100.00	99.99	100.00	100.02	100.00	100.00	100.00	100.00	99.99	100.00	100.00
(O)	(4)	(4)	(4)	(4)	(6)	(6)	(6)	(6)	(6)	(8)	(8)	(8)	(8)	(3)	(3)	(4)	(4)
Si	0.992	0.989	0.991	0.997	1.914	1.750	1.793	1.929	1.925	2.435	2.378	2.349	2.416	-	-	-	-
Ti	-	-	-	-	0.026	0.099	0.091	0.032	0.034	-	-	-	-	0.937	0.940	0.718	0.680
Al	-	-	-	-	0.114	0.307	0.235	0.101	0.104	1.577	1.625	1.649	1.590	0.007	-	0.078	0.070
Cr	-	-	-	-	0.013	-	-	-	0.007	-	-	-	-	-	-	-	-
Fe^{III}	-	-	-	-	-	-	-	-	-	-	-	-	-	0.119	0.119	0.487	0.570
Fe^{II}	0.440	0.503	0.455	0.467	0.178	0.269	0.360	0.202	0.211	excl	excl	-	-	0.854	0.863	1.623	1.591
Mn	0.006	0.005	0.006	-	-	-	-	-	-	-	-	-	-	0.012	0.014	0.021	0.021
Mg	1.563	1.504	1.547	1.529	0.856	0.683	0.606	0.835	0.831	excl	-	-	-	0.067	0.064	0.073	0.068
Ca	0.007	0.011	0.010	0.010	0.885	0.880	0.889	0.879	0.874	0.589	0.630	0.667	0.603	0.004	-	-	-
Na	-	-	-	-	0.022	0.021	0.049	0.020	-	0.262	0.341	0.310	0.346	-	-	-	-
K	-	-	-	-	-	-	-	-	-	0.087	0.012	0.012	0.017	-	-	-	-
Cation total	3.008	3.012	3.009	3.003	4.008	4.009	4.023	3.998	3.986	4.950	4.986	4.987	4.972	2.000	2.000	3.000	3.000
Mg/Mg+Fe	0.780	0.749	0.773	0.766	0.828	0.718	0.628	0.805	0.797	-	-	-	-	-	-	-	-
an										62.8	64.1	67.4	62.4				
ab										27.9	34.6	31.3	35.8				
or										9.3	1.2	1.3	1.8				

Table B5g
ELECTRON PROBE MICROANALYSES
Sample EV6 (870703)

	phenocrysts olivine				plagioclase	groundmass plagioclase				olivine	augite	
	150 core	151 rim	152 core	153 rim	154	155	156	157	158	159	160	161
SiO_2	39.32	37.87	39.47	38.05	53.79	54.25	53.54	55.77	55.09	35.08	46.77	50.99
TiO	-	-	-	-	-	-	-	0.19	-	-	5.21	1.39
Al_2O_3	-	-	-	-	29.08	28.73	29.10	27.59	27.42	-	4.02	2.80
Cr_2O_3	-	-	-	-	-	-	-	-	-	-	-	0.20
ΣFeO	17.64	22.79	17.10	23.25	0.47	0.43	0.69	0.55	0.99	39.13	16.21	10.04
MnO	-	0.28	-	-	-	-	-	-	-	0.47	-	-
MgO	43.04	38.93	43.30	38.50	0.22	0.18	-	-	0.54	25.01	10.01	15.39
CaO	-	0.13	0.12	0.20	11.96	11.77	12.44	10.64	10.96	0.31	16.70	18.82
Na_2O	-	-	-	-	4.25	4.44	4.00	4.61	4.53	-	1.09	0.37
K_2O	-	-	-	-	0.23	0.20	0.22	0.64	0.47	-	-	-
Total	100.00	100.00	99.99	100.00	100.01	100.00	99.99	99.99	100.00	100.00	100.01	100.00
(O)	(4)	(4)	(4)	(4)	(8)	(8)	(8)	(8)	(8)	(4)	(6)	(6)
Si	0.998	0.989	1.000	0.994	2.444	2.461	2.435	2.526	2.517	0.996	1.800	1.899
Ti	-	-	-	-	-	-	-	excl	-	-	0.151	0.039
Al	-	-	-	-	1.557	1.536	1.560	1.473	1.477	-	0.182	0.123
Cr	-	-	-	-	-	-	-	-	-	-	-	0.006
Fe^{II}	0.375	0.498	0.362	0.508	excl	excl	excl	excl	excl	0.929	0.522	0.313
Mn	-	0.006	-	-	-	-	-	-	-	0.011	-	-
Mg	1.629	1.515	1.635	1.499	excl	excl	-	-	excl	1.059	0.574	0.854
Ca	-	0.004	0.003	0.006	0.582	0.572	0.606	0.516	0.536	0.009	0.689	0.751
Na	-	-	-	-	0.374	0.390	0.353	0.405	0.401	-	0.081	0.026
K	-	-	-	-	0.013	0.011	0.013	0.037	0.028	-	-	-
Cation total	3.002	3.012	3.000	3.007	4.970	4.970	4.967	4.957	4.959	3.004	3.999	4.011
Mg/Mg+Fe	0.813	0.753	0.819	0.747	-	-	-	-	-	0.533	0.524	0.732
an					60.0	58.8	62.4	53.8	55.6			
ab					38.6	40.1	36.3	42.3	41.6			
or					1.4	1.2	1.3	3.9	2.9			

Table B5 h
ELECTRON PROBE MICROANALYSES
Sample EV20 (870717)

	glomerocryst (A) orthopyroxene core		clinopyroxene rim		glomerocryst (B) orthopyroxene core		clinopyroxene rim		olivine rim		phenocrysts olivine					microphenocrysts plagioclase		
	162	163	164	165	166	167	168	169	170	171	172 core	173 rim	174 rim	175 core	176 rim	177	178	179
SiO_2	55.11	55.51	53.25	53.02	54.61	56.32	53.32	54.17	38.41	38.76	38.85	38.00	37.18	38.49	38.21	53.15	52.76	53.21
TiO_2	0.17	-	0.49	0.56	0.28	-	0.56	0.39	-	-	-	-	-	-	-	-	-	-
Al_2O_3	3.08	2.63	2.27	2.31	2.52	1.40	1.87	1.09	-	-	-	-	-	-	-	29.61	29.99	29.58
Cr_2O_3	0.28	0.35	0.42	0.53	0.46	-	0.49	0.56	-	-	-	-	-	-	-	-	-	-
ΣFeO	9.79	9.82	7.04	7.15	11.18	10.20	7.23	7.49	21.08	21.69	20.22	23.15	26.01	21.83	22.38	0.38	0.37	0.30
MnO	-	-	-	-	-	-	-	-	0.22	-	-	-	0.31	-	0.23	-	-	-
MgO	29.71	29.95	16.89	17.37	28.74	30.01	17.44	19.34	40.28	39.36	40.71	38.63	36.34	39.51	38.96	-	-	0.17
CaO	1.86	1.74	19.64	19.07	2.20	2.08	19.09	16.96	-	0.19	0.22	0.22	0.16	0.17	0.23	12.76	12.95	12.65
Na_2O	-	-	-	-	-	-	-	-	-	-	-	-	-	-	-	3.85	3.72	3.91
K_2O	-	-	-	-	-	-	-	-	-	-	-	-	-	-	-	0.25	0.19	0.19
Total	100.00	100.00	100.00	100.01	99.99	100.01	100.00	100.00	99.99	100.00	100.00	100.00	100.00	100.00	100.01	100.00	99.98	100.01
(O)	(6)	(6)	(6)	(6)	(6)	(6)	(6)	(6)	(4)	(4)	(4)	(4)	(4)	(4)	(4)	(8)	(8)	(8)
Si	1.937	1.950	1.950	1.941	1.937	1.981	1.952	1.972	0.993	1.003	0.999	0.992	0.987	0.998	0.995	2.413	2.396	2.416
Ti	0.005	-	0.013	0.015	0.008	-	0.015	0.011	-	-	-	-	-	-	-	-	-	-
Al	0.128	0.109	0.098	0.100	0.105	0.058	0.081	0.047	-	-	-	-	-	-	-	1.585	1.605	1.583
Cr	0.008	0.010	0.012	0.015	0.013	-	0.014	0.016	-	-	-	-	-	-	-	-	-	-
Fe^{III}	-	-	-	-	-	-	-	-	-	-	-	-	-	-	-	-	-	-
Fe^{II}	0.288	0.288	0.216	0.219	0.332	0.300	0.221	0.228	0.456	0.470	0.435	0.506	0.577	0.473	0.487	excl	excl	excl
Mn	-	-	-	-	-	-	-	-	0.005	-	-	-	0.007	-	0.005	-	-	-
Mg	1.556	1.568	0.922	0.948	1.519	1.573	0.952	1.050	1.553	1.518	1.561	1.504	1.438	1.526	1.512	-	-	excl
Ca	0.070	0.066	0.770	0.748	0.084	0.078	0.749	0.662	-	0.005	0.006	0.006	0.005	0.005	0.006	0.621	0.630	0.616
Na	-	-	-	-	-	-	-	-	-	-	-	-	-	-	-	0.339	0.328	0.344
K	-	-	-	-	-	-	-	-	-	-	-	-	-	-	-	0.014	0.011	0.011
Cation total	3.992	3.991	3.981	3.986	3.998	3.990	3.984	3.986	3.007	2.996	3.001	3.008	3.014	3.002	3.005	4.972	4.970	4.970
Mg/Mg+Fe	0.844	0.845	0.810	0.812	0.821	0.840	0.811	0.822	0.773	0.764	0.782	0.748	0.713	0.763	0.756	-	-	-
an																63.7	65.0	63.4
ab																34.8	33.8	35.4
or																1.5	1.2	1.1

Table B5h
ELECTRON PROBE MICROANALYSES
Sample EV20 (870717) - continued

	groundmass olivine			augite			plagioclase			ilmenite
	180	181	182	183	184	185	186	187	188	189
SiO_2	36.74	36.90	37.97	49.63	51.89	49.92	55.17	54.68	54.14	-
TiO_2	-	-	-	2.06	1.12	1.68	-	-	-	48.74
Al_2O_3	-	-	-	4.37	2.64	4.07	27.93	28.46	29.00	-
Cr_2O_3	-	-	-	0.28	0.38	-	-	-	-	-
ΣFeO	29.89	27.90	24.56	9.50	8.40	9.77	0.68	0.53	0.48	49.32
MnO	0.38	0.29	0.23	-	-	-	-	-	-	0.54
MgO	32.75	34.70	37.01	14.55	15.48	15.11	0.28	0.19	-	21.40
CaO	0.24	0.22	0.23	19.34	20.08	19.05	10.99	11.18	11.56	-
Na_2O	-	-	-	0.27	-	0.40	4.46	4.63	4.53	-
K_2O	-	-	-	-	-	-	0.49	0.32	0.30	-
Total	100.00	100.01	100.00	100.00	99.99	100.00	100.00	99.99	100.01	100.00
(O)	(4)	(4)	(4)	(6)	(6)	(6)	(8)	(8)	(8)	(3)
Si	0.994	0.988	0.999	1.849	1.919	1.860	2.506	2.480	2.454	-
Ti	-	-	-	0.058	0.031	0.047	-	-	-	0.911
Al	-	-	-	0.192	0.115	0.179	1.495	1.522	1.549	-
Cr	-	-	-	0.008	0.011	-	-	-	-	-
Fe^{III}	-	-	-	-	-	-	-	-	-	0.177
Fe^{II}	0.676	0.625	0.540	0.296	0.260	0.304	excl	excl	excl	0.848
Mn	0.009	0.007	0.005	-	-	-	-	-	-	0.011
Mg	1.321	1.385	1.451	0.808	0.854	0.839	excl	excl	-	0.052
Ca	0.007	0.006	0.007	0.772	0.796	0.760	0.535	0.544	0.561	-
Na	-	-	-	0.019	-	0.029	0.393	0.407	0.398	-
K	-	-	-	-	-	-	0.028	0.018	0.017	-
Cation total	3.007	3.011	3.002	4.002	3.986	4.018	4.957	4.971	4.979	1.999
$Mg/Mg+Fe^{II}$	0.661	0.689	0.729	0.732	0.767	0.734	-	-	-	-
an							55.9	56.1	57.5	
ab							44.1	42.0	40.8	
or							3.0	1.9	1.8	

magmas with between 12.5 and 14.5% MgO by between about 5% and 20% (most commonly about 13%) olivine fractionation. More iron-rich magmas are transitional (SBDP9/237.6, plot no. 81), alkaline (EV24) or very alkaline (VA23, plot no. 41) in composition and are probably derived from parents with MgO ~15.5%. This group also includes the three basanite samples (olivine nephelinite) from hole SBDP4 (plot no. 59, 60, 61). The most iron-rich magmas, EV1 (the nodule-bearing basanite from South Riana) and EV11 are apparently derived from picritic parents with MgO ~17%. Note that the diagram only accounts for MgO and FeO, and each fractionation trend shown is equally valid for a wide range of magmas, differing in SiO_2 and other oxide contents.

A plot of Ni against (unrecalculated) MgO (fig. B9) shows a good positive correlation, consistent with depletion of both elements by olivine fractionation.

Two transitional basalt samples, analyses SBDP2/282.0 and SBDP2/293.0 (plot numbers 53 and 54), have very low Ni contents and Mg#, and are the most fractionated of those studied. Petrographically they are unusual coarse feldspar-rich basalts, lacking any phenocrysts. The Cr contents are much lower than any others (table B2), suggesting fractionation of pyroxene as well as olivine, and the slightly depleted CaO suggests that this may have been clinopyroxene. If so, this would have the effect of further increasing the amount of crystal fractionation required to derive them from a primary magma. There is no clear evidence for pyroxene fractionation in any other samples. However, Cr is highest in the two samples identified above as possible primary magmas, SBDP9/213.5 (460 ppm) and EV3 (450 ppm), and shows a general but vague tendency to decrease with Mg/Mg+Fe; its abundance seems to be similar in alkaline and tholeiitic types. Petrographically, small augite phenocrysts or glomerocrysts are present in about 20% of samples, and occasional pyroxene fractionation seems likely.

There is no evidence for plagioclase fractionation in any samples. With a few exceptions explicable by other processes, CaO and Al_2O_3 are remarkably constant throughout the suite, and Sr, as discussed below, has behaved as an incompatible element. Plagioclase microphenocrysts, where present, are usually only slightly larger than the groundmass plagioclase into which they grade, and their shape and low density makes significant crystal settling unlikely.

Frey *et al.* (1978) argued that the relatively high Al_2O_3/CaO values (≥1.6) of many tholeiitic basalts were difficult to generate from a likely upper mantle composition without clinopyroxene as well as olivine fractionation. However, in these samples olivine fractionation was much more important, and was responsible for producing basalts ranging from quartz-normative tholeiite to basanite from parental primary magmas ranging from olivine tholeiite to picritic basanite.

Partial melting: generation of parental primary magmas

As CaO and Al_2O_3 are relatively constant throughout the suite and MgO is largely controlled by olivine fractionation, the total alkali-silica plot (fig. B2) shows the most important major element variations. An apparently continuous spectrum is present, with total alkalis increasing with decreasing silica. Notably absent are members of the hawaiite-mugearite- benmoreite lineages which have higher alkali contents, further increasing with increasing silica (e.g. Coombs and Wilkinson, 1969). Such rocks are represented in the less voluminous Tertiary basalts of southern Tasmania,

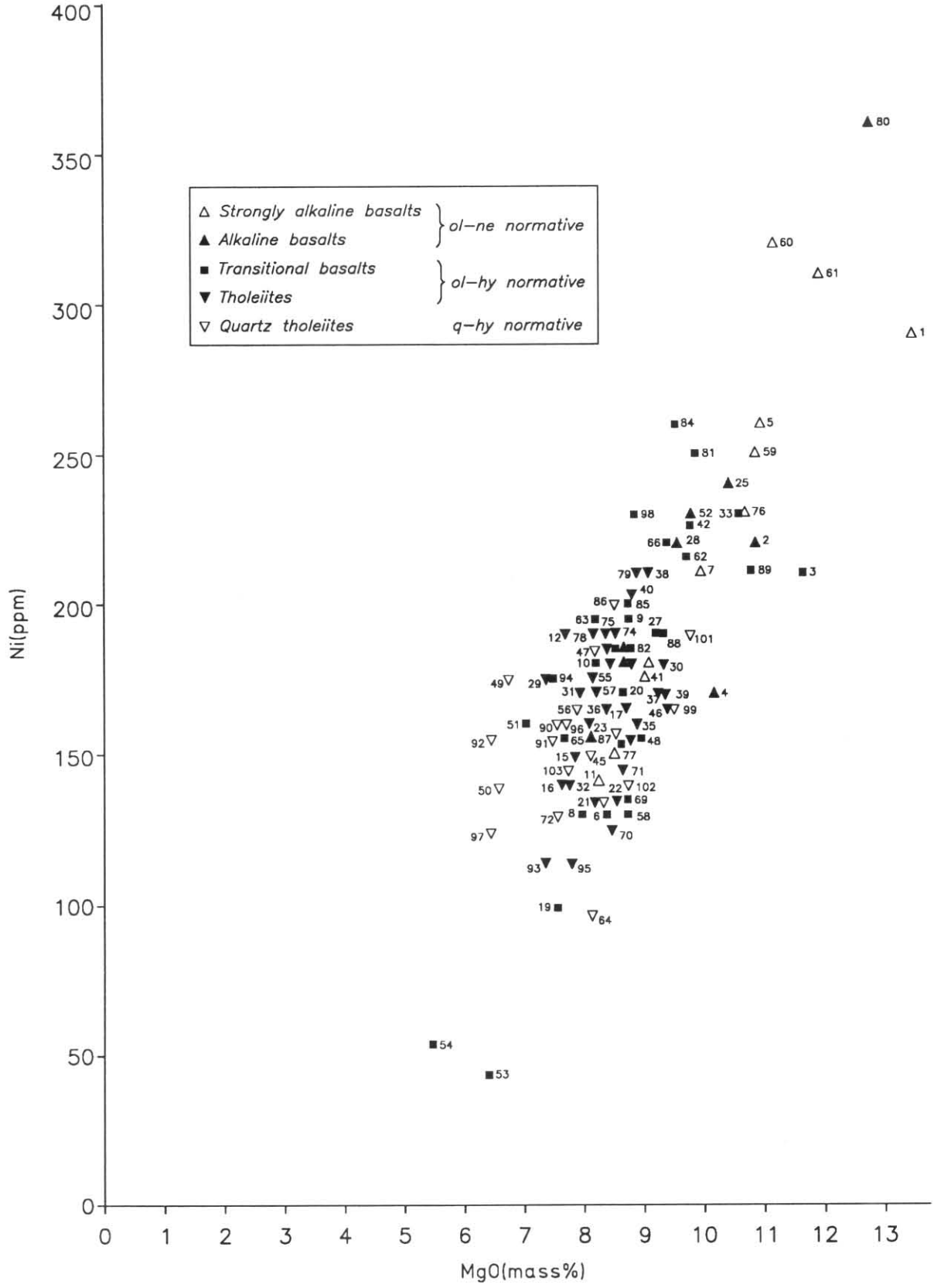

5 cm

Figure B9. Ni–MgO plot for Tertiary basaltic rocks

Table B5 i
ELECTRON PROBE MICROANALYSES
Sample SBDP2/2930 (872172)

	augite				plagioclase				alkali feldspar				ilmenite		titanomagnetite
	190	191	192	193	194	195	196	197	198	199	200	201	202	203	204
SiO_2	49.00	49.25	50.24	49.54	56.11	58.33	53.67	59.38	66.81	66.55	67.28	67.10	-	-	2.17
TiO_2	2.26	2.15	1.45	2.05	-	-	-	-	-	0.21	-	-	49.91	49.66	26.04
Al_2O_3	4.31	4.20	2.98	4.16	27.89	26.19	29.30	25.95	19.53	19.67	19.11	19.28	-	-	1.12
ΣFeO	9.58	10.35	12.20	9.18	0.37	0.36	0.36	-	-	-	-	0.26	49.03	49.26	68.48
MnO	-	-	0.37	-	-	-	-	-	-	-	-	-	-	-	-
MgO	13.01	12.90	12.50	13.35	-	-	-	-	-	-	-	-	0.65	0.68	0.87
CaO	21.46	20.85	19.77	21.46	9.92	8.25	12.21	7.88	0.95	0.79	0.34	0.55	0.41	0.40	1.33
Na_2O	0.38	0.31	0.48	0.25	5.26	6.26	4.16	6.08	6.68	6.67	6.06	6.95	-	-	-
K_2O	-	-	-	-	0.44	0.61	0.30	0.70	6.04	6.11	7.21	5.86	-	-	-
Total	100.00	100.01	99.99	99.99	99.99	100.00	100.00	99.99	100.01	100.00	100.00	00.00	100.00	100.00	100.01
(O)	(6)	(6)	(6)	(6)	(8)	(8)	(8)	(8)	(8)	(8)	(8)	(8)	(3)	(3)	(4)
Si	1.840	1.851	1.899	1.854	2.528	2.618	2.434	2.648	2.978	2.973	3.004	2.993	-	-	-
Ti	0.064	0.061	0.041	0.058	-	-	-	-	-	-	-	-	0.942	0.937	0.726
Al	0.191	0.186	0.133	0.184	1.481	1.385	1.566	1.363	1.026	1.036	1.005	1.013	-	-	0.049
Fe^{III}	-	-	-	-	-	-	-	-	-	-	-	-	0.116	0.126	0.499
Fe^{II}	0.301	0.325	0.386	0.287	excl	excl	excl	-	-	-	-	excl	0.913	0.908	1.626
Mn	-	-	0.012	-	-	-	-	-	-	-	-	-	0.014	0.014	0.027
Mg	0.728	0.722	0.704	0.745	-	-	-	-	-	-	-	-	0.015	0.015	0.073
Ca	0 .863	0.839	0.801	0.861	0.479	0.397	0.593	0.377	0.045	0.038	0.016	0.026	-	-	-
Na	0.028	0.023	0.036	0.018	0.460	0.545	0.366	0.526	0.577	0.577	0.525	0.601	-	-	-
K	-	-	-	-	0.025	0.035	0.017	0.040	0.343	0.348	0.410	0.334	-	-	-
Cation total	4.015	4.007	4.012	4.007	4.973	4.980	4.976	4.954	4.969	4.972	4.960	4.967	2.000	2.000	3.000
$Mg/Mg+Fe^{II}$	0.708	0.689	0.646	0.722	-	-	-	-	-	-	-	-	-	-	-
an					49.7	40.6	60.7	40.0	4.7	3.9	1.7	2.7			
ab					47.7	55.8	37.5	55.8	59.8	59.9	55.2	62.5			
or					2.6	3.6	1.8	4.3	35.5	36.2	43.1	34.7			

Table B5 j
ELECTRON PROBE MICROANALYSES

Sample EV16 (870713)

	phenocrysts olivine									microphenocrysts plagioclase			groundmass plagioclase			augite		pigeonite	
	205 core	206 rim	207 core	208 rim	209 core	210 rim	211 core	212 rim	213	214	215	216	217	218	219	220	221	222	223
SiO_2	38.14	37.27	38.38	37.32	38.25	36.65	39.09	36.82	35.43	52.81	53.34	53.22	57.28	53.83	53.86	52.79	50.79	51.01	52.74
TiO_2	-	-	-	-	-	-	-	-	-	-	-	-	-	0.26	-	0.65	0.84	0.52	0.65
Al_2O_3	-	-	-	-	-	-	-	-	-	29.88	29.48	29.13	26.44	26.94	27.49	1.67	1.32	1.21	0.79
Cr_2O_3	-	-	-	-	-	-	-	-	-	-	-	-	-	-	-	0.53	-	-	-
ΣFeO	21.66	26.44	21.09	26.14	22.00	30.43	18.46	30.14	36.10	0.27	0.28	0.84	0.95	2.12	1.62	9.63	19.31	26.74	19.18
MnO	0.22	0.23	-	0.23	-	0.29	-	0.31	0.44	-	-	-	-	-	-	-	0.39	0.40	0.35
NiO	0.31	0.30	-	-	-	-	-	-	-	-	-	-	-	-	-	-	-	-	-
MgO	39.49	35.62	40.39	36.19	39.63	32.41	42.31	32.57	27.86	0.18	-	-	0.34	-	0.87	16.28	12.49	13.52	21.64
CaO	0.18	0.13	0.13	0.12	0.13	0.22	0.14	0.17	0.18	12.81	12.54	12.60	8.82	12.95	11.59	18.22	14.47	6.25	4.65
Na_2O	-	-	-	-	-	-	-	-	-	3.90	4.20	3.92	5.76	3.31	4.30	0.24	0.39	0.34	-
K_2O	-	-	-	-	-	-	-	-	-	0.14	0.16	0.28	0.41	0.58	0.27	-	-	-	-
Total	100.00	99.99	99.99	100.00	100.01	100.00	100.00	100.01	100.01	99.99	100.00	99.99	100.00	99.99	100.00	100.01	100.00	99.99	100.00
(O)	(4)	(4)	(4)	(4)	(4)	(4)	(4)	(4)	(4)	(8)	(8)	(8)	(8)	(8)	(8)	(6)	(6)	(6)	(6)
Si	0.991	0.992	0.992	0.990	0.993	0.994	0.997	0.996	0.990	2.400	2.419	2.427	2.595	2.493	2.489	1.953	1.952	1.977	1.960
Ti	-	-	-	-	-	-	-	-	-	-	-	-	-	excl	-	0.018	0.024	0.015	0.018
Al	-	-	-	-	-	-	-	-	-	1.600	1.576	1.566	1.412	1.471	1.498	0.073	0.060	0.055	0.035
Cr	-	-	-	-	-	-	-	-	-	-	-	-	-	-	-	0.015	-	-	-
Fe^{II}	0.471	0.588	0.456	0.580	0.478	0.690	0.394	0.682	0.844	excl	excl	excl	excl	excl	excl	0.298	0.620	0.867	0.596
Mn	0.005	0.005	-	0.005	-	0.007	-	0.007	0.010	-	-	-	-	-	-	-	0.013	0.013	0.011
Ni	0.006	0.007	-	-	-	-	-	-	-	-	-	-	-	-	-	-	-	-	-
Mg	1.530	1.413	1.556	1.431	1.533	1.310	1.609	1.314	1.160	excl	-	-	excl	-	excl	0.897	0.716	0.781	1.199
Ca	0.005	0.004	0.004	0.003	0.004	0.006	0.004	0.005	0.005	0.624	0.609	0.616	0.428	0.642	0.574	0.722	0.596	0.260	0.185
Na	-	-	-	-	-	-	-	-	-	0.344	0.369	0.346	0.506	0.297	0.386	0.017	0.029	0.026	-
K	-	-	-	-	-	-	-	-	-	0.008	0.009	0.017	0.023	0.034	0.016	-	-	-	-
Cation total	3.008	3.009	3.008	3.009	3.008	3.007	3.004	3.004	3.009	4.976	4.982	4.990	4.964	4.937	4.963	3.993	4.010	3.994	4.004
Mg/Mg+Fe	0.765	0.706	0.773	0.712	0.763	0.655	0.803	0.658	0.579	-	-	-	-	-	-	0.751	0.536	0.474	0.668
an										63.9	61.7	62.9	44.7	66.0	58.8				
ab										35.2	37.4	35.4	52.8	30.5	39.5				
or										0.8	0.9	1.7	2.4	3.5	1.6				

Table B5 k
ELECTRON PROBE MICROANALYSES
Sample EV30 (870727)

	phenocrysts			groundmass							
	olivine			olivine		plagioclase				glass	
	224	225	226	227	228	229	230	231	232	233	234
SiO_2	39.69	38.80	39.22	37.15	38.44	54.04	53.40	54.09	54.00	63.74	59.03
TiO_2	-	-	-	-	-	-	-	-	-	1.33	1.31
Al_2O_3	-	0.42	-	-	-	28.98	29.39	29.08	28.83	13.59	12.94
ΣFeO	16.78	19.44	17.81	27.78	21.31	0.33	0.27	0.24	0.41	9.06	11.43
MnO	-	0.21	0.25	0.24	0.28	-	-	-	-	-	-
MgO	43.39	40.56	42.56	34.53	39.55	-	0.21	-	0.21	0.40	2.74
CaO	0.14	0.56	0.16	0.31	0.23	12.40	12.85	12.27	12.12	3.65	5.80
Na_2O	-	-	-	-	-	4.08	3.78	4.14	4.23	4.76	4.07
K_2O	-	-	-	-	-	0.16	0.11	0.19	0.21	1.97	1.47
P_2O_5	-	-	-	-	0.18	-	-	-	-	1.12	0.52
SO_3	-	-	-	-	-	-	-	-	-	0.29	0.77
Cl	-	-	-	-	-	-	-	-	-	0.10	-
Total	100.00	99.99	100.00	100.01	99.99	99.99	100.01	100.01	100.01	100.01	99.99
(O)	(4)	(4)	(4)	(4)	(4)	(8)	(8)	(8)	(8)		
Si	1.003	0.996	0.998	0.994	0.998	2.447	2.424	2.447	2.452		
Al	-	0.013	-	-	-	1.547	1.572	1.550	1.543		
Fe	0.355	0.417	0.379	0.621	0.462	excl	excl	excl	excl		
Mn	-	0.005	0.005	0.005	0.006	-	-	-	-		
Mg	1.635	1.552	1.615	1.377	1.530	-	excl	-	excl		
Ca	0.004	0.015	0.004	0.009	excl*	0.601	0.625	0.594	0.590		
Na	-	-	-	-	-	0.359	0.333	0.363	0.372		
K	-	-	-	-	-	0.009	0.006	0.011	0.012		
P	-	-	-	-	excl*	-	-	-	-		
Cation total	2.997	2.998	3.001	3.006	2.996	4.963	4.960	4.965	4.969		
Mg/Mg+Fe	0.822	0.788	0.810	0.689	0.768	-	-	-	-		
ab						62.1	64.8	61.4	60.5		
ab						37.0	34.5	37.5	38.2		
or						0.9	0.6	1.1	1.3		

where they have been termed the Southern Hobart Group or 'alkaline association' (Sutherland, 1976, 1984, 1985, 1988; Everard, 1984) in contrast to the tholeiitic and 'alkali basalt' associations which are similar to the basalts of the St Valentines Quadrangle.

Of the minor and trace elements, the most variable are the strongly incompatible elements P, Sr, Zr and Nb, which have relatively low abundances in tholeiites and are progressively more abundant in more alkaline rocks. Plots of Sr against Zr (fig. B11) and P_2O_5 against Zr (fig. B12) show a strong, positive and roughly linear correlation. A plot of Nb against Zr (not illustrated) or indeed of any pair of the above elements has a similar form. This is consistent with the generation of parental magmas ranging from picritic basanite to olivine tholeiite by progressively greater degrees of partial melting, if it is assumed that these elements are essentially completely partitioned into even a small proportion of melt. If the degree of partial melting is greater, P, Sr, Zr and Nb will be effectively diluted to lower concentrations.

If allowance is made for the slight concentration of incompatible elements caused by low pressure olivine fractionation, which can easily be estimated using Figure B8, the P_2O_5-basalt pyrolite model of Frey *et al.* (1978) can be used to estimate the amount of partial melting. On this basis, the South Riana basanite with 1.08% P_2O_5 (recalculated to 100% anhydrous) was derived by 9% olivine fractionation (fig. B8) from a parental magma with 0.98% P_2O_5, implying 6.1% partial melting of pyrolite (0.06% P_2O_5; Ringwood, 1966). Similarly:

(a) the basanite (olivine nephelinite) SBDP4/269.1 requires 6.8% partial melting.

(b) typical strongly alkaline basalts require 9-13%.

(c) typical alkaline basalts require 14-18%.

(d) typical transitional basalts require 16-24%.

(e) typical tholeiites and quartz tholeiites require 20-35% partial melting of pyrolite to produce their parental magmas.

These estimates are broadly similar to those of Frey *et al.* (1978) for similar Tasmanian and Victorian Tertiary basalts. Overlap and scatter in the estimates is due to several factors, including the arbitrary nature of the classification used, underestimation of the amount of fractionation in those samples that have fractionated pyroxene, and analytical error. Obviously, the model is also very sensitive to the assumed composition of upper mantle (pyrolite) and particularly its P_2O_5 content.

It is significant that the quartz-normative tholeiite samples are, in general, only slightly more fractionated than the olivine tholeiites (fig. B13), and appear to be derived from parental magmas generated by similar amounts of partial melting. Generally their incompatible elements and alkali contents are only slightly lower than olivine tholeiite samples, and SiO_2 slightly higher (fig. B2). Clearly they must be derived by olivine fractionation of olivine-normative parental primary magmas, as quartz-normative liquids cannot be directly generated by partial melting of upper mantle under any conditions. Possibly their parental magmas were derived from a zone of upper mantle that had already been slightly depleted in incompatible elements by an earlier partial melting episode. This is consistent with their apparently younger relative age, towards the top of the volcanic pile.

The three basanite samples from hole SBDP4 (251.1, 255.8, 269.1 m) are notable for their high CaO and low K_2O contents. In these respects, they differ from the South Riana basanite (EV1), but are similar to the olivine nephelinite of the Ringarooma Quadrangle (Brown and McClenaghan, 1982) and perhaps transitional to, but less undersaturated

Table B5 l
ELECTRON PROBE MICROANALYSES
Sample WA4/140m (830755)

	groundmass									
	augite				plagioclase				ilmenite	
	235	236	237	238	239	240	241	242	243	244
SiO_2	53.16	52.30	51.90	52.45	53.72	53.87	54.89	54.91	-	0.63
TiO_2	0.55	1.14	1.21	1.01	-	-	-	-	49.96	49.46
Al_2O_3	1.33	1.96	1.69	1.88	29.02	28.99	28.46	28.48	-	-
Cr_2O_3	-	-	-	0.22	-	-	-	-	-	-
ΣFeO	9.69	9.27	11.85	10.02	0.49	0.39	0.42	0.35	47.59	47.40
MnO	-	-	-	-	-	-	-	-	0.46	0.41
MgO	16.89	15.92	15.88	16.49	-	0.21	-	-	1.99	2.11
CaO	17.83	19.40	17.47	17.94	12.10	11.92	11.21	11.27	-	-
Na_2O	-	-	-	-	4.40	4.40	4.74	4.74	-	-
K_2O	0.55	-	-	-	0.26	0.23	0.27	0.26	-	-
Total	100.00	99.99	100.00	100.01	99.99	100.01	99.99	100.01	100.00	100.01
(O)	(6)	(6)	(6)	(6)	(8)	(8)	(8)	(8)	(3)	(3)
Si	1.966	1.936	1.935	1.940	2.440	2.446	2.483	2.482	-	excl
Ti	0.015	0.032	0.034	0.028	-	-	-	-	0.931	0.926
Al	0.058	0.086	0.074	0.082	1.553	1.551	1.517	1.517	-	-
Cr	-	-	-	0.006	-	-	-	-	-	-
Fe^{III}	-	-	-	-	-	-	-	-	0.138	0.148
Fe^{II}	0.300	0.287	0.370	0.310	excl	excl	excl	excl	0.848	0.839
Mn	-	-	-	-	-	-	-	-	0.010	0.009
Mg	0.931	0.879	0.883	0.909	-	excl	-	-	0.074	0.078
Ca	0.706	0.770	0.698	0.711	0.587	0.580	0.543	0.546	-	-
Na	-	-	-	-	0.388	0.387	0.416	0.415	-	-
K	0.026	-	-	-	0.015	0.013	0.016	0.015	-	-
Cation total	4.002	3.990	3.994	3.986	4.983	4.977	4.975	4.975	2.001	2.000
Mg/Mg+Fe	0.756	0.754	0.705	0.746	-	-	-	-	-	-
an					59.4	59.2	55.7	55.9		
ab					39.1	39.5	42.7	42.6		
or					1.5	1.3	1.6	1.5		

Table B5 m
ELECTRON PROBE MICROANALYSES
Sample SBDP5/2487 (872682)

	phenocrysts			groundmass						
	olivine			olivine			plagioclase			glass
	245	246	247	248	249	250	251	252	253	254
SiO_2	39.67	39.00	39.54	38.12	38.45	35.82	56.31	54.83	55.59	64.92
TiO_2	-	-	-	-	-	-	0.19	-	-	3.90
Al_2O_3	-	-	-	-	-	-	26.81	28.24	28.08	11.89
ΣFeO	16.48	19.20	16.62	24.60	22.50	34.85	1.00	0.44	0.35	8.10
MnO	-	-	-	0.24	-	0.40	-	-	-	-
MgO	43.85	41.80	43.67	36.75	38.89	28.71	-	0.25	-	0.26
CaO	-	-	0.17	0.28	0.15	0.23	10.40	11.35	10.95	2.03
Na_2O	-	-	-	-	-	-	4.90	4.70	4.84	2.37
K_2O	-	-	-	-	-	-	0.40	0.19	0.19	4.45
P_2O_5	-	-	-	-	-	-	-	-	-	1.46
SO_3	-	-	-	-	-	-	-	-	-	0.63
Total	100.00	100.00	100.00	99.99	99.99	100.01	100.01	100.00	100.00	100.01
(O)	(4)	(4)	(4)	(4)	(4)	(4)	(8)	(8)	(8)	
Si	1.001	0.998	0.999	1.003	1.000	0.994	2.557	2.486	2.507	
Ti	-	-	-	-	-	-	excl	-	-	
Al	-	-	-	-	-	-	1.435	1.509	1.493	
Fe as Fe^{II}	0.348	0.411	0.351	0.541	0.489	0.809	excl	excl	excl	
Mn	-	-	-	0.005	-	0.009	-	-	-	
Mg	1.650	1.594	1.645	1.440	1.507	1.187	-	excl	-	
Ca	-	-	0.005	0.008	0.004	0.007	0.506	0.551	0.529	
Na	-	-	-	-	-	-	0.431	0.413	0.424	
K	-	-	-	-	-	-	0.023	0.011	0.011	
Cation total	2.999	3.003	3.000	2.997	3.000	3.006	4.952	4.970	4.964	
$Mg/Mg+Fe^{II}$	0.826	0.795	0.824	0.727	0.755	0.595	-	-	-	
an							52.7	56.5	54.9	
ab							44.9	42.4	44.0	
or							2.4	1.1	1.1	

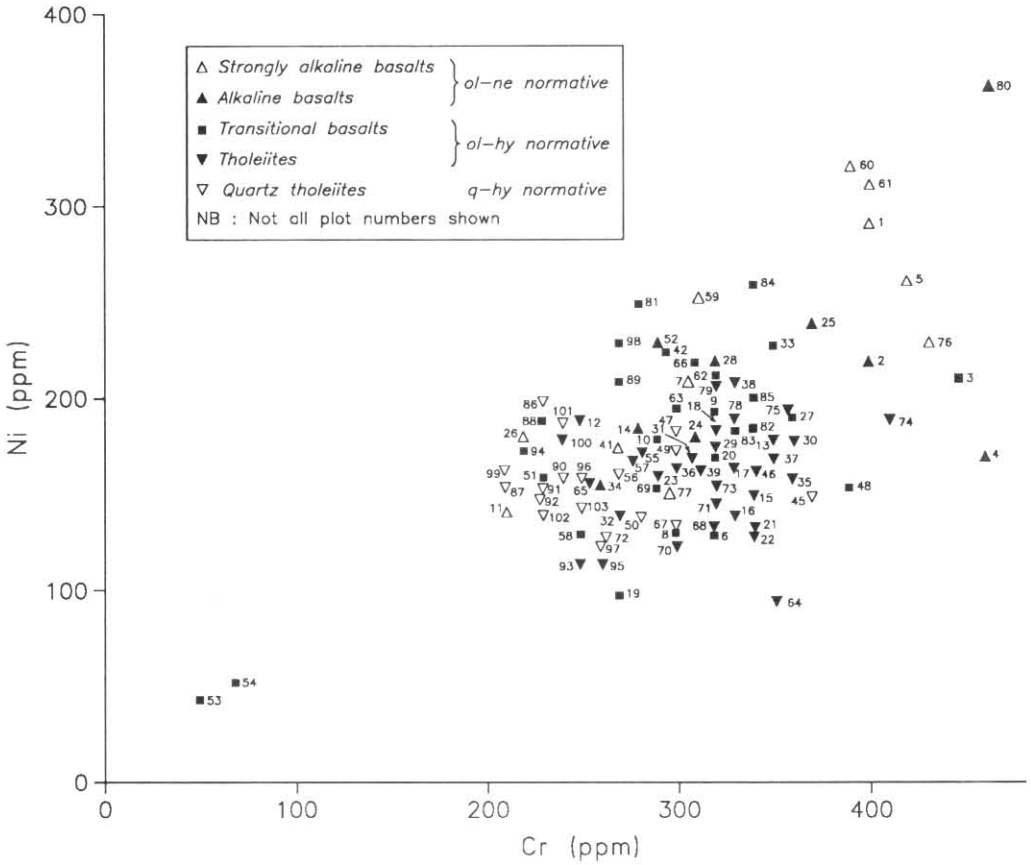

Figure B10. Ni–Cr plot for of Tertiary basaltic rocks

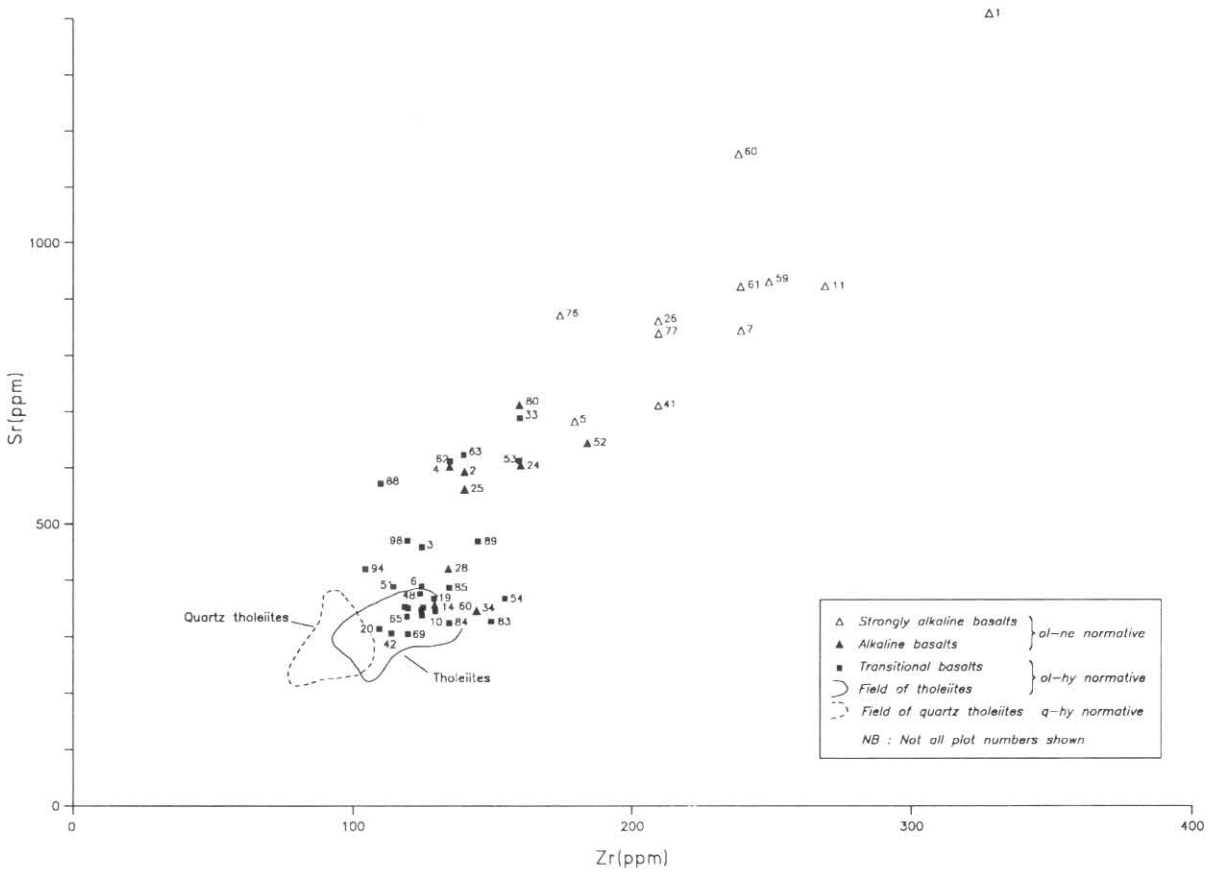

Figure B11. Zr–Sr plot for Tertiary basaltic rocks

5 cm

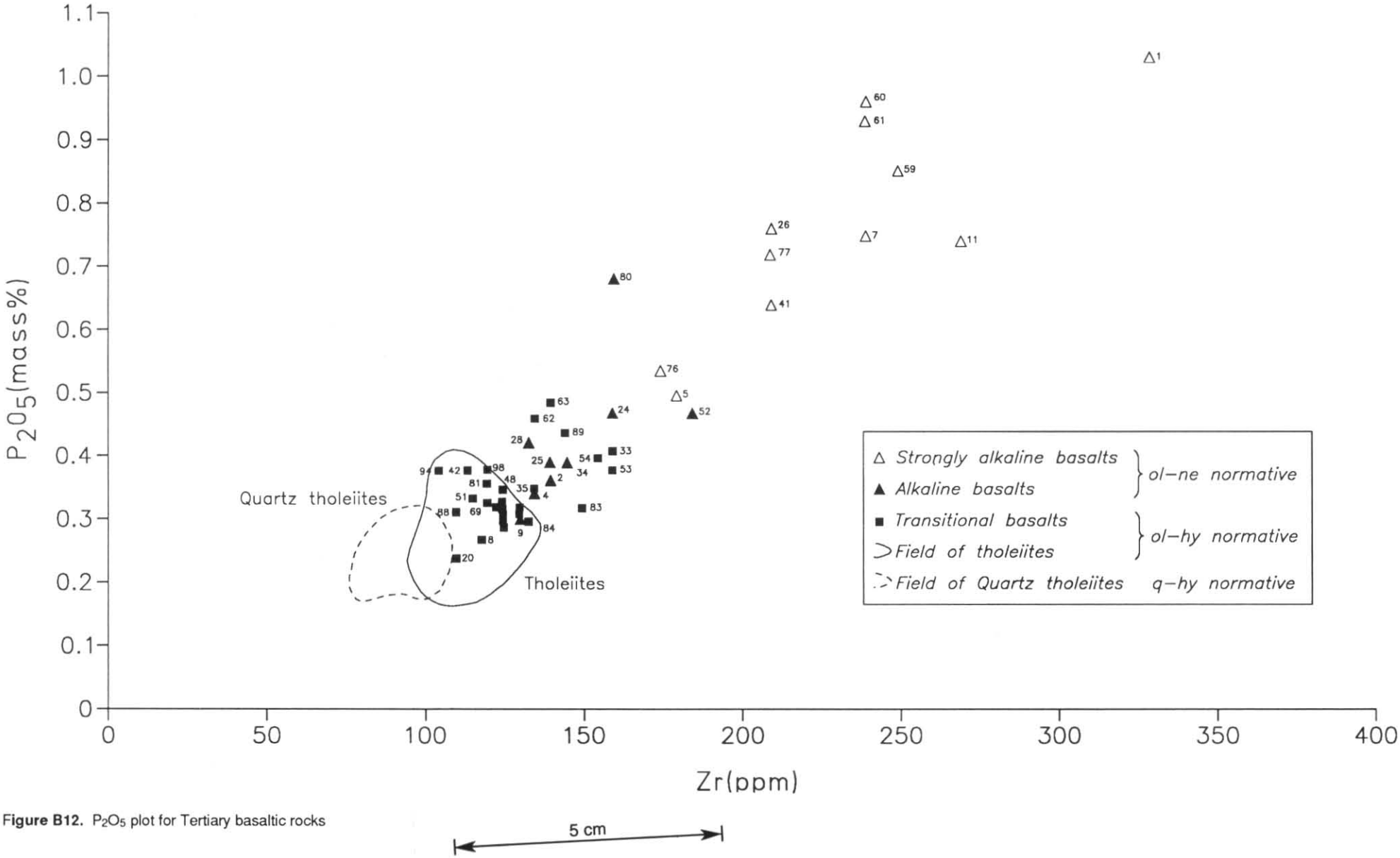

Figure B12. P_2O_5 plot for Tertiary basaltic rocks

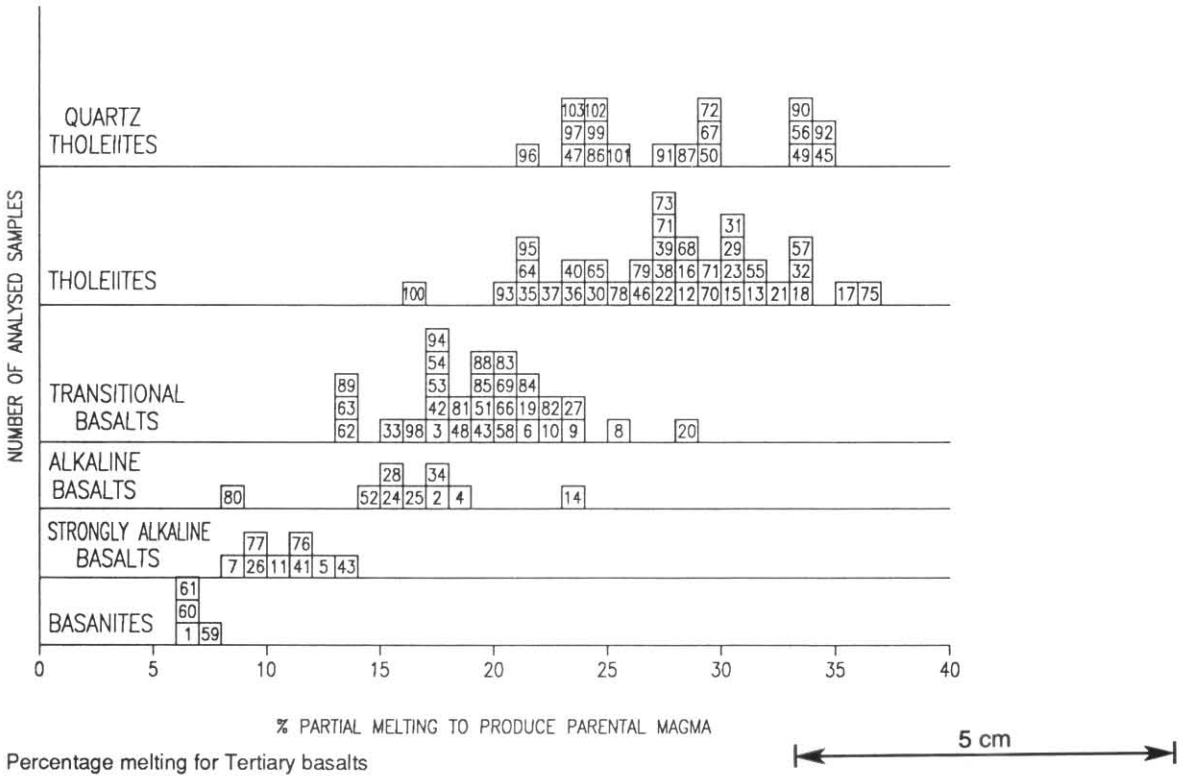

Figure B13. Percentage melting for Tertiary basalts

than, the rare olivine melilitite of Central Tasmania (e.g. Sutherland, 1973, 1988). Brey and Green (1975) have shown that the petrogenesis of such undersaturated, CaO-rich melts requires the pressure of CO_2 as well as H_2O during partial melting, causing the incongruent melting of clinopyroxene, in the presence of olivine, to orthopyroxene and a Ca_2SiO_4 normative melt. Low K_2O, on the other hand, is probably inherited from a K_2O-depleted source. The South Riana basanite, as well as the SBDP4 basanite samples, has low Al_2O_3, in common with many similar rocks.

Light rare earth elements (La, Ce and Nd) are sufficiently abundant in the basalts for determination by standard X-ray fluorescence methods. Although a full data set is not available, data are sufficient to show that these elements usually behave in a highly incompatible manner, similar to P, Sr, Zr and Nb, and increase from about 20 × chondritic abundance in tholeiite to 150 to 200 × chondrites in basanite (fig. B14). Ratios of P_2O_5/Ce are near 75, considered typical for alkali basalt by Sun and Hanson (1975). The outstanding exceptions are four basalts (three tholeiitic and one transitional) from the same interval of core in hole SBDP5 (159.3, 173.3, 219.5, 237.0 m, plot numbers 68-71). These have all elevated rare earth contents, similar to those of basanite, but their La:Ce:Nd ratios are normal. These rocks have no special petrographic or other chemical features (although they occur just below the palaeomagnetic reversal recognised by Lucas, 1988). Their high rare earth contents are probably inherited from a rare-earth enriched source (in comparison to that of the other samples), providing evidence for mantle heterogeneity and possibly incompatible element metasomatism.

Potassium also tends to increase from tholeiite to more alkaline basalt types, behaving to a large extent as an incompatible element. However, a plot of K_2O against Zr shows considerable scatter, and source heterogeneity or secondary process may be involved. Figure B15 also clearly shows the anomalously low K_2O nature of the three basanite samples from hole SBDP4 (plot numbers 59, 60, 61). These analyses are also depleted in Rb. A plot of Rb against K_2O (fig. B16) shows a generally good correlation corresponding to K/Rb of about 400, with two analyses, EV1 and EV34, with respectively anomalously low and anomalously high Rb. Barium also tends to be higher in alkaline basalt, but a plot of Ba against K_2O (not shown) has a great deal of scatter; for instance in transitional basalt samples Ba varies from 40 ppm (EV10) to 1300 ppm (SBDP2/282.0). Thus, although K, Rb and Ba behaved largely as incompatible elements, they are petrogenetically less useful than P, Sr, Zr or Nb because their variation is more random. They are relatively mobile and their abundance may partly reflect interaction with aqueous fluids and/or deuteric processes. Similar conclusions were reached by Frey *et al.* (1978, pp. 496-497, 502), and Hart *et al.* (1971) showed that their abundance was variable even within a single flow.

A plot of TiO_2 against Zr (fig. B17) shows that, although TiO_2 increases from tholeiites to more alkaline rocks, the increase is less rapid than for strongly incompatible elements (such as Zr). Some TiO_2 probably remains in the residue, at least for small amounts of partial melting which generate basanitic or strongly alkaline basaltic melts. Only after about 10-15% partial melting has occurred, and less alkaline and transitional to tholeiitic melts are produced, does TiO_2 become exhausted in the residue and begin to be diluted in the melt. This may correspond to the disappearance of a titaniferous phase from the residue.

Plots of V and Zr (fig. B18) and Co against Zr (not illustrated) show that vanadium and cobalt are moderately incompatible elements behaving similarly to titanium, increasing from tholeiite to alkaline basalt, but levelling out at around 200 ppm and 60 ppm respectively, in strongly alkaline basalt and basanite. Both elements are often associated with titanium in ilmenite and titanomagnetite.

Yttrium values vary only slightly (range 16-26 ppm) with appreciable scatter, but show a statistically significant increase from quartz tholeiite (mean 18.8 ± 1.5) to strongly alkaline basalt and basanite (mean 24.1 ± 1.4). This suggests that Y has a slight tendency to be partitioned into the melt during partial melting.

Copper varies over a factor of 4 (range 25-100 ppm), but this variation is largely random and cannot be clearly correlated with any other geochemical parameter. If anything, Cu tends to be higher in alkaline rocks (average 68 ppm) than in tholeiite and quartz tholeiite samples (average 51 ppm). This

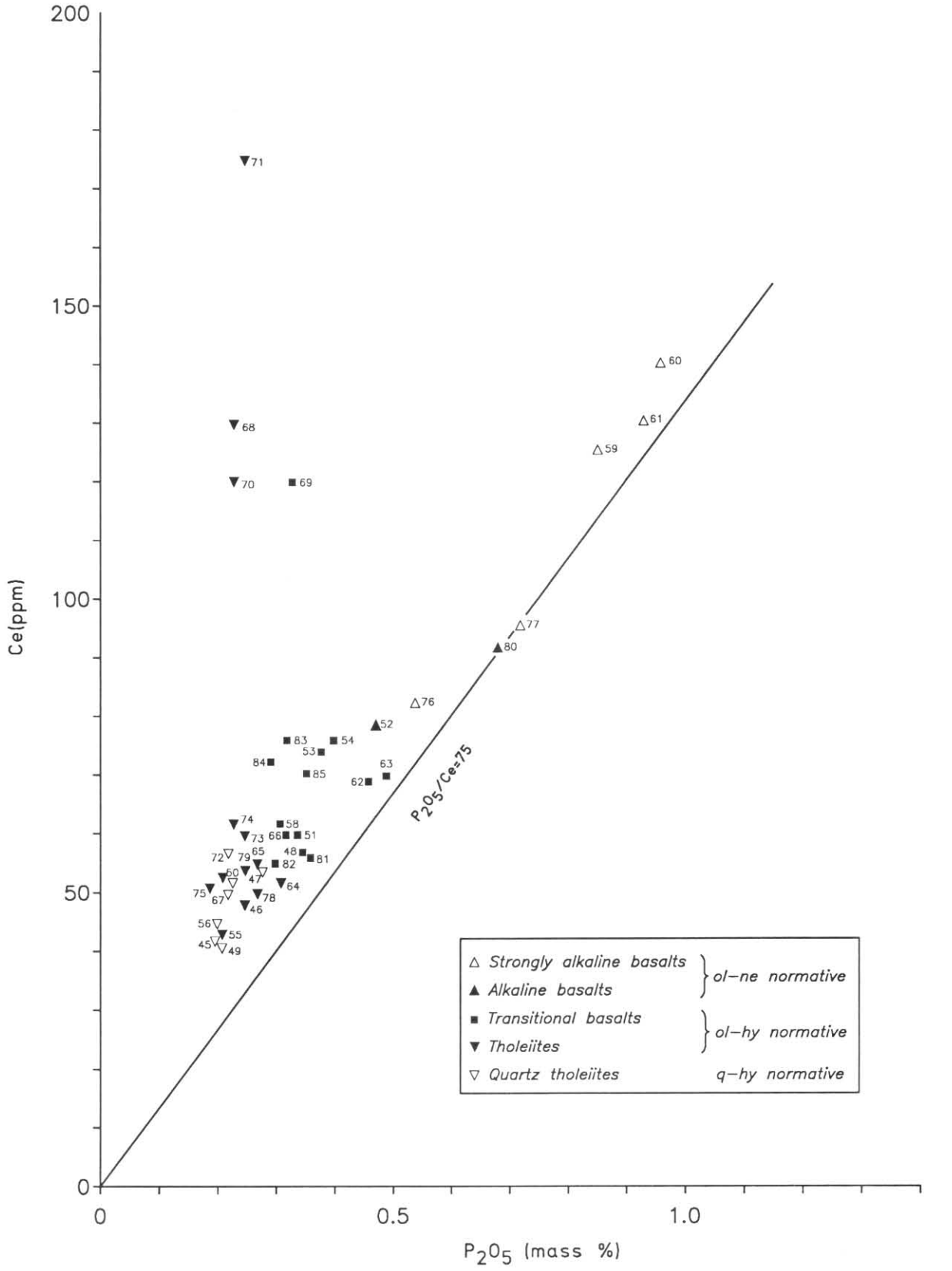

Figure B14. Ce–P_2O_5 plot for basaltic rocks

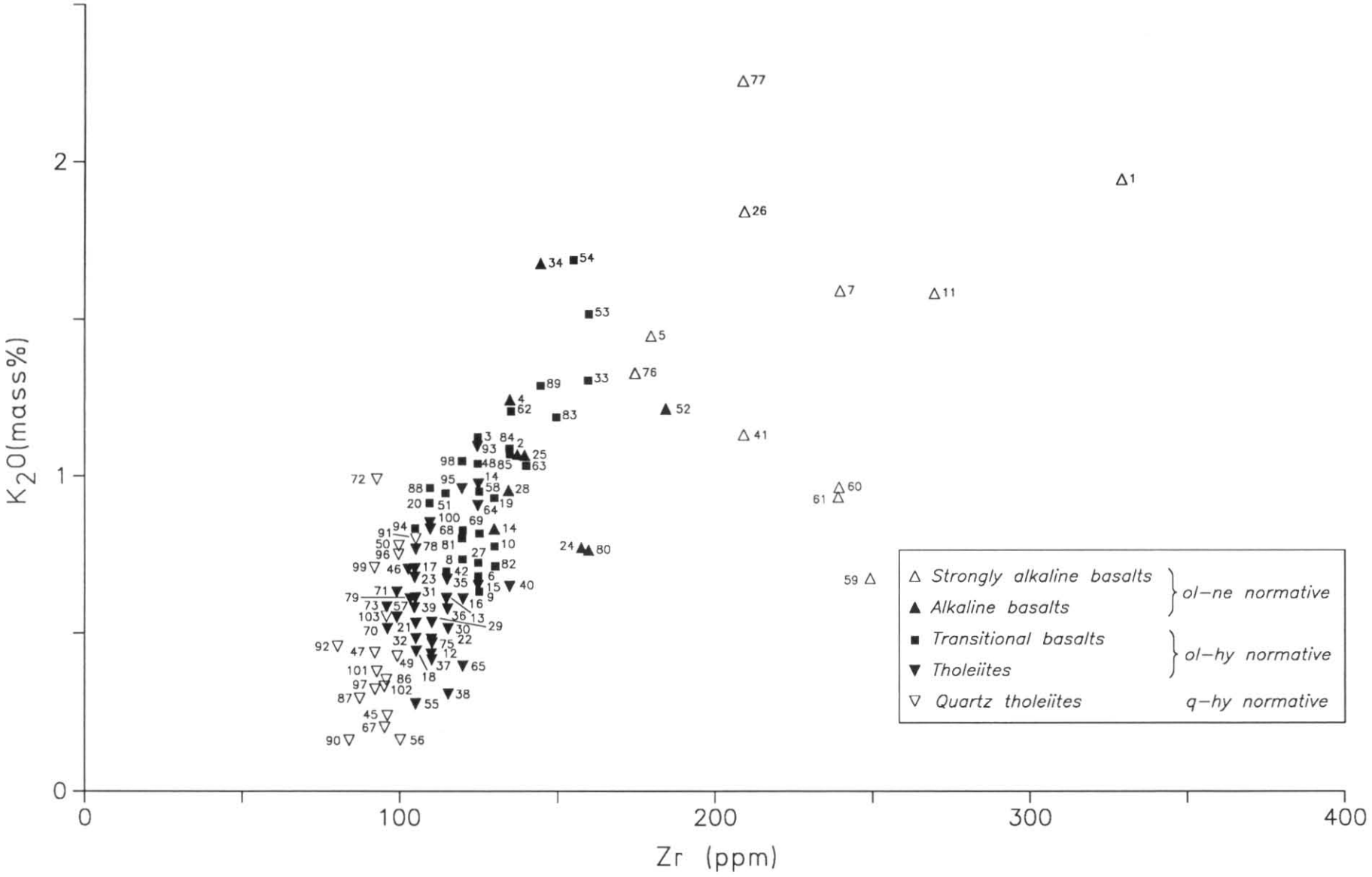

Figure B15. K_2O–Zr plot for Tertiary basaltic rocks

5 cm

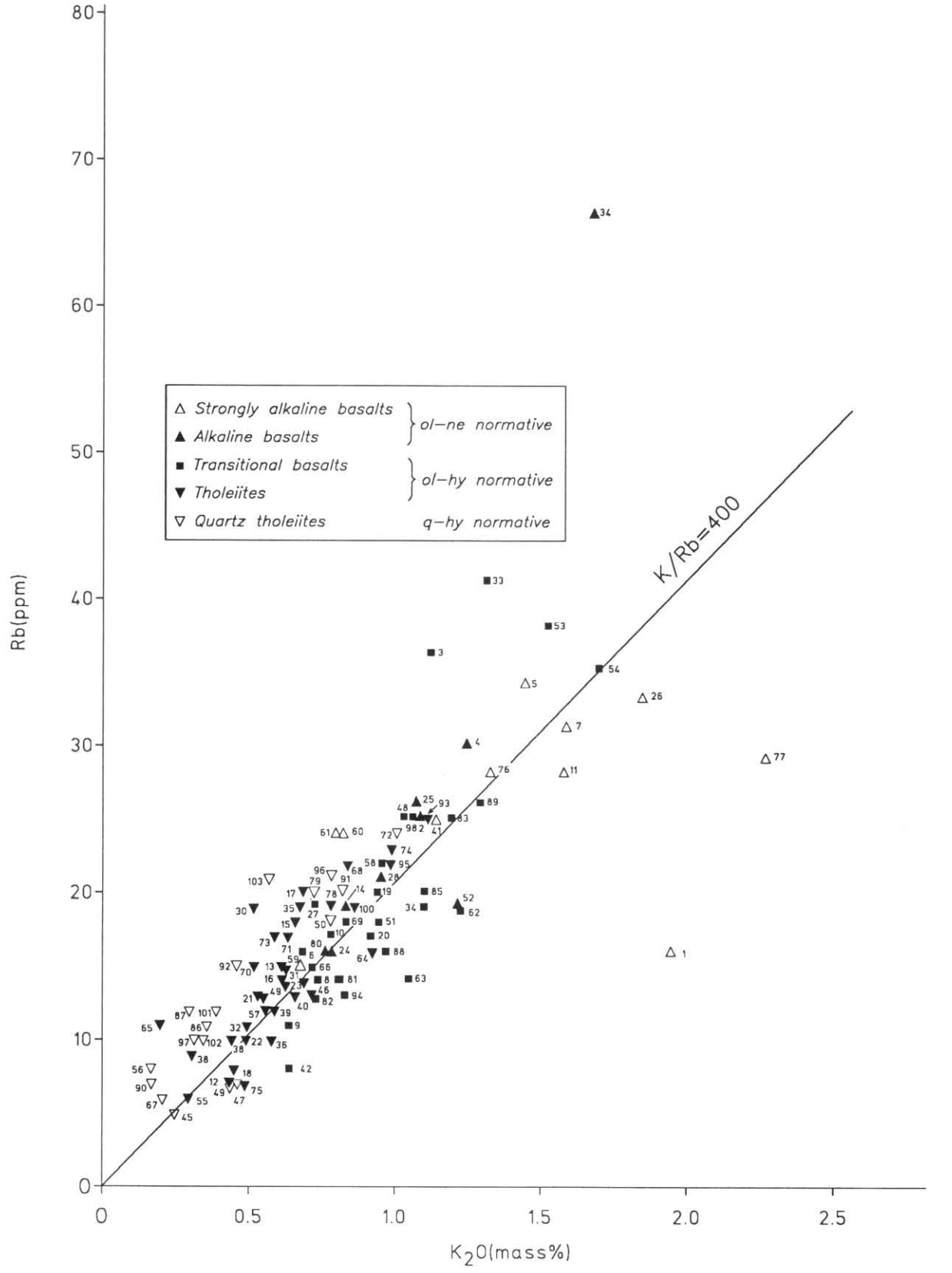

Figure B16. Rb–K_2O plot for Tertiary basaltic rocks

5 cm

is contrary to the observation of Prinz (1967). Possibly Cu is controlled by equilibrium with an immiscible sulphide melt (*cf.* Frey *et al.*, 197 p. 502).

The abundance of Mo, Sn and particularly W is puzzling, particularly as these elements would normally be below X-ray fluorescence detection limits in basalts. The highest Mo and Sn values are from hole SBDP2. Mo also appears to be higher in more alkaline rocks, but there is no clear correlation with chemistry. W values are highest in holes SBDP1 (average 408 ppm) and SBDP2 (average 231 ppm), but in the remaining holes (average 29 ppm) values are still far in excess of the world average of 0.7 ppm quoted for basalts (e.g. Turekian and Wedepohl, 1961; Evans and Krauskopf, 1969). Laboratory contamination or analytical problems are considered unlikely (R. A. Robie, pers. comm.) and the surface samples (EV1-39) have also anomalous W contents. The differences between drill holes indicate regional variations. The proximity of the Mt Bischoff tin and Kara tungsten deposits suggests the possibility that these elements may have been introduced into the magma from the country rock by wall rock reaction or a similar process, whilst it lay in relatively shallow magma chambers. Alternatively there may be a deep regional anomaly in these elements in north-west Tasmania. Further work is required on these questions.

The elements not so far discussed, As, Ag, Ta, Pb, Bi, Th and U, all have abundances near or below the detection limits of X-ray fluorescence, and thus it is not possible to draw any inferences from them.

SPINEL LHERZOLITE NODULES

Numerous spinel lherzolite nodules (≤100 mm) lie within a strongly undersaturated basanite, on a hill near South Riana [DQ156310]. In hand specimen, the nodules are usually well rounded and equidimensional or ellipsoidal in shape, or, less often, irregular or angular. Occasionally they appear to be embayed by the host rock. Pale green olivine and brownish orthopyroxene, with minor bright green clinopyroxene and black spinel, are visible to the naked eye.

In thin section (plate B1) the nodules have a granoblastic texture, consisting of interlocking anhedra, varying considerably in size (0.2-1 mm). The minerals, in decreasing order of abundance, are olivine, orthopyroxene, clinopyroxene and brown spinel. Extinction of olivine and pyroxenes is usually straight or, rarely, slightly undulose, suggesting that the grains are relatively unstrained. Grain boundaries are often strongly curved. Spinel grains are more irregular, sometimes slightly vermicular in shape, but the other minerals are never elongated and the nodules have no foliation. Occasionally near the margins of the nodules, reaction with the host rock has formed a zone of finely granular olivine and the margins of spinel grains are altered to an opaque mineral.

These features are characteristic of the protogranular type of lherzolite texture (Mercier and Nicolas, 1975) which is the commonest type in spinel lherzolite nodules from Tasmanian Tertiary basalts (Varne, 1977). Protogranular texture is considered by Mercier and Nicolas to be the original, oldest type, and may grade into the foliated, porphyroclastic texture by plastic flow, which in turn may recrystallise into various equigranular textures.

Electron probe microanalyses of grains from a single nodule (table B5, analyses 17-38) show that the minerals are remarkably homogeneous in composition (olivine averaging $Fo_{89.8}$, orthopyroxene $En_{90.4}$, clinopyroxene $Wo_{47.1}$ $En_{48.7}$ $Fs_{4.2}$). Pyroxenes have substantial Al_2O_3 contents, suggesting equilibrium at high temperatures, and spinel contains about 11% Cr_2O_3. Analyses from a second nodule (table B5, analyses 39-46) are not appreciably different. These mineral compositions are typical of spinel lherzolite nodules from Tasmanian Tertiary basalts (Varne, 1977), except for Na_2O and Al_2O_3 in clinpyroxene which is slightly lower than usual, suggesting a lower jadeite content.

After studying a large number of similar spinel lherzolite nodules, Varne (*ibid.*) concluded that their texture and mineralogy is of subsolidus rather than direct igneous origin, and in particular spinel and pyroxenes are derived from more aluminous pyroxenes as a result of falling temperature. Thus the nodules are neither residua of the source rock nor igneous cumulates, but fragments of the upper mantle genetically unrelated to their host rock and accidentally incorporated during ascent.

SUMMARY

The extensive flood basalts of the St Valentines Quadrangle vary widely in chemistry, texture and grain size.

Chemically, there is a continuous gradation with decreasing $Na_2O + K_2O$ and increasing SiO_2, from rare, strongly undersaturated basinites (which lack modal plagioclase and therefore could be termed olivine nephelinites), through alkali olivine basalts, to transitional basalts and olivine-normative tholeiites (the most common types) and finally to quartz-normative tholeiites. Fractionated alkaline rocks such as members of the hawaiite-mugearite-benmoreite trend are notably absent. Alkali olivine basalts are more common in lower parts of the volcanic pile and in the north-east of the quadrangle, and volcanism appears to have become progressively more tholeiitic with time and to the south-west.

Olivine phenocrysts, often embayed, are present and usually common in about 90% of samples, and in nearly all cases represent the low pressure liquidus phase. Usually smaller phenocrysts of clinopyroxene (20% of samples) and/or plagioclase (labradorite) microphenocrysts (also 20% of samples) may be present. A few samples contain unusual glomerocrysts in which augite and olivine surround, in apparent reaction relation to, a central core of orthopyroxene which probably crystallised at greater depth. The groundmass usually consists principally of plagioclase (labradorite), augite, ilmenite and titanomagnetite; in more alkaline rocks titanaugite replaces augite, alkali feldspar and apatite are more common, and nepheline and groundmass olivine may be present. Intergranular texture is the most common, but glassy to intersertal, subophitic to ophitic, and rare equigranular-consertal textures are also found. Grain size varies widely and, like texture, is largely controlled by the cooling history of the magma, and is not directly related to chemistry.

Only rare samples represent possible unfractionated primary magmas (100Mg/Mg + Fe ~ 68.8-73.0). The remainder were probably derived from more primitive parental magmas (olivine tholeiites to alkali picrites) by ≤20 mass% crystal fractionation of olivine and, less commonly, pyroxene. The incompatible elements P, Sr, Zr and Nb increase systematically from tholeiites to alkali olivine basalts and basanites; this is interpreted as due to varying amounts of partial melting. On the P_2O_5-based pyrolite model of Frey *et al.* (1978), the parental basanites were generated by 6-7% partial melting (with some variations in CaO due to differing amounts of CO_2 in the melt), alkali olivine basalts by 9-18%, transitional basalts by 16-24% and tholeiites by 20-35% partial melting. Light rare-earth elements (La, Ce, Nd), K_2O, Rb and Ba have also behaved similarly as incompatible elements, but show greater scatter, attributable to source inhomogeneity and/or more mobile behaviour.

Unusually high values of Sn, Mo and especially W are present in many samples and may represent a regional anomaly.

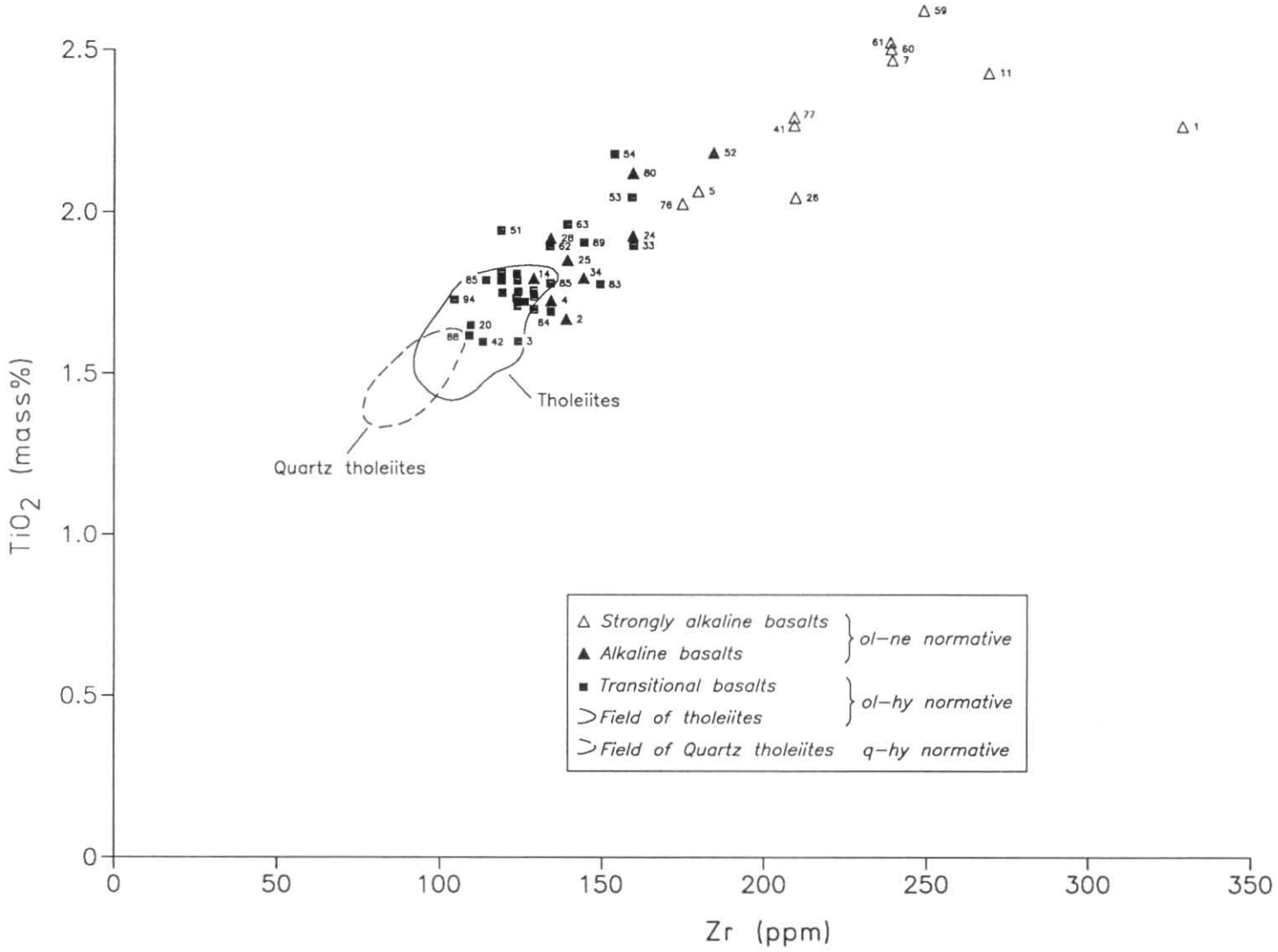

Figure B17. TiO_2-Zr plot for Tertiary basaltic rocks

5 cm

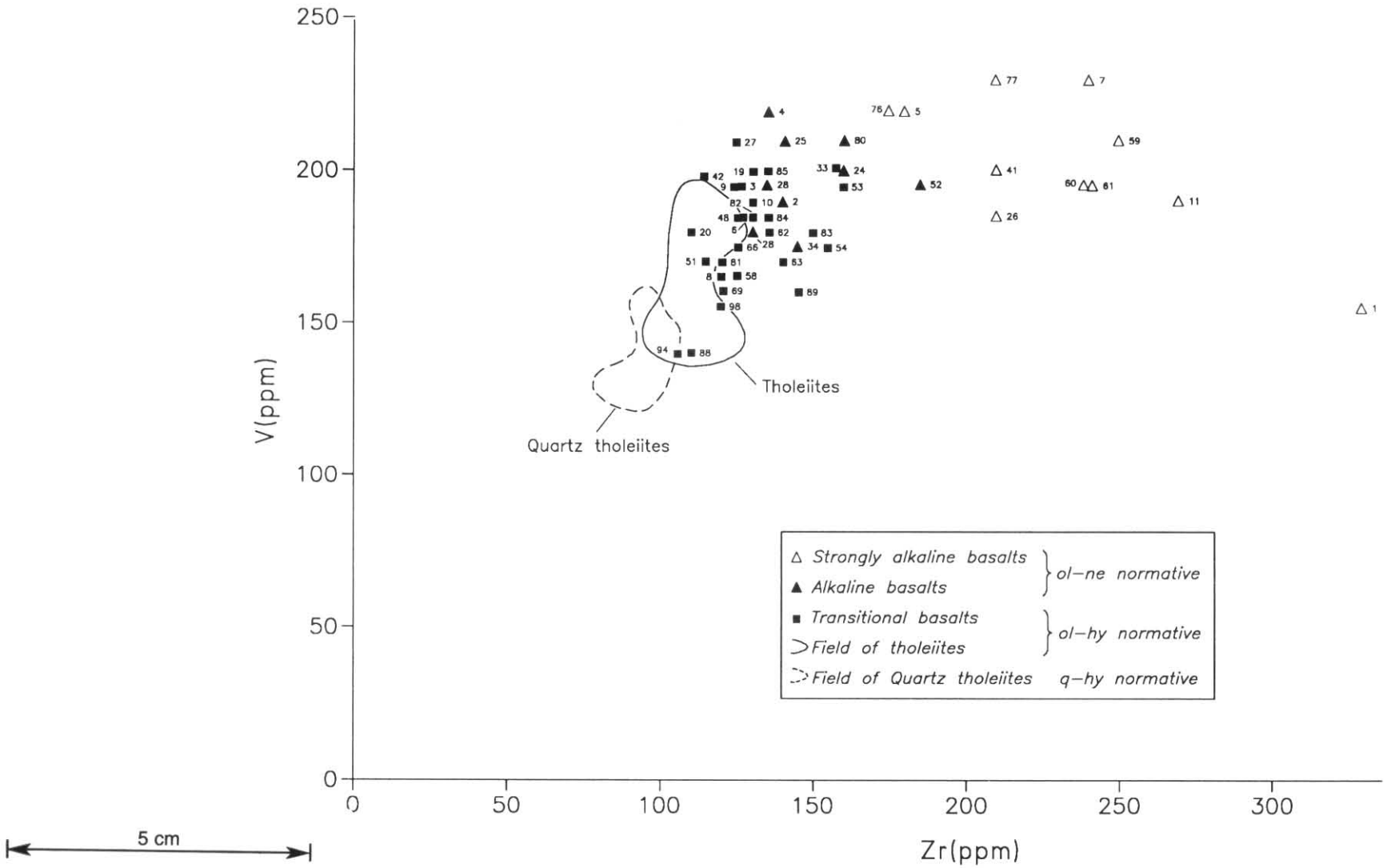

Figure B18. V-Zr plot for Tertiary basaltic rocks

Abundant spinel lherzolite nodules and related xenocrysts occur within a basanite on a hill near South Riana. Their mineralogy and granoblastic texture is typical of nodules from Tasmanian Tertiary basalts (Varne, 1977). They are probably accidental fragments of the upper mantle, genetically unrelated to the host magma into which they were incorporated during ascent.

REFERENCES

BAILLIE, P. W. 1987*a*. Completion report: Sub-basalt Drilling Project Hole 1. *Unpubl. Rep. Dep. Mines Tasm.* 1987/38.

BAILLIE, P. W. 1987*b*. Completion report: Sub-basalt Drilling Project Hole 2. *Unpubl. Rep. Dep. Mines Tasm.* 1987/40.

BAILLIE, P. W. 1987*c*. Completion report: Sub-basalt Drilling Project Hole 4. *Unpubl. Rep. Dep. Mines Tasm.* 1987/61.

BAILLIE, P. W.; GREEN, G. R. 1988a. Completion report: Sub-basalt Drilling Project Hole 6. *Unpubl. Rep. Dep. Mines Tasm.* 1988/06.

BAILLIE, P. W.; GREEN, G. R. 1988b. Completion report: Sub-basalt Drilling Project Hole 9. *Unpubl. Rep. Dep. Mines Tasm.* 1988/07.

BREY, G. P.; GREEN, D. H. 1975. The role of CO_2 in the genesis of olivine melilitite. *Contrib. Mineral. Petrol.* 49:93-103.

BROOKS, C. K. 1976. The Fe_2O_3/FeO ratio of basalt analyses: an appeal for a standard procedure. *Bull. geol. Soc. Denmark* 25:117-120.

BROWN, A.V.; FORSYTH, S. M. 1984. Chemistry of Tertiary basalt and palynology of sediments from B.H.P. drill holes, E.L. 33/79. *Unpubl. Rep. Dep. Mines Tasm.* 1984/39.

BROWN, A. V.; MCCLENAGHAN, M. P. 1982. Tertiary basaltic rocks, *in*MCCLENAGHAN *et al.*, Geology of the Ringarooma-Boobyalla area. *Bull. geol. Surv. Tasm.* 61:92-114.

BROWN, G. N. 1957. Pyroxenes from the early and middle stages of fractionation of the Skaergaard Intrusion, East Greenland. *Mineral. Mag.* 31:511-543.

BUDDINGTON, A. F.; LINDSLEY, D. H. 1964. Iron-titanium oxide minerals and synthetic equivalents. *J. Petrology* 5:310-357.

CARMICHAEL, I. S. E.; TURNER, F. J.; VERHOOGEN, J. 1974. *Igneous petrology*. McGraw Hill : New York.

CARTER, J. L. 1970. Mineralogy and chemistry of the earth's upper mantle based on the partial fusion - partial crystallisation model. *Bull. geol. Soc. Am.* 81:2021-2034.

COOMBS, D. S.; WILKINSON, J. F. G. 1969. Lineages and fractionation trends in undersaturated volcanic rocks from the East Otago volcanic province (New Zealand) and related rocks. *J. Petrology* 10:440-501.

DEER, W. A.; HOWIE, R. A.; ZUSSMAN, J. 1963. *Rock-forming minerals minerals. Vol. 4. Framework silicates*. Longmans : London.

EDWARDS, A. B. 1950. The petrology of the Cainozoic rocks of Tasmania. *Proc. R. Soc. Vict.* 62:97-120.

EVANS, H. T.; KRAUSKOPF, K. B. 1969. Tungsten (wolfram), *in:* WEDEPOHL, K. H. (ed.) *Handbook of geochemistry. Vol. II/5. Elements La (57) to U(92)*. Springer-Verlag : Berlin.

EVERARD, J. L. 1984. Petrology of Tertiary basalt, altered dolerite and tuff samples, *in* GULLINE, A. B. Geological atlas 1:50 000 series. Sheet 83(8412N). Sorell. Explan. *Rep. geol. Surv. Tasm.*

EVERARD, J. L. 1987*a*. Petrology of the Triassic basalt in TURNER, N. J.; CALVER, C. R. Geological atlas 1:50 000 series. Sheet 49(8514N). St Marys. *Explan. Rep. geol. Surv. Tasm.*

EVERARD, J. L. 1987*b*. Petrology of the Jurassic dolerite in TURNER, N. J.; CALVER, C. R. Geological atlas 1:50 000 series. Sheet 49(8514N). St Marys. *Explan. Rep. geol. Surv. Tasm.*

FLOYD, P. A.; WINCHESTER, J. A. 1975. Magma type and tectonic setting discrimination using immobile elements. *Earth planet. Sci. Lett.* 27:211-218.

FREY, F. A.; GREEN, D. H.; ROY, S. D. 1978. Integrated models of basalt petrogenesis: a study of quartz tholeiites to olivine melilitites from south eastern Australia utilizing geochemical and experimental petrological data. *J. Petrology* 19:463-513.

FULLER, R. E. 1939. Gravitative accumulation of olivine during the advance of basaltic flows. *J. Geol.* 47:303-313.

HART, S. R.; GUNN, B. M.; WATKINS, N. O. 1971. Interlava variation of alkali elements in Icelandic basalt. *Am. J. Sci.* 270:315-318.

IIRVING, A. J.; GREEN, D. H. 1976. Geochemistry and petrogenesis of the Newer basalts of Victoria and South Australia. *J. geol. Soc. Aust.* 23:45-66.

JOPLIN, G. A. 1963. Chemical analyses of Australian rocks. Part I: Igneous and metamorphic. *Bull. Bur. Geol. Geophys. Aust.* 65.

LE MAITRE, R. W. 1984. A proposal by the IUGS Subcommission on the Systematics of Igneous Rocks for a chemical classification of volcanic rocks based on the total alkali silica (TAS) diagram. *Aust. J. earth Sci.* 31:243-255.

LUCAS, D. S. 1988. *Magnetics of the Tertiary basalts of north-western Tasmania*. B.Sc.(Hons) thesis, University of Tasmania : Hobart.

MACDONALD, G. A.; KATSURA, T. 1964. Chemical composition of Hawaiian lavas. *J. Petrology* 5:82-133.

MCDOUGALL, I. 1961. Optical and chemical studies of pyroxenes in a differentiated Tasmanian dolerite. *Am. Mineral.* 44:661-687.

MATHEWS, W. H.; THORARINSSON, S.; CHURCH, N. B. 1964. Gravitative settling of olivine in pillows of an Icelandic basalt. *Am. J. Sci.* 262:1036-1040.

MERCIER, J. C. G.; NICOLAS, A. 1975. Textures and fabrics of upper mantle peridotites as illustrated by xenoliths from basalts. *J. Petrology* 16:454-487.

PEARCE, J. A.; CANN, J. R. 1973. Tectonic setting of basic volcanic rocks determined using trace element analyses. *Earth planet. Sci. Lett.* 19:290-300.

PRINZ, M. 1967. Geochemistry of basaltic rocks : trace elements, *in:* HESS, H. H.; POLDERVAART, A. (ed.) *Basalts, Vol. I*. Interscience : New York.

RINGWOOD, A. E. 1966. The chemical composition and origin of the earth, *in* HURLEY, P. M. (ed.). *Advances in earth science*. MIT Press : Cambridge, Mass.

ROEDER, P. L.; EMSLIE, R. F. 1970. Olivine-liquid equilibrium. *Contrib. mineral. Petrology* 29:275-289.

SATO, H. 1977. Nickel content of basaltic magmas: identification of primary magmas and a measure of the degree of olivine fractionation. *Lithos* 10:113-120.

SIMKIN, T.; SMITH, J. V. 1970. Minor element distribution in olivine. *J. Geol.* 78:304-325.

SMITH, J. V. 1974. *Feldspar minerals. II. Chemical and textural properties*. Springer-Verlag : Berlin.

STRECKEISEN, A. 1967. Classification and nomenclature of igneous rocks. *Neues Jb. Mineral., Abh.* 107:144-240.

STRECKEISEN, A. L. 1978. Classification and nomenclature of volcanic rocks, lamprophyres, carbonatites and melilitic rocks. *Neues Jb. Miner., Abh.* 134:1-14.

SUN, S. S.; HANSON, G. N. 1975. Evolution of the mantle: geochemical evidence from alkali basalt. *Geology* 3:297-302.

SUTHERLAND, F. L. 1969. A review of the Tasmanian Cainozoic Province. *Spec. Publ. geol. Soc. Aust.* 2:133-144.

SUTHERLAND, F. L. 1973. Igneous rocks, Central Plateau, *in:* BANKS, M. R. (ed.) *The Lake Country of Tasmania : a symposioum*. Royal Society of Tasmania : Hobart.

SUTHERLAND, F. L. 1974. High pressure inclusions in tholeiitic basalt and the range of lherzolite-bearing magmas in the Tasmanian Volcanic Plaince. *Earth planet. Sci. Lett.* 24:317-324.

SUTHERLAND, F. L. 1976. Cainozoic volcanic rocks, *in:* LEAMAN, D. E. Geological atlas 1:50 000 series. Sheet 82(8312S). Hobart. *Explan. Rep. geol. Surv. Tasm.*:35-56.

SUTHERLAND, F. L. 1984. Cainozoic basalts, *in:* FORSYTH, S. M. Geological atlas 1:50 000 series. Sheet 68(8313S). Oatlands. *Explan. Rep. Dep. Mines Tasm.*:103-120.

SUTHERLAND, F. L. 1985. Cainozoic volcanic rocks, *in:* FARMER, N. Geological atlas 1:50 000 series. Sheet 94(8311N). Kingborough. *Explan. Rep. geol. Surv. Tasm.*:73-83.

SUTHERLAND, F. L. 1989. Cainozoic volcanic rocks, *in:* FORSYTH, S.M. Geological atlas 1:50 000 series. Sheet 61 (8313N). Interlaken. *Explan. Rep. geol. Surv. Tasm.*

TUREKIAN, K. K.; WEDEPOHL, K. H. 1961. Distribution of the elements in some major units of the earth's crust. *Bull. geol. Soc. Am.* 72:175-192.

VARNE, R. 1977. On the origin of spinel lherzolite inclusions in basaltic rocks from Tasmania and elsewhere. *J. Petrology.* 18:1-23.

APPENDIX C

An unusual occurrence of ultramafic and mafic rocks north of Mt Bischoff, north-west Tasmania*

P. R. Williams
A. V. Brown

INTRODUCTION

Outcrops of ultramafic and mafic rocks in the Arthur River valley north of Mt Bischoff (fig. C1) were mapped during the Geological Survey of Tasmania's coverage of the St Valentines Quadrangle in north-western Tasmania. The occurrence was previously unrecorded, as was much of the sedimentary and volcanic sequence of the surrounding countryside. The ultramafic rock bodies are unusual to Tasmania, in that they are apparently undeformed, display their primary mineral compositions without extensive serpentinisation and appear to intrude the surrounding sedimentary/volcanic sequence as sills. A distinctive doleritic rock type intrudes the sedimentary/volcanic sequence in the same area as the ultramafic rocks. The purpose of this paper is to describe and contrast the igneous rock types in this unusual occurrence, and to compare the ultramafic rocks with those elsewhere in western Tasmania.

GEOLOGICAL SETTING

The area is underlain by a sequence of probable Eo-Cambrian or Early Cambrian greywacke, mudstone, basaltic lava, and subsidiary chert. These overlie the Proterozoic Mt Bischoff sequence with unconformity (Groves, 1971). The proportion of mudstone, chert and greywacke to basaltic lavas varies considerably, and in places greywacke is absent and lava flows are separated by thin mudstone beds and minor chert. In the region of ultramafic rocks there is an approximately equal abundance of greywacke and mudstone, with more chert than usual and less basaltic lava. The sequence is continuous with the rock exposed in the Cleveland mine area (Cox and Glasson, 1971; Collins, 1981). The greywacke from the sequence in the Arthur River is very poorly sorted, composed of angular grains of feldspar, quartz and rock fragments. The rock fragments are metaquartzite, similar to quartzite from the Tyennan region metamorphic rocks of central Tasmania. The presence of detrital garnet grains as well as metaquartzite suggests a Tyennan source area. Garnet has not been reported from Proterozoic rocks in north-western Tasmania. Detrital muscovite and biotite are also present. Chert interbedded with the mudstone and greywacke is usually finely laminated often with well preserved fine undulations, suggesting that it is a primary deposit. There is no evidence of detrital grains, implying that the chert may have been a chemical sediment.

BASALTIC ROCKS INTERBEDDED WITH THE SEDIMENTARY SEQUENCE

Basaltic rocks in the sequence increase in abundance to the north. The basalts form pillow structures (Groves and Solomon, 1964) and several exposures of pillow structure are observable on new Forestry roads in the area. Cusps of pillows are often filled with chert. In addition basaltic lapilli tuff is present, composed of rounded fragments of basalt in a fine-grained dark-coloured matrix with abundant pyroxene

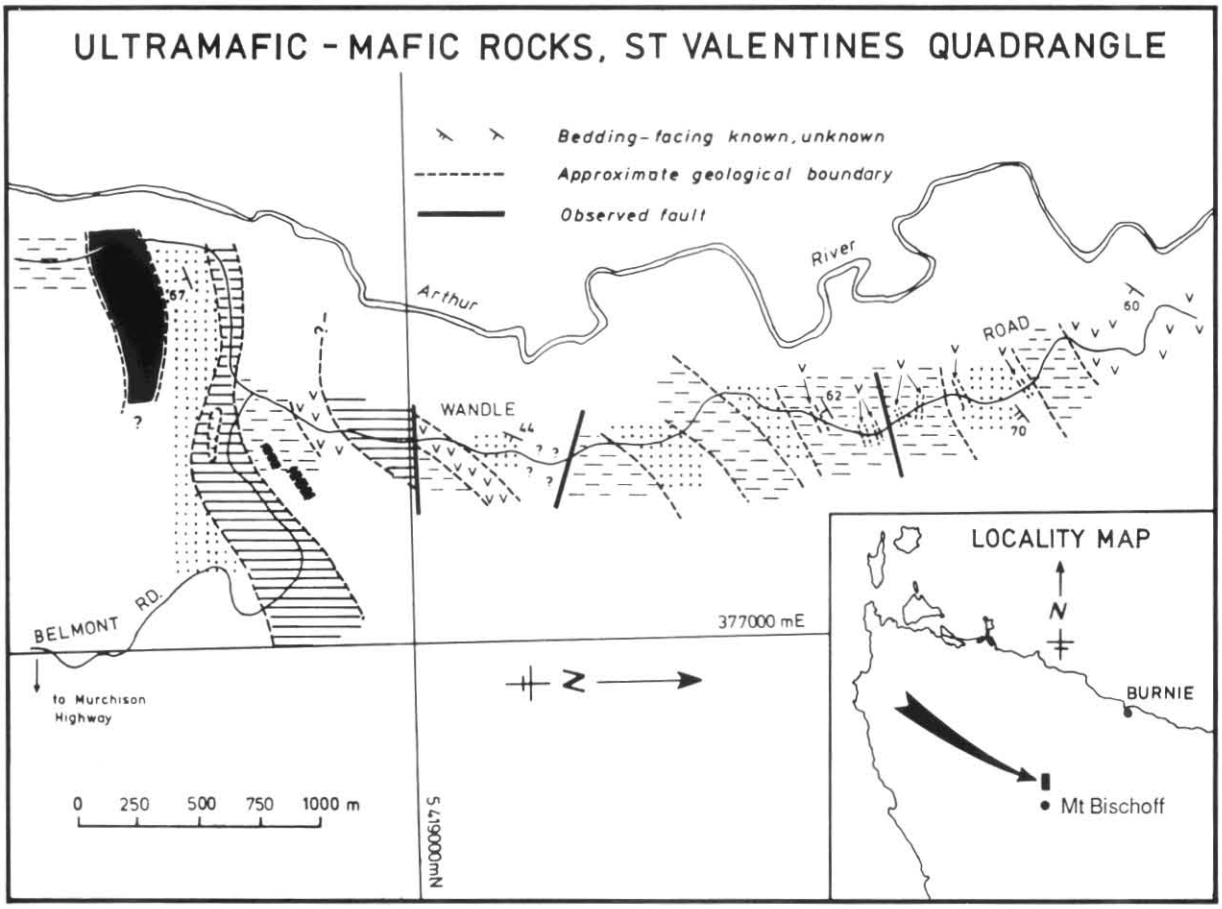

Figure C1. Geological map of the area around Belmont Road and Wandle Road in the Arthur River valley.

* Originally published in the Papers and Proceedings of the Royal Society of Tasmania, vol. 117, pp. 53-58 and reproduced with permission.

5 cm

crystals (crystal lithic lapilli tuff). The basalt is typically an equigranular or porphyritic rock with small phenocrysts of plagioclase and pyroxene in a matrix of feldspar laths, pyroxene crystals and chlorite showing an intersertal texture. The mineralogy and texture of these rocks has been described in detail by Groves and Solomon (1964). Chemical analyses of the basalt and tuff are shown in Table C1 (analyses 1-4).

Table C1
CHEMICAL ANALYSES

	1	2	3	4	5	6
	783165*	814513	783164	814514	814515	814512
SiO_2	46.60	47.44	50.00	47.80	50.97	49.55
TiO_2	1.70	3.38	1.00	1.95	0.25	0.39
Al_2O_3	14.20	12.31	13.30	13.26	13.56	14.15
Fe_2O_3	3.30	9.15	2.50	3.09	3.55	3.78
FeO	9.20	4.67	8.00	9.68	7.41	7.10
MnO	0.22	0.27	0.19	0.18	0.18	0.20
MgO	7.50	5.54	8.20	6.34	6.79	7.55
CaO	9.70	7.89	9.10	8.83	10.27	8.65
Na_2O	2.80	3.39	2.20	3.33	3.83	2.82
K_2O	1.00	0.86	0.53	0.22	0.34	0.21
P_2O_5	0.07	0.36	0.16	0.21	0.05	0.06
Loss	4.06	3.67	4.80	4.10	3.37	4.77
Cr	171	146	289	153	81	295
Ni	103	79	106	92	73	104
Rb	20	8	12	4	10	5
Sr	484	288	147	222	107	171
Y	22	33	25	20	8	14
Zr	111	216	80	111	9	17
Mg	52	43	59	47	55	56
Ti/Zr	92	94	75	105	166	317
Ti/Y	463	614	240	585	187	39
Zr/Y	5.05	6.55	3.20	5.55	1.31	1.21
Cr/Ni	1.66	1.85	2.73	1.66	1.11	2.49

	7	8	9	10	11	12
	783163	814511	813140	814510	814507	814508
SiO_2	50.30	52.69	38.48	38.64	40.38	40.84
TiO_2	0.39	0.55	0.03	0.03	0.04	0.05
Al_2O_3	14.00	13.26	4.41	4.34	5.42	5.40
Fe_2O_3	3.10	5.54	5.23	3.47	3.12	3.02
FeO	6.90	7.41	5.28	5.51	5.81	6.49
MnO	0.20	0.19	0.15	0.16	0.17	0.16
MgO	7.70	5.00	31.89	32.94	31.04	32.42
CaO	8.60	6.34	4.26	4.05	4.11	4.15
Na_2O	3.70	5.18	<0.03	0.10	0.07	0.21
K_2O	0.28	0.17	0.03	0.07	0.06	0.07
P_2O_5	0.03	0.07	0.01	0.02	0.02	0.03
Loss	4.60	2.65	9.86	9.68	8.87	6.62
Cr	258	81	3698	4249	4903	4363
Ni	119	63	1621	1703	1616	1657
Rb	4	<4	<4	<4	4	6
Sr	226	210	27	15	21	28
Y	15	18	<4	<4	<4	<4
Zr	<5	22	4	<4	<4	<4
Mg	59	42	85	87	87	86
Ti/Zr	468	150	45	45	60	75
Ti/Y	156	183	45	45	60	75
Zr/Y	0.33	1.22	1	1	1	1
Cr/Ni	2.17	1.29	2.28	2.50	2.53	2.63

* Sample numbers - Department of Mines analytical numbers

Analyses 1-4: Basaltic rocks from within the sedimentary sequence.
5-8: Fine-grained intrusive rocks.

INTRUSIVE ROCKS

Near the intersection of Belmont Road and Wandle Road, two major intrusions of ultramafic rock and one major intrusion of mafic (doleritic) rock have been identified (fig. C1). In addition there are several intrusions or extrusions of basalt between the two ultramafic bodies. The mafic and ultramafic rocks occur in the same zone, but no age relationship between them has been observed. The southern ultramafic body is regionally concordant, and where contacts with sedimentary rocks are exposed these parallel bedding. However, the northern ultramafic body has a faulted northern margin, and the surrounding mudstone is highly fractured. These fractures are filled with quartz and very iron-rich chlorite (with second order birefringence colours) and post-date cleavage. The fault is inferred to be Devonian in age, because the cleavage probably formed during a Devonian deformation event.

On the southern edge of the southern ultramafic body there is a sequence of graded contact metamorphosed greywacke beds with pelitic tops. The pelitic tops are spotted, and the spots are deformed into lozenges parallel to cleavage, implying that metamorphism occurred prior to deformation. There are no nearby dolerite dykes or pillow lavas. The metamorphism of the country rock, and absence of any deformation features suggesting solid state movement in the ultramafics is used to infer that the ultramafics intruded as a liquid-dominated magma. However, poor exposure away from road sections does not allow a metamorphic aureole to be mapped out. The spotting and grading define the sedimentary facing of the sequence, which is to the north in this area.

In the area between the two major ultramafic bodies smaller intrusions of ultramafic rock (about 30 m thick) are concordant with a sequence of indurated chert and mudstone with incipient metamorphic spotting and biotite development. The sequence includes basalt with mudstone xenoliths. The sedimentary rocks have been brecciated and the fractures filled with opaque minerals. The weight of evidence, therefore, strongly suggests that the ultramafic rocks were intruded as magma into the chert-greywacke-mudstone-pillowed basalt sequence. Later faulting has occurred along some primary boundaries, but other boundaries are undisturbed.

Mafic rocks have also been intruded into the sedimentary sequence (fig. C1). The body of dolerite south of the ultramafic rocks cross-cuts the chert sequence in that area at a low angle. Several small areas of porphyritic, fine- and medium-grained dolerite occur in the area between the two ultramafic intrusions and one large outcrop has a discordant boundary. At one of these localities fine-grained dolerite, in continuity with the medium-grained dolerite, may represent a chilled margin. They are inferred to be dykes, although the possibility that some may be sills cannot be ruled out. The age relationship between the dolerite and ultramafic rocks cannot be determined, although intruded into the same area.

The intrusive rocks range in texture from basaltic, with a grain size of about 0.02 mm, up to doleritic rocks, with a grain size of about 2 mm. Rare gabbroic rocks are present. The basaltic rocks are composed of patches of chlorite, large pyrite grains, abundant small anhedral grains of pyroxene which tend to aggregate in patches in a matrix of altered laths of plagioclase. These are much more altered rocks than the basalt interbedded with the sedimentary rocks, and the presence of fine-grained granular aggregates of small pyroxene grains has not been observed in the pillowed basalt. Rare altered feldspar phenocrysts (plagioclase) are present and rare augite posettes also occur. Very fine grained rocks contain abundant phenocrysts of plagioclase. Some calcite veins are also present.

In contrast the coarse-grained intrusive varieties contain subhedral augite crystals in a matrix of truncated feldspar laths (intergranular texture). Large chlorite phenocrysts with prismatic habit are clearly pseudomorphs after another ferro-magnesian mineral. Other specimens tend to ophitic to

sub-ophitic and tremolite occurs as fibrous aggregates in anhedral patches. Rocks of intermediate grain size show near anhedral pyroxene.

Very altered specimens are common and are composed dominantly of chlorite and feldspar (albite) with abundant opaque minerals. The rocks exhibit thick tremolite veins, fresh albite veins and sericitic patches. The absence of this type of alteration in the basaltic lava flows in the sedimentary rocks suggests that it may be primary or deuteric alteration. Chemical analyses of these mafic rocks are shown in Table C1 (analyses 5-8).

The ultramafic bodies grade from plagioclase and clinopyroxene bearing granular harzburgite at the top of the bodies to plagioclase bearing poikilitic lherzolite at the base. Overall the bodies are massive with little grain size variation. The bases are coarser than the tops and contain a larger percentage of euhedral crystals.

Olivine and accessory chrome spinel are the cumulate mineral phases while pyroxene and plagioclase are post-cumulate. No indication of layering or of mineral fabric (foliation) is seen. The distribution of plagioclase is irregular. In places, olivine crystals are mantled by mesh serpentine group minerals and outlined by fine-grained magnetite. Interstitial highly altered plagioclase usually forms as cuspate patches but occasional fresh subhedral grains are seen.

In the northern part of the largest body, exposed along Wandle Road, the plagioclase-bearing harzburgite has a panidiomorphic granular texture of rounded olivine and euhedral chrome spinel grains surrounded by anhedral post-cumulate granular orthopyroxene with minor irregular patches of clinopyroxene and plagioclase. Olivine and orthopyroxene make up approximately 95% of the rock.

Southwards the olivine grains become coarser and more euhedral, pyroxene remains dominantly granular but some orthopyroxene grains poikilitically enclose olivine. Post-cumulate plagioclase is more common. The southernmost outcrop of this body consists of plagioclase bearing poikilitic lherzolite. Olivine crystals are subhedral to euhedral and both orthopyroxene and clinopyroxene poikilitically enclose olivine and chrome spinel grains as well as occurring as anhedral intergranular grains.

The second body, exposed along Belmont Road, is similar to the basal part of the Wandle Road body but contains a greater percentage of post-cumulate plagioclase and is slightly coarser-grained. Overall, euhedral to subhedral olivine crystals are poikilitically enclosed by anhedral pyroxene crystals. Chemical analyses of rocks from the ultramafic bodies are shown in Table C1 (analyses 9-12).

Ultramafic bodies from western Tasmania are usually layered and the constituent minerals show plastic to solid state deformation characteristics. Neither of these features is found in the ultramafic rocks of the Wandle Road-Belmont Road area. All other Tasmanian ultramafic bodies have undergone a high degree of serpentinisation and usually consist of disseminated blocks within a sheared serpentinite sheath. No such features are found associated with the Wandle Road-Belmont Road bodies.

The nearest body of ultramafic rocks to the Wandle Road-Belmont Road area is the Heazlewood River Complex (Rubenach, 1973). Plagioclase-bearing harzburgite and lherzolite from this complex are usually interlayered with other ultramafic rock types. They consist dominantly of rounded to elongate anhedral olivine grains poikilitically enclosed by large subhedral grains of orthopyroxene. Plagioclase is either subhedral with an intergranular texture or post-cumulate and interstitial to the olivine and pyroxene crystals. Olivine grains are partly to completely replaced by serpentine-group minerals and plagioclase is replaced by saussurite or hydrogrossular (Rubenach, 1973).

SUMMARY

The sequence of mudstone, greywacke, chert and pillowed basalt exposed from along the Arthur River Valley for 14 km north north of Mt Bischoff is intruded by both ultramafic and mafic rocks. It is probable that the ultramafic rock intruded as magma, which caused thermal metamorphism of the surrounding sedimentary rocks. Boundary faults present appear to be Devonian in age, but the absence of internal deformation structures and extensive serpentinisation suggests that they have not moved significantly from their intrusive position.

Dolerite intrudes the sedimentary/volcanic sequence probably as dykes and differs significantly from the pillowed basalts in that it has lower Zr, Y and TiO_2 contents and different textural features. The intrusive rocks are also more altered.

ACKNOWLEDGEMENTS

Dr N. Farmer critically read the manuscript and made useful suggestions.

REFERENCES

Collins, P. L. F. 1981. The geology and genesis of the Cleveland tin deposit, western Tasmania: fluid inclusion and stable isotope studies. *Econ. Geol.* 76:365-392.

Cox, R.; Glasson, K. R. 1971. Economic geology of the Cleveland mine, Tasmania. *Econ. Geol.* 66:861-878.

Groves, D. I. 1971. The regional significance of the Don Hill fault zone of Mt Bischoff, Tasmania. *Tech. Rep. Dept. Mines Tasm.* 14:7-15.

Groves, D. I.; Solomon, M. 1964. The geology of the Mt Bischoff district. *Pap. Proc. R. Soc.Tasm.* 98:1-22.

Rubenach, M. 1973. *The Tasmanian ultramafic-gabbro and ophiolite complexes.* Ph.D. thesis, University of Tasmania : Hobart.

APPENDIX D

A new Cambrian fossil locality from Native Track Tier, north-west Tasmania

P. W. Baillie
*J. B. Jago**

INTRODUCTION

During completion of mapping in the St Valentines Quadrangle a new Cambrian fossil locality was found in the Native Track Tier area [DQ140218] within a mixed sequence of felsic volcanic and sedimentary rocks.

The volcanic rocks are variable and include agglomerate, crystal-lithic tuff, and fine-grained varieties. It is noteworthy that some of the volcanic rocks are very similar to the Comstock Tuff (Tyndall Group) of the Queenstown area.

The fossils are found as internal and external moulds within a buff or fawn-coloured siltstone which occurs within a conglomerate-sandstone-siltstone sequence. Poor outcrop precludes meaningful facies analysis of the sequence.

PALAEONTOLOGY

The Cambrian fossils from the locality are the best preserved yet found in Tasmania and consist predominantly of a mixed agnostid/polymerid fauna. Many of the specimens are complete.

The agnostids include *Valenagnostus, Aspidagnostus, Clavagnostus, Peronopsis, Agnostascus, Tasagnostus* and *Innitagnostus*.

Polymerids are represented by abundant *Nepea* and *Amphoton*, together with a pagetiid (possibly *Helepagetia*) and a papyriaspid.

Hyolithids are common in the fauna, together with possible brachiopods.

AGE AND CORRELATION

The age of the fauna is Late Middle Cambrian in either the *Lejopyge laevigata* III Zone or the *Damesella torosa* - *Ascionepea janitrix* Zone (i.e. latest Middle Cambrian).

The fauna is similar in faunal content and age to the main Cambrian fossil locality in the St Valentines Peak area (Jago *et al.*, 1975) and is an approximate correlate of the Comstock Tuff (Jago, 1979).

This locality provides important new stratigraphic information with respect to the Mt Read Volcanics in north-western Tasmania.

REFERENCES

JAGO, J. B. 1979. Tasmanian Cambrian biostratigraphy - a preliminary report. *J. geol. Soc. Aust.* 26:223-230.

JAGO, J. B.; PIKE, G. A.; MILLS, D. 1975. Cambrian stratigraphy of the St Valentines Peak area, north-western Tasmania. *Pap. Proc. R. Soc. Tasm.* 109:85-90.

* South Australian Institute of Technology.

This Appendix was originally issued as *Unpubl. Rep. Dep. Mines Tasm.* 1985/15.

I. C. CARTER, Acting Government Printer, Tasmania

Printed on paper produced in Tasmania